QUANTIFICATION IN NON-INVASIVE CARDIAC IMAGING: CT AND MR

KWANTIFICATIE MET NIET-INVASIEVE BEELDVORMING VAN HET HART: CT EN MR

ALEXIA ROSSI

Financial support by
Medis medical imaging systems BV (Leiden, the Netherlands)
Department of Radiology, Erasmus MC, Rotterdam, the Netherlands
Pie Medical Imaging BV, Maastricht
for the publication of this thesis is gratefully acknowledged.

ISBN: 978-94-6191-778-2
Printed by Ipskamp Drukkers B.V., Enschede
Cover design: A.W. Everaers, A. Rossi
Layout: A.W. Everaers

QUANTIFICATION IN NON-INVASIVE CARDIAC IMAGING: CT AND MR

KWANTIFICATIE MET NIET-INVASIEVE BEELDVORMING VAN HET HART:

CT EN MR

Proefschrift

ter verkrijging van de graad van doctor aan de
Erasmus Universiteit Rotterdam
op gezag van de
rector magnificus

Prof.dr. H.G. Schmidt

en volgens besluit van het College voor Promoties.

De openbare verdediging zal plaatsvinden op
vrijdag 28 juni 2013 om 9.30 uur

door

Alexia Rossi

geboren te Pordenone, Italië

PROMOTIECOMMISSIE

PROMOTOREN	Prof.dr. J.W. Roos-Hesselink
	Prof.dr. G.P. Krestin
OVERIGE LEDEN	Prof.dr. M.G.M. Hunink
	Prof.dr. A.J.J.C. Bogers
	Prof.dr. J.H.C. Reiber
COPROMOTOR	Dr. R.J. van Geuns

Follow your heart wherever it may go

CONTENTS

PREFACE 11

CHAPTER 1 13
Introduction and thesis outline

PART 1: ISCHEMIC HEART DISEASE 23

CHAPTER 2 25
Coronary CT angiography for patients with suspected coronary artery disease.
2013 accepted for publication in Heart
A Rossi, A Dharampal, PJ de Feyter

CHAPTER 3 43
Diagnostic accuracy of 128-slice dual source CT coronary angiography: a randomized comparison of different acquisition protocols.
European Radiology, 2012; 23(3): 614-622
LA Neefjes, A Rossi, TS Genders, K Nieman, SL Papadopoulou, AS Dharampal, CJ Schultz, AC Weustink, ML Dijkshoorn, GJ Ten Kate, A Dedic, M van Straten, F Cademartiri, MG Hunink, GP Krestin, PJ de Feyter, NR Mollet

CHAPTER 4 61
Quantitative CT coronary angiography - Does it predict functionally significant coronary stenoses?
2013 (submitted for publication)
A Rossi, S-L Papadopolou, F Pugliese, B Russo, AS Dharampal, A Dedic, PH Kitslaar, A Broersen, B Meijboom, R-J van Geuns, A Wragg , J Ligthart, C Schultz, SE Petersen, K Nieman, GP Krestin, PJ de Feyter

CHAPTER 5 81
Myocardial Perfusion with Multislice Computed Tomography in Stable Angina Pectoris.
2013 accepted for publication in Radiology
A Rossi, D Merkus, E Klotz, N Mollet, PJ de Feyter, GP Krestin

CHAPTER 6 119
Quantification of myocardial blood flow by adenosine stress CT perfusion imaging in pigs during various degrees of stenosis correlates well with coronary artery blood flow and fractional flow reserve.
European Heart Journal Cardiovascular Imaging, 2012. Epub ahead of print.
A Rossi, A Uitterdijk, M Dijkshoorn, E Klotz, A Dharampal, M van Straten, WJ van der Giessen, N Mollet, RJ van Geuns, GP Krestin, DJ Duncker, PJ de Feyter, D Merkus

CHAPTER 7 137
Diagnostic performance of hyperaemic myocardial blood flow obtained by dynamic computed tomography - Does it predict functional significance in intermediate coronary lesions?
2013 (submitted for publication)
A Rossi, A Dharampal, A Wragg, L Ceri Davies, RJ van Geuns, E Klotz, P Kitslaar, A Broersen, A Mathur, K Nieman, MG Hunink, PJ de Feyter, SE Petersen, F Pugliese

CHAPTER 8 161
Patient with microvascular obstruction and myocardial bridging: multimodality approach with dynamic CT perfusion imaging, invasive coronary angiography, index of microvascular resistance and fractional flow reserve.
2013 (submitted for publication)
A Rossi, A Dharampal, PJ de Feyter, C Schultz

PART 2: AORTIC VALVE STENOSIS 165

CHAPTER 9 167
Ascending aorta dilatation in patients with bicuspid aortic valve: prospective CMR study.
European Radiology, 2012; 23(3): 642-649
A Rossi, D van der Linde, SC Yap, T Lapinskas, S Kirschbaum, T Springeling, M Witsenburg, J Cuypers, A Moelker, GP Krestin, A van Dijk, M Johnson, RJ van Geuns, JW Roos-Hesselink.

CHAPTER 10 185
Ascending aortic diameters in congenital aortic stenosis: cardiac magnetic resonance versus transthoracic echocardiography.
Echocardiography, 2013. Epub ahead of print.
D van der Linde, A Rossi, SC Yap, JS McGhie, AE van den Bosch, SWM Kirschbaum, B Russo, APJ van Dijk, A Moelker, GP Krestin, RJ van Geuns, JW Roos-Hesselink.

CHAPTER 11 201
Aortic annulus and leaflet calcification from contrast MSCT predict the need for baloon post-dilatation after TAVI with Medtronic CoreValve prosthesis.
Eurointervention, 2011; 7(5): 564-72
C Schultz, A Rossi, N van Mieghem, R van der Boon, S-L Papadopoulou, R van Domburg, A Moelker, N Mollet, GP Krestin, RJ van Geuns, K Nieman, PJ de Feyter, PW Serruys, P de Jaegere

PART 3: PREGNANCY AND HEART DISEASE 219

CHAPTER 12 221
Quantitative cardiac magnetic resonance in pregnant women: cross-sectional analysis of physiological parameters throughout pregnancy and the impact on the supine position.
Journal of Cardiovascular Magnetic Resonance, 2011; 13 (1): 31-37
A Rossi, J Cornette, Y Karamermer, T Springeling, P Opic, A Moelker, GP Krestin, E Steegers, M Johnson, JW Roos-Hesselink, RJ van Geuns

CHAPTER 13 235
Hemodynamic adaptation to pregnancy in patients with structural heart disease: a prospective MRI study.
2013 (submitted for publication)
A Rossi, J Cornette, TP Ruys, D Rizopoulos, Y Karamermer, E Steegers, M Ouhlous, GP Krestin, RJ van Geuns, JW Roos-Hesselink

SUMMARY AND CONCLUSIONS 249

CHAPTER 14 251
Summary 251
Samenvatting 259
General Discussion and Conclusions 267
PhD portfolio 277
List of Publications 285
Acknowledgements 293
About the Author 299
Abbreviations 303

PREFACE

CHAPTER 1

INTRODUCTION AND THESIS OUTLINE

The diagnosis and management of cardiac disease require a precise assessment of morphological and functional cardiac parameters. This thesis is divided in three parts. **Part 1** emphasizes the role of cardiac computed tomography (CT) in the diagnosis of patients with ischemic heart disease. **Part 2** describes the role of cardiac magnetic resonance (CMR) and cardiac CT in the diagnosis, interventional planning, and follow-up of patients with aortic valve stenosis. **Part 3** provides an evaluation of the role of CMR in pregnant patients with structural heart disease. The aim of this thesis was to gain insights in clinical applications of quantitative CT and MR.

ISCHEMIC HEART DISEASE

Coronary artery disease (CAD) is one of the major causes of mortality and morbidity throughout the world [1]. Since its introduction in 2000, CT coronary angiography (CTCA) has developed into a well-established, non-invasive imaging modality for direct visualization of coronary arteries, coronary stenosis, and atherosclerotic plaques. One of the major drawbacks of CTCA is the radiation dose. Indeed, CT and CTCA in particular, is a major contributor to medical ionising radiation exposure, which is assumed to increase the lifetime attributable risk of cancer. Therefore efforts should be taken to keep the radiation dose of CTCA as low as reasonably achievable. Radiation dose is inversely related to image noise and, by implication, to image quality. Efforts to decrease radiation exposure and patient dose should aim to deliver an image quality that allows confident image interpretation. In Chapter 2 the enormous increase of evidence supporting the role of CTCA in the diagnosis of patients with suspected CAD is summarised. In Chapter 3 the diagnostic performance and radiation exposure of two low dose CTCA protocols, available on dual source CT (DSCT) scanners, in the detection of obstructive coronary stenosis are evaluated.

Numerous single centre studies have compared CTCA to invasive coronary angiography (ICA) as a reference standard for stenosis severity. Several pooled meta-analysis data have shown the high diagnostic performance of CTCA with sensitivities ranging from 91% to 99% and specificities ranging from 74% to 96%. All these single centre studies were susceptible to referral and selection biases. Subsequently, three prospective multicentre studies [2-4] have been published showing sensitivities and specificities ranging from 85% to 99% and 64% to 90%, respectively. While all these studies highlighted the high diagnostic performance of CTCA to detect and particularly exclude anatomically obstructive CAD, the less-than-perfect specificity demonstrates the general overestimation of coronary stenosis severity with a high rate of false positive findings. An additional drawback is that, similarly to ICA, CTCA is an anatomical modality and it is often insufficient to predict functional significance of coronary stenosis [5]. According to the current guidelines the treatment of patients with CAD should be based on the combination of anatomical and functional significance of coronary stenosis [6]. Therefore, additional functional testing is often required to guide patient management. The value of cardiac CT to assess physiologic consequences of CAD has been explored by several methods.

In this thesis two new methods have been evaluated concerning this goal.

1 Quantitative CTCA

Studies using intravascular ultrasound (IVUS) have demonstrated that cross-sectional measurements of coronary artery stenosis are correlated well with fractional flow reserve (FFR) [7, 8] which is commonly used during ICA to identify functionally significant coronary stenosis. Similarly to IVUS, quantitative CTCA, using automated border lumen detection algorithms, allows assessment of cross-sectional parameters like the minimum lumen area, the percentage area stenosis, and the overall plaque burden [9]. In Chapter 4 the diagnostic accuracy of quantitative CTCA was compared to the diagnostic performance of visual CTCA to detect functionally significant coronary artery stenosis using FFR as the reference standard.

2 Physiological stress testing by CT perfusion imaging

Recently, CT-technical developments have been introduced that allow myocardial perfusion imaging during pharmacological stress to analyse the impedance of a coronary stenosis on myocardial blood flow [10, 11]. Some insights into CT myocardial perfusion studies are discussed in Chapter 5. The feasibility of dynamic stress CT perfusion imaging is investigated in an animal model with various degrees of coronary blood flow reduction (Chapter 6). The diagnostic performance of dynamic stress CT perfusion imaging in the detection of functionally significant stenosis based on FFR is evaluated in patients with chest pain referred to ICA and compared with the diagnostic performance of visual CTCA and quantitative CTCA (Chapter 7). In Chapter 8 a multimodality approach including dynamic stress CT perfusion imaging, ICA, index of microvascular resistance, and fractional flow reserve is presented in a patient with microvascular obstruction and myocardial bridging.

AORTIC VALVE STENOSIS

Aortic stenosis is the third most prevalent form of cardiovascular disease after hypertension and coronary atherosclerosis. It may be congenital in origin or secondary to another process. Bicuspid aortic valve (BAV) is the most common congenital cardiovascular anomaly with a prevalence of 1-2% in the general population [12]. The presence of a BAV is associated with an increased incidence of complications as aortic valve stenosis, aortic valve regurgitation, aneurysmal dilatation of the ascending aorta and aortic dissection [13].

Dilatation of the ascending aorta is one of the most consistent findings in BAV [14]. However, there is still controversy regarding the pathogenesis of aortic dilatation in the presence of BAV. Hemodynamic derangements of the BAV, including abnormal flow turbulence, poststenotic dilatation, and increased stroke volumes of aortic insufficiency [15-17] are believed to be the most common cause for aneurysmal dilatation of the aortic root and ascending aorta.

Histological abnormalities of the aortic media in patients with BAV are well documented [18]. Studies have demonstrated that the aortic media above a BAV is abnormal regardless of valve function [19] and is also present in the pulmonary trunk [20], suggesting the presence of an underlying systemic disorder. Familial links have been identified in BAV also suggesting an autosomal dominant inheritance pattern with reduced penetrance [21]. Chapter 9 describes the natural progression of aortic dilatation and its association with aortic valve stenosis in asymptomatic patients with BAV using CMR.

Stringent follow-up is necessary to determine the optimal timing of surgical replacement of the aortic valve and/or ascending aorta [22]. So far, transthoracic echocardiography (TTE) has been considered the reference standard for the evaluation of the severity of aortic stenosis in BAV patients. However, the acoustic window in obese patients and patients with chronic obstructive pulmonary disease may be inadequate for a comprehensive examination of the aortic valve and the ascending aorta. CMR can be used to characterize aortic valve disease in patients with inconclusive findings at TTE providing ancillary data that may affect patient management: quantification of left ventricular volumes, quantification of the severity of aortic stenosis and regurgitation, quantification of flow across the aortic valve, and measurements of the thoracic aorta diameters. In Chapter 10 correlation and agreement between CMR and TTE aortic measurements are investigated in young patients with congenital aortic stenosis.

Transcatheter aortic valve implantation (TAVI) is an emerging therapeutic option for symptomatic patients with severe aortic stenosis who are not eligible for surgical treatment [23]. Heavy calcification of the aortic root is an almost universal finding in patients with severe symptomatic aortic stenosis [24]. The reference standard for the measurement of calcification is non-contrast cardiac CT, yet the precise anatomical distribution of calcifications can be better appreciated on contrast-enhanced CT examinations usually showing dense calcification of the aortic leaflets. Dense calcification may contribute to deformation of the deployed frame of the prosthesis, which may result in malposition and paraprosthetic aortic valve regurgitation (PAR). Undersizing, where the prosthesis is small relative to the native annulus, is another factor, which may cause PAR after TAVI [25]. Balloon dilatation of the prosthesis is able to reduce the amount of regurgitation when significant PAR is encountered after deployment of the prosthesis. In Chapter 11 measurements of aortic valve calcifications on contrast-enhanced cardiac CT are compared to those performed on non-contrast cardiac CT in patients with severe aortic valve stenosis who underwent TAVI. Moreover, the predictors of the need for balloon dilatation after TAVI are investigated.

PREGNANCY AND HEART DISEASE

Increasing numbers of women with pre-existing heart disease are reaching childbearing age and are deciding to become pregnant [26, 27]. Pregnancy induces marked physiological changes in cardiac parameters with a 30-50% increase in cardiac output through an increase both in stroke volume and heart rate. CMR has become the reference standard in the assessment of cardiac hemodynamic parameters and ventricular function [28] as it can safely be performed after the first gestational trimester [29]. When a pregnant woman lays on her back the gravid uterus partially compresses the inferior vena cava with the consequent reduction of venous filling load and cardiac output. Therefore, the choice of positioning is an important factor during CMR acquisition. In Chapter 12 the effects of postural changes on cardiac dimensions and function during mid and late pregnancy are evaluated in healthy subjects.

While usually well tolerated in healthy women, pregnancy can induce adverse effects in women with pre-existing heart disease on both right and left-sided lesions [30]. Therefore, heart function should be closely monitored during pregnancy in these patients. In Chapter 13 the effects of pregnancy on left ventricular ejection fraction are evaluated in a longitudinal prospective CMR study investigating women with structural heart disease.

REFERENCES

1. Murray CJ, Lopez AD. Mortality by cause for eight regions of the world: Global burden of disease study. *Lancet*. 1997;349:1269-1276
2. Meijboom WB, Meijs MF, Schuijf JD, Cramer MJ, Mollet NR, van Mieghem CA, Nieman K, van Werkhoven JM, Pundziute G, Weustink AC, de Vos AM, Pugliese F, Rensing B, Jukema JW, Bax JJ, Prokop M, Doevendans PA, Hunink MG, Krestin GP, de Feyter PJ. Diagnostic accuracy of 64-slice computed tomography coronary angiography: A prospective, multicenter, multivendor study. *J Am Coll Cardiol*. 2008;52:2135-2144
3. Budoff MJ, Dowe D, Jollis JG, Gitter M, Sutherland J, Halamert E, Scherer M, Bellinger R, Martin A, Benton R, Delago A, Min JK. Diagnostic performance of 64-multidetector row coronary computed tomographic angiography for evaluation of coronary artery stenosis in individuals without known coronary artery disease: Results from the prospective multicenter accuracy (assessment by coronary computed tomographic angiography of individuals undergoing invasive coronary angiography) trial. *J Am Coll Cardiol*. 2008;52:1724-1732
4. Miller JM, Rochitte CE, Dewey M, Arbab-Zadeh A, Niinuma H, Gottlieb I, Paul N, Clouse ME, Shapiro EP, Hoe J, Lardo AC, Bush DE, de Roos A, Cox C, Brinker J, Lima JA. Diagnostic performance of coronary angiography by 64-row ct. *N Engl J Med*. 2008;359:2324-2336
5. Meijboom WB, Van Mieghem CA, van Pelt N, Weustink A, Pugliese F, Mollet NR, Boersma E, Regar E, van Geuns RJ, de Jaegere PJ, Serruys PW, Krestin GP, de Feyter PJ. Comprehensive assessment of coronary artery stenoses: Computed tomography coronary angiography versus conventional coronary angiography and correlation with fractional flow reserve in patients with stable angina. *J Am Coll Cardiol*. 2008;52:636-643
6. Wijns W, Kolh P, Danchin N, Di Mario C, Falk V, Folliguet T, Garg S, Huber K, James S, Knuuti J, Lopez-Sendon J, Marco J, Menicanti L, Ostojic M, Piepoli MF, Pirlet C, Pomar JL, Reifart N, Ribichini FL, Schalij MJ, Sergeant P, Serruys PW, Silber S, Sousa Uva M, Taggart D. Guidelines on myocardial revascularization. *Eur Heart J*. 2010;31:2501-2555
7. Takagi A, Tsurumi Y, Ishii Y, Suzuki K, Kawana M, Kasanuki H. Clinical potential of intravascular ultrasound for physiological assessment of coronary stenosis: Relationship between quantitative ultrasound tomography and pressure-derived fractional flow reserve. *Circulation*. 1999;100:250-255
8. Koo BK, Yang HM, Doh JH, Choe H, Lee SY, Yoon CH, Cho YK, Nam CW, Hur SH, Lim HS, Yoon MH, Park KW, Na SH, Youn TJ, Chung WY, Ma S, Park SK, Kim HS, Tahk SJ. Optimal intravascular ultrasound criteria and their accuracy for defining the functional significance of intermediate coronary stenoses of different locations. *JACC Cardiovasc Interv*. 2011;4:803-811
9. Kristensen TS, Engstrom T, Kelbaek H, von der Recke P, Nielsen MB, Kofoed KF. Correlation between coronary computed tomographic angiography and fractional flow reserve. *Int J Cardiol*. 2010;144:200-205
10. Bamberg F, Becker A, Schwarz F, Marcus RP, Greif M, von Ziegler F, Blankstein R, Hoffmann U, Sommer WH, Hoffmann VS, Johnson TR, Becker HC, Wintersperger BJ, Reiser MF, Nikolaou K. Detection of hemodynamically significant coronary artery stenosis: Incremental diagnostic value of dynamic ct-based myocardial perfusion imaging. *Radiology*. 2011;260:689-698

11. Blankstein R, Shturman LD, Rogers IS, Rocha-Filho JA, Okada DR, Sarwar A, Soni AV, Bezerra H, Ghoshhajra BB, Petranovic M, Loureiro R, Feuchtner G, Gewirtz H, Hoffmann U, Mamuya WS, Brady TJ, Cury RC. Adenosine-induced stress myocardial perfusion imaging using dual-source cardiac computed tomography. *J Am Coll Cardiol*. 2009;54:1072-1084

12. Ward C. Clinical significance of the bicuspid aortic valve. *Heart*. 2000;83:81-85

13. Roberts WC, Ko JM. Frequency by decades of unicuspid, bicuspid, and tricuspid aortic valves in adults having isolated aortic valve replacement for aortic stenosis, with or without associated aortic regurgitation. *Circulation*. 2005;111:920-925

14. Nkomo VT, Enriquez-Sarano M, Ammash NM, Melton LJ, 3rd, Bailey KR, Desjardins V, Horn RA, Tajik AJ. Bicuspid aortic valve associated with aortic dilatation: A community-based study. *Arterioscler Thromb Vasc Biol*. 2003;23:351-356

15. Robicsek F, Thubrikar MJ, Cook JW, Fowler B. The congenitally bicuspid aortic valve: How does it function? Why does it fail? *Ann Thorac Surg*. 2004;77:177-185

16. Ferencik M, Pape LA. Changes in size of ascending aorta and aortic valve function with time in patients with congenitally bicuspid aortic valves. *Am J Cardiol*. 2003;92:43-46

17. Keane MG, Wiegers SE, Plappert T, Pochettino A, Bavaria JE, Sutton MG. Bicuspid aortic valves are associated with aortic dilatation out of proportion to coexistent valvular lesions. *Circulation*. 2000;102:III35-39

18. McKusick VA. Association of congenital bicuspid aortic valve and erdheim's cystic medial necrosis. *Lancet*. 1972;1:1026-1027

19. Niwa K, Perloff JK, Bhuta SM, Laks H, Drinkwater DC, Child JS, Miner PD. Structural abnormalities of great arterial walls in congenital heart disease: Light and electron microscopic analyses. *Circulation*. 2001;103:393-400

20. de Sa M, Moshkovitz Y, Butany J, David TE. Histologic abnormalities of the ascending aorta and pulmonary trunk in patients with bicuspid aortic valve disease: Clinical relevance to the ross procedure. *J Thorac Cardiovasc Surg*. 1999;118:588-594

21. Cripe L, Andelfinger G, Martin LJ, Shooner K, Benson DW. Bicuspid aortic valve is heritable. *J Am Coll Cardiol*. 2004;44:138-143

22. Hiratzka LF, Bakris GL, Beckman JA, Bersin RM, Carr VF, Casey DE, Jr., Eagle KA, Hermann LK, Isselbacher EM, Kazerooni EA, Kouchoukos NT, Lytle BW, Milewicz DM, Reich DL, Sen S, Shinn JA, Svensson LG, Williams DM. 2010 accf/aha/aats/acr/asa/sca/scai/sir/sts/svm guidelines for the diagnosis and management of patients with thoracic aortic disease. A report of the american college of cardiology foundation/american heart association task force on practice guidelines, american association for thoracic surgery, american college of radiology,american stroke association, society of cardiovascular anesthesiologists, society for cardiovascular angiography and interventions, society of interventional radiology, society of thoracic surgeons,and society for vascular medicine. *J Am Coll Cardiol*. 2010;55:e27-e129

23. Leon MB, Smith CR, Mack M, Miller DC, Moses JW, Svensson LG, Tuzcu EM, Webb JG, Fontana GP, Makkar RR, Brown DL, Block PC, Guyton RA, Pichard AD, Bavaria JE, Herrmann HC, Douglas PS, Petersen JL, Akin JJ, Anderson WN, Wang D, Pocock S. Transcatheter aortic-valve implantation for aortic stenosis in patients who cannot undergo surgery. *N Engl J Med*. 2010;363:1597-1607

24. Rosenhek R, Binder T, Porenta G, Lang I, Christ G, Schemper M, Maurer G, Baumgartner H. Predictors of outcome in severe, asymptomatic aortic stenosis. *N Engl J Med*. 2000;343:611-617

25. Detaint D, Lepage L, Himbert D, Brochet E, Messika-Zeitoun D, Iung B, Vahanian A. Determinants of significant paravalvular regurgitation after transcatheter aortic valve: Implantation impact of device and annulus discongruence. *JACC Cardiovasc Interv*. 2009;2:821-827

26. Drenthen W, Pieper PG, Roos-Hesselink JW, van Lottum WA, Voors AA, Mulder BJ, van Dijk AP, Vliegen HW, Yap SC, Moons P, Ebels T, van Veldhuisen DJ. Outcome of pregnancy in women with congenital heart disease: A literature review. *J Am Coll Cardiol*. 2007;49:2303-2311

27. Karamermer Y, Roos-Hesselink JW. Pregnancy and adult congenital heart disease. *Expert Rev Cardiovasc Ther*. 2007;5:859-869

28. Kilner PJ, Geva T, Kaemmerer H, Trindade PT, Schwitter J, Webb GD. Recommendations for cardiovascular magnetic resonance in adults with congenital heart disease from the respective working groups of the european society of cardiology. *Eur Heart J*. 2010;31:794-805

29. Kanal E, Barkovich AJ, Bell C, Borgstede JP, Bradley WG, Jr., Froelich JW, Gilk T, Gimbel JR, Gosbee J, Kuhni-Kaminski E, Lester JW, Jr., Nyenhuis J, Parag Y, Schaefer DJ, Sebek-Scoumis EA, Weinreb J, Zaremba LA, Wilcox P, Lucey L, Sass N. Acr guidance document for safe mr practices: 2007. *AJR Am J Roentgenol*. 2007;188:1447-1474

30. Uebing A, Arvanitis P, Li W, Diller GP, Babu-Narayan SV, Okonko D, Koltsida E, Papadopoulos M, Johnson MR, Lupton MG, Yentis SM, Steer PJ, Gatzoulis MA. Effect of pregnancy on clinical status and ventricular function in women with heart disease. *Int J Cardiol*. 2010;139:50-59

PART 1: ISCHEMIC HEART DISEASE

CHAPTER 2

CORONARY CT ANGIOGRAPHY FOR PATIENTS WITH SUSPECTED CORONARY ARTERY DISEASE

2013 Accepted for publication in Heart

A Rossi
AS Dharampal
PJ de Feyter

INTRODUCTION

Since the introduction of coronary computer tomography angiography (CCTA) there has been an enormous growth in the quantity of evidence to support the role of CCTA in the diagnosis of patients with suspected coronary artery disease (CAD). Yet, the question remains: at what level of diagnostic accuracy efficacy is CCTA today? Have we attained sufficient reliable evidence to fully appreciate the role of CCTA in cardiologic practice?

HIERARCHICAL MODEL OF DIAGNOSTIC EFFICACY

The technical details and potential clinical applications of CCTA have been reported in 2 recent reviews in "Education in Heart" [1,2]. In this current state-of-the-art exposition of CCTA for patients with suspected CAD it appears useful to arrange the available evidence according to a hierarchical model of efficacy of diagnostic imaging first described by Fryback and Thornburg in 1991 [3]. Efficacy is defined as:" the probability of benefit to individuals in a defined population from medical technology (CCTA) applied for a given medical problem under ideal conditions" [3].

The model consists of 6 levels of efficacy: *level 1* - technical efficacy, *level 2*-diagnostic accuracy efficacy, *level 3*- diagnostic thinking accuracy, *level 4*- therapeutic efficacy, *level 5*- patient outcome efficacy, *level 6*- societal efficacy. The goal of the model not only involves the traditional view of the assessment of diagnostic imaging to generate optimal quality images and hence optimal diagnosis, but rather is a comprehensive assessment of patient and societal benefit of CCTA [3].

This review is an update of the current position of CCTA in the diagnosis of patients with suspected CAD.

TECHNICAL EFFICACY

The spatial resolution of 64 - or more slices CCTA in the laboratory setting is 0.3-0.4 mm^3 (isotropic spatial resolution allowing undistorted reconstruction of images in any plane), but in the clinical setting this is 0.5 mm^3 to 0.6 mm^3. The spatial resolution of CCTA is still limited compared to the 0.1 to 0.2 mm of invasive coronary angiography (ICA). The temporal resolution (time required for the acquisition of data necessary for the generation of one slice) of CCTA depends mainly on the gantry rotation time which with current scanners ranges between 280 ms to 420 ms per rotation, resulting in a temporal resolution of maximally 75 ms (i.e ¼ the rotation time in case of a dual source CT scanner) to 210 ms (i.e. ½ the rotation time in single source scanner). Although this is acceptable for CCTA imaging, it falls short of

the 4 ms to 8 ms of ICA. Low heart rates less than 60 to 65 beats/minute (bpm) are required to generate nearly motion free coronary images. The scan time (time required for data acquisition of the entire coronary tree) ranges between 6 s to 8 s for 64-slice CT scanners, but is dramatically reduced with the use of 256 to 320-slice CT scanners that allow coverage of the entire heart in one single rotation with data acquisition during one heart beat. These fast scanners have reduced CT susceptibility to the occurrence of arrhythmias.

The radiation dose of earlier type of CCTA scanners was worrisome (with effective dose of 15 mSv to 20 mSv), but newly introduced technically CT improvements together with radiation dose reduction protocols, including prospective ECG triggered ("step-and-shoot") scanning, low tube potential (100 kVp instead of 120 kVp) in patients less than 90 kg have now reduced the effective dose to 3.5 ± 2.1 mSv, with preservation of diagnostic image quality and no increase in downstream testing due to poor image quality [4-6]. In a preliminary report a prospectively ECG triggered high pitch helical acquisition protocol enabling coverage of the heart in one heart beat combined with low tube voltage (80 kVp) and currents (50 mAs) and iterative reconstruction further reduced the radiation dose to less than 1 mSv[7]. These results require confirmation by other large sized studies in various patient populations.

DIAGNOSTIC ACCURACY EFFICIENCY

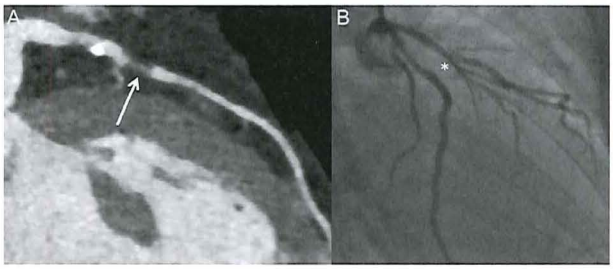

Figure 1. CCTA in the detection of coronary artery disease.
CCTA was performed in a 59-year-old man with atypical chest pain, positive family history for coronary artery disease, hypercholesterolemia and inconclusive stress test. Curved multiplanar reconstruction of the left anterior descending coronary artery, LAD, (A) shows a severe coronary lesion due to a non-calcified atherosclerotic plaque in the proximal part of the vessel (arrow). Invasive coronary angiography (B) confirms the obstructive coronary lesion in the LAD (star).

Numerous single centre and multicentre studies attest to high diagnostic accuracy of CCTA (Figure 1) and highlight the ability of CCTA to exclude the presence of obstructive CAD (≥50% diameter stenosis) in patients with suspected CAD (Figure 2). A recent pooled analysis of 3674 patients, examined between December 2006 and March 2009, showed the diagnostic performance of 64- or more slice CCTA with high patient sensitivity and specificity of 98% and 82% respectively [8] (Table 1) with ICA as standard of reference. The per-segment calculated sensitivity was lower, but the specificity was higher with 91% and 94% respectively. The three reported per vessel analysis outcomes were in between those of patient- and segment analysis (Table 1).

Table 1

Diagnostic performance of 64-or more slice CCTA.
Systematic review including 18 studies and 3674 patients [8]

ANALYSIS	SENSITIVITY,% (95% CI)	SPECIFICITY, % (95% CI)	PPV, % (95% CI)	NPV, % (95% CI)
PATIENT	98 (97-99)	82 (79-84)	91 (76-100)	99 (83-100)
VESSEL	95 (94-96)	90 (89-90)	75 (53-95)	99 (93-100)
SEGMENT	91 (90-92)	94 (94-95)	69 (44-86)	99 (98-100)

PPV = positive predictive value; NPV = negative predictive value

The multicenter trials had a sensitivity and specificity ranging from 85% to 99% and 64% to 90% respectively (Table 2) [9-11].

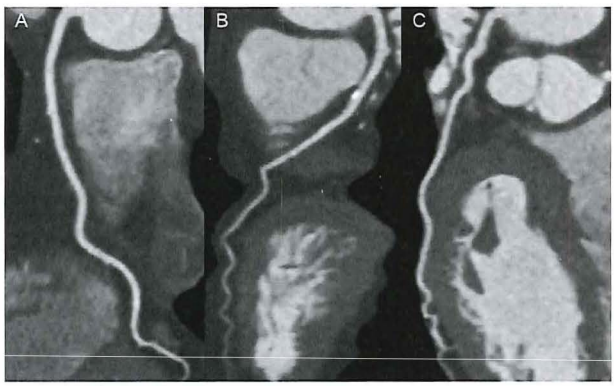

Figure 2. CCTA for ruling out coronary artery disease.
CCTA was performed in a 45-year-old woman with atypical chest pain, hypertension and inconclusive stress test. Curved multiplanar reconstructions of right coronary artery (A), left anterior descending coronary artery (B) and left circumflex coronary artery (C) show non-obstructive coronary artery disease.

Von Balmoos et al. reported the diagnostic accuracy of CCTA which was achieved with low dose radiation by using a "step-and shoot" protocol. The sensitivities and specificities of per patient, per vessel or per segment analysis, remained high with an average estimated effec-

Table 2

Patient diagnostic performance 64-slice CCTA: multicenter studies.

STUDY	N	CAD, %	SENSITIVITY,%	SPECIFICITY, %	PPV, %	NPV, %
ACCURACY [9]	230	25	95	83	64	99
CORE [10]	291	56	85	90	91	83
MEIJBOOM [11]	360	68	99	64	86	97

PPV = positive predictive number; NPV = negative predictive number

tive radiation dose of 2.7 mSv (95%CI: 2.2 mSv - 3.2 mSv) (Table 3)[12]. However this was achieved with non-diagnostic image quality that occurred in 2.4% of the coronary segments.

Table 3

Diagnostic performance of low dose CCTA (2.7 mSv; 95% CI 2.2-3.2).
Systematic review: 16 studies comprising 960 patients [12].

ANALYSIS	N	POOLED SENSITIVITY, % (95% CI)	POOLED SPECIFICITY, % (95% CI)	TP	TN	FP	FN
PATIENT	789	100 (98-100)	89 (85-92)	455	296	36	2
VESSEL	2622	97 (95-98)	93 (89-96)	839	1625	129	28
SEGMENT	11518	91 (86-95)	96 (94-97)	1429	9528	415	146

TP = true positive; FP = false positive; FN = false negative; TN = true negative

A serious limitation of all these studies was the retrospective nature of the study design and they all suffered from the inevitable referral bias because these patients were referred for ICA.

An additional significant problem, seriously limiting the clinical value of a positive CT outcome is that CCTA identified coronary obstructions (≥50% diameter stenosis) but it cannot reliably predict the presence of myocardial ischemia (Table 4)[13-16]. The limited positive predictive value of CCTA to detect myocardial ischemia is usually caused by overestimation of calcified lesions due to blooming artefacts or motion artefacts (Figure 3).

Table 4

Relation 64 slice CCTA (< 50% or >50%) and functional testing.

AUTHOR	TEST	N	AGREEMENT, % <50%/ TEST	AGREEMENT, % ≥50%/ TEST
SCHUIJF [13]	SPECT	114	77	50
GAEMPERLI [14]	SPECT	78	97	59
GROOTHUIS [15]	MRP	145	88	58
MEIJBOOM [16]	FFR	89*	93	51

* *number if coronary stenoses*

The prognostic accuracy of CCTA in combination with the diagnostic accuracy efficacy is important for diagnostic and therapeutic patient management. A recently published systematic review evaluating 9592 patients with a median follow-up of 1.7 years revealed that a normal CCTA was associated with an excellent prognosis and that an increasing burden of non-

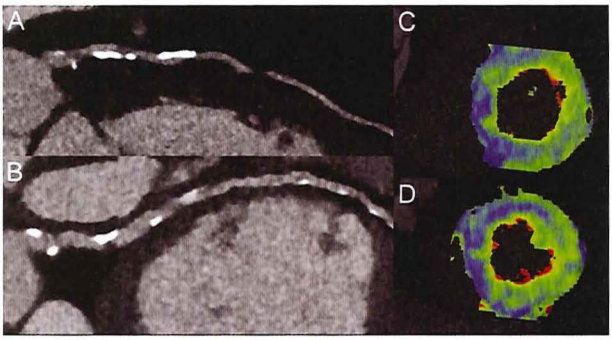

Figure 3. 70-year-old man with hypertension and progressive dyspnea. Calcium score was 1580 Agatston. CCTA demonstrates diffuse atherosclerotic disease in the left anterior descending, LAD, (A) coronary artery and in the left circumflex, LCX (B) coronary artery. A stack artefact is visible in the mid-distal LAD coronary artery. Short-axis color-coded dynamic CT perfusion images acquired during the infusion of adenosine show a diffused reduced myocardial perfusion in the anterior, septal and inferior myocardial wall (blue areas) in a left dominant coronary system. Both LAD and LCX lesions were determined to be hemodynamically significant at fractional flow reserve measurements.

obstructive or obstructive CAD was associated with increasing rate of major adverse cardiovascular events (Table 5) [17]. The prognostic accuracy was reported from a prospective multicenter study, CONFIRM, including 23,854 symptomatic patients who underwent ≥ 64-slice CCTA and were followed for 2.3 ± 1.1 years during which period 404 all-cause deaths occurred [18]. The risk adjusted per patient analysis revealed that patients with non-obstructive CAD (<50% stenosis) or obstructive CAD (≥ 50% stenosis) had a risk adjusted hazard ratio of 1.6 (95%CI 1.2 to 2.2) and 2.6 (95%CI 1.9 to 3.5) respectively with normal CCTA as the reference. Similar outcomes were observed if patients were classified into normal, non-obstructive CAD, 1-vessel disease (VD), 2-VD or 3-VD with higher mortality with increasing disease burden. Absence of CAD was associated with a favourable prognosis with an annualized all-cause death rate of 0.28%. These prognostic studies

Table 5

CCTA prognosis in symptomatic patients.

Annualized event rate per 100 patients per year from 18 studies comprising 9,592 patients. Median follow-up : 20 months [17].

CCTA	MACE, %	ALL-CAUSE DEATH, %	MI, %	REVASCULARIZATION,%
NO CAD	0.2	0.2	0	0
CAD <50%	1.42	0.7	0.3	1.3
CAD >50%	8.8	2.2	2.1	24.8

have some limitations. The total all-cause mortality, although important, is not a CAD specific endpoint (like cardiac death or MI) and the revascularization rate is biased by the index CCTA because treating physicians were not blinded and anatomic CT abnormalities may easily have led to referral for ICA and subsequent revascularization. In addition there was no adjustment for other confounding co-variables such as medication or left ventricular ejection fraction.

DIAGNOSTIC THINKING EFFICACY

A relevant question for the clinician is: in which patient population does CCTA achieve the greatest diagnostic benefit or where is virtually no benefit to be expected? According to Bayesian theorem patients with intermediate pre-test probability of CAD will gain most benefit from CCTA [19]. The accuracy of a negative CCTA scan to rule out CAD is high in patients with intermediate pre-test probability of CAD and this obviates the need for further downstream diagnostic testing (Figure 4). Unfortunately, a positive CCTA is associated with a relatively insufficient increase in post-test probability of CAD in particular in the per-vessel and per-segment analysis (Table 1). This results in a high number of false positive outcomes and unnecessary number of referrals to ICA.

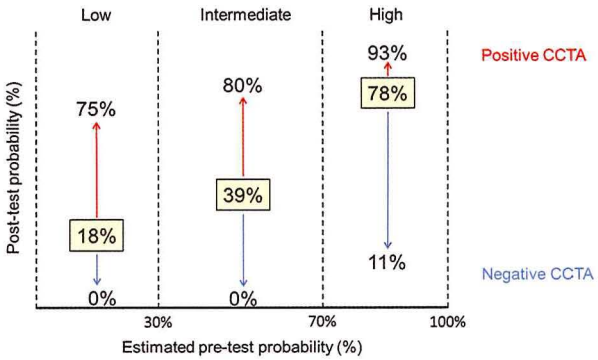

Figure 4. Influence of pre-test probability of CAD on post-test probability after CCTA.

Bayesian theory: the diagnostic performance of CCTA in patients at low, intermediate and high pre-test probability of CAD by Meijboom et al.[19].

A low pre-test probability favoured high negative predictive value (NPV) at cost of positive predictive value (PPV) (high false positive rate). A high pre-test probability favoured high PPV at cost of NPV (high false negative rate). An intermediate pre-test probability favoured high NPV but only moderate PPV.

CCTA is not useful in patients with high pre-test probability of CAD as a negative CCTA is associated with a relatively high number of false negative outcomes requiring further downstream testing to avoid "missing" patients with significant CAD. A positive CT scan provides only limited increase of the post-test probability of CAD and direct referral to ICA is preferred. In addition the CCTA diagnostic accuracy in patients with high pre-test probability is lower due to the higher prevalence of coronary calcifications or diffuse CAD which render precise assessment of obstructions more difficult.

Patients with low pre-test probability of CAD may not benefit from CCTA either. A negative scan does not significantly decrease the post-test probability in these patients as this was already low and a positive scan is associated with a considerable number of false positive outcomes leading to over-diagnosis and unnecessary referral to ICA .

THERAPEUTIC EFFICACY

Here a relevant question would be: does CCTA change patient management? This depends on the diagnostic and prognostic accuracy of CCTA to determine further need of testing.

In patients with intermediate pre-test probability CCTA results in reclassification to either low post-test (in case of negative CCTA which is associated with an excellent prognosis) or high post-test (in case of positive CCTA and associated with high adverse event rate) probability groups that would be associated with a clinically relevant change of diagnostic and therapeutic management. Patients with low post-test probability do not require further testing and may be safely discharged. In contrast patients with high post-test probability may be directly referred for ICA with or without fractional flow reserve (FFR). Obviously this is related to the achieved post-test probability level and the associated diagnostic certainty of a negative CT scan to exclude CAD or a positive CT scan to rule in CAD. The level of diagnostic certainty is arbitrary and depends on whether additional testing is deemed necessary that may improve patient management and prognosis. In general one may assume that a post-test probability of <5% or >90% indicates sufficient diagnostic certainty and no further testing is helpful. Further testing is indicated if the post-test probability is between 5% and 90%.

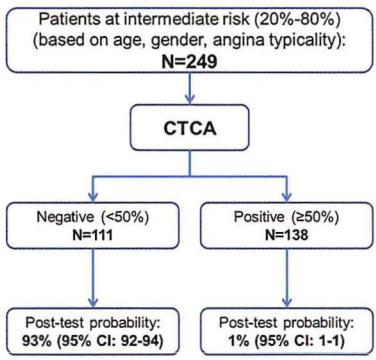

Figure 5. Therapeutic efficacy CCTA.
Data from a recent study of 249 patients with intermediate pre-test probability of CAD (prevalence of CAD by ICA of 53%) [20]. A negative CCTA virtually ruled out the presence of CAD while a positive CCTA achieved a high probability of CAD and patients required referral to ICA.

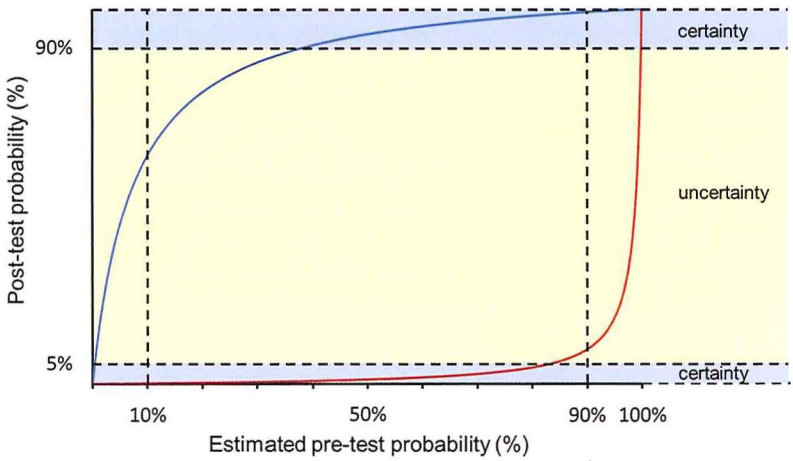

In a recent study of 249 patients with intermediate pre-test probability a negative CCTA virtually ruled out the presence of CAD [20] (Figure 5). These patients have an excellent prognosis and can be safely discharged [17, 18]. In contrast patients with a positive CCTA achieved a high probability of CAD and these patients required referral to ICA and in case of multivessel CAD invasive FFR to consider revascularization to relief symptoms and improve prognosis (Figure 5).

The post-test probability is related to the estimated pre-test probability and the sensitivity and specificity of the test [21].

The diagnostic performance of SPECT, MRI and CCTA in patients with intermediate pre-test probability is shown in Figure 6. Sensitivities and specificities were obtained from a recent extensive review [22]. The positive predictive value of CCTA was highest, but most important was the very high negative predictive value of CCTA that outperformed the negative predictive value of the two other non-invasive tests. This supports the use of CCTA as a first line

Figure 6. Revised probability of CAD.

Revised probability of CAD. This figure shows the revised (post-test) probability of CAD (y-axis) as a function of prior (pre-test) probability (x-axis) of CAD for positive and negative SPECT, MR-perfusion and CCTA results based on the data presented in 8, 22. SPECT+, MRI+ and CCTA+ represent the solid lines for a positive test result and SPECT-, MRI- and CCTA- represent the dashed lines for a negative test result.

	SENSITIVITY (%)	SPECIFICITY (%)
SPECT 22	88	61
MR-PERFUSION 22	89	76
CCTA 8	98	82

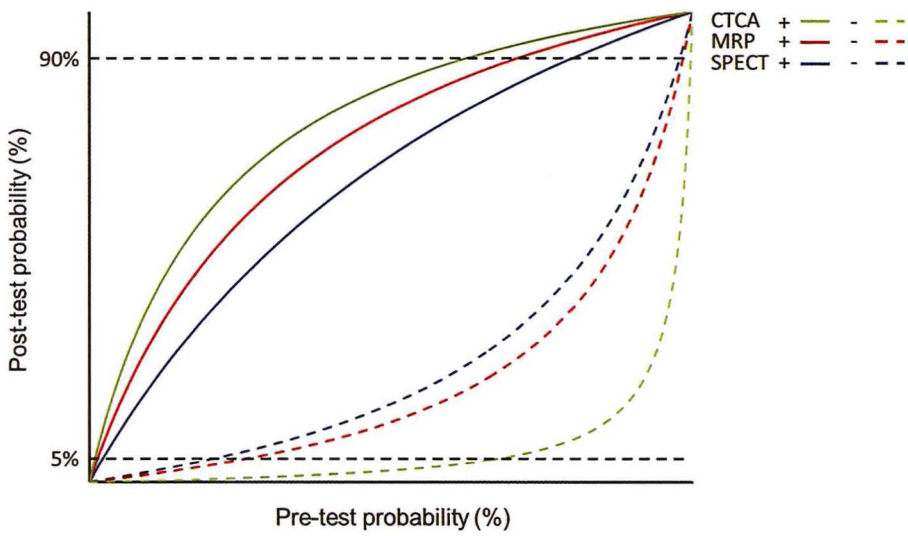

diagnostic test to act as gatekeeper of ICA because a negative CCTA scan virtually rules out the presence of significant CAD.

It seems reasonable to expect that the outcome of non-invasive diagnostic imaging tests would exert a significant impact on referral to ICA or change in medical treatment. Yet, this was disappointing. The SPARC study that evaluated the impact of SPECT, PET and CCTA on management of patients with suspected CAD demonstrated that there was only a modest impact. CCTA was associated with a relatively higher referral to ICA than SPECT and PET [23].

PATIENT OUTCOME EFFICACY AND SOCIETAL EFFICACY

Today no (comparative) effectiveness studies are available that evaluate the benefits and harms of CCTA in terms of improved clinical outcomes or cost effectiveness at the societal level to asses the role of CCTA as an alternative to other non-invasive diagnostic imaging strategies in patients with suspected CAD.

The importance of comparative effectiveness studies is well recognized and is now considered a prerequisite to judge the definitive role of CCTA in the diagnosis and management of symptomatic coronary patients [24].

We have to await the finalisation of the ongoing PROMISE (Prospective Multicenter Imaging for Evaluation of Chest Pain) study which is randomizing symptomatic patients suspected of having CAD to either a usual stress testing (functional) strategy or a CCTA strategy (anatomy) with clinical outcomes and costs as endpoints.

NEW CT DEVELOPMENTS: CT FUNCTIONAL IMAGING

The physiological significance of a coronary obstruction is dependent on both the vessel wall morphology (anatomy) and coronary blood flow. The combined information of the presence of a coronary obstruction (local or diffuse) and coronary blood flow limitation is crucial for optimal decision-making for patients with chest pain.

One of the main shortcomings of CCTA is the fact that CCTA cannot adequately predict the functional significance of a coronary obstruction (≥50% diameter stenosis) (Table 4). This has prompted the search for a single CT examination combining CT functional imaging with CT coronary anatomical imaging. Several CT functional imaging approaches are now being

investigated including CT-FFR, CT myocardial perfusion and CT intracoronary attenuation gradient assessment.

However, the primary endpoint of the study, the per-patient diagnostic accuracy of CT-FFR plus CTCA, was not achieved. CT- FFR is a promising technique that recently is introduced in clinical practice. The technique uses computational fluid dynamics (CFD) with simulated hyperemia that enables prediction of blood flow and pressure fields in coronary arteries. This then allows calculation of the fractional flow reserve of a coronary stenosis from data derived from a usual single CCTA. A multicenter prospective study demonstrated that CT-FFR correlated reasonably well with the standard of reference invasive FFR [25]. CT-FFR drawbacks currently are the extreme need for computational ability and analysis time and the need for high quality CT images. Other studies are needed to confirm the robustness and reliability of the technique.

CT myocardial perfusion can be evaluated by assessing the myocardial contrast enhancement at rest or during pharmacological stress to analyze the impact of a coronary obstruction on myocardial blood flow [26]. The method is technically demanding but dynamic CT perfusion is able to provide absolute measurement of the myocardial blood flow thereby allowing functional assessment of individual coronary artery territories (Figure 3). The initial results are promising but serious problems that need to be resolved are the additional (unacceptable) high radiation dose and the limited collection of sufficient contrast enhanced samples during the passage of contrast through the myocardium that may cause inexact determination of the myocardial blood flow.

CT measurement of the gradient of intraluminal attenuation along the proximal to distal course of a coronary artery provides information about the coronary blood flow. The difference between the attenuation proximal and distal of an obstruction allows to predict the degree of a coronary stenosis and preliminary results suggested that this method can moderately predict stenosis severity [27, 28]. However the gradient is only measured at rest and it is unknown how the technique would perform under conditions of stress induced hyperemia.

The addition of non-invasive CT functional imaging to CT coronary anatomical imaging is clinically significant as it augments the diagnostic performance and prognostic power which is expected to translate in improved patient management and improved prognosis.

CCTA AREAS OF UNCERTAINTY

CCTA does not only provide information about the coronary arteries but also about heart, great thoracic vessels, portions of the lungs, mediastinum, chest wall, spine and upper abdomen. This will inevitably result in the detection of incidental findings that may require adequate interpretation and subsequent management that may cause unforeseen complex

medico-legal consequences. A multidisciplinary cardiologic and radiologic approach is recommended to face these problems.

The life time attributable risk of cancer associated with ionizing radiation from CCTA scanning may lead to adverse events that should be taken into account when comparing the effectiveness of CCTA with other non-radiation diagnostic modalities.

The assessment of the severity of a coronary obstruction is expected to be more precise using CT imaging compared to 2-D ICA imaging, in particular with complex, asymmetrical, irregular lesions. However there is concern about the grading of the severity of CT coronary obstructions by visual assessment. Quantitative CCTA, using automated border lumen detection algorithms have shown that these measurements were more precise than visual assessment. But compared to IVUS there was still overestimation (minimum lumen area and diameter stenosis) and underestimation (minimal lumen area and area stenosis) [29, 30]. It remains to be seen that quantitative CCTA better predicts hemodynamic consequences of coronary obstructions than visual assessment.

Another area of debate is whether usual functional testing should be the first–line diagnostic test (now endorsed by European Guidelines) or may CCTA, with its established higher diagnostic accuracy to exclude the presence of significant stenosis, be an effective alternative anatomic test. More scientific clinical evidence is needed to settle this important issue.

CCTA PERSPECTIVE

CCTA has matured, due to the ever increasing enhancement in temporal and spatial resolution in recent years, as a robust non-invasive imaging technique. Yet, it should not be regarded as a replacement of ICA that still is the anatomic "standard of reference" for the assessment of coronary revascularization.

The high negative predictive value of CCTA effectively identifies patients without significant CAD. This supports the use of CCTA as a viable alternative to established functional tests to act as an effective gatekeeper for ICA (Figure 7).

The high sensitivity of CCTA indicates that CCTA can identify the majority of patients with significant CAD, but at the cost of a rather high false positive rate due to overestimation of the severity of stenoses. This is further complicated by the fact that CCTA cannot reliably predict which identified obstruction is haemodynamically significant. Current paradigm dictates that therapeutic interventions should only be applied to stenoses that are coronary flow-limiting. Further non-invasive functional testing is recommended in CT- anatomic non-high risk patients (single or double vessel disease), which in case of ischemia may be referred for revascularization. CT- anatomic high-risk patients (left main, left anterior descending coronary

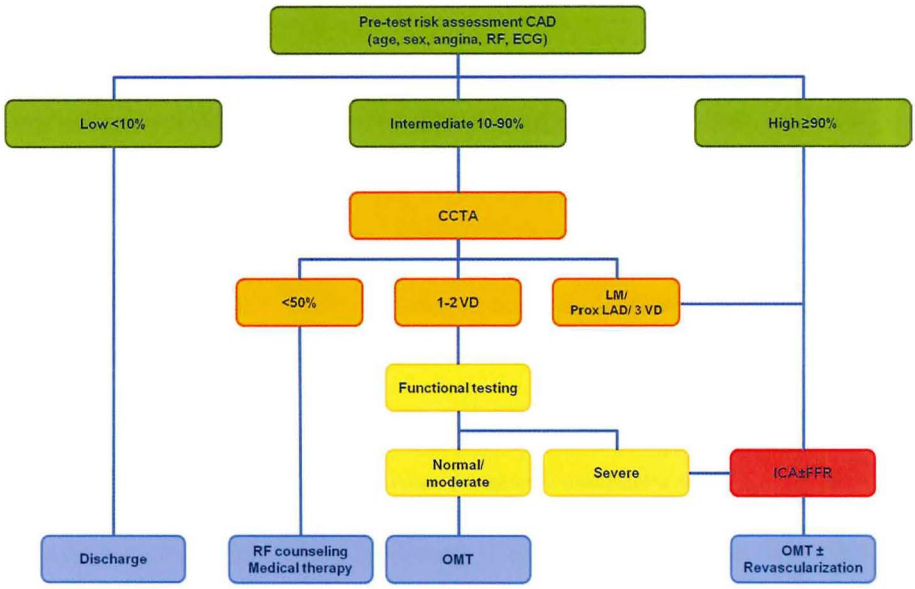

Figure 7. Diagnostic algorithm for patients with stable angina.
CAD: coronary artery disease; RF: risk factors: CCTA: coronary CT angiography; VD: vessel disease; LM: left main; LAD: left anterior descending coronary artery; ICA: invasive coronary angiography; FFR: fractional flow reserve; OMT: optimal medical therapy

artery, three-vessel disease) may be directly referred to ICA with FFR to guide functional lesion revascularization.

Preliminary studies have shown that the combination of CT-anatomy and CT- function in one examination is feasible, but establishment of the reliable robustness of the combined technique needs further clinical testing.

Further directions of CCTA should focus on the continued improvement of spatial and temporal resolution, the development of approaches that minimise calcification blooming effects and reduce radiation exposure with preservation of diagnostic image quality and advancement of CT techniques that increase the reliability of the application of a single protocol for CT-anatomic and CT-functional CAD assessment.

Formal guidelines for the use of CCTA do not exist. Before acceptance of CCTA as an inferior, similar or superior imaging technique compared to established non-invasive functional tests we need evidence from comparative effectiveness research with patient outcome and costs as endpoints.

REFERENCES

1. Achenbach S, Daniel WG. Cardiac imaging in the patient with chest pain: Coronary ct angiography. *Heart*. 2010;96:1241-1246
2. Schuijf JD, Achenbach S, de Feyter PJ, Bax JJ. Current applications and limitations of coronary computed tomography angiography in stable coronary artery disease. *Heart*. 2011;97:330-337
3. Fryback DG, Thornbury JR. The efficacy of diagnostic imaging. *Med Decis Making*. 1991;11:88-94
4. Hausleiter J, Meyer T, Hermann F, Hadamitzky M, Krebs M, Gerber TC, McCollough C, Martinoff S, Kastrati A, Schomig A, Achenbach S. Estimated radiation dose associated with cardiac ct angiography. *JAMA*. 2009;301:500-507
5. Hausleiter J, Meyer TS, Martuscelli E, Spagnolo P, Yamamoto H, Carrascosa P, Anger T, Lehmkuhl L, Alkadhi H, Martinoff S, Hadamitzky M, Hein F, Bischoff B, Kuse M, Schomig A, Achenbach S. Image quality and radiation exposure with prospectively ecg-triggered axial scanning for coronary ct angiography: The multicenter, multivendor, randomized protection-iii study. *JACC Cardiovasc Imaging*. 2012;5:484-493
6. Raff GL, Chinnaiyan KM, Share DA, Goraya TY, Kazerooni EA, Moscucci M, Gentry RE, Abidov A. Radiation dose from cardiac computed tomography before and after implementation of radiation dose-reduction techniques. *JAMA*. 2009;301:2340-2348
7. Schuhbaeck A, Achenbach S, Layritz C, Eisentopf J, Hecker F, Pflederer T, Gauss S, Rixe J, Kalender W, Daniel WG, Lell M, Ropers D. Image quality of ultra-low radiation exposure coronary ct angiography with an effective dose <0.1 msv using high-pitch spiral acquisition and raw data-based iterative reconstruction. *Eur Radiol*. 2012
8. Paech DC, Weston AR. A systematic review of the clinical effectiveness of 64-slice or higher computed tomography angiography as an alternative to invasive coronary angiography in the investigation of suspected coronary artery disease. *BMC Cardiovasc Disord*. 2011;11:32
9. Budoff MJ, Dowe D, Jollis JG, Gitter M, Sutherland J, Halamert E, Scherer M, Bellinger R, Martin A, Benton R, Delago A, Min JK. Diagnostic performance of 64-multidetector row coronary computed tomographic angiography for evaluation of coronary artery stenosis in individuals without known coronary artery disease: Results from the prospective multicenter accuracy (assessment by coronary computed tomographic angiography of individuals undergoing invasive coronary angiography) trial. *J Am Coll Cardiol*. 2008;52:1724-1732
10. Miller JM, Rochitte CE, Dewey M, Arbab-Zadeh A, Niinuma H, Gottlieb I, Paul N, Clouse ME, Shapiro EP, Hoe J, Lardo AC, Bush DE, de Roos A, Cox C, Brinker J, Lima JA. Diagnostic performance of coronary angiography by 64-row ct. *N Engl J Med*. 2008;359:2324-2336
11. Meijboom WB, Meijs MF, Schuijf JD, Cramer MJ, Mollet NR, van Mieghem CA, Nieman K, van Werkhoven JM, Pundziute G, Weustink AC, de Vos AM, Pugliese F, Rensing B, Jukema JW, Bax JJ, Prokop M, Doevendans PA, Hunink MG, Krestin GP, de Feyter PJ. Diagnostic accuracy of 64-slice computed tomography coronary angiography: A prospective, multicenter, multivendor study. *J Am Coll Cardiol*. 2008;52:2135-2144
12. von Ballmoos MW, Haring B, Juillerat P, Alkadhi H. Meta-analysis: Diagnostic performance of low-radiation-dose coronary computed tomography angiography. *Ann Intern Med*. 2011;154:413-420

13. Schuijf JD, Wijns W, Jukema JW, Atsma DE, de Roos A, Lamb HJ, Stokkel MP, Dibbets-Schneider P, Decramer I, De Bondt P, van der Wall EE, Vanhoenacker PK, Bax JJ. Relationship between noninvasive coronary angiography with multi-slice computed tomography and myocardial perfusion imaging. *J Am Coll Cardiol*. 2006;48:2508-2514
14. Gaemperli O, Schepis T, Valenta I, Koepfli P, Husmann L, Scheffel H, Leschka S, Eberli FR, Luscher TF, Alkadhi H, Kaufmann PA. Functionally relevant coronary artery disease: Comparison of 64-section ct angiography with myocardial perfusion spect. *Radiology*. 2008;248:414-423
15. Groothuis JG, Beek AM, Brinckman SL, Meijerink MR, Koestner SC, Nijveldt R, Gotte MJ, Hofman MB, van Kuijk C, van Rossum AC. Low to intermediate probability of coronary artery disease: Comparison of coronary ct angiography with first-pass mr myocardial perfusion imaging. *Radiology*. 2010;254:384-392
16. Meijboom WB, Van Mieghem CA, van Pelt N, Weustink A, Pugliese F, Mollet NR, Boersma E, Regar E, van Geuns RJ, de Jaegere PJ, Serruys PW, Krestin GP, de Feyter PJ. Comprehensive assessment of coronary artery stenoses: Computed tomography coronary angiography versus conventional coronary angiography and correlation with fractional flow reserve in patients with stable angina. *J Am Coll Cardiol*. 2008;52:636-643
17. Hulten EA, Carbonaro S, Petrillo SP, Mitchell JD, Villines TC. Prognostic value of cardiac computed tomography angiography: A systematic review and meta-analysis. *J Am Coll Cardiol*. 2011;57:1237-1247
18. Min JK, Dunning A, Lin FY, Achenbach S, Al-Mallah M, Budoff MJ, Cademartiri F, Callister TQ, Chang HJ, Cheng V, Chinnaiyan K, Chow BJ, Delago A, Hadamitzky M, Hausleiter J, Kaufmann P, Maffei E, Raff G, Shaw LJ, Villines T, Berman DS. Age- and sex-related differences in all-cause mortality risk based on coronary computed tomography angiography findings results from the international multicenter confirm (coronary ct angiography evaluation for clinical outcomes: An international multicenter registry) of 23,854 patients without known coronary artery disease. *J Am Coll Cardiol*. 2011;58:849-860
19. Meijboom WB, van Mieghem CA, Mollet NR, Pugliese F, Weustink AC, van Pelt N, Cademartiri F, Nieman K, Boersma E, de Jaegere P, Krestin GP, de Feyter PJ. 64-slice computed tomography coronary angiography in patients with high, intermediate, or low pretest probability of significant coronary artery disease. *J Am Coll Cardiol*. 2007;50:1469-1475
20. Weustink AC, Mollet NR, Neefjes LA, Meijboom WB, Galema TW, van Mieghem CA, Kyrzopoulous S, Eu RN, Nieman K, Cademartiri F, van Geuns RJ, Boersma E, Krestin GP, de Feyter PJ. Diagnostic accuracy and clinical utility of noninvasive testing for coronary artery disease. *Ann Intern Med*. 2010;152:630-639
21. Diamond GA, Forrester JS. Posterior probability in clinical trials. *Ann Intern Med*. 1984;100:457
22. Jaarsma C, Leiner T, Bekkers SC, Crijns HJ, Wildberger JE, Nagel E, Nelemans PJ, Schalla S. Diagnostic performance of noninvasive myocardial perfusion imaging using single-photon emission computed tomography, cardiac magnetic resonance, and positron emission tomography imaging for the detection of obstructive coronary artery disease: A meta-analysis. *J Am Coll Cardiol*. 2012;59:1719-1728

23. Hachamovitch R, Nutter B, Hlatky MA, Shaw LJ, Ridner ML, Dorbala S, Beanlands RS, Chow BJ, Branscomb E, Chareonthaitawee P, Weigold WG, Voros S, Abbara S, Yasuda T, Jacobs JE, Lesser J, Berman DS, Thomson LE, Raman S, Heller GV, Schussheim A, Brunken R, Williams KA, Farkas S, Delbeke D, Schoepf UJ, Reichek N, Rabinowitz S, Sigman SR, Patterson R, Corn CR, White R, Kazerooni E, Corbett J, Bokhari S, Machac J, Guarneri E, Borges-Neto S, Millstine JW, Caldwell J, Arrighi J, Hoffmann U, Budoff M, Lima J, Johnson JR, Johnson B, Gaber M, Williams JA, Foster C, Hainer J, Di Carli MF. Patient management after noninvasive cardiac imaging results from sparc (study of myocardial perfusion and coronary anatomy imaging roles in coronary artery disease). *J Am Coll Cardiol*. 2012;59:462-474

24. Hlatky MA, Douglas PS, Cook NL, Wells B, Benjamin EJ, Dickersin K, Goff DC, Hirsch AT, Hylek EM, Peterson ED, Roger VL, Selby JV, Udelson JE, Lauer MS. Future directions for cardiovascular disease comparative effectiveness research: Report of a workshop sponsored by the national heart, lung, and blood institute. *J Am Coll Cardiol*. 2012;60:569-580

25. Min JK, Leipsic J, Pencina MJ, Berman DS, Koo BK, van Mieghem C, Erglis A, Lin FY, Dunning AM, Apruzzese P, Budoff MJ, Cole JH, Jaffer FA, Leon MB, Malpeso J, Mancini GB, Park SJ, Schwartz RS, Shaw LJ, Mauri L. Diagnostic accuracy of fractional flow reserve from anatomic ct angiography. *JAMA*. 2012;308:1237-1245

26. Techasith T, Cury RC. Stress myocardial ct perfusion: An update and future perspective. *JACC Cardiovasc Imaging*. 2011;4:905-916

27. Chow BJ, Kass M, Gagne O, Chen L, Yam Y, Dick A, Wells GA. Can differences in corrected coronary opacification measured with computed tomography predict resting coronary artery flow? *J Am Coll Cardiol*. 2011;57:1280-1288

28. Choi JH, Min JK, Labounty TM, Lin FY, Mendoza DD, Shin DH, Ariaratnam NS, Koduru S, Granada JF, Gerber TC, Oh JK, Gwon HC, Choe YH. Intracoronary transluminal attenuation gradient in coronary ct angiography for determining coronary artery stenosis. *JACC Cardiovasc Imaging*. 2011;4:1149-1157

29. Boogers MJ, Schuijf JD, Kitslaar PH, van Werkhoven JM, de Graaf FR, Boersma E, van Velzen JE, Dijkstra J, Adame IM, Kroft LJ, de Roos A, Schreur JH, Heijenbrok MW, Jukema JW, Reiber JH, Bax JJ. Automated quantification of stenosis severity on 64-slice ct: A comparison with quantitative coronary angiography. *JACC Cardiovasc Imaging*. 2010;3:699-709

30. Voros S, Rinehart S, Qian Z, Joshi P, Vazquez G, Fischer C, Belur P, Hulten E, Villines TC. Coronary atherosclerosis imaging by coronary ct angiography: Current status, correlation with intravascular interrogation and meta-analysis. *JACC Cardiovasc Imaging*. 2011;4:537-548

CHAPTER 3

DIAGNOSTIC ACCURACY OF 128-SLICE DUAL-SOURCE CT CORONARY ANGIOGRAPHY: A RANDOMIZED COMPARISON OF DIFFERENT ACQUISITION PROTOCOLS

European Radiology, 2012; 23(3): 614-622

LA Neefjes
A Rossi
TSS Genders
K Nieman
SL Papadopoulou
AS Dharampal
CJ Schultz
AC Weustink
ML Dijkshoorn
G-JR ten Kate
A Dedic
M van Straten
F Cademartiri
MG Hunink
GP Krestin
PJ de Feyter
NR Mollet

ABSTRACT

Objectives: To compare the diagnostic performance and radiation exposure of 128-slice dual-source CT coronary angiography (CTCA) protocols to detect coronary stenosis with more than 50 % lumen obstruction.

Methods: We prospectively included 459 symptomatic patients referred for CTCA. Patients were randomized between high-pitch spiral vs. narrow-window sequential CTCA protocols (heart rate below 65 bpm, group A), or between wide-window sequential vs. retrospective spiral (heart rate above 65 bpm, group B). Diagnostic performance of CTCA was compared with quantitative coronary angiography in 267 patients.

Results: In group A (231 patients, 146 men, mean heart rate 58±7 bpm), high-pitch spiral CTCA yielded a lower per segment sensitivity compared to sequential CTCA (89 % vs. 97 %, P00.01). Specificity, PPV and NPV were comparable (95 %, 62 %, 99 % vs. 96 %, 73 %, 100 %, P>0.05) but radiation dose was lower (1.16±0.60 vs. 3.82±1.65 mSv, P<0.001). In group B (228 patients, 132 men, mean heart rate 75±11 bpm), per-segment sensitivity, specificity, PPV and NPV were comparable (94 %, 95 %, 67 %, 99 % vs. 92 %, 95 %, 66 %, 99 %, P>0.05). Radiation dose of sequential CTCA was lower compared to retrospective CTCA (6.12±2.58 vs. 8.13±4.52 mSv, P<0.001). Diagnostic performance was comparable in both groups.

Conclusion: Sequential CTCA should be used in patients with regular heart rates using 128-slice dual-source CT, providing optimal diagnostic accuracy with as low as reasonably achievable (ALARA) radiation dose.

INTRODUCTION

CT coronary angiography (CTCA) is currently considered a reliable technique to detect and especially rule out significant stenoses in patients with stable angina with a low or intermediate pre-test probability of having coronary artery disease (CAD) [1-6]. However, its non-invasive nature has been challenged during past years in publications reporting increased lifetime attributable risk estimates of developing cancer associated with high radiation exposure [7,8]. These studies prompted CT vendors to develop hardware and software improvements to reduce radiation exposure, e.g. tube current modulation (ECG-pulsing), automated tube current modulation adapted to the body size, implementation of prospective sequential (step-and-shoot) protocols and lower tube voltages [9-13].

In addition to these radiation-lowering techniques, 128 slice dual-source CT (DSCT) systems offer a high temporal resolution of 75 ms, a pitch up to 3.4 and two wide detector arrays. Hence this DSCT system provides two low dose CTCA protocols: a) a newly introduced prospective high-pitch spiral protocol which allows CT data acquisition of the entire heart within 1 heart beat and b) a prospective sequential protocol for patients with low and high (above 65 bpm) heart rates. However, the diagnostic performance and effect on radiation exposure of these low dose CTCA protocols in patients with various heart rates is currently widely debated [14-17].

The purpose of this study was to determine and compare the diagnostic performance and radiation exposure of different CTCA protocols using 128-slice DSCT to detect or rule out obstructive CAD.

MATERIALS AND METHODS

STUDY POPULATION

The institutional review board approved the study and all patients gave informed consent. Between May 2009 and November 2010, 549 symptomatic patients with stable anginal complaints were referred to CTCA in our institution. Patients with known allergy to iodinated contrast material (n=8), impaired renal function (serum creatinine above 120 μmol/L) (n=18), history of bypass surgery (n=18), persistent arrhythmias (n=17) and patients who refused to give informed consent (n=25) were excluded.

CTCA was carried out as part of the clinical diagnostic work-up of these 463 symptomatic patients suspected of having obstructive CAD. In general, patients with negative CTCA in combination with a negative stress test and/or good response to medical treatment were not referred to conventional coronary angiography (CCA). Exceptions to this rule were made at the discretion of the referring physician (e.g. discordance between symptoms and the results of diagnostic tests). Finally, 267 patients (58 %) underwent CCA within 5 weeks after CTCA and were used for primary data analysis. The remaining 196 patients with only CTCA were used to account for verification bias.

All patients received nitroglycerin (0.4 mg/dose) sublingually just before CT. Patients with a heart rate above 65 bpm received a single dose of 100 mg metoprolol orally 1 h before CT. A heart rate above 65 bpm was accepted in patients with contraindications to β-blockade or patients not sufficiently responding to the administered β-blocker.

Patients were categorized into two groups based on pre-CT heart rate (after administration of β-blocker). Group A comprised patients with a heart rate below 65 bpm and group B patients with a heart rate at least 65 bpm. Patients in group A were randomized to undergo either prospective high-pitch spiral CTCA or prospective sequential CTCA with a narrow CT acquisition window. Patients in group B were randomized to undergo either prospective sequential CTCA with a wide CT acquisition window or retrospective spiral CTCA. Patients were randomized using a block randomization (block size 10).

CT DATA ACQUISITION AND POST PROCESSING

All CTs was performed using a 128-slice DSCT system (Somatom Definition Flash, Siemens Healthcare, Forchheim, Germany). This CT system has two X-ray tubes and two detector arrays rotating in the same plane with an angular offset of 95°. Gantry rotation time is 280 ms, which provides a temporal resolution of 75 ms using a heart rate independent single-segment reconstruction. Detector collimation is 2x64x0.6 mm. A z-axis flying focal spot is applied which results in an acquisition of 2x128 slices per rotation. In the high-pitch spiral

mode prospective ECG-triggering was used to obtain a single data set in a single heart beat [18] starting at 55 % of the R–R interval.

In the sequential mode prospective ECG-triggering was used with a narrow (group A, 62–75 % of the R–R interval) or wide (group B, 31–75 %) CT acquisition window [19]. The entire heart was covered in three or four heart beats.

In the retrospective spiral mode retrospective ECGgating was used in combination with prospective ECGpulsing with maximum tube current output during 31– 75 % of the R–R interval. Outside this window, 4 % of the reference tube current was used.

Tube voltage and reference tube current were adapted to the body mass index (BMI) of the patient: no greater than 30 kg/m^2 BMI, 100 kV and 370 mAs; greater than 30 kg/m^2 BMI, 120 kV and 320 mAs.

We used a volume of 75 mL iodinated contrast media (Ultravist 370 mg I/mL, Bayer-Schering AG, Berlin, Germany) with a flow rate of 6.0 mL/s (high-pitch spiral) or 80–100 mL (CT acquisition time dependent) with a flow rate of 5.5 mL/s (sequential and retrospective spiral) followed by a saline chaser of 45 mL with the same flow rate.

Data sets were reconstructed with a slice thickness of 0.75 mm, an increment of 0.4 mm, a field of view of 180 mm, a medium-soft convolution kernel (B26) and additionally a sharp convolution kernel (B46) in patients exhibiting coronary calcium. Data sets were reconstructed in the optimal diastolic and, if applicable, systolic phase to obtain maximum image quality.

CT ANALYSIS

All data sets were sent to an off-line workstation (MMWP, Siemens Healthcare, Forchheim, Germany). Two independent observers, L.A.N. and A.R. (with both 5 years' experience in cardiovascular imaging), evaluated all CTCA data sets to assess the presence or absence of CAD and categorize the lesions (no more than 50 % or more than 50 % lumen diameter reduction) per coronary segment (modified American Heart Association (AHA) 16-segment model [20]. More than 50 % lumen diameter reduction was considered obstructive disease. Additionally the image quality per segment was assessed (1=poor image quality due to major artefacts; no diagnostic evaluation possible. 2=minor or no artefacts present; adequate image quality for reliable evaluation). Discrepancies were resolved in consensus. Small-sized coronary segments (less than 1.5 mm diameter, manually measured at its origin) (n=1,117/7,803), segments distal to an occlusion (n=74/7,803) or stented segments (n=97/7,803) were excluded. Segments with non-diagnostic image quality were considered significantly obstructed with a maximum of one assumed obstructive segment per vessel in order not to underestimate the disease severity in this symptomatic patient population.

EFFECTIVE DOSE ESTIMATION

The dose length product (DLP) per CTCA was assessed and we calculated the mean estimated radiation dose by multiplying the DLP by the conversion coefficient of 0.014 mSv mGy^{-1} cm^{-1} for the chest [21].

QUANTITATIVE CORONARY ANGIOGRAPHY (QCA)

One cardiologist (K.N., 8 years of experience in CCA), unaware of the CTCA results, evaluated all coronary angiograms. Lumen diameter reduction of all available nonstented segments (at least 1.5 mm diameter) was assessed and categorized (no more than 50 % or more than 50 % lumen diameter reduction) using a validated QCA algorithm (CAAS, version 5.7, Pie Medical Imaging, Maastricht, The Netherlands). Lumen reduction of more than 50 % was considered significant obstructive disease.

STATISTICAL ANALYSIS

Statistical analysis was performed using commercially available software (Stata, version 11 for Windows; StataCorp, College Station, Texas, USA and SPSS, version 15.0 for windows, SPSS, Chicago, USA).

Continuous variables are shown as mean (SD) or median (IQR) and categorical variables as number (%). The t test or Mann–Whitney U test was used to compare continuous variables and the Chi-square test or the Fisher exact test for the comparison of categorical variables.

The diagnostic performance including sensitivity, specificity, positive predictive value (PPV) and negative predictive value (NPV) of CTCA for the detection or exclusion of significant coronary stenosis compared to QCA was calculated with corresponding 95 % confidence intervals (CIs) in those patients that underwent CCA. These parameters were calculated per patient, per vessel and per segment. To take into account the correlation between different segments in a patient, we analysed measures of diagnostic accuracy on a vessel level and segment level by using generalized estimating equations, with the assumption of a binomial distribution of the dependent variable, a logit-link function, the patient as cluster, an equal-correlation model within each cluster, and the robust sandwich estimator of the variance. The analyses were performed separately for randomization within group A and group B. An indicator variable was used to estimate the difference between the CTCA protocols in each randomization group. To account for verification bias the data were re-analysed using inverse probability weighting [22,23]. The probability of verification with CCA was calculated at the patient level using all patients who underwent CTCA, and based on a logistic regression

model with verification as the dependent variable with the following predictors: chest pain type, presence of previously diagnosed CAD and CTCA result per segment. Subsequently, the accuracy analyses were performed using only the patients who underwent angiography, each patient weighted by the inverse of their probability of undergoing CCA (verification). Interobserver variability and agreement between CTCA and CCA to detect obstructive CAD were described with kappa statistics.

RESULTS

Our initial study population comprised 463 consecutive patients scheduled for CTCA of which 233 were classified into group A (below 65 bpm pre-CT heart rate) and 230 patients into group B (above 65 bpm) to be examined according to the assigned protocol after randomization (Figure 1). Two patients randomized to undergo high-pitch spiral CTCA experienced a sudden increase in heart rate of above 75 bpm immediately before the CT examination. Owing to the increased probability of non-diagnostic results, both were excluded from the study and underwent retrospective spiral CTCA [14]. Two patients in group B, assigned to undergo retrospective spiral CTCA, were excluded because of lack of contrast material in the coronary arteries because of technical failure of the contrast material injector (n=1) or contrast extravasation subcutaneously (n=1).

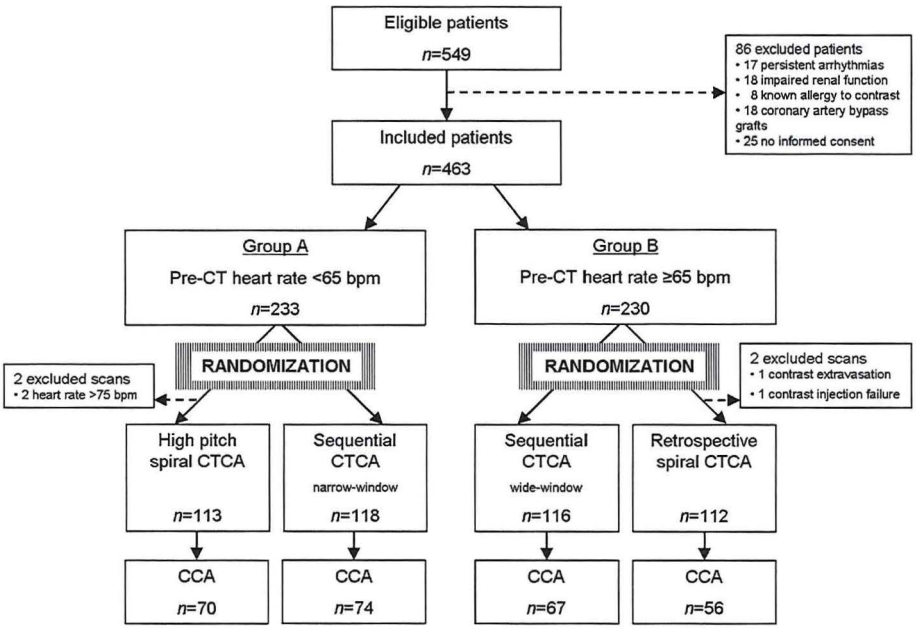

Figure 1. Patient inclusion. Study design flow chart. CCA conventional coronary angiography, CTCA CT coronary angiography.

In total 459 patients underwent CTCA of which finally 267 patients (58 %) also underwent CCA (group A: high-pitch spiral, n=70; narrow-window sequential, n=74; group B: wide-window sequential, n=67 and retrospective spiral, n=56).

Table 1 Patients characteristics

	ALL PATIENTS	PATIENTS WITH CCA	PATIENTS WITHOUT CCA
	n=459	n=267	n=192
Age (years)	59 (11)	62 (11)	55 (11)
Sex (male)	278 (61%)	181 (68%)	97 (50%)
Heart rate (bpm)	67 (12)	65 (12)	69 (12)
Risk factors			
Hypertension†	258 (56%)	166 (62%)	92 (48%)
Diabetes Mellitus‡	77 (17%)	46 (17%)	31 (16%)
Smoking‖	152 (33%)	94 (35%)	58 (30%)
Hypercholesterolemia§	269 (59%)	177 (66%)	95 (48%)
Family history of CAD	243 (53%)	140 (52%)	103 (54%)
Body Mass Index (kg/m2)	27 (5)	27 (5)	27 (5)
Typical angina pectoris¶	205 (45%)	161 (60%)	44 (23%)
Atypical angina pectoris¶	85 (19%)	34 (13%)	51 (27%)
Non aginal chest pain¶	169 (37%)	72 (27%)	97 (51%)
Known CAD in history	71 (16%)	64 (24%)	7 (3%)
Calcium score	45 (0-381)	242 (38-196)	1 (0-44)
CCA			
No CAD	-	31 (12%)	-
Non-obstructive CAD	-	30 (11%)	-
Obstructive CAD	-	206 (77%)	-

Continuous data is expressed as mean (SD) and dichotomous data as n (%). *The Calcium Score is expressed as median (Inter Quartile Range). CAD, Coronary Artery Disease; CCA, conventional coronary angiography; CTCA Computed Tomography Coronary Angiography; †Blood pressure >140/90 mm Hg or treatment for hypertension. ‡Treatment with oral anti-diabetic medicine or insulin. ‖Currently and/or in the past. §Total cholesterol >180ml/dl or treatment for hypercholesterolemia. ¶ According to chest discomfort classification of Diamond et al.(J Am Coll of Cardiol 1983;1:574-5).

Patient characteristics are shown in Table 1. In group A, the mean heart rate of patients examined with the high-pitch spiral CTCA protocol (57±6 bpm) was slightly lower than the heart rate in patients examined with the sequential CTCA protocol (60±7 bpm, p00.01). In group B, the mean heart rate was similar between patients examined with the sequential CTCA protocol or the retrospective spiral CTCA protocol (75±10 vs. 75±12 bpm, respectively, P=0.93).

The patients that underwent both CTCA and CCA exhibited a prevalence of significant CAD based on CCA results of 79 % (high-pitch spiral), 78 % (narrow-window sequential), 76 % (wide-window sequential) and 75 % (retrospective spiral).

DIAGNOSTIC ACCURACY

The diagnostic performance, including the sensitivity, specificity, PPV and NPV, of the 128-slice DSCT to detect or rule out significant coronary stenoses compared to CCA is shown in Table 2.

SEGMENT-BY-SEGMENT ANALYSIS

Group A
In group A the number of non-assessable segments (quality score 1) was significantly higher in the high-pitch spiral group (70 of 832 segments (8 %)) compared to the narrow-window sequential group (23 of 906 segments (3 %), P<0.001).

The sensitivity on a per-segment level was significantly lower for the high-pitch spiral CTCA protocol than for the narrow-window sequential protocol (89 % vs. 97 %, P0 0.01). High-pitch spiral CTCA incorrectly classified 15 segments of 133 diseased segments as having no significant stenoses vs. 4 incorrectly classified segments of 133 diseased segments using a narrow-window sequential protocol. No significant difference was found in specificity, PPV or NPV in group A (95 % vs. 96 %, P=0.50; 62 % vs. 73 %, P=0.07; and 99 % vs. 100 %, P=0.07, respectively).

Group B
No significant difference in the number of non-assessable segments was found between the narrow-window sequential and the retrospective spiral CTCA protocol (22/801 (3 %) vs. 18/657 (3 %), P=0.99). Sensitivity (94 % vs. 92 %, P=0.62), specificity (95 % vs. 95 %, P=0.79), PPV (67 % vs. 66 %, P=0.81) and NPV (99 % vs. 99 %, P=0.94) on a per-segment level were comparable between both protocols.

Table 2 Diagnostic performance of 128-slice dual source CT coronary angiography for the detection of >50% coronary stenosis on CCA; analysis for 4 different scan protocols.

							VERIFICATION BIAS CORRECTED ANALYSIS				UNCORRECTED ANALYSIS			
	n	TP	TN	FP	FN	kappa	Sensitivity %	Specificity %	PPV %	NPV %	Sensitivity %	Specificity %	PPV %	NPV %
SEGMENT-BASED ANALYSIS§														
High-pitch Spiral	832	118	626	73	15	0.67	89 (83-94)	95 (92-98)	62 (54-70)	99 (98-100)	89 (84-94)	89 (86-93)	63 (55-71)	98 (96-99)
Sequential narrow scan window	906	129	719	54	4	0.78	97 (94-100)	96 (94-99)	73 (65-80)	100 (99-100)	97 (94-100)	93 (90-95)	73 (65-80)	99 (99-100)
Sequential wide scan window	801	104	642	47	8	0.75	94 (89-98)	95 (93-97)	67 (59-76)	99 (99-100)	93 (88-98)	93 (91-95)	69 (61-78)	99 (98-100)
Retrospective Spiral	657	75	534	41	7	0.72	92 (85-98)	95 (93-98)	66 (56-75)	99 (99-100)	92 (86-98)	93 (90-96)	66 (57-75)	99 (98-100)
VESSEL-BASED ANALYSIS§														
High-pitch Spiral	270	92	137	36	5	0.69	95 (90-99)	90 (84-96)	71 (62-80)	99 (98-100)	95 (88-98)	79 (72-86)	73 (64-81)	97 (92-99)
Sequential narrow scan window	293	94	169	30	0	0.78	100*	92 (87-97)	76 (68-85)	100*	100 (96-100)†	84 (78-90)	77 (69-85)	100 (98-100)†
Sequential wide scan window	264	84	150	29	1	0.76	99 (96-100)	88 (82-94)	71 (61-80)	100 (99-100)	99 (96-100)	84 (78-89)	74 (66-83)	99 (98-100)
Retrospective Spiral	217	63	130	22	2	0.76	97 (92-100)	91 (86-96)	73 (62-83)	99 (98-100)	97 (92-100)	85 (80-91)	74 (65-83)	99 (96-100)
PATIENT-BASED ANALYSIS														
High-pitch Spiral	70	55	10	5	0	0.76	100*	91 (80-100)	89 (80-99)	100*	100 (94-100)†	67 (38-88)‡	92 (85-99)	100 (69-100)†
Sequential narrow scan window	74	58	11	5	0	0.78	100*	91 (79-100)	91 (82-99)	100*	100 (94-100)†	69 (41-89)‡	92 (85-99)	100 (72-100)†
Sequential wide scan window	67	51	10	6	0	0.72	100*	78 (55-100)	86 (75-97)	100*	100 (93-100)†	63 (35-85)‡	90 (82-97)	100 (69-100)†
Retrospective Spiral	56	42	8	6	0	0.67	100*	78 (55-100)	85 (72-98)	100*	100 (92-100)†	57 (29-82)‡	88 (78-97)	100 (63-100)†

*Corrected CI could not be calculated; †One-sided exact 97.5% CI; ‡exact 95% CI; §Analyses performed using generalized estimating equations unless indicated otherwise. TP, true positive; TN, true negative; FP, false positive; FN, false negative; PPV, positive predictive value; NPV, negative predictive value. Values in parentheses represent 95% CI unless indicated otherwise.

Interobserver variability for the detection of obstructive CAD on a per-segment level was good in all patients (κ value 0.77).

VESSEL-BY-VESSEL ANALYSIS

Group A

Using the high-pitch spiral protocol 5 obstructed vessels were missed: 1 right coronary artery (RCA), 2 left anterior descending arteries (LAD) and 2 left circumflex arteries (LCX), whereas none were missed using the narrowwindow sequential protocol. The lack of confidence intervals for the 100% sensitivity and NPV of the narrow-window sequential protocol hampers statistical comparison between the high-pitch spiral and the sequantial protocol but no significant difference is assumed. Specificity and PPV on a per-vessel level are comparable (90% vs. 92%, P=0.65 and 71% vs 76%, P=0.36).

Group B

Wide-window sequential CTCA missed 1 obstructed vessel (LCX) and retrospective spiral CTCA missed 2 (LAD, LCX).

Sensitivity (99 % vs. 97 %, P=0.41), specificity (88 % vs. 91 %, P=0.45), PPV (71 % vs. 73 %, P=0.77) and NPV (100 % vs. 99 %, P=0.54) on a per-vessel level were comparable between the wide-window sequential protocol and the retrospective spiral protocol.

PATIENT-BY-PATIENT ANALYSIS

Group A

None of the patients with significant CAD were missed by either the high-pitch spiral or the narrow-window sequential CTCA protocol. Consequently the sensitivity and NPV on a per-patient level of both CTCA protocols are 100 % and no statistical difference is assumed. Specificity and PPV are comparable between both protocols (91 % vs. 91 %, P=NS and 89 % vs. 91 %, P=NS).

Group B

All patients with obstructive disease on CCA were detected by CTCA using the wide-window sequential (Fig. 2) or the retrospective spiral CTCA protocol. Consequently the sensitivity and NPV on a per-patient level are 100 % for both protocols and no statistical difference is assumed. Specificity and PPV were similar (78 % vs. 78 %, P=NS and 86% vs. 85%, P=NS).

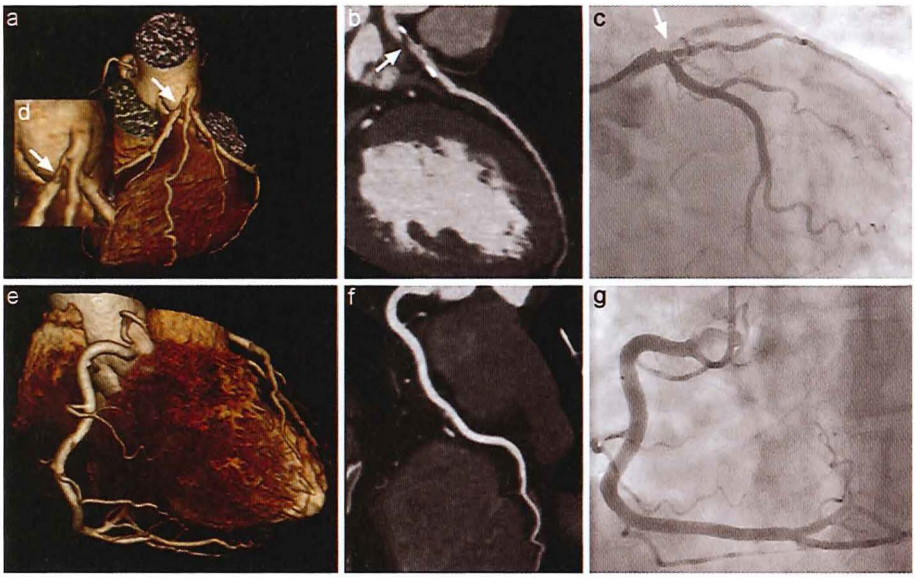

Figure 2. Prospective sequential CT coronary angiography protocol with a wide CT data acquisition window in a patient with a high heart rate. Male, 57 years old, presenting with atypical angina pectoris and a positive exercise test. Mean heart rate during CT was 74 bpm. Estimated radiation dose of the wide window sequential CTCA protocol was 3.9 mSv. Volume rendered CTCA images (VRT) reveal the anatomy of the left anterior descending coronary artery (LAD) (a) and the right coronary artery (RCA) (e). The curved multiplanar reconstruction image (cMPR) (b) and the VRT inlay (d) disclose a subtotal occlusion (arrow) of the proximal LAD, which was confirmed by CCA (c). The cMPR image (f) shows a non-diseased RCA which was confirmed by CCA (g).

RADIATION DOSE

In group A the estimated radiation dose was significantly lower with the high-pitch spiral protocol than with the narrow-window sequential protocol (tube voltage 100 kV, 0.74±0.15 vs. 2.65±1.01 mSv, P<0.001; 120 kV, 1.60± 0.57 vs. 4.65±1.51 mSv, P<0.001) (Table 3). In group B the estimated radiation dose was significantly lower with the wide-window sequential protocol than with the retrospective spiral protocol (tube voltage 100 kV, 4.05±1.46 vs. 5.66±2.30 mSv, P<0.001; 120 kV, 7.53±2.18 vs. 10.21± 4.89 mSv, P<0.001) (Table 3).

DISCUSSION

Our results show that sequential CT data acquisition provides good diagnostic performance at a low radiation dose in both groups undergoing CTCA. Consequently, sequential CTCA should be used as the first-line protocol in concordance with the as low as reasonably achiev-

able (ALARA) principle. Further dose reduction can be achieved with high-pitch spiral CTCA in patients with low heart rates, albeit at the expense of a lower diagnostic performance.

The strength of CTCA is its high NPV and preliminary data suggest that CTCA is even the preferred first-line diagnostic investigation in patients with low-to-intermediate risk of having significant CAD compared to exercise ECG-testing [24]. As a first-line test, CTCA should be as

Table 3 Estimated radiation exposure

		DLP (MGY•CM)	ESTIMATED DOSE* (MSV)
All patients (n=459)			
Group A	High Pitch Spiral	82.69 (42.80)	1.16 (0.60)
	Sequential narrow scan window	273.13 (117.82)	3.82 (1.65)
Group B	Sequential wide scan window	437.39 (183.87)	6.12 (2.58)
	Retrospective Spiral	581.24 (323.15)	8.13 (4.52)
Tube Voltage			
100 kV (n=204)			
Group A	High Pitch Spiral	52.83 (11.02)	0.74 (0.15)
	Sequential narrow scan window	189.02 (72.37)	2.65 (1.01)
Group B	Sequential wide scan window	288.87 (103.89)	4.05 (1.46)
	Retrospective Spiral	403.92 (163.81)	5.66 (2.30)
120 kV (n=255)			
Group A	High Pitch Spiral	114.18 (41.30)	1.60 (0.57)
	Sequential narrow scan window	331.64 (107.66)	4.65 (1.51)
Group B	Sequential wide scan window	537.94 (156.10)	7.53 (2.18)
	Retrospective Spiral	729.00 (348.99)	10.21 (4.89)

Data is expressed as mean (SD). *Estimated dose was calculated by multiplying the DLP by the conversion coefficient of 0.014 mSv•mGy-1•cm-1 for the chest. DLP, dose length product.

safe and non-invasive as possible because the vast majority of patients do not have significant CAD. The introduction of radiation-lowering techniques has boosted the implementation of CTCA in a clinical routine setting. However, data on the impact of diagnostic accuracy using 128-slice dual-source CTCA protocols are scarce. Some preliminary studies reported high diagnostic accuracy of high-pitch spiral CTCA in patients with low heart rates [15,25]. Our results are in line with these previously published studies but we found two important limitations with respect to high-pitch spiral CTCA. Firstly, we detected significantly more non-assessable segments with high pitch spiral CTCA vs. sequential CTCA. Secondly, we found a significantly lower sensitivity on a per-segment level. These observations indicate that sequential CTCA outperforms high-pitch spiral CTCA on a per-segment level. Although this difference is not found on a per-vessel or per patient level, we believe that a negative high-pitch spiral CTCA does not reliably exclude the presence of a significant stenosis because of a relatively high frequency of non assessable segments (8 %) mainly based on motion artefacts.

The results of our study indicate that the use of βblockers in patients with high heart rates (above 65 bpm) is an effective tool to reduce radiation exposure if the heart rate can be reduced to below 65 bpm, which allows the selection of a low dose CTCA protocol. If the use of βblockers is not sufficient to reduce the heart rate below 65 bpm or in the presence of contraindications, a widewindow sequential CTCA protocol can be used as it provides similar diagnostic performance compared to retrospective spiral CTCA in patients with heart rates above 65 bpm.

Our results also demonstrate that radiation exposure can be significantly reduced using lower kV voltages (100 kV instead 120 kV) in patients with a BMI of less than 30 kg/m^2,which is in line with previous studies [11,26]. The potential of this tool is currently not fully used as the selection of kV voltage based on BMI is rather arbitrary. Thus, the selection of the appropriate protocol tailored to individual patient characteristics such as heart rate and geometry provides significant reduction of radiation dose while maintaining diagnostic accuracy. In the near future further dose lowering by optimized use of lower tube voltages is to be expected owing to (1) the recent introduction of automated tube voltage selection based on patient geometry which provides an optimal balance between tube current and tube voltage [27] and (2) the widespread application of iterative reconstruction, which limits the disadvantages of the use of lower tube voltages as it provides a significantly higher contrast-to-noise ratio compared to conventional reconstruction algorithms [28].

Our study had a major limitation. Only a part of the included patients underwent CCA after the CTCA at the discretion of underwent CTCA. A limitation of our study is the exclusive inclusion of patients with stable heart rates and thus the results are not applicable to patients suffering any kind of arrhythmia including atrial fibrillation. Furthermore it is debatable whether a heart rate of 65 bpm is the correct cut-off heart rate for the selection of CTCA protocol and acquisition window. We did extract these values from data of a retrospective acquisition protocol [19] and future studies are mandatory to determine the correct settings for sequential acquisition protocols.

In conclusion, we demonstrated that a sequential CTCA protocol should be the first choice in patients undergoing CT coronary angiography, combining high diagnostic performance with few non-assessable segments and relatively low radiation exposure.

REFERENCES

1. von Ballmoos MW, Haring B, Juillerat P, Alkadhi H (2011) Metaanalysis: diagnostic performance of low-radiation-dose coronary computed tomography angiography. Ann Intern Med 154:413–420
2. Mowatt G, Cummins E, Waugh N et al (2008) Systematic review of the clinical effectiveness and cost-effectiveness of 64-slice or higher computed tomography angiography as an alternative to invasive coronary angiography in the investigation of coronary artery disease. Health Technol Assess 12:iii–iv, ix–143
3. Vanhoenacker PK, Heijenbrok-Kal MH, Van Heste R et al (2007) Diagnostic performance of multidetector CT angiography for assessment of coronary artery disease: meta-analysis. Radiology 244:419–428
4. Weustink AC, Meijboom WB, Mollet NR et al (2007) Reliable high-speed coronary computed tomography in symptomatic patients. J Am Coll Cardiol 50:786–794
5. Pugliese F, Mollet NR, Hunink MG et al (2008) Diagnostic performance of coronary CT angiography by using different generations of multisection scanners: single-center experience. Radiology 246:384–393
6. Taylor AJ, Cerqueira M, Hodgson JM et al (2010) ACCF/SCCT/ ACR/AHA/ASE/ASNC/NASCI/SCAI/ SCMR 2010 appropriate use criteria for cardiac computed tomography. A report of the American College of Cardiology Foundation Appropriate Use Criteria Task Force, the Society of Cardiovascular Computed Tomography, the American College of Radiology, the American Heart Association, the American Society of Echocardiography, the American Society of Nuclear Cardiology, the North American Society for Cardiovascular Imaging, the Society for Cardiovascular Angiography and Interventions, and the Society for Cardiovascular Magnetic Resonance. J Am Coll Cardiol 56:1864–1894
7. Einstein AJ, Henzlova MJ, Rajagopalan S (2007) Estimating risk of cancer associated with radiation exposure from 64-slice computed tomography coronary angiography. JAMA 298:317–323
8. Gerber TC, Carr JJ, Arai AE et al (2009) Ionizing radiation in cardiac imaging: a science advisory from the American Heart Association Committee on Cardiac Imaging of the Council on Clinical Cardiology and Committee on Cardiovascular Imaging and Intervention of the Council on Cardiovascular Radiology and Intervention. Circulation 119:1056–1065
9. Roobottom CA, Mitchell G, Morgan-Hughes G (2010) Radiationreduction strategies in cardiac computed tomographic angiography. Clin Radiol 65:859–867
10. Bischoff B, Hein F, Meyer T et al (2010) Comparison of sequential and helical scanning for radiation dose and image quality: results of the Prospective Multicenter Study on Radiation Dose Estimates of Cardiac CT Angiography (PROTECTION) I Study. AJR 194:1495–1499
11. Hausleiter J, Martinoff S, Hadamitzky M et al (2010) Image quality and radiation exposure with a low tube voltage protocol for coronary CT angiography results of the PROTECTION II Trial. JACC Cardiovasc Imaging 3:1113–1123
12. Halliburton SS, Abbara S, Chen MY et al (2011) SCCT guidelines on radiation dose and dose-optimization strategies in cardiovascular CT. J Cardiovasc Comput Tomogr 5:198–224
13. Sun ML, Lu B, Wu RZ et al (2011) Diagnostic accuracy of dualsource CT coronary angiography with prospective ECG-triggering on different heart rate patients. Eur Radiol 21:1635–1642

14. Achenbach S, Marwan M, Ropers D et al (2010) Coronary computed tomography angiography with a consistent dose below 1 mSv using prospectively electrocardiogram-triggered high-pitch spiral acquisition. Eur Hear J 31:340–346
15. Alkadhi H, Stolzmann P, Desbiolles L et al (2010) Low-dose, 128slice, dual-source CT coronary angiography: accuracy and radiation dose of the high-pitch and the step-and-shoot mode. Heart 96:933–938
16. Leschka S, Stolzmann P, Desbiolles L et al (2009) Diagnostic accuracy of high-pitch dual-source CT for the assessment of coronary stenoses: first experience. Eur Radiol 19:2896–2903
17. Sommer WH, Albrecht E, Bamberg F et al (2010) Feasibility and radiation dose of high-pitch acquisition protocols in patients undergoing dual-source cardiac CT. AJR 195:1306–1312
18. Ertel D, Lell MM, Harig F, Flohr T, Schmidt B, Kalender WA (2009) Cardiac spiral dual-source CT with high pitch: a feasibility study. Eur Radiol 19:2357–2362
19. Weustink AC, Mollet NR, Pugliese F et al (2008) Optimal electrocardiographic pulsing windows and heart rate: effect on image quality and radiation exposure at dual-source coronary CT angiography. Radiology 248:792–798
20. Austen WG, Edwards JE, Frye RL et al (1975) A reporting system on patients evaluated for coronary artery disease. Report of the Ad Hoc Committee for Grading of Coronary Artery Disease, Council on Cardiovascular Surgery, American Heart Association. Circulation 51:5–40
21. Shrimpton P (2004) Assessment of patient dose in CT. http:// www.msct.eu/PDF_FILES/Appendix%20 paediatric%20CT%20 Dosimetry.pdf. Accessed 20 Nov 2008
22. Begg CB, Greenes RA (1983) Assessment of diagnostic tests when disease verification is subject to selection bias. Biometrics 39:207–215
23. Hunink MG, Polak JF, Barlan MM, O'Leary DH (1993) Detection and quantification of carotid artery stenosis: efficacy of various Doppler velocity parameters. AJR 160:619–625
24. Weustink AC, Mollet NR, Neefjes LA et al (2010) Diagnostic accuracy and clinical utility of noninvasive testing for coronary artery disease. Ann Intern Med 152:630–639
25. Achenbach S, Goroll T, Seltmann M et al (2011) Detection of coronary artery stenoses by low-dose, prospectively ECGtriggered, high-pitch spiral coronary CT angiography. JACC Cardiovasc Imaging 4:328–337
26. Leschka S, Stolzmann P, Schmid FT et al (2008) Low kilovoltage cardiac dual-source CT: attenuation, noise, and radiation dose. Eur Radiol 18:1809–1817
27. Yu L, Li H, Fletcher JG, McCollough CH (2010) Automatic selection of tube potential for radiation dose reduction in CT: a general strategy. Med Phys 37:234–243
28. Leipsic J, Labounty TM, Heilbron B et al (2010) Estimated radiation dose reduction using adaptive statistical iterative reconstruction in coronary CT angiography: the ERASIR study. AJR 195:655–660

CHAPTER 4

QUANTITATIVE CT CORONARY ANGIOGRAPHY - DOES IT PREDICT FUNCTIONALLY SIGNIFICANT CORONARY STENOSES?

2013 Submitted for publication.

A Rossi
S-L Papadopolou
F Pugliese
B Russo
AS Dharampal
A Dedic
PH Kitslaar
A Broersen
B Meijboom
RJ van Geuns
A Wragg
J Ligthart
C Schultz
SE Petersen
K Nieman
GP Krestin
PJ de Feyter

ABSTRACT

Background: Coronary lesions with a diameter narrowing ≥ 50% on visual CT coronary angiography (CTCA) are generally considered for referral to invasive coronary angiography (ICA). However, similarly to ICA, visual CTCA is often inaccurate in detecting functionally significant coronary lesions. We sought to compare the diagnostic performance of quantitative CTCA with visual CTCA for the detection of functionally significant coronary lesions using fractional flow reserve (FFR) as reference standard.

Methods and results: CTCA and FFR measurements were obtained in 99 symptomatic patients. In total, 144 coronary lesions detected on CTCA were visually graded for stenosis severity. Quantitative CTCA measurements included lesion length, minimal lumen area (MLA), percentage area stenosis (%AS) and plaque burden [((vessel area – lumen area)/ vessel area)*100]. Optimal cut-off values of CTCA-derived parameters were determined and their diagnostic accuracy for the detection of flow-limiting coronary lesions (FFR ≤0.80) was compared to visual CTCA.

FFR was ≤0.80 in 54/144 (38%) coronary lesions. Optimal cut-off values to predict flow-limiting coronary lesion were 10 mm for lesion length, 1.8 mm^2 for MLA, 73% for %AS, and 76% for plaque burden. No significant difference in sensitivity was found between visual CTCA and quantitative CTCA parameters ($p>0.05$). Specificity of visual CTCA (42%; 95%CI: 32-52) was lower than that of MLA (68%; 95%CI: 57-77; $p=0.001$), %AS (76%, 95%CI: 65-84; $p<0.001$) and plaque burden (63%; 95%CI: 52-73; $p=0.004$). The specificity of lesion length was comparable to that of visual CTCA.

Conclusions: Quantitative CTCA improves the prediction of functionally significant coronary lesions compared to visual CTCA assessment but remains insufficient. Functional assessment is still needed in lesions of moderate stenosis to guide patient's management.

INTRODUCTION

Computed tomography coronary angiography (CTCA) is a reliable, non-invasive imaging modality to visualize coronary artery disease, with a high diagnostic accuracy compared to invasive coronary angiography (ICA).[1-3] In addition, CTCA can provide cross-sectional information beyond lumenography, similar to intravascular ultrasound (IVUS), including plaque burden and morphology.

In daily practice, lesions with a diameter stenosis ≥50% on visual CTCA are generally considered for referral to ICA. However, similarly to ICA, CTCA is an anatomical imaging technique, thus it may result in both underestimation and overestimation of a lesion's severity and is often inaccurate in identifying functionally significant coronary lesions which cause ischemia [4,5]. Current guidelines suggest that treatment decisions based on the hemodynamic impact of a coronary lesion may improve clinical outcome [6-8]. Therefore it would be relevant if the cross-sectional quantitative parameters derived from CTCA could be optimized to predict the functional significance of a coronary stenosis.

The aim of this study was to compare the diagnostic performance of CTCA-derived cross-sectional quantitative parameters with visual CTCA in the detection of functionally significant coronary lesions using fractional flow reserve (FFR) as the reference standard.

METHODS

STUDY POPULATION

We retrospectively included patients with stable angina who underwent both CTCA and ICA and a subsequent measurement of FFR in 2 teaching hospitals. The decision to measure FFR was based on the visual assessment of ICA and was made at the discretion of the interventional cardiologist. Due to the potential hemodynamic interaction between 2 or more stenoses in series [9,10], we only included patients with a single coronary lesion per coronary vessel.

Exclusion criteria were impaired renal function (creatinine clearance <60 ml/min), known allergy to iodine contrast material, calcium-score per vessel >400, left main coronary lesions, and poor image quality. Poor image quality was defined as severe motion artifacts or poor contrast opacification.

All patients gave written informed consent to undergo CTCA as part of research protocols approved by the institutional review boards of the participating institutions. FFR was carried out as part of routine clinical management.

CTCA ACQUISITION

All patients received nitroglycerin (0.4 mg/ dose) sublingually just prior to the CT scan, provided there were no contraindications and patients with a heart rate above 65 beats per minute (bpm) received preparation with beta-blockers (50-100 mg metoprolol per os 1 hour prior to scanning or 1-30 mg metoprolol intravenously directly before scanning). The CT scan was performed using either a 64-slice dual source scanner (Somatom Definition, Siemens Medical Solutions, Forchheim, Germany) or a 128-slice second-generation dual source CT scanner (Somatom Definition Flash, Siemens Medical Solutions, Forchheim, Germany). First, all patients underwent an unenhanced scan for the calculation of the calcium score with the Agatston method (32 x 1.2 mm collimation, 120-kV tube voltage, 75 mAs tube current and 3-mm slice thickness with increment 1.5-mm). The CT angiographic scan parameters were: 1) for the 64-dual source CT scanner a gantry rotation time of 330 ms; 32x2x0.6 mm collimation with z-flying focal spot for both detectors, gantry rotation time 330 ms, tube voltage 120 kV and tube current of 320 to 412 mAs per rotation 2) for the 128-dual source CT scanner a gantry rotation time of 280 ms; 64x2x0.6 mm collimation with z-flying focal spot for both detectors, tube voltage 100 kV or 120 kV and tube current of 320 to 412 mAs per rotation. A bolus of iodinated contrast agent (370 mgI/mL, Ultravist; Schering, Berlin, Germany, or 300 mgI/ml, Omnipaque, GE Healthcare, Milwaukee, MI), which varied between 60 and 100 mL depending on the expected scan time, was injected intravenously at an injection rate of either 5.5 mL/s or 7 mL/s (depending on the type of contrast agent used) followed by a 45 mL saline chaser at the same injection rate. The iodine delivery rates achieved

with both injection protocols were similar (2.0-2.1 gl/s). A bolus tracking technique was used to synchronize the start of image acquisition with the arrival of the iodinated contrast agent in the coronary arteries. With the 64-slice DSCT scanner, an ECG-gated spiral scan mode with ECG-pulsing was used for image acquisition. When scanning with the 128-slice DSCT either the prospectively ECG triggered sequential scan mode ('step-and-shoot') or the retrospective ECG-gated spiral scan mode with ECG-pulsing or a high pitch spiral scan mode was used, depending on the heart rate.

All CT images were reconstructed with a slice thickness of 0.75 mm and an increment of 0.4 mm. Images were analyzed using medium-to-smooth convolution kernels for non-calcified lesions and sharp convolution kernels for calcified lesions. More details about the CT protocol were previously described in detail [11].

FFR MEASUREMENTS

Fractional flow reserve was measured with a sensor-tipped 0.014-inch guidewire (Pressure Wire, Radi Medical Systems, Uppsala, Sweden). The pressure sensor was positioned just distal to the stenosis and maximal myocardial hyperemia was induced by a continuous intravenous infusion of adenosine in a femoral vein (140 μg/kg/minute for a minimum of 2 min). FFR was calculated as the ratio of mean distal pressure measured by the pressure wire divided by the mean proximal pressure measured by the guiding catheter. A coronary stenosis with an FFR value $\leq$0.80 was considered functionally significant [12].

CTCA IMAGE ANALYSIS

First, the CTCA datasets were evaluated visually and the coronary lesion was graded as non-obstructive (<50% lumen narrowing), moderate ($\leq$50%-70 lumen narrowing) and severe ($\geq$70% lumen narrowing). Afterwards, all datasets were transferred to an offline workstation for analysis using semi-automated plaque analysis software (QAngioCT Research Edition v1.3.61, Medis Medical Imaging Systems, Leiden, The Netherlands). The location and the extent of the region of interest (ROI) were manually defined using proximal and distal markers as the coronary vessel region where the lumen diameter was reduced at least of 30% compared to the normal vessel. Planimetry of the inner lumen and outer vessel areas was performed following a stepwise approach as previously described [13-15]. In summary, a centerline originating from the ostium was automatically extracted; then straightened multiplanar reformatted images were generated and the lumen and vessel borders were detected longitudinally on four different vessel views by the software; based on these longitudinal contours, cross-sectional images at 0.5 mm intervals were calculated in order to create transversal lumen and vessel wall contours, which were examined and, if necessary, adjusted by a single

experienced observer. Based on the detected contours proximal and distal from the lesion region a reference area function is derived for both lumen and vessel areas, modeling the tapering of a healthy vessel. From these data the following cross-sectional CT-CA-derived parameters were provided automatically by the software: lesion length, minimum lumen area (MLA) and percent area stenosis (%AS) at the level of the MLA defined by *[(1-(MLA/reference lumen area))*100]*. In addition plaque burden was calculated for the whole coronary lesion by the following equation: [((vessel area – lumen area)/vessel area)*100], Figure 1.

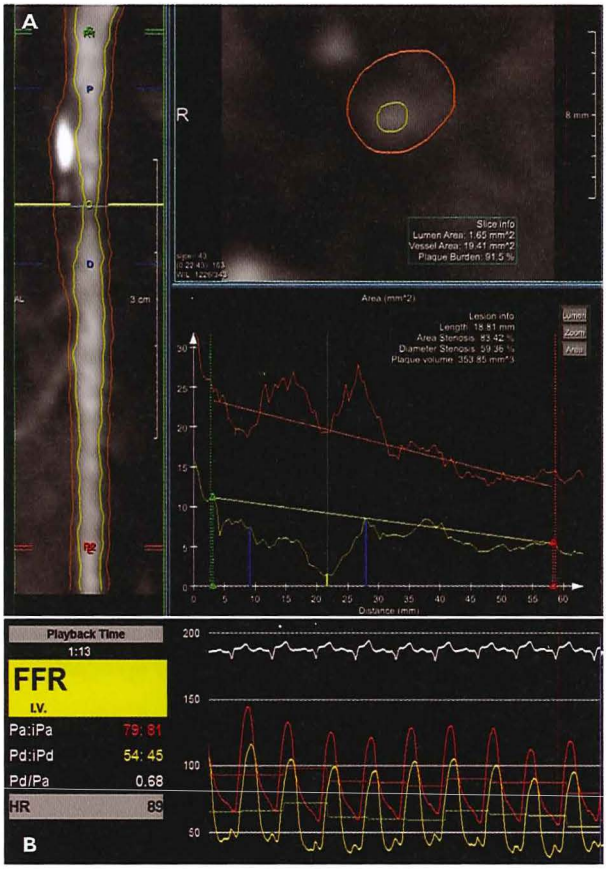

Figure 1. Quantitative CT coronary angiography (CTCA) and fractional flow reserve (FFR) measurement in a moderate coronary lesion.

Example of a patient with a moderate (50-70% lumen narrowing by visual CTCA) coronary lesion due a partly calcified plaque in the left descending coronary artery (LAD). Panel A shows the screenshot of the quantitative CTCA analysis using dedicated software. The lesion was assessed as moderate by visual CTCA. Lumen (yellow) and wall (orange) contours were semi-automatically detected. At the level of the minimal lumen area (yellow line), lumen area, percentage area stenosis and plaque burden were measured as 1.6 mm^2, 83% and 91%, respectively. The FFR was 0.68 (panel B).

STATISTICAL ANALYSIS

Statistical analysis was performed using commercially available software (IBM SPSS Statistic, version 20). Results are reported in accordance with the STARD criteria [16]. Continuous variables were presented as means ± standard deviation (SD) or medians with interquartile range (IQR) when not normally distributed and compared with the unpaired t-test or the Mann-Whitney test, respectively. Categorical variables were presented as frequencies and percentages and compared using the chi-square test. The association between the cross-sectional CTCA-derived parameters and FFR was assessed for each interrogated vessel using

the Spearman rank correlation coefficient. For the per-lesion data analysis, a linear generalized estimated equation model was used to account for the clustering between lesions in the same subject. Multivariate analyses were performed to identify independent predictors of FFR as continuous variable. In case multicollinearity was present ($r>0.7$), the multivariate analysis was performed using separate models for the two correlated variables. Receiver operating characteristics (ROC) curves were used to assess the optimal cut-off values of CTCA-derived parameters to predict FFR ≤ 0.80, defined as the values with the best combination of sensitivity and specificity, provided that sensitivity was at least 80%. Diagnostic performance of visual CTCA and quantitative CTCA parameters for the detection of functionally significant lesions were evaluated on a per-lesion level and expressed as sensitivity, specificity, positive and negative predictive values and their corresponding 95% confidence intervals. The McNemar test was used to compare the sensitivities and specificities of quantitative CTCA versus visual CTCA.

Table 1. Baseline clinical characteristics.

	ALL (N=99)	FFR >0.80 (N=55)	FFR ≤0.80 (N=44)	P*
MEN	77 (78%)	40 (73%)	37 (84%)	0.177
AGE (YRS)	61±11	60±12	62±10	0.222
RISK FACTORS				
SMOKER	17 (17%)	7 (13%)	10 (23%)	0.190
HYPERTENSION†	63 (64%)	36 (66%)	27 (61%)	0.674
DYSLIPIDEMIA‡	75 (76%)	40 (73%)	35 (79%)	0.432
DIABETES§	22 (22%)	16 (29%)	6 (14%)	0.066
FAMILY HISTORY OF CAD∫	51 (52%)	29 (53%)	22 (50%)	0.787
CALCIUM SCORE (AGATSTON)	284 (43-629)	197 (36-631)	355 (100-640)	0.428

Values are median (IQR) or n (percentage). * Comparison between fractional flow reserve (FFR) >0.80 versus FFR ≤0.80.

† Blood pressure ≥ 140/90 mmHg or treatment for hypertension; ‡ Total cholesterol >180 mg/dl or treatment for hypercholesterolemia; § Treatment with oral anti-diabetic medication or insulin; ∫ Family history of coronary artery disease having first- or second- degree relatives with premature CAD (age <55 years).

Coronary lesions were divided into three groups based on visual assessment: non-obstructive (<50% lumen narrowing), moderate (≤50%-<70% lumen narrowing) and severe (≥70% lumen narrowing). The cut-off values of the cross-sectional CTCA-derived parameters derived from the ROC curves were used individually (MLA; %AS and plaque burden) and in combination (MLA and plaque burden; %AS and plaque burden) to investigate whether they could decrease the number of misclassified lesions in the three categories of lesions' severity.

When the combined approach was used a positive outcome was adjudicated if both quantitative CTCA parameters were positive as defined by the optimal cut-off values. A misclassified lesion was defined as a mismatch between CTCA results and FFR measurements.

Statistical significance was defined as $p<0.05$.

RESULTS

STUDY POPULATION

In total 124 patients were considered for inclusion in the study. Twenty-five patients were excluded due to extreme calcifications (vessel calcium score >400) in the target vessel (n=17), left main coronary lesions (n=2), and poor image quality (n=6). Therefore, 144 coronary lesions in 99 patients were finally included in the analysis. Baseline clinical characteristics and

Table 2. Cross-sectional CT-derived parameters, vessel distribution and FFR.

	ALL (N=144)	FFR >0.80 (N=90)	FFR ≤0.80 (N=54)	P*
FFR	0.83 (0.75-0.90)	0.88 (0.84-0.93)	0.72 (0.68-0.77)	<0.001
LESION LENGTH (MM)	13 (9-19)	11 (8-17)	16 (11-25)	0.001
MLA (MM2)	1.8 (1.0-2.7)	2.3 (1.5-2.8)	1.0 (0.3-1.6)	<0.001
%AS	71 (62-82)	67 (56-73)	84 (74-91)	<0.001
PLAQUE BURDEN (%)	76 (71-79)	73 (69-77)	79 (76-82)	<0.001
VESSEL				0.050
RCA	36 (25%)	24 (27%)	12 (22%)	
LAD	76 (53%)	41 (46%)	35 (65%)	
LCX	32 (22%)	25 (28%)	7 (13%)	
LESION LOCATION				0.121
PROXIMAL	76 (53%)	43 (48%)	33 (61%)	
MID	68 (47%)	47 (52%)	21 (39%)	

Values are median (IQR) or n (percentage). * Comparison between fractional flow reserve (FFR) >0.80 versus FFR ≤0.80.

MLA = Minimal Lumen Area; %AS = Percentage Area Stenosis; RCA = Right Coronary Artery; LAD = Left Anterior Descending Coronary Artery; LCX = Left Circumflex Coronary Artery

cross-sectional CTCA-derived parameters are shown in Table 1 and Table 2, respectively. The range of FFR values was between 0.24 and 1.00; 35% (35/99) of the patients had multivessel FFR measurements. The FFR was ≤0.80 in 54 lesions (38%). There was no difference in baseline clinical characteristics between patients with FFR ≤0.80 or FFR >0.80. Coronary lesions with FFR ≤0.80 were longer lesions with smaller lumen area, more severe stenoses and higher plaque burden than those with FFR >0.80 (Table 2).

FFR VERSUS CROSS-SECTIONAL CTCA-DERIVED PARAMETERS

There was a significant positive correlation between FFR and MLA and a significant negative correlation between FFR and lesion length, %AS and plaque burden (Table 3). Multicollinearity was present between MLA and %AS, thus they were tested in two separate multivariate models. Multivariate linear analysis for the MLA model included lesion length, MLA and plaque burden; both MLA and plaque burden were independent predictors of FFR as a continuous variable (Table 4).

Table 3. Correlation and univariate analysis between quantitative CTCA and FFR.

	R	ß	95% CI	P
LESION LENGTH (MM)	-0.41	-0.003	-0.006 to -0.001	0.008
MLA (MM2)	0.58	0.051	0.034 to 0.068	<0.001
%AS	-0.57	-0.004	-0.006 to -0.003	<0.001
PLAQUE BURDEN (%)	-0.57	-0.987	-1.242 to -0.732	<0.001

CTCA = CT Coronary Angiography; FFR = Fractional Flow Reserve; MLA = Minimal Lumen Area; %AS = Percentage Area Stenosis

Multivariate linear analysis for the %AS model included lesion length, %AS and plaque burden; the independent predictors of FFR as a continuous variable were %AS and plaque burden (Table 4).

ROC analysis yielded an area under the curve (AUC) of 0.66 (0.57-0.75) for lesion length, 0.82 (0.75-0.89) for MLA, 0.83 (0.75-0.90) for %AS and 0.80 (0.73-0.87) for plaque burden. Optimal cut-off values to predict the functional significance of coronary lesions were 1.8 mm^2 for MLA, 73% for %AS, and 76% for plaque burden; Figure 2.

Table 4. Results of multivariate linear analysis to predict FFR as continuous variable.

	ß	95% CI	P
MLA MODEL			
INTERCEPT	1.214	0.969 to 1.459	<0.001
LESION LENGTH (MM)	-0.002	-0.004 to 0.001	0.124
MLA (MM2)	0.028	0.011 to 0.045	0.001
PLAQUE BURDEN (%)	-0.566	-0.854 to -0.277	<0.001
%AS MODEL			
INTERCEPT	1.523	1.362 to 1.683	<0.001
LESION LENGTH (MM)	-0.001	-0.004 to 0.001	0.303
% AS	-0.003	-0.004 to -0.002	<0.001
PLAQUE BURDEN (%)	-0.657	-0.880 to -0.433	<0.001

CTCA = CT Coronary Angiography; FFR = Fractional Flow Reserve; MLA = Minimal Lumen Area; %AS = Percentage Area Stenosis

DIAGNOSTIC PERFORMANCE OF VISUAL CTCA AND CROSS-SECTIONAL QUANTITATIVE CTCA-DERIVED PARAMETERS IN PREDICTING FUNCTIONALLY SIGNIFICANT CORONARY LESIONS

The diagnostic performance of visual CTCA and quantitative CTCA using the optimal cut-off values for the assessment of functionally significant coronary lesions (FFR ≤0.80) is detailed in Table 5. No significant difference was found for sensitivity between visual CTCA

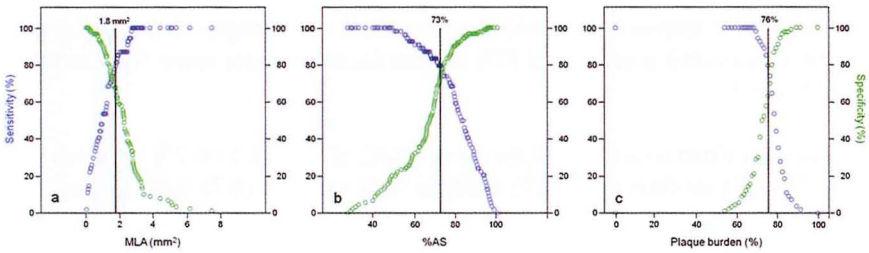

Figure 2. Plots of sensitivity and specificity for increasing values of MLA (a), %AS (b) and plaque burden (c) as calculated with receiver operating characteristics curves.

Continuous values of MLA (a), %AS (b) and plaque burden (c) are reported on the X-axis; sensitivity and specificity values are reported on the left and right Y-axis, respectively. The optimal cutoff value, defined as the best combination of sensitivity and specificity providing a sensitivity of at least 80%, is indicated.

Table 5. Diagnostic accuracy of visual CTCA and MLA, %AS and plaque burden from quantitative CTCA in the detection of flow-limiting coronary lesions as defined by a FFR≤0.80.

	TP	TN	FP	FN	SENSITIVITY % (95%CI)*	SPECIFICITY % (95%CI)*	PPV % (95%CI)*	NPV % (95%CI)*
VISUAL ASSESSMENT	50	38	52	4	93 (82-97)	42 (31-54)	49 (38-60)	90 (77-96)
MLA (MM2)	43	61	29	11	80 (67-88)	68 (57-77)**	60 (46-72)	85 (75-91)
%AS	43	68	22	11	80 (65-89)	76 (65-84) **	66 (53-77)	86 (76-92)
PLAQUE BURDEN (%)	43	57	33	11	80 (66-89)	63 (52-73)**	57 (43-69)	84 (72-91)

(95%CI) = 95% confidence interval; CTCA = CT Coronary Angiography; FFR = Fractional Flow Reserve; MLA = Minimal Lumen Area; %AS = Percentage Area Stenosis; AUC = area under the curve; TP = true positive; TN = true negative; PPV = positive predictive value; NPV = negative predictive value.

* Sensitivity, specificity, PPV and NPV calculated using the optimal cut-off value for each cross-sectional CTCA parameter.

** $p<0.05$ derived from McNemar comparing the specificities of lesion length, MLA, %AS, MLD, %DS and plaque burden with the specificity of visual assessment

and quantitative CTCA in terms of MLA, %AS and plaque burden ($p>0.05$). Specificity of MLA, %AS and plaque burden was significant higher than the specificity of visual CTCA ($p=0.001$, $p<0.001$ and $p=0.004$, respectively) for the detection of functionally significant coronary lesions.

MODERATE CORONARY LESIONS

Visual CTCA showed 42 (29%) non-obstructive lesions, 85 (59%) moderate lesions and 17 (12%) severe lesions. In the moderate lesion category 46 lesions were misclassified by visual CTCA; the use of %AS and plaque burden in combination decreased the number of lesions incorrectly classified from 46/85 (54%) to 20/85 (24%) of which 15 lesions were incorrectly classified as non-functionally significant (Table 6).

DISCUSSION

In this exploratory study we sought to investigate the ability of quantitative cross-sectional parameters derived by CTCA to predict the functional significance of coronary lesions using FFR as the reference standard.

The major findings of our study were the following: 1) MLA, %AS, and plaque burden were independent predictors of FFR as continuous variable over a wide range of coronary stenosis severity; 2) the optimal cut-off values to predict the functional significance of coronary lesions were 1.8 mm^2, 73% and 76% for MLA, %AS and

Table 6. Diagnostic performance of CTCA cross-sectional parameters to predict functionally significant lesions (FFR≤0.80).

	VISUAL ASSESSMENT					
	NON-OBSTRUCTIVE STENOSES (N=42)		MODERATE STENOSES (N=85)		SEVERE STENOSES (N=17)	
FFR>0.80	38		46		6	
FFR≤0.80	4		39		11	
	MLA (MM^2)					
	>1.8	≤1.8	>1.8	≤1.8	>1.8	≤1.8
FFR>0.80	28	10	29	17	4	2
FFR≤0.80	1	3	10	29	0	11
	AS (%)					
	<73	≥73	<73	≥73	<73	≥73
FFR>0.80	33	5	31	15	4	2
FFR≤0.80	1	3	10	29	0	11
	PLAQUE BURDEN (%)					
	<76	≥76	<76	≥76	<76	≥76
FFR>0.80	27	11	29	17	1	5
FFR≤0.80	1	3	10	29	0	11
	MLA (MM^2) AND PLAQUE BURDEN (%)					
	MLA>1.8 PB<76	MLA≤1.8 PB≥76	MLA>1.8 PB<76	MLA≤1.8 PB≥76	MLA>1.8 PB<76	MLA≤1.8 PB≥76
FFR>0.80	34	4	36	10	4	2
FFR≤0.80	1	3	15	24	0	11
	AS (%) AND PLAQUE BURDEN (%)					
	AS<73 PB<76	AS≥73 PB≥76	AS<73 PB<76	AS≥73 PB≥76	AS<73 PB<76	AS≥73 PB≥76
FFR>0.80	36	2	41	5	4	2
FFR≤0.80	1	3	15	24	0	11

Values are numbers.

For each CT parameter and for each stenosis category: upper left cell = true negative; upper right cell = false positive; lower left cell = false negative; lower right cell = true positive.

CTCA = CT Coronary Angiography; FFR = Fractional Flow Reserve; MLA = Minimal Lumen Area; %AS = Percentage Area Stenosis; PB = Plaque Burden.

plaque burden, respectively; 3) in the moderate lesion category the combined use of %AS and plaque burden decreased the number of lesions incorrectly classified from 46/85 (54%) to 20/85 (24%) of which 15 lesions were incorrectly classified as non-functionally significant lesions.

PREDICTORS OF FUNCTIONAL SIGNIFICANCE OF A CORONARY LESION AND THEIR OPTIMAL CUT-OFF VALUES

As shown in previous IVUS studies [17,18], MLA is important in determining coronary blood flow based on the Bernoulli equation. However, other important factors can affect coronary flow: the degree of diameter stenosis, lesion length, plaque burden, vessel size, lesion morphology, plaque characteristics, blood viscosity, collateral circulation, and supplied myocardium [19]. Several of these parameters can be measured using CTCA [14]. In our study we found that MLA, %AS and plaque burden were independent predictors of FFR. In another study by Kristensen et al. [20], the lesion length was also shown to be an independent predictor of FFR, although the correlation coefficient was weak ($r=-0.32$) and comparable to the one we found. This discrepancy might be explained by the inclusion of severe lesions in our population additionally to moderate lesions; consequently, a very severe lesion would result in an abnormal FFR even if it is short ("pin-point" coronary lesions), potentially decreasing the average length of the flow-limiting lesions.

Several IVUS studies have validated an MLA of 3.0 mm^2 or 4.0 mm^2 as an anatomic predictor for physiological lesion significance [21,22]. However, it has been shown that these cut-off values are not accurate; especially when applied in small vessels (diameter<2.5 mm) [17] a smaller cut-off value should be used. In our study, similarly to the finding reported by Kristensen et al. [20], we found a MLA CT-derived cut-off value of 1.8 mm^2 which is smaller compared to the IVUS-derived one reported by Kang et al.[17] This may be related to inherent differences between invasive and non-invasive imaging modalities. For instance, to avoid the induction of coronary spasm by the IVUS catheter, intracoronary nitrates are usually given before imaging at the dose of 100-200 μg causing a status of coronary vasodilation greater than the one induced by nitrates administered orally before the CTCA acquisition. In addition, IVUS does not assess severe coronary lesions due the large profile of the IVUS catheter which is unable to pass through small coronary lumen.

CTCA-DERIVED PARAMETERS IN PREDICTING FLOW-LIMITING CORONARY LESIONS

Previous investigations have demonstrated that, similarly to ICA, the anatomical assessment of a coronary stenosis by CTCA correlates poorly with the functional significance of the

stenosis defined by FFR [4,5]. As previously shown in a study by Tonino et al., there was a high rate of non-functionally significant lesions in the range of angiographic severity 50% to 70% diameter stenosis [23]. Similarly, in our study 54% of the coronary stenoses with an angiographic severity between 50% and 70% were not functionally significant. The use of quantitative CTCA decreased the number of misclassified lesions by half, mainly by reducing the number of lesions incorrectly classified as functionally significant from 46 to 20. However, 15 of these misclassified lesions were incorrectly classified as non-functionally significant, highlighting the fact that the increase in the specificity comes at the expense of a decrease in the sensitivity. Similarly, Godoy et al. [24] and Gaemperli et al.[25] found only a moderate diagnostic accuracy of quantitative CTCA for the detection of myocardial ischemia by SPECT. The modest association of anatomic assessment by quantitative CTCA with functional assessment may be explained by the complexity of factors leading to myocardial ischemia [26]. As proposed by Marzilli et al. [27] obstructive epicardial coronary stenosis is only one of the contributors to myocardial ischemia and inflammation, endothelial dysfunction, microvascular dysfunction, platelet dysfunction, thrombosis and vasomotor dysfunction should be also considered.

LIMITATIONS

Firstly, our study was a retrospective study performed in a relatively small number of patients; the possibility of a type II error should be considered. Secondly, we included only patients referred for ICA with moderate-to severely diseased coronary arteries. Future studies with a prospective design are needed to evaluate the diagnostic accuracy of quantitative CTCA for the selection of patients who will benefit most from revascularization. In addition, the discriminatory power of CTCA cross-sectional quantitative parameters in the detection of functionally significant coronary lesions needs further investigation in the typical population, at low to intermediate pre-test probability of CAD, referred for CTCA. Thirdly, we excluded vessels with poor image quality on CTCA; good image quality is a prerequisite for the reliable calculation of CT-derived cross-sectional parameters.

CLINICAL IMPLICATIONS AND FUTURE DIRECTIONS

The interest in overcoming the mismatch between anatomy and function in cardiac imaging has initiated intense research to assess the feasibility of new non-invasive diagnostic techniques. In this study we determined whether the analysis of quantitative cross-sectional CTCA parameters could improve the prediction of functionally significant lesions without further irradiation, contrast or drug administration. In our study stenosis quantification prolonged the post-processing analysis time by 5 to 10 minutes, mainly depending on the amount of calcium per lesion, with a significant reduction of the number of moderate lesions incorrectly

classified as functionally significant. Several automated software programs are now commercially available for stenosis quantification and their use may be useful in clinical routine.

The possibility of a non-invasive FFR measurement has been shown with promising results [28]. In a multicenter study involving 252 patients with stable angina, non-invasive FFR in addition to CTCA improved the diagnostic accuracy and discrimination of CTCA alone for the diagnosis of functional significant lesions [29]. Similarly to our results, the diagnostic specificity and positive predictive value remained low and further studies are warranted to determine the potential clinical implication of this more comprehensive coronary lesion assessment.

The safety and feasibility of stress myocardial CT perfusion imaging has been also demonstrated in few experimental and human studies [30-34]. The addition of stress myocardial CT perfusion imaging to the standard CTCA can provide complementary anatomical and functional information in a single examination. However, CT perfusion imaging involves increased patient radiation exposure, increased contrast volume and potential patient's discomfort related to the administration of a pharmacological stress agent.

CONCLUSION

CTCA cross-sectional quantitative parameters improve the prediction of flow-limiting lesions, compared to visual assessment, but remain insufficient. Functional assessment is still needed for lesions of moderate severity to guide patient's management.

ACKNOWLEDGEMENTS:

FP, SEP: This work forms part of the research themes contributing to the translational research portfolio of the Cardiovascular Biomedical Research Unit at Barts which is supported and funded by the National Institute for Health Research (NIHR).

DISCLOSURES:

PK is employed by Medis medical imaging systems bv and has a research appointment at the Leiden University Medical Center.

GPK has a consultancy relationship with GE Healthcare.

REFERENCES

1. Meijboom WB, Meijs MF, Schuijf JD, et al. Diagnostic accuracy of 64-slice computed tomography coronary angiography: a prospective, multicenter, multivendor study. *J Am Coll Cardiol.* Dec 16 2008;52(25):2135-2144.
2. Miller JM, Dewey M, Vavere AL, et al. Coronary CT angiography using 64 detector rows: methods and design of the multi-centre trial CORE-64. *Eur Radiol.* Apr 2009;19(4):816-828.
3. Budoff MJ, Dowe D, Jollis JG, et al. Diagnostic performance of 64-multidetector row coronary computed tomographic angiography for evaluation of coronary artery stenosis in individuals without known coronary artery disease: results from the prospective multicenter ACCURACY (Assessment by Coronary Computed Tomographic Angiography of Individuals Undergoing Invasive Coronary Angiography) trial. *J Am Coll Cardiol.* Nov 18 2008;52(21):1724-1732.
4. Sarno G, Decraemer I, Vanhoenacker PK, et al. On the inappropriateness of noninvasive multidetector computed tomography coronary angiography to trigger coronary revascularization: a comparison with invasive angiography. *JACC Cardiovasc Interv.* Jun 2009;2(6):550-557.
5. Meijboom WB, Van Mieghem CA, van Pelt N, et al. Comprehensive assessment of coronary artery stenoses: computed tomography coronary angiography versus conventional coronary angiography and correlation with fractional flow reserve in patients with stable angina. *J Am Coll Cardiol.* Aug 19 2008;52(8):636-643.
6. Hachamovitch R, Hayes SW, Friedman JD, Cohen I, Berman DS. Comparison of the short-term survival benefit associated with revascularization compared with medical therapy in patients with no prior coronary artery disease undergoing stress myocardial perfusion single photon emission computed tomography. *Circulation.* Jun 17 2003;107(23):2900-2907.
7. Kolh P, Wijns W, Danchin N, et al. Guidelines on myocardial revascularization. *Eur J Cardiothorac Surg.* Sep 2010;38 Suppl:S1-S52.
8. Wijns W, Kolh P, Danchin N, et al. Guidelines on myocardial revascularization. *Eur Heart J.* Oct 2010;31(20):2501-2555.
9. Pijls NH, De Bruyne B, Bech GJ, et al. Coronary pressure measurement to assess the hemodynamic significance of serial stenoses within one coronary artery: validation in humans. *Circulation.* Nov 7 2000;102(19):2371-2377.
10. De Bruyne B, Pijls NH, Heyndrickx GR, Hodeige D, Kirkeeide R, Gould KL. Pressure-derived fractional flow reserve to assess serial epicardial stenoses: theoretical basis and animal validation. *Circulation.* Apr 18 2000;101(15):1840-1847.
11. Neefjes LA, Dharampal AS, Rossi A, et al. Image Quality and Radiation Exposure Using Different Low-Dose Scan Protocols in Dual-Source CT Coronary Angiography: Randomized Study. *Radiology.* Dec 2011;261(3):779-786.
12. Tonino PA, De Bruyne B, Pijls NH, et al. Fractional flow reserve versus angiography for guiding percutaneous coronary intervention. *N Engl J Med.* Jan 15 2009;360(3):213-224.

13. Boogers MJ, Schuijf JD, Kitslaar PH, et al. Automated quantification of stenosis severity on 64-slice CT: a comparison with quantitative coronary angiography. *JACC Cardiovasc Imaging.* Jul 2010;3(7):699-709.
14. Papadopoulou SL, Neefjes LA, Garcia-Garcia HM, et al. Natural history of coronary atherosclerosis by multislice computed tomography. *JACC Cardiovasc Imaging.* Mar 2012;5(3 Suppl):S28-37.
15. Boogers MJ, Broersen A, van Velzen JE, et al. Automated quantification of coronary plaque with computed tomography: comparison with intravascular ultrasound using a dedicated registration algorithm for fusion-based quantification. *Eur Heart J.* Apr 2012;33(8):1007-1016.
16. Bossuyt PM, Reitsma JB, Bruns DE, et al. The STARD statement for reporting studies of diagnostic accuracy: explanation and elaboration. *Ann Intern Med.* Jan 7 2003;138(1):W1-12.
17. Kang SJ, Lee JY, Ahn JM, et al. Validation of intravascular ultrasound-derived parameters with fractional flow reserve for assessment of coronary stenosis severity. *Circ Cardiovasc Interv.* Feb 1 2011;4(1):65-71.
18. Koo BK, Yang HM, Doh JH, et al. Optimal intravascular ultrasound criteria and their accuracy for defining the functional significance of intermediate coronary stenoses of different locations. *JACC Cardiovasc Interv.* Jul 2011;4(7):803-811.
19. Park SJ, Ahn JM, Kang SJ. Paradigm shift to functional angioplasty: new insights for fractional flow reserve- and intravascular ultrasound-guided percutaneous coronary intervention. *Circulation.* Aug 23 2011;124(8):951-957.
20. Kristensen TS, Engstrom T, Kelbaek H, von der Recke P, Nielsen MB, Kofoed KF. Correlation between coronary computed tomographic angiography and fractional flow reserve. *Int J Cardiol.* Oct 8 2010;144(2):200-205.
21. Takagi A, Tsurumi Y, Ishii Y, Suzuki K, Kawana M, Kasanuki H. Clinical potential of intravascular ultrasound for physiological assessment of coronary stenosis: relationship between quantitative ultrasound tomography and pressure-derived fractional flow reserve. *Circulation.* Jul 20 1999;100(3):250-255.
22. Nishioka T, Amanullah AM, Luo H, et al. Clinical validation of intravascular ultrasound imaging for assessment of coronary stenosis severity: comparison with stress myocardial perfusion imaging. *J Am Coll Cardiol.* Jun 1999;33(7):1870-1878.
23. Tonino PA, Fearon WF, De Bruyne B, et al. Angiographic versus functional severity of coronary artery stenoses in the FAME study fractional flow reserve versus angiography in multivessel evaluation. *J Am Coll Cardiol.* Jun 22 2010;55(25):2816-2821.
24. Godoy GK, Vavere A, Miller JM, et al. Quantitative coronary arterial stenosis assessment by multidetector CT and invasive coronary angiography for identifying patients with myocardial perfusion abnormalities. *J Nucl Cardiol.* Oct 2012;19(5):922-930.
25. Gaemperli O, Schepis T, Valenta I, et al. Functionally relevant coronary artery disease: comparison of 64-section CT angiography with myocardial perfusion SPECT. *Radiology.* Aug 2008;248(2):414-423.
26. Gould KL. Does coronary flow trump coronary anatomy? *JACC Cardiovasc Imaging.* Aug 2009;2(8):1009-1023.
27. Marzilli M, Merz CN, Boden WE, et al. Obstructive coronary atherosclerosis and ischemic heart disease: an elusive link! *J Am Coll Cardiol.* Sep 11 2012;60(11):951-956.

28. Koo BK, Erglis A, Doh JH, et al. Diagnosis of ischemia-causing coronary stenoses by noninvasive fractional flow reserve computed from coronary computed tomographic angiograms. Results from the prospective multicenter DISCOVER-FLOW (Diagnosis of Ischemia-Causing Stenoses Obtained Via Noninvasive Fractional Flow Reserve) study. *J Am Coll Cardiol.* Nov 1 2011;58(19):1989-1997.
29. Min JK, Leipsic J, Pencina MJ, et al. Diagnostic accuracy of fractional flow reserve from anatomic CT angiography. *JAMA.* Sep 26 2012;308(12):1237-1245.
30. Bamberg F, Becker A, Schwarz F, et al. Detection of Hemodynamically Significant Coronary Artery Stenosis: Incremental Diagnostic Value of Dynamic CT-based Myocardial Perfusion Imaging. *Radiology.* Sep 2011;260(3):689-698.
31. Ho KT, Chua KC, Klotz E, Panknin C. Stress and rest dynamic myocardial perfusion imaging by evaluation of complete time-attenuation curves with dual-source CT. *JACC Cardiovasc Imaging.* Aug 2010;3(8):811-820.
32. Ko BS, Cameron JD, Meredith IT, et al. Computed tomography stress myocardial perfusion imaging in patients considered for revascularization: a comparison with fractional flow reserve. *Eur Heart J.* Aug 2 2011.
33. Bamberg F, Hinkel R, Schwarz F, et al. Accuracy of dynamic computed tomography adenosine stress myocardial perfusion imaging in estimating myocardial blood flow at various degrees of coronary artery stenosis using a porcine animal model. *Invest Radiol.* Jan 2012;47(1):71-77.
34. Rossi A, Uitterdijk A, Dijkshoorn M, et al. Quantification of myocardial blood flow by adenosine-stress CT perfusion imaging in pigs during various degrees of stenosis correlates well with coronary artery blood flow and fractional flow reserve. *Eur Heart J Cardiovasc Imaging.* Jul 26 2012.

CHAPTER 5

MYOCARDIAL PERFUSION WITH MULTISLICE COMPUTED TOMOGRAPHY IN STABLE ANGINA PECTORIS.

2013 Accepted for publication in Radiology.

A Rossi
D Merkus
E Klotz
N Mollet
PJ de Feyter
GP Krestin

ESSENTIALS

(1) Optimal management of symptomatic patients with coronary artery disease requires both anatomical and functional information. CT coronary angiography is a well-established non invasive imaging technique for the detection of coronary artery stenoses but it has limited accuracy in determining whether a coronary stenosis causes myocardial ischemia.

(2) New technical developments, such as improved temporal and spatial resolution and increased coverage, allow CT to evaluate myocardial perfusion during pharmacological stress.

(3) Preliminary reports of myocardial CT perfusion imaging are promising but several key issues must be addressed before CT perfusion can be implemented in clinical practice. Foremost, the radiation dose of CT perfusion imaging is of concern. Perfusion imaging protocols should be optimized to minimize radiation dose with preservation of image quality.

(4) Standard CT coronary angiography with complementary CT perfusion imaging provides comprehensive anatomical and functional information of coronary lesions.

SUMMARY STATEMENT

The addition of CT myocardial perfusion imaging to the standard CT coronary angiography provides complementary anatomical and functional information in a single examination which may be helpful to improve patient management.

ABSTRACT

CT coronary angiography (CTCA) is a well-established non invasive imaging modality for detection of coronary stenosis but it has limited accuracy in determining whether a coronary stenosis is hemodynamically significant. An additional functional test is often required because both anatomical and functional information is needed for guiding patient's management.

Recent developments in CT technology allow CT evaluation of myocardial perfusion during vasodilator stress, thereby providing information about myocardial ischemia. Several single-center studies have established the feasibility of stress myocardial CT perfusion (CTP) imaging in small groups of patients and have shown that stress myocardial CTP in combination with CTCA improved the diagnostic accuracy in comparison with CTCA alone. However CTP acquisition protocols must be optimized in terms of acquisition and reconstruction parameters, contrast material protocol injections and radiation dose. Further research is needed to establish the clinical usefulness of this novel technique.

In this review we provide an overview of (1) the physiology of coronary circulation and myocardial perfusion, (2) describe the technical pre-requisites, challenges and mathematical modeling related to CTP imaging, (3) note recent advances in CT scanners and CTP protocols, and (4) discuss the interpretation of CTP images. Finally we review, summarize the current literature and discuss future directions for research.

BACKGROUND

WHY IS THERE A NEED FOR CT MYOCARDIAL PERFUSION IMAGING?

CT coronary angiography (CTCA) has high reliability to exclude coronary artery disease (high negative predictive value) but it is limited in detecting obstructive coronary artery stenoses as reflected by a moderate positive predictive value [1-3]. CTCA has low predictive value in assessing the physiological importance of coronary stenoses in particular in the presence of intermediate lesions (40-70% diameter stenosis) when compared to myocardial perfusion as depicted by nuclear medicine [4-6] or intracoronary pressure measurements (Figure 1) [7]. The assessment of the hemodynamic significance of a lesion is important as this guides patient management. Non-flow-limiting coronary stenoses require optimal medical management [8, 9] while flow-limiting lesions may need revascularization with either percutaneous coronary intervention or coronary artery by-pass graft [10]. Therefore optimal management of symptomatic patients with coronary artery disease (CAD) requires information about anatomy and physiology. So far, this complementary information can be acquired using a number of different imaging modalities or hybrid scanners but recently, an awareness of the potential of CT to offer both anatomy and function in a single, stand-alone examination has initiated intense research to assess feasibility and future clinical implementation [11-21] of this technique.

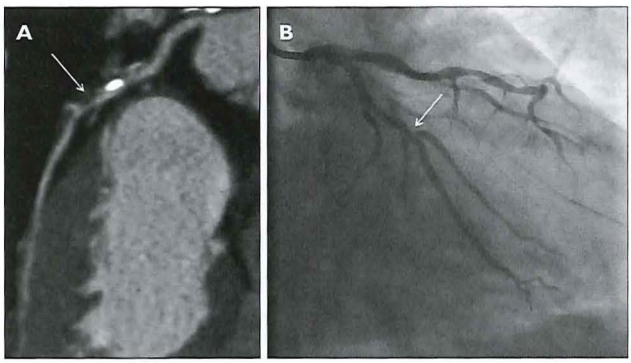

Figure 1. 54-year-old man with hypercholesterolemia and stable angina. Curved multiplanar reformat of the circumflex coronary artery from CT coronary angiography (dual source CT scanner) shows an intermediate coronary stenosis (arrow) due to a non calcified plaque (A) confirmed by conventional coronary angiography (B). The coronary artery lesion was determined not to be hemodynamically significant at FFR measurement (FFR of 0.92).

REGULATION OF CORONARY BLOOD FLOW DISTAL TO A CORONARY ARTERY STENOSIS

The function of the heart is critically dependent on aerobic metabolism. Since, even under resting conditions, the heart utilizes approximately 80% of the oxygen that is extracted from the coronary blood flow (CBF), any increase in oxygen demand must be met by an increase

in oxygen supply by increase of CBF [22]. CBF is determined by the pressure-gradient across the coronary vasculature and coronary vascular resistance. In normal, healthy individuals, the pressure-gradient across the coronary vasculature (i.e. arterial pressure-coronary venous pressure) is relatively constant. However, the presence of a stenosis in a large coronary artery creates an additional resistance, which causes a pressure-drop across the stenosis, thereby decreasing the effective perfusion pressure of the respective coronary vessel. The magnitude of the pressure-drop across the stenosis is determined by the severity as well as the flow through the stenosis.

The coronary vasculature is capable of maintaining basal resting flow constant over a wide range of perfusion pressures (from approximately 40-150 mmHg), by autoregulation, i.e. adjusting coronary (micro)vascular resistance (Figure 2). Thus, when coronary perfusion pressure is decreased, either by a decrease in aortic pressure or by the presence of a coronary artery stenosis, the distal coronary arterioles dilate, thereby decreasing their resistance and increasing intravascular blood volume to maintain basal myocardial flow [23, 24]. However, the capacity of the coronary vasculature to dilate is limited, and at rest condition becomes exhausted in the presence of severe coronary artery stenoses with >85% lumen reduction. During hyperemia, induced by exercise or pharmacological stress, the impairment of hyperemic flow starts already with 50% lumen reduction [25, 26].

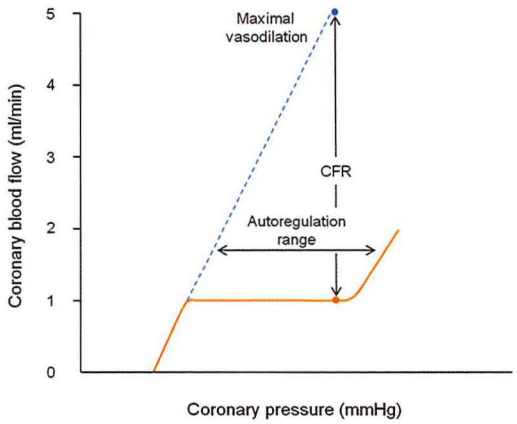

Figure 2. Relation between coronary blood flow and coronary pressure in the left ventricle. At rest the autoregulation mechanism maintains coronary blood flow constant over a wide range of coronary perfusion pressure. During stress conditions, induced by exercise or pharmacological stress, the basal coronary flow (orange circle) increased by a factor 5 (blue circle) when coronary arteries are normal. The ratio of coronary blood flow during stress to the resting flow is called coronary flow reserve (CFR).

In a maximally vasodilated bed, CBF is linearly related to coronary perfusion pressure. Coronary flow reserve (CFR) is the ratio of coronary blood flow during exercise or pharmacological induced maximal coronary vasodilation to the resting flow distal to the stenosis [26]. The CFR is an integrated measure of flow through both the large epicardial coronary arteries and the microcirculation. In the absence of a coronary stenosis and normal microcirculation the CFR may be a factor 5 or more. A reduced CFR may result from either an epicardial stenosis or dysfunctional coronary microcirculation or both [22, 25, 27, 28].

The inability of CFR to indicate which component is affected led to the introduction of the concept of fractional flow reserve (FFR). Indeed FFR can assess the functional importance of an epicardial coronary stenosis alone. FFR is defined as the maximal achievable blood flow to a myocardial territory in the presence of a stenosis as a ratio to the normal achievable blood flow to the same myocardial territory if the same artery was normal [29]. In clinical practice the FFR is measured as the ratio of the distal coronary pressure to the proximal aortic pressure. A coronary stenosis associated to a FFR<0.80 is usually considered clinically significant and should be treated [9, 30].

Vasodilator capacity is not homogeneously distributed in the myocardium. The subendocardium is burdened with higher extravascular compressive forces and consequent lower vasodilator capacity compared to the subepicardium. In addition, under rest conditions, the oxygen demand and consequently the CBF is higher in the subendocardium than in the subepicardium. This translates into a lower CFR of the subendocardium compared to the subepicardium. The post-stenotic pressure break point, where autoregulation fails, is 40 mmHg for the subendocardium and 25 mmHg for the subepicardium. These factors make subendocardium more sensitive to ischemia which starts from the inner layers of the left ventricle wall with a trans-mural spread from endocardium to epicardium [31-33].

TECHNICAL CONSIDERATIONS FOR CT PERFUSION IMAGING

Cardiac CT is a well-established modality for the evaluation of coronary anatomy and cardiac ventricular function. Imaging of myocardial perfusion with CT was performed as early as 1980's [34-36] but its routine clinical use has remained elusive due to overwhelming technical issues that could not be met with earlier CT technology. Recently, the technical improvements of the CT scanners, such as increased temporal and spatial resolution and increased coverage, have renewed the interest in performing myocardial CT perfusion (CTP) imaging.

PRE-REQUISITES FOR CT MYOCARDIAL PERFUSION IMAGING

CONTRAST MATERIAL

CT perfusion techniques image the transit of the contrast material from the coronary arteries to the myocardium. Because iodine contrast material attenuates X-ray proportional to its concentration, hypoattenuated areas in the myocardium represent myocardial regions of hypoperfusion and/or reduced intravascular blood volume.

TIME OF CT ACQUISITION

CT perfusion imaging should be performed during the early portion of first pass circulation when iodine contrast is mainly intravascular [37]. Indeed in the myocardium the highest contrast

level is reached at 1 minute after the injection followed by an initially rapid and then slower decline [37].

TEMPORAL RESOLUTION

The use of adenosine during stress myocardial perfusion test induces an increase of the heart rate of 10-20 beats above the heart rate at rest. Higher heart rates carry a higher likelihood of motion artifacts which compromises the evaluation of myocardial CTP imaging. Temporal resolution is, simply, how fast a single image of the heart can be obtained. Thereby the highest possible temporal resolution is needed to reduce cardiac motion artifacts. Indeed, even if no directly visible artifacts are present, insufficient temporal resolution limits the correct partial volume free delineation of the myocardial wall. The introduction of 64 detector CT scanners led to a substantial improvement, over previous 16 detector CT scanners, of temporal resolution of up to 165 ms. However this temporal resolution is still too limited in subjects with high heart rates. Dual source CT (DSCT) was designed to further improve the temporal resolution. DSCT is equipped with two x-rays and two detectors with an angular offset of 90° (first generation) or 95° (second generation). Due to this configuration the data needed for the full image reconstruction are sampled during a quarter rotation scanning instead of half rotation requested by single source CT [38, 39]. DSCT systems feature a temporal resolution of 83 ms (first generation) or 75 ms (second generation) which allows scanning at higher heart rates resulting from the heart rate increase of adenosine stress perfusion. In addition to a high temporal resolution, for dynamic, i.e., repetitive, scanning of the heart a sufficiently high temporal sampling rate (i.e., frequency at which the CT scanner acquires consecutive CT datasets over time) is also required to accurately assess the temporal changes of contrast enhancement over time.

SPATIAL AND CONTRAST RESOLUTION

High spatial resolution is an important pre-requisite in the assessment of myocardial perfusion. The higher spatial resolution of the multi-slice CT technology and capability to virtually freeze motion compared to nuclear modalities allows reliable assessment of subendocardial versus subepicardial myocardial perfusion. Myocardial CTP has relatively poor contrast resolution. After administration of contrast material the difference in HU between the normal and the hypoperfused myocardium remains small in the order of 50 HU as reported by George et al [40]. Because iodine is a chemical element with high atomic number lowering tube voltage increases its attenuation [41]. The lowest kV setting is recommended to obtain maximum attenuation difference. Because lowering kV settings increases image noise 100 kV should be used in most patients reserving 80 kV for very slim patients (BMI<25) and 120 kV for heavier patients (BMI >30).

Z AXIS COVERAGE

64-slice CT and first generation DSCT enable the acquisition of a limited area of the myocardium per gantry rotation (coverage) if the table remains in the same position as was the case in the initial CTP reports [42]. The ideal detector array for myocardial perfusion imaging would be wide enough to cover the entire left ventricle myocardium within one gantry ro-

tation. This can be achieved, for example, with a 320-slice CT which has a detector width of 16 cm and provides 12 to 14 cm of cranio-caudal coverage per gantry rotation. This in principle allows acquisition of the heart in within a fraction of a single heart beat with a lower probability of irregularities of the cardiac rhythm and more homogeneous attenuation of the myocardium. Unfortunately the limited temporal resolution of this system (175 ms) makes it less suited for higher heart rates.

Recently myocardial perfusion imaging technology has been incorporated in the second generation DSCT with ECG-triggered sequential scan CT data acquired at 2 different table positions with the table moving back and forth between the 2 scan positions (shuttle mode). Given a detector size of 38 mm and an overlap of 10% between the two consecutive scan positions the final coverage is limited to only 7.3 cm. This coverage should be large enough to collect information about myocardial perfusion in end-systolic phase when the size of the heart is smaller and the thickness of the myocardial wall is higher (compared to diastolic phase) [21]. Performing the acquisition during the systolic phase provides some advantages for CTP imaging. The systolic phase is shorter than the diastolic phase but it has a quite stable length of about 200 ms and it is not affected by extrasystolic events. In addition the intraventricular amount of contrast medium is lower compared to the diastolic phase reducing the beam hardening artifact and thereby the fluctuation of the CT numbers [21].

ACQUISITION OF IMAGES

Myocardial CTP imaging can be performed in two ways: static CTP imaging and dynamic CTP imaging.

STATIC CTP IMAGING

Static CTP imaging refers to the assessment of myocardial perfusion obtained from a single data sample of contrast-enhancement acquired during first-pass myocardial enhancement of CTCA. This snapshot sample is obtained from the entire heart, i.e from base to apex, as the table moves through the gantry during CTCA data acquisition during several heart beats.

The assessment of myocardial perfusion is qualitative by comparing the attenuation of the ischemic area to the density of a remote normal myocardium or normalizing it to the left ventricular cavity. Myocardial ischemia may not be detected in cases of balanced ischemia as may occur in patients with CAD involving all three coronary vessels.

Static CTP imaging is highly dependent on the contrast bolus timing. A drawback of static CTP is that the peak attenuation may be missed because only one sample of data is acquired. In addition, if data are obtained from sequential heart beats there can be heterogeneous attenuation from base to apex.

Recently static CT perfusion imaging has been performed using the dual energy mode. Currently there are three different ways to perform dual energy myocardial CTP. The first is the use of a DSCT scanner in which the two tubes operate at two different kV settings that allows acquiring simultaneously two different datasets at low (100 kV) and high kV (140 kV) [20, 43-48]. A merged dataset which combines the lower noise of the higher energy level and the higher contrast resolution of the lower energy level is used to create a better definition between normal perfused and hypoperfused myocardium and allows one to construct iodine concentration maps (Figure 3). The amount of iodine per voxel can be quantified with normalization

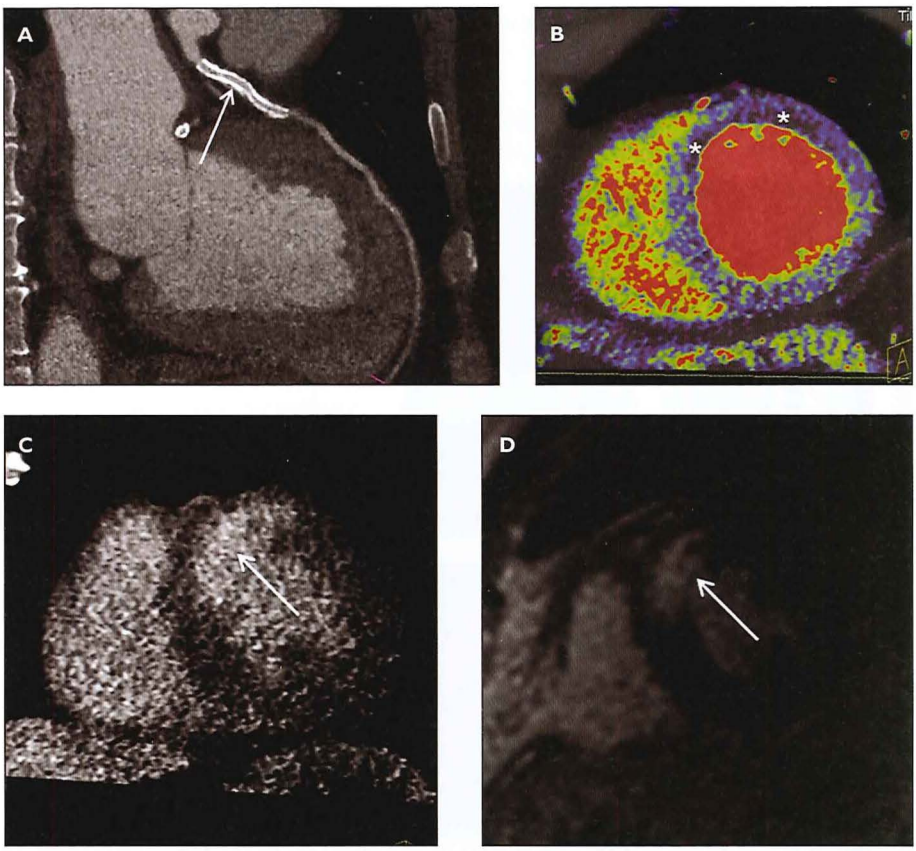

Figure 3. 58-year-old man with history of antero-septal infarction and prior LAD stent placement. Curved multiplanar reformat of the left anterior descending coronary artery (A) shows a patent stent (arrow) in the proximal part of the vessel. Iodine concentration map of the myocardium from dual energy CT (dual source CT scanner) acquisition (B) reveals a subendocardial hypoperfused area in the anterior and antero-septal myocardial segments suggestive for myocardial infarction (*). CT delayed enhancement image (C) shows a hyperdense area in the anterior and antero-septal myocardial segments representing myocardial infarction (arrow). . T1 weighted-inversion recovery gradient echo sequence 20 minutes after infusion of gadolinium (TR: 6.3; TE: 1.5; flip angle 20°; inversion pulse of 180°; matrix 192 x 160) (D) shows a hyperintense area in the same myocardial territories described above confirming the presence of myocardial infarction (arrow).

of the iodine of the ischemic area to normal myocardium or the left ventricular cavity. This is achieved at the price of a reduction of the temporal resolution by 50% because images are acquired from one half of the gantry rotation. However a second generation DSCT algorithm permits maintaining the high temporal resolution of DSCT (75 ms) when used in dual energy mode [49]. The second approach uses a CT scanner with a single x-ray source which rapidly switches between 80 kV and 140 kV [50, 51], which operates at a rotation time of 0.5 s and therefore has a temporal resolution of only 250 ms. The third approach uses a sandwich detector technology. The two detectors are superimposed and are composed of different materials. The top layer detector absorbs low energy X-ray photons, whereas the bottom-layer detector absorbs higher energy X-ray photons [52].

DYNAMIC CTP IMAGING

Dynamic CTP imaging refers to the assessment of myocardial perfusion obtained from multiple samples of myocardial attenuation at sequential time points of contrast enhancement after injection of a short contrast bolus to create time-attenuation curves (TAC). This can be performed while the table is stationary or in shuttle mode [53]. With the shuttle mode technique CT data are acquired at two alternative table positions by moving the table back and forth thereby covering the entire myocardium in end-systolic phase. The big advantage of dynamic imaging is

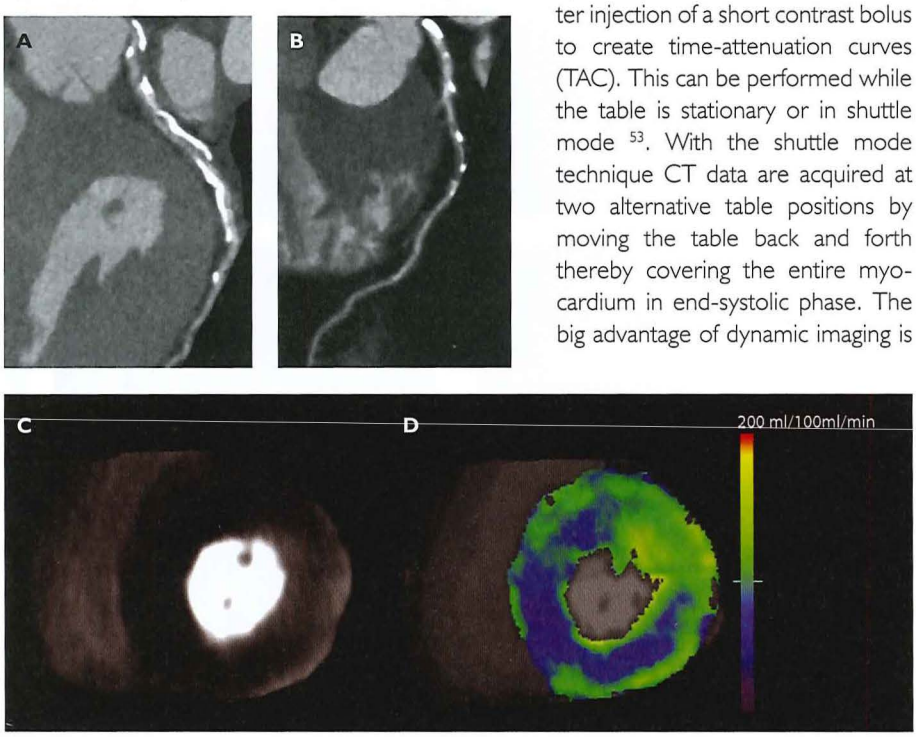

Figure 4. 60-year-old man with typical angina. Curved multiplanar reformat images show extensive highly calcified plaques in the left anterior descending coronary artery, LAD, (A) and in the circumflex coronary artery, CX (B). Stress dynamic CT perfusion imaging, acquired using a dual source CT scanner, shows a perfusion defect in the anterior, antero-septal, infero-septal, and inferior myocardial wall (C) in a patient with left dominant coronary system. The color-code map (D) demonstrates substantially reduced myocardial perfusion in the anterior and antero-septal walls (86 ml/100ml/min) related to the LAD as well as the inferior and infero-septal wall (48 ml/100ml/min) related to the CX.

the ability to quantify myocardial blood flow (MBF) (Figure 4), myocardial blood volume and potentially other hemodynamic parameters by applying different mathematical models to the TACs. The parameters utilized and how accurately they can be determined strongly depend on the temporal sampling rate. While it would be desirable to scan the whole heart during the heartbeat necessary to sample TAC this is either technically impossible (see shuttle mode technique) or requires unacceptable radiation burden. In addition dynamic acquisition may suffer from respiratory motion artifacts but correction algorithm is available [21].

CT PERFUSION IMAGING PROTOCOLS

PRE-MEDICATION AND PATIENT PREPARATION

Patients are advised to avoid caffeine before stress imaging because this may affect the vasodilator capacity of adenosine during stress. Although recent studies reported no effects of β-blockers on coronary flow reserve [54-56], the use of β-blockers before stress perfusion imaging is still contraindicated because they may mask ischemia.

Nitrates are contraindicated because they may interfere with adenosine, compromising the accuracy of ischemia detection [57].

In addition to the normal set-up for CTCA an additional intravenous catheter and an infusion pump for the stress agent are necessary for the acquisition of a stress phase. A 12-lead electrocardiography and a blood pressure monitor should also be present in the CT suite for continuous monitoring of the patient throughout the entire exam.

SCAN ACQUISITION

A myocardial CTP protocol should comprise a rest and a stress scan acquisition similar to nuclear medicine myocardial perfusion imaging (Figure 5). When the stress imaging is performed first, the detection of myocardial ischemia is optimized because the myocardium is not contaminated by previous injection of contrast material. In addition, the administration of β-blockers and nitrates before the rest scan is allowed without interfering with perfusion assessment. On the other hand, a rest CTCA scan followed by a stress scan is more suitable in clinical practice, as only patients with obstructive coronary stenoses or with highly calcified coronary arteries (or with stents) should undergo the stress phase and patients with absence of coronary artery disease do not require stress testing. The major disadvantage of this approach is the contamination by contrast material of the myocardium during the second acquisition which may mask an area of ischemia.

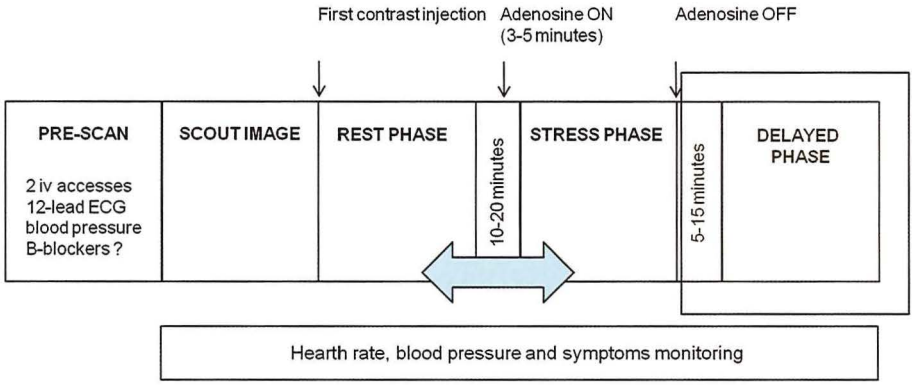

Figure 5. CTP imaging protocol. More details are explained in the text.

A delay of 10-20 minutes should be utilized between the two CT acquisitions to avoid contrast contamination of the myocardium and to resolve the effects of pharmacological stress. The resolution of pharmacologic stress can be determined by noting the resolution of ischemic related symptoms and the return of heart rate to baseline.

The rest phase is usually acquired using a prospective ECG triggering scan protocol [58, 59] or prospective ECG triggering high pitch spiral protocol [58, 60], implemented in a second generation DSCT, to minimize radiation dose. This phase is used for the evaluation of both myocardial perfusion at rest and coronary anatomy.

Stress phase imaging is performed under pharmacologically induced stress. The most common stress agents used in perfusion imaging are non-selective vasodilator agents: adenosine and dipyridamole. Adenosine acts directly on adenosine receptors causing coronary vasodilation while dipyrimadole increases the endogenous level of adenosine decreasing adenosine's reuptake by endothelial cells. The principle differences between adenosine and dipyrimadole are in their duration of action and method of infusion. The half-life of adenosine is few seconds and it is rapidly removed from the body. Dipyrimadole has longer half-life than adenosine, and aminophylline, an antagonist of adenosine receptors, may be required to reverse its effects. Adenosine is continuously infused at the dose of 0.14 mg/kg/min over 3 to 5 minutes while dipyridamole is infused at the dose of 0.56 mg/kg over 4 to 6 minutes. Both agents induce reflex tachycardia as the result of sympathetic stimulation and a decrease in systemic blood pressure which may alter the pressure gradient from aorta to the coronary venous bed and hence could reduce myocardial perfusion. They are both contraindicated in patients with asthma, chronic obstructive pulmonary disease and advanced atrio-ventricular block without functioning pacemaker [61].

Ragadenoson has also been used for stress myocardial perfusion imaging. It is a selective A_{2A} adenosine receptor leading to a selective coronary vasodilation and reducing the side effects in patients with airway disease. It is administered as a fixed unit intravenously followed by a

Table 1. Stress CT perfusion scan protocols.

	64-SLICE CT	WIDE DETECTOR CT (320-SLICE CT)	FIRST GENERATION DSCT	FIRST GENERATION DUAL ENERGY CT	SECOND GENERATION DSCT (SHUTTLE MODE)	SECOND GENERATION DUAL ENERGY CT
SCAN MODE	ECG gated retrospective scan	ECG triggered prospective scan (targeting 70 - 90% RR interval)	ECG gated retrospective scan with tube current modulation	ECG gated retrospective scan with tube current modulation	ECG triggered prospective scan	ECG gated retrospective scan with tube current modulation
DETECTOR COLLIMATION	64 x 0.5 mm	320 x 0.5 mm	2 x 32 x 0.6 mm (z-flying focal spot technique)	2 x 32 x 0.6 mm (z-flying focal spot technique)	2 x 64 x 0.6 mm (z-flying focal spot technique)	2 x 64 x 0.6 mm (z-flying focal spot technique)
TUBE CURRENT	400 mA	320-500 mAs (based on BMI)	330-370 mAs (based on BMI)	150 mAs/rot (tube A) 165 mAs/rot (tube B)	300 mAs/rot	150 mAs/rot (tube A) 165 mAs/rot (tube B)
VOLTAGE	120 kV	120 kV	100 or 120 kV (based on BMI)	140 kV (tube A) 100 kV (tube B)	100 kV	140 kV (tube A) 100 kV (tube B)
GANTRY ROTATION	400 ms	350 ms	330 ms	330 ms	285 ms	285 ms
TEMPORAL RESOLUTION	200 ms	175 ms	83 ms	165 ms	75 ms	75 ms (hybrid reconstruction algorithm)
AMOUNT OF CONTRAST	90-95 ml @ 5 ml/s	50-70 ml @ 4-5 ml/s	65 ml @ 4-5 ml/s	60 ml @ 6 ml/s + 50 ml 70%/30% saline/contrast @ 6 ml/s	50 ml @ 5 ml/s	100 ml @ 5-6 ml/s
TYPE OF PERFUSION IMAGING	Static	Static	Static	Static	Dynamic	Static

ADVANTAGES		Temporal uniform contrast enhancement from base to apex No slab misregistration artifacts	High temporal resolution (83 ms)	Iodine map	Quantification of MBF	Iodine map Maintained temporal resolution (75 ms)
DISADVANTAGES	Low temporal resolution Prolonged scan time and breath-holding No temporal uniform contrast enhancement from base to apex Slab misregistration artifacts High radiation dose	Low temporal resolution	Prolonged scan time and breath-holding No temporal uniform contrast enhancement from base to apex Slab misregistration artifacts High radiation dose	Reduced temporal resolution (165 ms)	Limited coverage (73 mm) High radiation dose	

saline chaser and the peak of vasodilation is reached at 2 to 4 minutes after injection. It is contraindicated in patients with second or third atrio-ventricular block without pacemaker.

Scan protocols for stress CTP imaging using different CT scanners are reported in table 1.

A third optional CT delayed scan can be performed to complete the CTP protocol for the discrimination between viable and non-viable myocardium. No additional administration of contrast material is needed because it employs the effect of contrast material injected during the previous CT acquisitions. In our department the acquisition is prospectively ECG-triggered at systolic phase and it is performed 5-10 minutes after the second CT scan [62, 63]. Low tube voltage settings (80 or 100 kV) seem to be advantageous by improving the contrast resolution between normal and infarcted myocardium [64]. Tube current is optimized based on patient size ranging between 320 mAs (patients with BMI<30) and 370 mAS (patients with BMI>30). Further research is needed to establish the role of delayed enhancement phase in a CTP protocol for the detection of myocardial infarction.

ANALYSIS OF MYOCARDIAL CT PERFUSION IMAGING

VISUAL ANALYSIS OF CTP IMAGING

Visual assessment of CTP images is the most common approach for qualitative assessment of myocardial perfusion. The normal myocardium enhances homogeneously after the injection of intravenous contrast material. During the first pass, contrast material diffuses to the interstitial space with homogeneous incremental increase of myocarial signal intensity over time that is directly proportional to iodine content in the tissue. Normal left ventricular myocardial enhancement demonstrates substantially lower attenuation in the lateral wall when compared with the anterior, septal and inferior walls in patients with normal coronary arteries. The lateral myocardial wall is located adjacent to the air within the lungs and it is not subjected to the same beam-hardening effect (see paragraph "Artifacts") as the inferior and the septal myocardium which are located near more dense thoracic structures. This may result in a lower attenuation. [65]. The increased attenuation during the first pass is followed by the wash out of the contrast material. Ischemic myocardium demonstrates decreased wash-in and delayed time to peak attenuation with normal wash-out of contrast material (Figure 6) [42]. Infarcted myocardium shows both a slow wash-in and a slow wash-out of the contrast material [62] resulting in lower delayed peak attenuation.

First pass CTP imaging, with and without pharmacological stress, has been used to identify areas of decreased myocardial perfusion in a similar manner to radionuclide perfusion imaging and magnetic resonance perfusion imaging [15, 17, 62, 66-72]. Areas of reduced perfusion appear hypo-enhanced compared to the normal myocardium which implies either myocardial ischemia or myocardial infarction. In addition, delayed enhancement CT imaging, performed

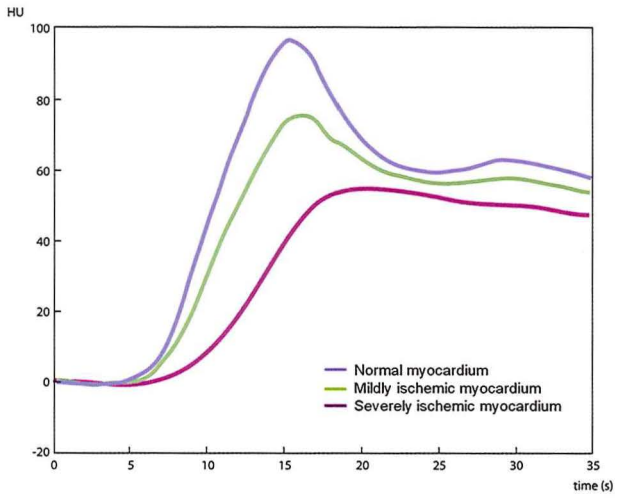

Figure 6. Comparison of wash-in and wash-out kinetics of iodinated contrast material in a normal myocardium (blue line), in a moderate ischemic myocardium (green line) and in severe ischemic myocardium (purple line).

5-15 minutes after the first injection of contrast material, can depict findings specific for irreversible cell damage and it has been used to discriminate between viable and infarcted (non viable) myocardium. Hyper-enhanced bright myocardial areas, confined to a specific vessel territory and with an endo-epicardial spread pattern, during delayed CT imaging are scar tissue caused by myocardial infarction [63, 73-75].

QUANTITATIVE CTP IMAGING

Semi-quantitative or fully quantitative evaluation of myocardial perfusion by CT scanners is feasible by assessment of the inflow and outflow characteristics of iodine contrast agent in the myocardium over time.

SEMI-QUANTITATIVE ANALYSIS OF CTP IMAGING

The semi-quantitative approach assesses the mean signal attenuation of the myocardium within a region of interest over time resulting in TACs (Figure 7). Several parameters which are indexes of regional myocardial flow can be extracted from that curve: upslope, time to peak, maximal signal density, and time to 50% of maximal signal density. The upslope method [14, 42] initially applied to magnetic resonance studies [76], is considered the most reliable semi-quantitative parameter for evaluating perfusion imaging [77]. The upslope of a TAC is calculated applying a linear fit line to the time-attenuation data. Only the upslope of the TAC curve is required to assess semi-quantitatively myocardial perfusion with this method, thereby reducing the sampling points and the radiation dose.

FULLY-QUANTITATIVE ANALYSIS OF CTP IMAGING

Mathematical modeling of myocardial tissue TACs follows similar indicator dilution principles as have been used for the analysis of cerebral ischemia as well as organ and tumor perfu-

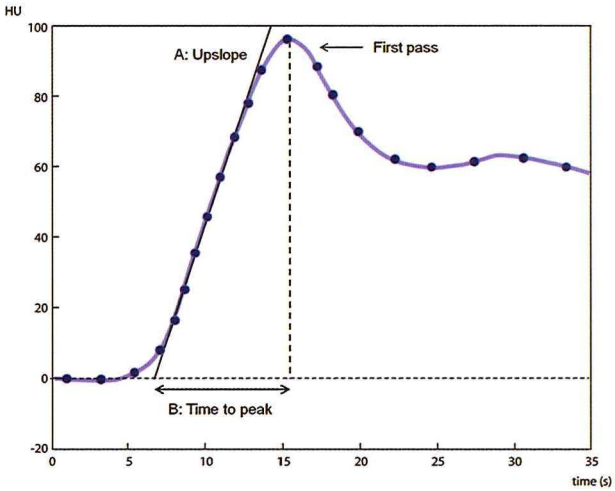

Figure 7. Time-attenuation curve of normal myocardium within a region of interest obtained by fitting several sampling (circles) of the myocardium over time.
(A: upslope of the curve; B: time to peak; dashed line: maximal signal intensity).

sion. The myocardium, however, particularly if measured under stress, is substantially more challenging than these applications in the brain. In order to acquire optimal data, each system parameter challenges current technical limitations. Ideally data should be obtained from a detector wide enough to cover the whole heart in end-systolic phase (10 to 12 cm), with a 360 degree temporal resolution of less than 100 ms (avoiding partial reconstruction artifacts). In addition the system should be capable of acquiring data for every heartbeat for a total duration of about 30 s. As the optimal injection protocol would be as short as possible (not exceeding about 5 s of injection time) in order to get a "sharp" arterial input function (AIF) the iodine sensitivity of the system would have to be good enough to still provide acceptable contrast to noise ratio despite lower enhancement levels. While partial solutions for each of these requirements can be found, a complete system that fulfills all is not yet available.

Currently the rather high radiation exposure during CTP is of concern. The minimum radiation exposure required to sample one point of the TAC is on the order of 1 mSv [11, 21, 78, 79]. Acquiring dynamic data at 80 bpm for 30 s would require 40 scans and result in about 40 time sample points (scans) for one study (rest or stress). Although further dose reduction techniques might still reduce these values it is unlikely that they will decrease by one order of magnitude. A balance should be sought between radiation dose and adequate clinical information derived from dynamic CTP. In this respect quantitative dynamic myocardial perfusion imaging is now an active research area and a full discussion of all the approaches under investigation is beyond the scope of this review. We will only discuss some basic principles and limitations.

The extraction fraction of the myocardium for small tracer molecules such as iodine contrast media is high and any modeling that assumes that the tracer stays intravascular for any relevant amount of time is probably not correct.

Vasodilatory "stress" studies pose specific challenges: as the heart rate and actual cardiac work increase only by a small amount the flow extraction product, i.e. the actual extravascular flow that reaches interstitial space, remains relatively constant in the normal myocardium. The additional "stress" blood flow is mainly intracapillary with a very short transit time (about 2s or potentially even less). As a consequence, temporal undersampling affects stress studies more than rest studies and the normal myocardium more than ischemic myocardium.

Maximum enhancement (Mullani-Gould) method
This method was only used for region of interest (ROI) analysis in the initial electron beam CT studies [34-36, 80] and has not been used since. MBF is calculated by dividing the peak of the tissue TAC by the area under the AIF until this peak is reached. The restrictions are more severe than for the maximum slope method and agreement to comparison techniques was achieved only by using a large relatively arbitrary empirical correction factor.

Maximum slope method
The maximum slope method can be derived from the Fick principle and calculates MBF by dividing the maximum gradient of the tissue TAC by the peak of the AIF. This derivation is the methodological basis of all upslope techniques even if an explicit AIF is not available. It has been used for ROI based rest perfusion assessment with CT [81, 82]. The method provides accurate MBF values only if the maximum gradient is reached earlier than the transit time of the tissue. If the maximum gradient is reached later MBF values will increasingly be underestimated. As the maximum tissue gradient is reached simultaneously with the peak of the AIF the accuracy directly depends on the ratio of the injection time (or more strictly the bolus width or the time the AIF rises from zero to its peak) and the tissue transit time. Because the average transit time after stress (and particularly for the normal myocardium) is smaller than for rest and for ischemic areas, ratios of slopes or absolute values will tend to be smaller than expected. Further underestimation will occur if not the true maximum of the slope but rather the average of the upslope of the TAC is calculated.

Gamma variate curve fitting
This technique was used for the ROI analysis of electron beam CT animal data. Linear combinations of gamma variate functions are fit to the AIF and the tissue TACs. Mean transit time (MTT) and blood volume values were then calculated from the moments of the fit curves and MBF calculated using the central volume principle [24] . This study showed that the capillary MTT can be as small as 2 seconds. Despite otherwise best case conditions (intra-atrial CM injection, one scan every heart beat) the CFR determined after adenosine was not higher than 2 compared to the expected higher physiological value

Deconvolution method
In this approach the tissue TACs are fit by convolving the AIF with a parametric impulse residue function that models the temporal course of intra / extravascular tracer exchange as it would occur for an infinitesimally short bolus.

The simplest "complete" model which is frequently used is the "adiabatic approximation to the tissue homogeneity model" [83]. In order to reliably calculate intracapillary transit time this model explicitly requires that the temporal sampling rate must be better than the shortest transit time. So et al. [84] have recently used this approach in a clinical study acquiring data for every heart beat over 4 cm detector width. Nevertheless the CFR of the normal myocardium was not larger than about 2. The dose for 4 cm coverage was about 10 mSv.

Hybrid deconvolution / maximum slope
This approach combines deconvolution with the maximum slope method and was designed for the relatively low sampling rate (2 to 3s) of the shuttle mode. TACs are fit by convolving the AIF with a simplified impulse residue function that does not explicitly contain intravascular MTT but models the flow extraction product (ktrans). MBF is then determined from the maximum slope of the fit model curve making the slope determination more robust and more accurate [21]. This makes it particularly suited for parameter image calculation. Otherwise the approach shares the limitations of the maximum slope method: it underestimates CFR. Nevertheless it appears to have sufficient discriminatory power to quantitatively differentiate areas of relevant flow compromise and has been successfully used in several clinical studies [11, 14, 78]. The dose for 7.3 cm coverage is about 10 mSv.

IMAGE INTERPRETATION

The traditional approach uses both rest and stress myocardial perfusion imaging [85]. A perfusion defect is classified as non-reversible (or fixed) or reversible. In patients with scar tissue due to prior myocardial infarction a non-reversible pattern is seen: the perfusion defect appears during stress and remains visible at rest. A reversible perfusion defect is seen only on stress images and it is a sign of hemodynamically significant stenosis inducing reversible ischemia.

A second approach evaluates myocardial perfusion only during stress. The discrimination of a stress perfusion defect between viable and non-viable myocardium can be assessed performing CT delayed enhancement imaging (Figure 8 and Figure 9).

Stunned myocardium is viable myocardium salvaged by coronary reperfusion that shows post-ischemic dysfunction after reperfusion and it is associated with normal CTP at rest. Hibernating myocardium is ischemic myocardium in which ischemic cells remain viable but contraction is chronically depressed with reduced resting myocardial blood flow [86, 87] .

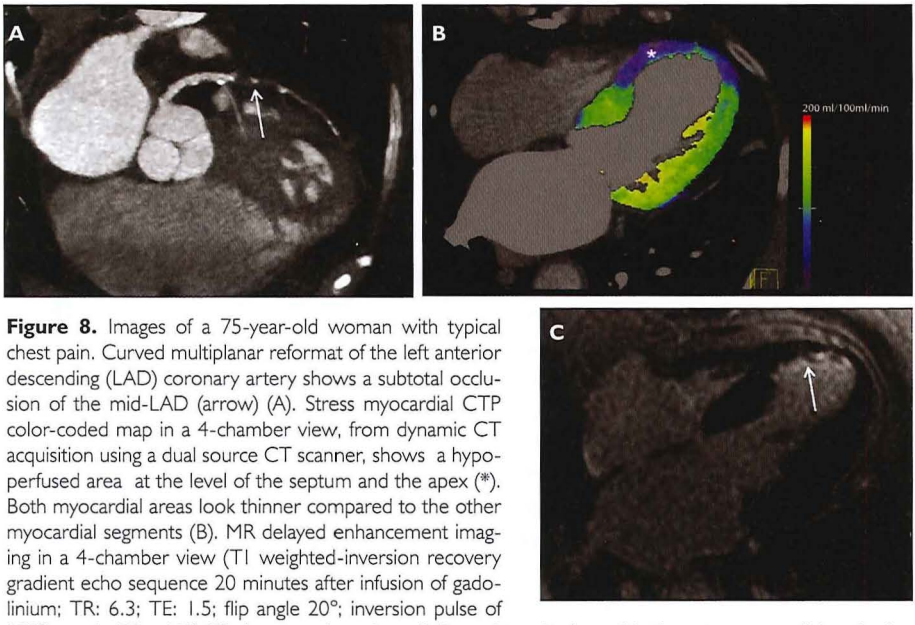

Figure 8. Images of a 75-year-old woman with typical chest pain. Curved multiplanar reformat of the left anterior descending (LAD) coronary artery shows a subtotal occlusion of the mid-LAD (arrow) (A). Stress myocardial CTP color-coded map in a 4-chamber view, from dynamic CT acquisition using a dual source CT scanner, shows a hypoperfused area at the level of the septum and the apex (*). Both myocardial areas look thinner compared to the other myocardial segments (B). MR delayed enhancement imaging in a 4-chamber view (T1 weighted-inversion recovery gradient echo sequence 20 minutes after infusion of gadolinium; TR: 6.3; TE: 1.5; flip angle 20°; inversion pulse of 180°; matrix 192 x 160) (C) shows a sub-endocardial hyperintensity (arrow) in the same myocardial territories revealing the presence of myocardial infarction.

ARTIFACTS

Several artifacts may mimic or mask a perfusion defect in myocardial CTP imaging. The high heart rate induced by the administration of adenosine increases the likelihood of cardiac motion artifacts that can appear as a myocardial perfusion defect. A good rule is to examine different cardiac phases. The persistence of a hypoperfused area in all phases suggests a true perfusion defect while an artifact usually disappears by examining additional cardiac phases.

The presence of very dense structures such as bone (sternum and spine) and contrast material in the left ventricular and atrial cavities or descending aorta can cause beam hardening. These high density objects preferentially absorb the low energy photons thereby increasing the mean energy of the remaining X-ray beam. This may result in a false hypo-enhanced area in the myocardium that can be misinterpreted as a perfusion defect. Beam hardening occurs more often in the postero-basal myocardial wall and its presence has also been related to the heart rate [88]. Beam hardening correction algorithms should be used to ensure an accurate assessment of myocardial perfusion [89, 90].

Misalignment artifacts occur by imaging the heart over several heart beats. They are more common with CT scanners which do not provide full cardiac coverage requiring spiral or shuttle mode scan protocols.

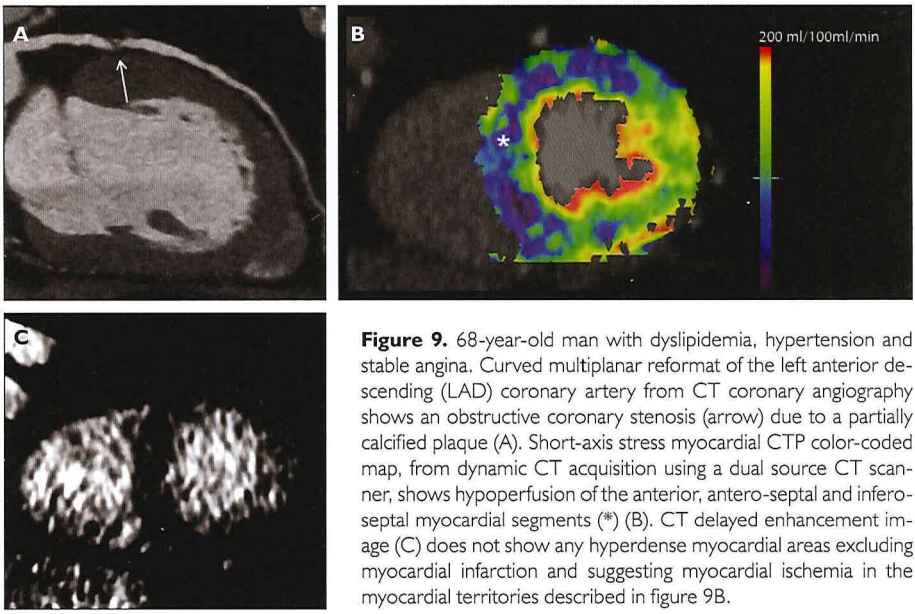

Figure 9. 68-year-old man with dyslipidemia, hypertension and stable angina. Curved multiplanar reformat of the left anterior descending (LAD) coronary artery from CT coronary angiography shows an obstructive coronary stenosis (arrow) due to a partially calcified plaque (A). Short-axis stress myocardial CTP color-coded map, from dynamic CT acquisition using a dual source CT scanner, shows hypoperfusion of the anterior, antero-septal and infero-septal myocardial segments (*) (B). CT delayed enhancement image (C) does not show any hyperdense myocardial areas excluding myocardial infarction and suggesting myocardial ischemia in the myocardial territories described in figure 9B.

CURRENT STATUS OF CTP IMAGING

First attempts of CTP imaging at rest were done in the late 1970's using first generation single-slice CT scanners [91-93]. However, it is only with the recent developments of the multi-slice CT scanners that reliable detection of myocardial ischemia with CT during pharmacological stress has become feasible.

Table 2,3, and 4 summarize the CTP studies performed to date.

STATIC CT PERFUSION IMAGING

Kurata et al. [66] were the first to explore the feasibility of CTP imaging during infusion of adenosine, showing a good agreement (83%) between stress CT and stress SPECT. The number of non-assessable myocardial territories during stress was higher (68/141) than at rest (126/141) revealing that the temporal resolution of 16-slice CT was not sufficient to provide diagnostic image quality at the higher heart rates which occur during adenosine stress acquisition.

The introduction of 64-slice CT led to an improvement in the performance of adenosine CTP imaging. George et al [94] demonstrated the feasibility of adenosine CTP imaging in a ca-

Table 2. Studies using stress static CTP imaging

AUTHOR	STUDY POPULATION	CT SCANNER	CT PROTOCOL	STRESSOR	IMAGE ANALYSIS	REFERENCE STANDARD	CT EFFECTIVE DOSE (mSv)[a]	SENSITIVITY	SPECIFICITY	PPV	NPV
GEORGE ET AL. [94] (2006)	Animal study	64- slice CT	ECG-GR scan	Adenosine (0.14 mg/kg/min)	Regional signal density ratio normalized to left ventricular blood pool between ischemic and remote myocardial	Microspheres MBF	N.A.	N.A.	N.A.	N.A.	N.A.
KURATA ET AL. [66] (2005)	Human study (12 patients)	16-slice CT	1. Stress CTP ECG-GR scan 2. Rest ECG-GR scan (coronaries-perfusion)	Adenosine (0.16 mg/kg/min)	Visual assessment	Stress SPECT	NA	NA	NA	NA	NA
BLANKSTEIN ET AL. [15] (2009)	Human study (34 patients)	First generation DSCT	1. Stress CTP ECG-GR scan 2. Rest ECG-TP scan (coronaries-perfusion). 3. ECG -TP DE scan.	Adenosine (0.14 mg/kg/min)	Visual assessment	Rest and stress SPECT	9.1 (k=0.017)	84%	80%	71%	90%
ROCHA-FILHO ET AL. [72] (2010)	Human study (35 patients)	First generation DSCT	1. Stress CTP ECG-GR scan 2. Rest ECG-TP scan (coronaries-perfusion).	Adenosine (0.14 mg/kg/min)	Visual assessment	QCA	9.8 (k=0.017)	90%	69%	77%	85%
FEUTCHER ET AL. [18] (2011)	Human study (25 patients)	Second generation DSCT	1. Stress CTP high pitch spiral 2. Rest high pitch spiral CT/ ECG-TP	Adenosine (0.14 mg/kg/min)	Visual assessment	MR (stress perfusion and delayed enhancement)	0.93 (k=0.014)	78%	88%	83%	84%

CURY ET AL. [16] (2011)	Human study (26 patients)	64-row CT	1. Stress CTP ECG-GR scan 2. Rest ECG-GR scan	Dypirimadole (0.56 mg/min)	Visual assessment	SPECT	14.4 (both CT scans) (k=0.014)	94%	78%	89%	87%

DSCT: dual-source CT; CTP: CT perfusion; ECG-GR: ECG gated retrospective scan; ECG-TP scan: ECG triggered prospective scan; MBF: myocardial blood flow; DE: delayed enhancement; NA: non-assessable

a: radiation dose only for the stress perfusion acquisition

nine model of LAD stenosis showing that first-pass myocardial perfusion information can be extracted from these CT images. Later studies confirmed the potential of CTP imaging in humans. Blankstein et al. [15] evaluated 34 patients who underwent DSCT, nuclear stress testing and coronary angiography. Stress CTP imaging alone had a sensitivity of 93% and a specificity of 74% in detecting flow-limiting stenosis using SPECT as reference standard. The same investigators [72] then showed that stress CTP imaging adds incremental value to CTCA in the detection of obstructive coronary stenoses. The combined protocol was superior and had a sensitivity of 91%, a specificity of 93%, a PPV of 86% and a NPV of 93% compared to 83%, 71%, 66% and 87%, respectively of CTCA alone. George et al. [32] quantified the transmural extent of perfusion abnormalities on CTP images acquired during the infusion of adenosine. They found that the transmural perfusion ratio, defined as the ratio of the attenuation density of the specific subendocardium attenuation and the mean attenuation density of the entire subepicardial layer, was inversely related to the percent diameter stenosis measured by quantitative angiography. A similar finding was also demonstrated by Cury and colleagues using dypiridamole as stress agent [16].

Ko et al. [19] investigated 42 patients who underwent CTP imaging but, in contrast to earlier studies, they used invasive FFR as reference standard. Although the specificity in predicting ischemia was very high (98%) when CTCA and CTP imaging were concordant (obstructive coronary stenosis and perfusion defect or non-obstructive coronary stenosis and normal myocardial perfusion) the overall diagnostic accuracy was only 80%. Indeed, CTCA and CTP imaging were concordant in only 58% of the sampled territories.

Another possible clinical application of stress CTP imaging is the assessment of coronary stents. Magalhaes et al [95] demonstrated that the combination of CTCA and stress CTP imaging improved the diagnostic accuracy to detect in-stent restenosis to overcome "blooming" artifacts.

The addition of a stress CT scan to the conventional cardiac CT protocol raises the total radiation dose to the patient. A "low dose" CTP protocol has been reported by Feuchtner et al [18] who performed stress high pitch spiral CTP imaging in 25

Table 3. Studies using static dual energy CT perfusion imaging

AUTHOR	STUDY POPULATION	CT SCANNER	CT PROTOCOL	STRESSOR	IMAGE ANALYSIS	REFERENCE STANDARD	CT EFFECTIVE DOSE (mSv)[a]	SENSITIVITY	SPECIFICITY	PPV	NPV
KO ET AL. [20] (2011)	Human study (50 patients)	First generation DSCT	1. Stress CTP ECG-GR scan in dual energy mode	Adenosine (0.14 mg/kg/min)	Visual assessment	MRI	5.8 (k=0.017)	89%	79%	74%	91%
WEININGER ET AL. [97] (2010)	Human study (20 patients)	Second generation DSCT						87%	79%	50%	81%
	10 (Group A)		Group A: 1. Rest ECG-TP scan (coronaries-perfusion). 2. Stress dynamic CTP (shuttle mode) 3. ECG-TG DE scan.	Adenosine (0.14 mg/kg/min)	Visual assessment	Rest/stress first pass MRI Rest/stress SPECT	12.8±2.4	86% (MRI) 84% (SPECT)	98% (MRI) 92% (SPECT)	96% (MRI) 92% (SPECT)	94% (MRI) 88% (SPECT)
	10 (Group B)		Group B: 1. Stress CTP ECG-GR scan in dual energy mode. 2. ECG-TP DE scan.	Adenosine (0.14 mg/kg/min)	Visual assessment	Rest/stress first pass MRI Rest/stress SPECT	15.2±2.7	93% (MRI) 94% (SPECT)	99% (MRI) 98% (SPECT)	96% (MRI) 94% (SPECT)	96% (MRI) 94% (SPECT)

DSCT: dual-source CT; CTP: CT perfusion; ECG-GR: ECG gated retrospective scan; ECG-TP scan: ECG triggered prospective scan; MBF: myocardial blood flow; MRI: magnetic resonance imaging; SPECT: single photon emission computed tomography; DE: delayed enhancement; NA: non-assessable

a: radiation dose only for the stress perfusion acquisition

Table 4. Studies using stress dynamic CT perfusion imaging

AUTHOR	STUDY POPULATION	CT SCANNER	CT PROTOCOL	STRESSOR	IMAGE ANALYSIS	REFERENCE STANDARD	CT EFFECTIVE DOSE (mSv)[a]	SENSITIVITY	SPECIFICITY	PPV	NPV
GEORGE ET AL. [42] (2007)	Animal study	64-slice CT		Adenosine (0.14 mg/kg/min)	Semi-quantitative perfusion analysis (upslope method). Absolute quantification of MBF (model dependent deconvolution analysis).	Microspheres MBF	NA	NA	NA	NA	NA
MAHNKEN ET AL. [21] (2010)	Animal study	Second generation DSCT	Stress dynamic CTP (shuttle mode)	Adenosine (0.24 mg/kg/min)	Absolute quantification of MBF (compartment model).	NA	NA	NA	NA	NA	NA
CHRISTIAN ET AL.[99] (2010)	Animal study	64-slice CT	Stress CTP ECG-GR scan	Adenosine (0.80 mg/kg/min)	Semi-quantitative perfusion analysis (slope integral ratio).	Microspheres MBF	NA	NA	NA	NA	NA
BAMBERG ET AL. [12] (2012)	Animal study	Second generation DSCT	Stress dynamic CTP (shuttle mode)	Adenosine (0.14 mg/kg/min)	Absolute quantification of MBF (compartment model)	Microspheres MBF	11.3	NA	NA	NA	NA
KIDO ET AL. [100] (2008)	Human study (14 patients)	16-slice CT	Non ECG gated CTP scan	Adenosine (0.16 mg/kg/min)	Absolute quantification of MBF (Patlak plot method)	Stress SPECT	NA	87%	79%	50%	81%
BASTARRIKA ET AL. [14] (2010)	Human study (10 patients)	Second generation DSCT	1. Rest ECG-TP scan (coronaries-perfusion) 2. Stress dynamic CTP (shuttle mode) 3. ECG-TP DE scan	Adenosine (0.14 mg/kg/min)	Visual assessment Semiquantitative perfusion analysis (upslope method) Absolute quantification of MBF (compartment model).	First pass MR	12.5 (k=0.017)	NA	NA	NA	NA

HO ET AL. [78] **(2010)**	Human study (35 patients)	Second generation DSCT	1.Rest dynamic CTP (shuttle mode) 2. Stress dynamic CTP (shuttle mode) 3. Rest ECG-TP scan (coronaries)	Dypiridamole (0.56 mg/kg over 4 minutes)	Absolute quantification of MBF (compartment model)	SPECT	9.2 (k=0.014)	83%	78%	79%	82%
BAMBERG ET AL. [11] **(2011)**	Human study (33 patients)	Second generation DSCT	1. Rest ECG-TP scan 2. Stress dynamic CTP (shuttle mode)	Adenosine (0.14 mg/kg/min)	Absolute quantification of MBF (compartment model)	FFR	10.0±2.0 (k=0.017)	91%	98%	78%	99%
SO ET AL. [84] **(2012)**	Human study (26 patients)	64-slice CT	1. Rest dynamic CTP ECG-GR scan 2. Stress dynamic CTP ECG-GR scan	Dypiridamole (0.56 mg/kg over 4 minutes)	Absolute quantification of MBF	SPECT	9.7 (k=0.014)	95%	35%	83%	67%

DSCT: dual-source CT; CTP: CT perfusion; ECG-GR: ECG gated retrospective scan; ECG-TP scan: ECG triggered prospective scan; MBF: myocardial blood flow; DE: delayed enhancement; NA: non-assessable

a: radiation dose only for the stress perfusion acquisition

patients in combination with rest high pitch spiral CTCA/prospective CTCA. For the detection of any myocardial perfusion defect during the stress phase high pitch spiral CT showed a sensitivity of 78% and a specificity of 87% compared to cardiac MR (combination of stress perfusion and delayed enhancement imaging). Radiation exposure of the entire stress/rest CT protocol was only 2.5 mSv.

Dual Energy CT (DECT) scan mode has been investigated for the detection of myocardial perfusion defects. Preliminary results reported by Ruzsics et al. [48] showed that DECT has a sensitivity of 96% and a specificity of 95% in the detection of fixed perfusion defects using SPECT as reference standard. Recently Arnoldi and colleagues [96] demonstrated that the diagnostic performance of DECT, in particular using the iodine map, is higher than that of single energy CT in the detection of reversible and fixed myocardial perfusion defects seen on SPECT. The role of DECT in the setting of adenosine stress has also been tested by Ko et al. [20] They found that DECT had a sensitivity of 89% and a specificity of 78% in the detection of ischemic myocardial segments in a group of patients with known CAD, using MRI as the reference standard. Weininger et al. [97] determined the diagnostic accuracy of stress DECT in a small group of patients with acute chest pain. They reported a sensitivity and a specificity of 93% and 99% and 94% and 98% using MRI or SPECT, respectively, as reference standard.

DYNAMIC CT PERFUSION IMAGING

Quantification of MBF using dynamic CT scanning and iodine contrast material was first reported using the ultrafast electron beam CT scanners in the late 1980's. Several animal [34, 36] and human studies [35] reported a good correlation between electron beam CT-derived MBF and microspheres, the experimental reference standard, or indicator dilution methods. The latest technical developments of CT scanners, specifically improved temporal resolution and coverage, have prompted the study of stress dynamic perfusion imaging in animal models and its diagnostic performance in clinical practice. So et al.[98] performed dynamic perfusion imaging using a 16-slice CT in a porcine model with acute myocardial infarction. CT-derived MBF correlated well with microspheres-derived MBF and there was a good agreement with histology findings. George et al. [42] demonstrated a strong correlation between CT-derived MBF (using 64-slice CT in a canine model) and microspheres with only a modest overestimation of flow. Recently Manhken et al [21] illustrated the feasibility of a dynamic quantitative whole heart perfusion using the shuttle-mode technique implemented in the 128-slice dual source CT in a porcine model with a balloon-induced high grade coronary stenosis. Bamberg et al. studied 7 pigs with various degrees of LAD coronary stenosis (50% and 75% diameter stenosis). They demonstrated a moderate positive correlation between CT-MBF and microsphere-MBF [12]. Only few human studies investigated the diagnostic performance of CT in performing stress dynamic perfusion imaging. So et al. [84] studied 26 patients at rest and under dypiridamole stress with 64-slice CT, with a total myocardial coverage of 4 cm. They found that CFR and myocardial blood volume reserve of myocardial territories downstream of moderate or se-

vere coronary stenosis were significantly lower than those in regions supplied by normal coronary arteries. The average CFR in normal myocardial territories was only 2.3. Ho et al.[78] performed rest and stress dynamic perfusion in 35 patients referred to SPECT imaging. Sensitivity, specificity, PPV and NPV of CTP to detect ischemic myocardial segments was 83%, 78%, 79% and 82%, respectively. Similar to the finding reported by So and colleagues, CFR of normal myocardial territories was low (1.5) suggesting that current modeling techniques used in CT underestimated MBF. Bastarrika et al. [14] compared dynamic CTP imaging with MR in 10 patients. Sensitivity, specificity, PPV and NPV of detecting perfusion defects at CT was 86%, 98%, 94% and 96%, respectively. Bamberg et al.[11] found that a cut-point of 75ml/100ml/min discriminated between non-hemodynamic and hemodynamic significant coronary stenoses.

It should be kept in mind that all the reported human studies investigating the diagnostic accuracy of dynamic CTP imaging used SPECT, FFR, and MRI which do not provide absolute quantification of MBF which can be achieved with PET or PET-CT.

FUTURE STUDIES

Preliminary reports of myocardial CTP imaging are promising, but several problems need to be resolved before CTP can be implemented in routine clinical practice. So far there has not been consensus on the optimal scan mode to use for the acquisition of CTP. Foremost there is concern about the radiation dose of CTCA in combination with CTP. Only patients with intermediate lesions should be referred for CTP. Optimization of radiation dose reduction protocols should be developed with preservation of image quality. Iterative reconstruction should be helpful in this respect. Future studies should establish the usefulness of CTCA and CTP in symptomatic patients with prior stent implantation or coronary artery bypass graft, and in patients with acute chest pain and low likelihood of coronary artery disease in the emergency department. In particular, CTCA and CTP may be helpful in patients with severe coronary calcifications which seriously affect the assessment of the anatomic severity of coronary narrowings. Finally the role of CTCA and CTP with regard to other stand-alone hybrid imaging modalities (SPECT-CT, PET-CT) needs to be established preferably in large multicenter studies, including patient outcomes and cost-effectiveness.

CONCLUSIONS

The safety and feasibility of stress myocardial CT perfusion imaging has been recently demonstrated. The addition of myocardial CT perfusion imaging to the standard CT coronary angiography provides complementary anatomical and functional information in a single examination which may be helpful to improve patient management and outcome.

REFERENCES

1. Miller JM, Rochitte CE, Dewey M, Arbab-Zadeh A, Niinuma H, Gottlieb I, Paul N, Clouse ME, Shapiro EP, Hoe J, Lardo AC, Bush DE, de Roos A, Cox C, Brinker J, Lima JA. Diagnostic performance of coronary angiography by 64-row ct. *N Engl J Med.* 2008;359:2324-2336
2. Budoff MJ, Dowe D, Jollis JG, Gitter M, Sutherland J, Halamert E, Scherer M, Bellinger R, Martin A, Benton R, Delago A, Min JK. Diagnostic performance of 64-multidetector row coronary computed tomographic angiography for evaluation of coronary artery stenosis in individuals without known coronary artery disease: Results from the prospective multicenter accuracy (assessment by coronary computed tomographic angiography of individuals undergoing invasive coronary angiography) trial. *J Am Coll Cardiol.* 2008;52:1724-1732
3. Meijboom WB, Meijs MF, Schuijf JD, Cramer MJ, Mollet NR, van Mieghem CA, Nieman K, van Werkhoven JM, Pundziute G, Weustink AC, de Vos AM, Pugliese F, Rensing B, Jukema JW, Bax JJ, Prokop M, Doevendans PA, Hunink MG, Krestin GP, de Feyter PJ. Diagnostic accuracy of 64-slice computed tomography coronary angiography: A prospective, multicenter, multivendor study. *J Am Coll Cardiol.* 2008;52:2135-2144
4. Di Carli MF, Dorbala S, Curillova Z, Kwong RJ, Goldhaber SZ, Rybicki FJ, Hachamovitch R. Relationship between ct coronary angiography and stress perfusion imaging in patients with suspected ischemic heart disease assessed by integrated pet-ct imaging. *J Nucl Cardiol.* 2007;14:799-809
5. Hacker M, Jakobs T, Matthiesen F, Vollmar C, Nikolaou K, Becker C, Knez A, Pfluger T, Reiser M, Hahn K, Tiling R. Comparison of spiral multidetector ct angiography and myocardial perfusion imaging in the noninvasive detection of functionally relevant coronary artery lesions: First clinical experiences. *J Nucl Med.* 2005;46:1294-1300
6. Schuijf JD, Wijns W, Jukema JW, Atsma DE, de Roos A, Lamb HJ, Stokkel MP, Dibbets-Schneider P, Decramer I, De Bondt P, van der Wall EE, Vanhoenacker PK, Bax JJ. Relationship between noninvasive coronary angiography with multi-slice computed tomography and myocardial perfusion imaging. *J Am Coll Cardiol.* 2006;48:2508-2514
7. Meijboom WB, Van Mieghem CA, van Pelt N, Weustink A, Pugliese F, Mollet NR, Boersma E, Regar E, van Geuns RJ, de Jaegere PJ, Serruys PW, Krestin GP, de Feyter PJ. Comprehensive assessment of coronary artery stenoses: Computed tomography coronary angiography versus conventional coronary angiography and correlation with fractional flow reserve in patients with stable angina. *J Am Coll Cardiol.* 2008;52:636-643
8. Weintraub WS, Spertus JA, Kolm P, Maron DJ, Zhang Z, Jurkovitz C, Zhang W, Hartigan PM, Lewis C, Veledar E, Bowen J, Dunbar SB, Deaton C, Kaufman S, O'Rourke RA, Goeree R, Barnett PG, Teo KK, Boden WE, Group CTR, Mancini GB. Effect of pci on quality of life in patients with stable coronary disease. *N Engl J Med.* 2008;359:677-687

9. Tonino PA, De Bruyne B, Pijls NH, Siebert U, Ikeno F, van' t Veer M, Klauss V, Manoharan G, Engstrom T, Oldroyd KG, Ver Lee PN, MacCarthy PA, Fearon WF, Investigators FS. Fractional flow reserve versus angiography for guiding percutaneous coronary intervention. *N Engl J Med.* 2009;360:213-224

10. Hachamovitch R, Hayes SW, Friedman JD, Cohen I, Berman DS. Comparison of the short-term survival benefit associated with revascularization compared with medical therapy in patients with no prior coronary artery disease undergoing stress myocardial perfusion single photon emission computed tomography. *Circulation.* 2003;107:2900-2907

11. Bamberg F, Becker A, Schwarz F, Marcus RP, Greif M, von Ziegler F, Blankstein R, Hoffmann U, Sommer WH, Hoffmann VS, Johnson TR, Becker HC, Wintersperger BJ, Reiser MF, Nikolaou K. Detection of hemodynamically significant coronary artery stenosis: Incremental diagnostic value of dynamic ct-based myocardial perfusion imaging. *Radiology.* 2011;260:689-698

12. Bamberg F, Hinkel R, Schwarz F, Sandner TA, Baloch E, Marcus R, Becker A, Kupatt C, Wintersperger BJ, Johnson TR, Theisen D, Klotz E, Reiser MF, Nikolaou K. Accuracy of dynamic computed tomography adenosine stress myocardial perfusion imaging in estimating myocardial blood flow at various degrees of coronary artery stenosis using a porcine animal model. *Invest Radiol.* 2012;47:71-77

13. Bamberg F, Klotz E, Flohr T, Becker A, Becker CR, Schmidt B, Wintersperger BJ, Reiser MF, Nikolaou K. Dynamic myocardial stress perfusion imaging using fast dual-source ct with alternating table positions: Initial experience. *Eur Radiol.* 2010;20:1168-1173

14. Bastarrika G, Ramos-Duran L, Rosenblum MA, Kang DK, Rowe GW, Schoepf UJ. Adenosine-stress dynamic myocardial ct perfusion imaging: Initial clinical experience. *Invest Radiol.* 2010;45:306-313

15. Blankstein R, Shturman LD, Rogers IS, Rocha-Filho JA, Okada DR, Sarwar A, Soni AV, Bezerra H, Ghoshhajra BB, Petranovic M, Loureiro R, Feuchtner G, Gewirtz H, Hoffmann U, Mamuya WS, Brady TJ, Cury RC. Adenosine-induced stress myocardial perfusion imaging using dual-source cardiac computed tomography. *J Am Coll Cardiol.* 2009;54:1072-1084

16. Cury RC, Magalhaes TA, Paladino AT, Shiozaki AA, Perini M, Senra T, Lemos PA, Rochitte CE. Dipyridamole stress and rest transmural myocardial perfusion ratio evaluation by 64 detector-row computed tomography. *J Cardiovasc Comput Tomogr.* 2011;5:443-448

17. Cury RC, Nieman K, Shapiro MD, Butler J, Nomura CH, Ferencik M, Hoffmann U, Abbara S, Jassal DS, Yasuda T, Gold HK, Jang IK, Brady TJ. Comprehensive assessment of myocardial perfusion defects, regional wall motion, and left ventricular function by using 64-section multidetector ct. *Radiology.* 2008;248:466-475

18. Feuchtner G, Goetti R, Plass A, Wieser M, Scheffel H, Wyss C, Stolzmann P, Donati O, Schnabl J, Falk V, Alkadhi H, Leschka S, Cury RC. Adenosine stress high-pitch 128-slice dual-source myocardial computed tomography perfusion for imaging of reversible myocardial ischemia: Comparison with magnetic resonance imaging. *Circ Cardiovasc Imaging.* 2011;4:540-549

19. Ko BS, Cameron JD, Meredith IT, Leung M, Antonis PR, Nasis A, Crossett M, Hope SA, Lehman SJ, Troupis J, Defrance T, Seneviratne SK. Computed tomography stress myocardial perfusion imaging in patients considered for revascularization: A comparison with fractional flow reserve. *Eur Heart J.* 2011

20. Ko SM, Choi JW, Song MG, Shin JK, Chee HK, Chung HW, Kim DH. Myocardial perfusion imaging using adenosine-induced stress dual-energy computed tomography of the heart: Comparison with cardiac magnetic resonance imaging and conventional coronary angiography. *Eur Radiol.* 2011;21:26-35
21. Mahnken AH, Klotz E, Pietsch H, Schmidt B, Allmendinger T, Haberland U, Kalender WA, Flohr T. Quantitative whole heart stress perfusion ct imaging as noninvasive assessment of hemodynamics in coronary artery stenosis: Preliminary animal experience. *Invest Radiol.* 2010;45:298-305
22. Duncker DJ, Bache RJ. Regulation of coronary blood flow during exercise. *Physiol Rev.* 2008;88:1009-1086
23. Wu XS, Ewert DL, Liu YH, Ritman EL. In vivo relation of intramyocardial blood volume to myocardial perfusion. Evidence supporting microvascular site for autoregulation. *Circulation.* 1992;85:730-737
24. Lerman LO, Siripornpitak S, Maffei NL, Sheedy PF, 2nd, Ritman EL. Measurement of in vivo myocardial microcirculatory function with electron beam ct. *J Comput Assist Tomogr.* 1999;23:390-398
25. Gould KL, Lipscomb K, Hamilton GW. Physiologic basis for assessing critical coronary stenosis. Instantaneous flow response and regional distribution during coronary hyperemia as measures of coronary flow reserve. *Am J Cardiol.* 1974;33:87-94
26. Gould KL, Kirkeeide RL, Buchi M. Coronary flow reserve as a physiologic measure of stenosis severity. *J Am Coll Cardiol.* 1990;15:459-474
27. Uren NG, Melin JA, De Bruyne B, Wijns W, Baudhuin T, Camici PG. Relation between myocardial blood flow and the severity of coronary-artery stenosis. *N Engl J Med.* 1994;330:1782-1788
28. Canty JM, Jr., Smith TP, Jr. Adenosine-recruitable flow reserve is absent during myocardial ischemia in unanesthetized dogs studied in the basal state. *Circ Res.* 1995;76:1079-1087
29. Pijls NH, van Son JA, Kirkeeide RL, De Bruyne B, Gould KL. Experimental basis of determining maximum coronary, myocardial, and collateral blood flow by pressure measurements for assessing functional stenosis severity before and after percutaneous transluminal coronary angioplasty. *Circulation.* 1993;87:1354-1367
30. Pijls NH, De Bruyne B, Peels K, Van Der Voort PH, Bonnier HJ, Bartunek JKJJ, Koolen JJ. Measurement of fractional flow reserve to assess the functional severity of coronary-artery stenoses. *N Engl J Med.* 1996;334:1703-1708
31. Reimer KA, Jennings RB. The "wavefront phenomenon" of myocardial ischemic cell death. Ii. Transmural progression of necrosis within the framework of ischemic bed size (myocardium at risk) and collateral flow. *Lab Invest.* 1979;40:633-644
32. George RT, Arbab-Zadeh A, Miller JM, Kitagawa K, Chang HJ, Bluemke DA, Becker L, Yousuf O, Texter J, Lardo AC, Lima JA. Adenosine stress 64- and 256-row detector computed tomography angiography and perfusion imaging: A pilot study evaluating the transmural extent of perfusion abnormalities to predict atherosclerosis causing myocardial ischemia. *Circ Cardiovasc Imaging.* 2009;2:174-182
33. Ball RM, Bache RJ. Distribution of myocardial blood flow in the exercising dog with restricted coronary artery inflow. *Circ Res.* 1976;38:60-66

34. Rumberger JA, Feiring AJ, Lipton MJ, Higgins CB, Ell SR, Marcus ML. Use of ultrafast computed tomography to quantitate regional myocardial perfusion: A preliminary report. *J Am Coll Cardiol.* 1987;9:59-69

35. Bell MR, Lerman LO, Rumberger JA. Validation of minimally invasive measurement of myocardial perfusion using electron beam computed tomography and application in human volunteers. *Heart.* 1999;81:628-635

36. Rumberger JA, Bell MR. Measurement of myocardial perfusion and cardiac output using intravenous injection methods by ultrafast (cine) computed tomography. *Invest Radiol.* 1992;27 Suppl 2:S40-46

37. Newhouse JH, Murphy RX, Jr. Tissue distribution of soluble contrast: Effect of dose variation and changes with time. *AJR Am J Roentgenol.* 1981;136:463-467

38. Flohr TG, McCollough CH, Bruder H, Petersilka M, Gruber K, Suss C, Grasruck M, Stierstorfer K, Krauss B, Raupach R, Primak AN, Kuttner A, Achenbach S, Becker C, Kopp A, Ohnesorge BM. First performance evaluation of a dual-source ct (dsct) system. *Eur Radiol.* 2006;16:256-268

39. Lell M, Marwan M, Schepis T, Pflederer T, Anders K, Flohr T, Allmendinger T, Kalender W, Ertel D, Thierfelder C, Kuettner A, Ropers D, Daniel WG, Achenbach S. Prospectively ecg-triggered high-pitch spiral acquisition for coronary ct angiography using dual source ct: Technique and initial experience. *Eur Radiol.* 2009;19:2576-2583

40. George RT, Arbab-Zadeh A, Cerci RJ, Vavere AL, Kitagawa K, Dewey M, Rochitte CE, Arai AE, Paul N, Rybicki FJ, Lardo AC, Clouse ME, Lima JA. Diagnostic performance of combined noninvasive coronary angiography and myocardial perfusion imaging using 320-mdct: The ct angiography and perfusion methods of the core320 multicenter multinational diagnostic study. *AJR Am J Roentgenol.* 2011;197:829-837

41. Keller MR, Kessler RM, Brooks RA, Kirkland LR. Optimum energy for performing ct iodinated constrast studies. *Br J Radiol.* 1980;53:576-579

42. George RT, Jerosch-Herold M, Silva C, Kitagawa K, Bluemke DA, Lima JA, Lardo AC. Quantification of myocardial perfusion using dynamic 64-detector computed tomography. *Invest Radiol.* 2007;42:815-822

43. Schwarz F, Ruzsics B, Schoepf UJ, Bastarrika G, Chiaramida SA, Abro JA, Brothers RL, Vogt S, Schmidt B, Costello P, Zwerner PL. Dual-energy ct of the heart--principles and protocols. *Eur J Radiol.* 2008;68:423-433

44. Johnson TR, Krauss B, Sedlmair M, Grasruck M, Bruder H, Morhard D, Fink C, Weckbach S, Lenhard M, Schmidt B, Flohr T, Reiser MF, Becker CR. Material differentiation by dual energy ct: Initial experience. *Eur Radiol.* 2007;17:1510-1517

45. Kang DK, Schoepf UJ, Bastarrika G, Nance JW, Jr., Abro JA, Ruzsics B. Dual-energy computed tomography for integrative imaging of coronary artery disease: Principles and clinical applications. *Semin Ultrasound CT MR.* 2010;31:276-291

46. Nagao M, Kido T, Watanabe K, Saeki H, Okayama H, Kurata A, Hosokawa K, Higashino H, Mochizuki T. Functional assessment of coronary artery flow using adenosine stress dual-energy ct: A preliminary study. *Int J Cardiovasc Imaging.* 2010

47. Meyer M, Nance JW, Jr., Schoepf UJ, Moscariello A, Weininger M, Rowe GW, Ruzsics B, Kang DK, Chiaramida SA, Schoenberg SO, Fink C, Henzler T. Cost-effectiveness of substituting dual-energy ct for spect in the assessment of myocardial perfusion for the workup of coronary artery disease. *Eur J Radiol.* 2011

48. Ruzsics B, Schwarz F, Schoepf UJ, Lee YS, Bastarrika G, Chiaramida SA, Costello P, Zwerner PL. Comparison of dual-energy computed tomography of the heart with single photon emission computed tomography for assessment of coronary artery stenosis and of the myocardial blood supply. *Am J Cardiol.* 2009;104:318-326

49. Nance JW, Jr., Bastarrika G, Kang DK, Ruzsics B, Vogt S, Schmidt B, Raupach R, Flohr TG, Schoepf UJ. High-temporal resolution dual-energy computed tomography of the heart using a novel hybrid image reconstruction algorithm: Initial experience. *J Comput Assist Tomogr.* 2011;35:119-125

50. So A, Lee TY, Imai Y, Narayanan S, Hsieh J, Kramer J, Procknow K, Leipsic J, Labounty T, Min J. Quantitative myocardial perfusion imaging using rapid kvp switch dual-energy ct: Preliminary experience. *J Cardiovasc Comput Tomogr.* 2011;5:430-442

51. Matsumoto K, Jinzaki M, Tanami Y, Ueno A, Yamada M, Kuribayashi S. Virtual monochromatic spectral imaging with fast kilovoltage switching: Improved image quality as compared with that obtained with conventional 120-kvp ct. *Radiology.* 2011;259:257-262

52. Boll DT, Merkle EM, Paulson EK, Fleiter TR. Coronary stent patency: Dual-energy multidetector ct assessment in a pilot study with anthropomorphic phantom. *Radiology.* 2008;247:687-695

53. Haberland U, Klotz E, Abolmaali N. Performance assessment of dynamic spiral scan modes with variable pitch for quantitative perfusion computed tomography. *Invest Radiol.* 2010;45:378-386

54. Bottcher M, Refsgaard J, Madsen MM, Randsbaek F, Kaltoft A, Botker HE, Nielsen TT. Effect of antianginal medication on resting myocardial perfusion and pharmacologically induced hyperemia. *J Nucl Cardiol.* 2003;10:345-352

55. Yoon AJ, Melduni RM, Duncan SA, Ostfeld RJ, Travin MI. The effect of beta-blockers on the diagnostic accuracy of vasodilator pharmacologic spect myocardial perfusion imaging. *J Nucl Cardiol.* 2009;16:358-367

56. Scanlan JG, Gustafson DE, Chevalier PA, Robb RA, Ritman EL. Evaluation of ischemic heart disease with a prototype volume imaging computed tomographic (ct) scanner: Preliminary experiments. *Am J Cardiol.* 1980;46:1263-1268

57. Zoghbi GJ, Dorfman TA, Iskandrian AE. The effects of medications on myocardial perfusion. *J Am Coll Cardiol.* 2008;52:401-416

58. Neefjes LA, Dharampal AS, Rossi A, Nieman K, Weustink AC, Dijkshoorn ML, Ten Kate GJ, Dedic A, Papadopoulou SL, van Straten M, Cademartiri F, Krestin GP, de Feyter PJ, Mollet NR. Image quality and radiation exposure using different low-dose scan protocols in dual-source ct coronary angiography: Randomized study. *Radiology.* 2011;261:779-786

59. Dewey M, Zimmermann E, Deissenrieder F, Laule M, Dubel HP, Schlattmann P, Knebel F, Rutsch W, Hamm B. Noninvasive coronary angiography by 320-row computed tomography with lower radiation exposure and maintained diagnostic accuracy: Comparison of results with cardiac catheterization in a head-to-head pilot investigation. *Circulation*. 2009;120:867-875

60. Achenbach S, Goroll T, Seltmann M, Pflederer T, Anders K, Ropers D, Daniel WG, Uder M, Lell M, Marwan M. Detection of coronary artery stenoses by low-dose, prospectively ecg-triggered, high-pitch spiral coronary ct angiography. *JACC Cardiovasc Imaging*. 2011;4:328-337

61. Druz RS. Current advances in vasodilator pharmacological stress perfusion imaging. *Semin Nucl Med*. 2009;39:204-209

62. Gerber BL, Belge B, Legros GJ, Lim P, Poncelet A, Pasquet A, Gisellu G, Coche E, Vanoverschelde JL. Characterization of acute and chronic myocardial infarcts by multidetector computed tomography: Comparison with contrast-enhanced magnetic resonance. *Circulation*. 2006;113:823-833

63. Buecker A, Katoh M, Krombach GA, Spuentrup E, Bruners P, Gunther RW, Niendorf T, Mahnken AH. A feasibility study of contrast enhancement of acute myocardial infarction in multislice computed tomography: Comparison with magnetic resonance imaging and gross morphology in pigs. *Invest Radiol*. 2005;40:700-704

64. Mahnken AH, Bruners P, Muhlenbruch G, Emmerich M, Hohl C, Gunther RW, Wildberger JE. Low tube voltage improves computed tomography imaging of delayed myocardial contrast enhancement in an experimental acute myocardial infarction model. *Invest Radiol*. 2007;42:123-129

65. Crossett MP, Schneider-Kolsky M, Troupis J. Normal perfusion of the left ventricular myocardium using 320 mdct. *J Cardiovasc Comput Tomogr*. 2011;5:406-411

66. Kurata A, Mochizuki T, Koyama Y, Haraikawa T, Suzuki J, Shigematsu Y, Higaki J. Myocardial perfusion imaging using adenosine triphosphate stress multi-slice spiral computed tomography: Alternative to stress myocardial perfusion scintigraphy. *Circ J*. 2005;69:550-557

67. Hoffmann U, Millea R, Enzweiler C, Ferencik M, Gulick S, Titus J, Achenbach S, Kwait D, Sosnovik D, Brady TJ. Acute myocardial infarction: Contrast-enhanced multi-detector row ct in a porcine model. *Radiology*. 2004;231:697-701

68. Nieman K, Shapiro MD, Ferencik M, Nomura CH, Abbara S, Hoffmann U, Gold HK, Jang IK, Brady TJ, Cury RC. Reperfused myocardial infarction: Contrast-enhanced 64-section ct in comparison to mr imaging. *Radiology*. 2008;247:49-56

69. Mahnken AH, Koos R, Katoh M, Wildberger JE, Spuentrup E, Buecker A, Gunther RW, Kuhl HP. Assessment of myocardial viability in reperfused acute myocardial infarction using 16-slice computed tomography in comparison to magnetic resonance imaging. *J Am Coll Cardiol*. 2005;45:2042-2047

70. Henneman MM, Schuijf JD, Dibbets-Schneider P, Stokkel MP, van der Geest RJ, van der Wall EE, Bax JJ. Comparison of multislice computed tomography to gated single-photon emission computed tomography for imaging of healed myocardial infarcts. *Am J Cardiol*. 2008;101:144-148

71. Nikolaou K, Sanz J, Poon M, Wintersperger BJ, Ohnesorge B, Rius T, Fayad ZA, Reiser MF, Becker CR. Assessment of myocardial perfusion and viability from routine contrast-enhanced 16-detector-row computed tomography of the heart: Preliminary results. *Eur Radiol*. 2005;15:864-871

72. Rocha-Filho JA, Blankstein R, Shturman LD, Bezerra HG, Okada DR, Rogers IS, Ghoshhajra B, Hoffmann U, Feuchtner G, Mamuya WS, Brady TJ, Cury RC. Incremental value of adenosine-induced stress myocardial perfusion imaging with dual-source ct at cardiac ct angiography. *Radiology*. 2010;254:410-419
73. Baks T, Cademartiri F, Moelker AD, Weustink AC, van Geuns RJ, Mollet NR, Krestin GP, Duncker DJ, de Feyter PJ. Multislice computed tomography and magnetic resonance imaging for the assessment of reperfused acute myocardial infarction. *J Am Coll Cardiol*. 2006;48:144-152
74. Schuleri KH, Centola M, George RT, Amado LC, Evers KS, Kitagawa K, Vavere AL, Evers R, Hare JM, Cox C, McVeigh ER, Lima JA, Lardo AC. Characterization of peri-infarct zone heterogeneity by contrast-enhanced multidetector computed tomography: A comparison with magnetic resonance imaging. *J Am Coll Cardiol*. 2009;53:1699-1707
75. le Polain de Waroux JB, Pouleur AC, Goffinet C, Pasquet A, Vanoverschelde JL, Gerber BL. Combined coronary and late-enhanced multidetector-computed tomography for delineation of the etiology of left ventricular dysfunction: Comparison with coronary angiography and contrast-enhanced cardiac magnetic resonance imaging. *Eur Heart J*. 2008;29:2544-2551
76. Al-Saadi N, Nagel E, Gross M, Bornstedt A, Schnackenburg B, Klein C, Klimek W, Oswald H, Fleck E. Noninvasive detection of myocardial ischemia from perfusion reserve based on cardiovascular magnetic resonance. *Circulation*. 2000;101:1379-1383
77. al-Saadi N, Gross M, Bornstedt A, Schnackenburg B, Klein C, Fleck E, Nagel E. Comparison of various parameters for determining an index of myocardial perfusion reserve in detecting coronary stenosis with cardiovascular magnetic resonance tomography. *Z Kardiol*. 2001;90:824-834
78. Ho KT, Chua KC, Klotz E, Panknin C. Stress and rest dynamic myocardial perfusion imaging by evaluation of complete time-attenuation curves with dual-source ct. *JACC Cardiovasc Imaging*. 2010;3:811-820
79. Wang Y, Qin L, Shi X, Zeng Y, Jing H, Schoepf UJ, Jin Z. Adenosine-stress dynamic myocardial perfusion imaging with second-generation dual-source ct: Comparison with conventional catheter coronary angiography and spect nuclear myocardial perfusion imaging. *AJR Am J Roentgenol*. 2012;198:521-529
80. Gould RG, Lipton MJ, McNamara MT, Sievers RE, Koshold S, Higgins CB. Measurement of regional myocardial blood flow in dogs by ultrafast ct. *Invest Radiol*. 1988;23:348-353
81. Rienmuller R, Baumgartner C, Kern R, Harb S, Aigner R, Fueger G, Weihs W. [quantitative determination of left ventricular myocardial perfusion with electron beam computerized tomography]. *Herz*. 1997;22:63-71
82. Groves AM, Goh V, Rajasekharan S, Kayani I, Endozo R, Dickson JC, Menezes LJ, Shastry M, Habib SB, Ell PJ, Hutton BF. Ct coronary angiography: Quantitative assessment of myocardial perfusion using test bolus data-initial experience. *Eur Radiol*. 2008;18:2155-2163
83. St Lawrence KS, Lee TY. An adiabatic approximation to the tissue homogeneity model for water exchange in the brain: I. Theoretical derivation. *J Cereb Blood Flow Metab*. 1998;18:1365-1377
84. So A, Wisenberg G, Islam A, Amann J, Romano W, Brown J, Humen D, Jablonsky G, Li JY, Hsieh J, Lee TY. Non-invasive assessment of functionally relevant coronary artery stenoses with quantitative ct perfusion: Preliminary clinical experiences. *Eur Radiol*. 2012;22:39-50

85. Pennell DJ, Sechtem UP, Higgins CB, Manning WJ, Pohost GM, Rademakers FE, van Rossum AC, Shaw LJ, Yucel EK, Society for Cardiovascular Magnetic R, Working Group on Cardiovascular Magnetic Resonance of the European Society of C. Clinical indications for cardiovascular magnetic resonance (cmr): Consensus panel report. *Eur Heart J*. 2004;25:1940-1965

86. Braunwald E, Kloner RA. The stunned myocardium: Prolonged, postischemic ventricular dysfunction. *Circulation*. 1982;66:1146-1149

87. Rahimtoola SH, Dilsizian V, Kramer CM, Marwick TH, Vanoverschelde JL. Chronic ischemic left ventricular dysfunction: From pathophysiology to imaging and its integration into clinical practice. *JACC Cardiovasc Imaging*. 2008;1:536-555

88. Rodriguez-Granillo GA, Rosales MA, Degrossi E, Rodriguez AE. Signal density of left ventricular myocardial segments and impact of beam hardening artifact: Implications for myocardial perfusion assessment by multidetector ct coronary angiography. *Int J Cardiovasc Imaging*. 2010;26:345-354

89. Stenner P, Schmidt B, Allmendinger T, Flohr T, Kachelrie M. Dynamic iterative beam hardening correction (dibhc) in myocardial perfusion imaging using contrast-enhanced computed tomography. *Invest Radiol*. 2010;45:314-323

90. Kitagawa K, George RT, Arbab-Zadeh A, Lima JA, Lardo AC. Characterization and correction of beam-hardening artifacts during dynamic volume ct assessment of myocardial perfusion. *Radiology*. 2010;256:111-118

91. Adams DF, Hessel SJ, Judy PF, Stein JA, Abrams HL. Computed tomography of the normal and infarcted myocardium. *AJR Am J Roentgenol*. 1976;126:786-791

92. Siemers PT, Higgins CB, Schmidt W, Ashburn W, Hagan P. Detection, quantitation and contrast enhancement of myocardial infarction utilizing computerized axial tomography: Comparison with histochemical staining and 99mtc-pyrophosphate imaging. *Invest Radiol*. 1978;13:103-109

93. Powell WJ, Jr., wittenberg J, Maturi RA, Dinsmore RE, Miller SW. Detection of edema associated with myocardial ischemia by computerized tomography in isolated, arrested canine hearts. *Circulation*. 1977;55:99-108

94. George RT, Silva C, Cordeiro MA, DiPaula A, Thompson DR, McCarthy WF, Ichihara T, Lima JA, Lardo AC. Multidetector computed tomography myocardial perfusion imaging during adenosine stress. *J Am Coll Cardiol*. 2006;48:153-160

95. Magalhaes TA, Cury RC, Pereira AC, Moreira Vde M, Lemos PA, Kalil-Filho R, Rochitte CE. Additional value of dipyridamole stress myocardial perfusion by 64-row computed tomography in patients with coronary stents. *J Cardiovasc Comput Tomogr*. 2011;5:449-458

96. Arnoldi E, Lee YS, Ruzsics B, Weininger M, Spears JR, Rowley CP, Chiaramida SA, Costello P, Reiser MF, Schoepf UJ. Ct detection of myocardial blood volume deficits: Dual-energy ct compared with single-energy ct spectra. *J Cardiovasc Comput Tomogr*. 2011;5:421-429

97. Weininger M, Schoepf UJ, Ramachandra A, Fink C, Rowe GW, Costello P, Henzler T. Adenosine-stress dynamic real-time myocardial perfusion ct and adenosine-stress first-pass dual-energy myocardial perfusion ct for the assessment of acute chest pain: Initial results. *Eur J Radiol*. 2010

98. So A, Hsieh J, Li JY, Hadway J, Kong HF, Lee TY. Quantitative myocardial perfusion measurement using ct perfusion: A validation study in a porcine model of reperfused acute myocardial infarction. *Int J Cardiovasc Imaging*. 2011

99. Christian TF, Frankish ML, Sisemoore JH, Christian MR, Gentchos G, Bell SP, Jerosch-Herold M. Myocardial perfusion imaging with first-pass computed tomographic imaging: Measurement of coronary flow reserve in an animal model of regional hyperemia. *J Nucl Cardiol*. 2010;17:625-630

100. Kido T, Kurata A, Higashino H, Inoue Y, Kanza RE, Okayama H, Higaki J, Murase K, Mochizuki T. Quantification of regional myocardial blood flow using first-pass multidetector-row computed tomography and adenosine triphosphate in coronary artery disease. *Circ J*. 2008;72:1086-1091

CHAPTER 6

QUANTIFICATION OF MYOCARDIAL BLOOD FLOW BY ADENOSINE-STRESS CT PERFUSION IMAGING IN PIGS DURING VARIOUS DEGREES OF STENOSIS CORRELATES WELL WITH CORONARY ARTERY BLOOD FLOW AND FRACTIONAL FLOW RESERVE

2012, European Heart Journal Cardiovascular Imaging.

A Rossi
A Uitterdijk
M Dijkshoorn
E Klotz
A Dharampal
M van Straten
WJ van der Giessen
N Mollet
RJ van Geuns
GP Krestin
DJ Duncker
PJ de Feyter
D Merkus

ABSTRACT

Aims: Only few preliminary experimental studies demonstrated the feasibility of adenosine stress CT myocardial perfusion to calculate absolute myocardial blood flow (MBF), thereby providing information whether a coronary stenosis is flow-limiting. Therefore the aim of our study was to determine whether adenosine stress myocardial perfusion imaging by Dual Source CT (DSCT) enables non-invasive quantification of regional myocardial blood flow (MBF) in an animal model with various degrees of coronary flow reduction.

Methods and Results: In seven pigs a coronary flow probe and an adjustable hydraulic occluder were placed around the left anterior descending coronary artery to monitor the distal coronary artery blood flow (CBF) while several degrees of coronary flow reduction were induced. CT perfusion (CT-MBF) was acquired during adenosine stress with no CBF reduction, an intermediate (15-39%) and a severe (40-95%) CBF reductions. Standards of reference were CBF and fractional flow reserve measurements (FFR). FFR was simultaneously derived from distal coronary artery pressure and aortic pressure measurements. CT-MBF decreased progressively with increasing CBF reduction severity from 2.68 [2.31-2.81] ml/g/min (normal CBF) to 1.96 [1.83-2.33] ml/g/min (intermediate CBF-reduction) and to 1.55 [1.14-2.06] ml/g/min (severe CBF-reduction) (both $p<0.001$). We observed very good correlations between CT-MBF and CBF ($r=0.85$, $p<0.001$) and CT-MBF and FFR ($r=0.85$, $p<0.001$).

Conclusion: Adenosine stress DSCT myocardial perfusion imaging allows quantification of regional MBF under various degrees of CBF reduction.

INTRODUCTION

Current guidelines indicate that in patients with stable angina pectoris both anatomy and functional severity of coronary obstructions should be assessed for guiding patient management [1]. Optimal medical treatment is preferred in symptomatic patients with no or moderate ischemia, while revascularization is required in symptomatic patients with substantial myocardial ischemia,[2-4] and Percutaneous Coronary Intervention (PCI) is recommended for lesions with impaired Fractional Flow Reserve (FFR) in patients with multi-vessel disease [5-8].

Coronary CT Angiography (CTA) is a well-established, non-invasive imaging modality for detection and ruling-out coronary atherosclerosis [9-11]. Coronary CTA cannot, however, accurately predict whether an intermediate lesion is flow-limiting therefore requiring the use of additional functional testing [12, 13]. Yet, little information is available about the ability to use CT for the quantitative assessment of myocardial blood flow (MBF) at different levels of coronary artery stenosis. Only few preliminary experimental studies demonstrated the feasibility of adenosine stress CT myocardial perfusion to determine absolute MBF, thereby providing information about the functional severity of coronary lesions [2, 14, 15].

The purpose of our study was two-fold: 1) to quantify regional CT-derived MBF (CT-MBF) at different degrees of coronary flow reduction in a well established large animal model; 2) to correlate CT-MBF with coronary artery blood flow (CBF), the experimental reference standard, and with FFR, the clinical reference standard.

MATERIALS AND METHODS

ANIMAL PREPARATION

All procedures were conducted in compliance with the "Guide for the Care and Use of Laboratory Animals" (NIH Publication No. 85-23 revised 1996), and with prior approval of the Animal Care Committee of our institution. Nine, 5-6 months old, crossbred Yorkshire X Landrace swine (34.2±3.6kg) were sedated with an intramuscular injection of ketamine (20 mg/kg, Anisane, Raamsdonksveer, The Netherlands), midazolam (1 mg/kg, Actavis, Baarn, The Netherlands) and atropine sulphate (1mg, Pharmachemie, Haarlem, The Netherlands). Anesthesia was induced with an intravenous injection of pentobarbital sodium (15 mg/kg, Faculty of Veterinary Medicine, Utrecht, The Netherlands). Animals were intubated and mechanically ventilated with a mixture of O_2 and N_2 (1:2 v/v) [16]. Anesthesia was maintained by intravenous pentobarbital sodium infusion (15mg/kg/h). A left thoracotomy was performed in the fourth intercostal space and the pericardium was opened. Fluid-filled polyvinylchloride catheters were placed in the aortic arch, for measurement of pressure and for blood gas analysis to maintain blood gases within the physiological range. Catheters were also placed in the pulmonary artery for infusion of drugs and contrast material. Subsequently, the left anterior descending coronary artery (LAD) was dissected free for placement of a flow probe (Transonic Systems Europe B.V., Maastricht, The Netherlands) and a remote controlled silicone hydraulic vascular occluder (Fine Science Tools GmbH, Heidelberg, Germany). In addition, a fluid-filled polyvinylchloride angiocatheter for the measurement of distal coronary pressure and determination of FFR was into the LAD distal to the occluder. Flow probe, occluder and catheters were exteriorized, the chest was closed and anesthetized animals were transported to the CT suite using a mobile ventilator (Carina™, Dräger Medical, Best, The Netherlands).

EXPERIMENTAL AND CT IMAGING PROTOCOLS

A dual source CT (DSCT) scanner (SOMATOM Definition Flash, Siemens Healthcare, Forchheim, Germany) was used for perfusion imaging. All animals were placed in supine position. First, animals underwent DSCT myocardial perfusion imaging at rest. Subsequently, DSCT myocardial perfusion imaging was performed during maximal vasodilation. Maximal vasodilation was obtained during the infusion of 500 μg/kg/min adenosine (Adenoscan, Sanofi-Aventis Frankfurt, Germany). At this dose, adenosine resulted in marked systemic vasodilation and hypotension. In order to maintain blood pressure, the α_1-adrenoceptor agonist phenylephrine was co-infused (~5μg/kg/min iv, Pharmacy Erasmus MC, Rotterdam, The Netherlands) with adenosine. Since swine lack significant α_1-adrenergic coronary microvascular constrictor responses [17], phenylephrine can be used to oppose the systemic effects of adenosine, while leaving adenosine-induced coronary vasodilation unperturbed [16].Under maximal vasodilation the hydraulic occluder was manually inflated to sequentially obtain at least one intermediate

degree of flow-limiting coronary stenosis and at least one severe degree of flow-limiting stenosis. Total occlusion was performed to delineate the LAD perfusion territory. CT perfusion imaging was repeated at each severity level of flow reduction using a novel electrocardiogram (ECG) triggered dynamic scan mode. All scans were performed in cranio-caudal direction during end-expiratory breath-hold obtained by interrupting the mechanical ventilator. The data were acquired at two alternative table positions while the table was moving back and forth [18]. Image acquisition was triggered at 200ms after the R-wave. The scan coverage was 73mm resulting from a detector width of 38.4mm and 10% overlap between both scan ranges. The minimum cycle time for the alternating scan is 950ms. For the range of heart rates in this study we acquired data every second or third heart beat. Hence volume scan of the total heart was obtained every 2 to 3 seconds. The tube voltage was 100 kV for each X-ray tube and the total tube current-time product was 300mAs/rot. Prior to each scan 36ml of contrast material (Ultravist 370, Bayer Schering Pharma, Berlin, Germany) was injected through a pulmonary artery line at a flow rate of 6mL/s, followed by a saline chaser of 30mL at 6mL/s. Data acquisition started 2 seconds before the contrast medium injection and lasted for 30s. The delay between two consecutive scans was 20 minutes. Depending on the heart rate, the volume CT dose index (CTDIvol) ranged from 115.1 to 168.5 (mean 149.5±80.0) mGy. The corresponding dose length product (DLP) was 844.0 to 1129.0 (mean 1012.2±14.1) mGycm.

During each experiment heart rate, aortic pressure, mean coronary artery pressure and coronary blood flow (CBF) were continuously recorded (Codas, DATAQ) and stored for off-line analysis using a custom written software in MatLab (the Math Works). FFR was calculated as the ratio of distal coronary artery pressure and aortic pressure.

At the end of the experiment, animals were sacrificed with an intravenous overdose of pentobarbital sodium.

DATA ANALYSIS

All CT images were evaluated by one cardiac radiologist with four-years experience in cardiac imaging (A.R.). To assess intra- and inter-observer agreement, MBF of the ischemic myocardial territories was measured on 10 randomly chosen CT datasets by two independent observers (AR and AD). One observer (AR), who was blinded to the previous results, measured the datasets twice, separated by at least 12 weeks. Both observers were blinded to all CBF and FFR measurements.

CT images were reconstructed with a slice thickness of 3mm and an increment of 1.5mm using a medium-smooth kernel (B30f). The dynamic data were analyzed using commercial software, Volume Perfusion CT Body on a standard workstation (MMWP, Siemens Healthcare, Germany). Reconstruction and post-processing analysis of the CT perfusion images was

previously described.[14] Briefly, the left ventricular myocardium was segmented manually placing a volume of interest (VOI) and using a combination of a system of blood pool removal and HU thresholding (Figure 1 - A1 and A2). Afterwards, the arterial input function was sampled drawing a region of interest (ROI) in the descending aorta at the cranial and the caudal ends of the two image stacks (Figure 1B). The data from both ROIs were then combined into one arterial input function (Figure 1C) and time attenuation curves (TAC) were built for each voxel within the VOI. A dedicated parametric deconvolution technique based on a two-compartment model of intra- and extravascular space was applied to fit the TACs (Figure 2 B1 and B2). CT-derived MBF (CT-MBF) in ml/100ml/min of each voxel was then calculated using the maximum slope of the fit curves and quantitative three-dimensional color maps representing the MBF distribution in the myocardium were generated (Figure 2A). CT myocardial perfusion in ml/g/min was calculated assuming a myocardium specific density of 1.05 g/ml.

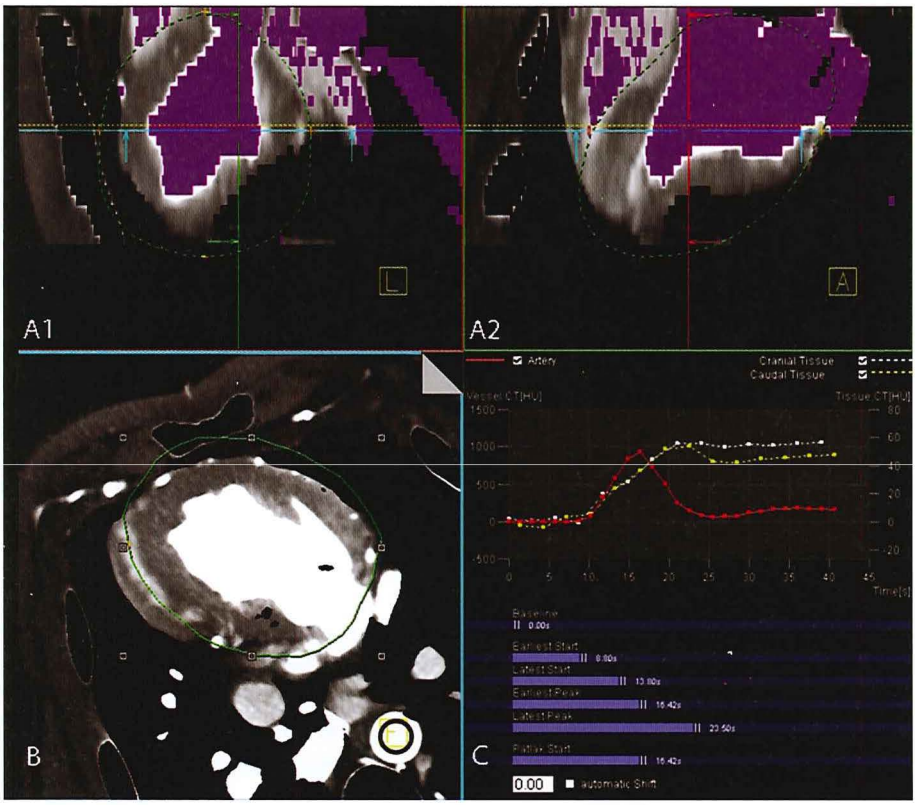

Figure 1: CT-perfusion imaging post-processing. Screenshot of the post-processing software. Panels A1 and A2 show the segmentation of the left ventricle. The left ventricle myocardium is isolated using in combination a Hounsfield unit based thresholding and a peak enhancement analysis within a volume of interest, VOI (green line). The arterial input function is sampled from two regions of interest placed in the descending aorta of the cranial (panel B) and caudal part of the image stack. One arterial input function is then obtained (red time-attenuation curve, TAC) in panel C combining the information of both ROIs.

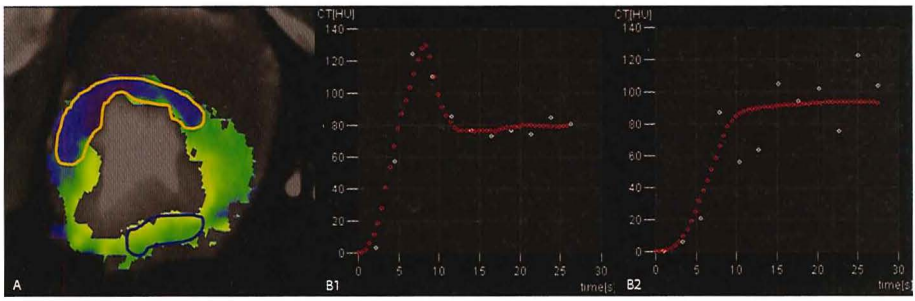

Figure 2: Ischemic and remote myocardial territory. Quantitative three-dimensional color-map representing the distribution of myocardial blood flow (A). During maximal vasodilation the ischemic anterior wall shows reduced perfusion (blue area) whereas the normal myocardium appears greenish (remote myocardium). A dedicated parametric deconvolution technique based on a two compartment model of intra- and extravascular space was used to fit the TACs in a representative normal (B1) and ischemic (B2) myocardium. The white dots are the measured enhancement values. The upslope of the time attenuation curve of the ischemic myocardium is less steep compared to the remote myocardium.

The LAD perfusion territory of each animal was first defined using the color code MBF maps during total occlusion of the LAD. Afterwards a VOI was manually placed in the most representative ischemic area of the LAD territory for each degree of CBF reduction within the same animal. A VOI was manually drawn also in the remote myocardium (inferior wall). CT-MBF was then obtained for both regions.

STATISTICAL ANALYSIS

Statistical analysis was performed using a dedicated statistical software program (SPSS PASW, version 17.0.2, IMB, Chicago, Illinois, USA). Measurements are presented as median [interquartile range]. All measurements were pooled and afterwards classified in three groups according to CBF: no-CBF reduction, intermediate CBF reduction (range: 15-39%), severe CBF reduction (range: 40-95%). When CBF measurements were not available the classification in different groups was based on FFR measurements. All measurements at rest and during maximal vasodilation were compared using Wilcoxon Signed Rank test. For each degree of coronary flow reduction CT-MBF were compared between the ischemic and remote myocardial territories using Wilcoxon Signed Rank test. CT-MBF, CBF and FFR were compared between different degrees of CBF reduction applying Kruskal-Wallis test for multiple independent samples. Mann-Whitney test was applied for post hoc comparison. Correlation analysis was performed to evaluate the association between CT-MBF and CBF and FFR. Linear regression models were then fitted to asses the value of CT-MBF to predict CBF and FFR. A p-value <0.05 was considered statistically significant.

RESULTS

Two pigs died before CT imaging due to ventricular fibrillation. In 7 animals instrumentation and CT myocardial perfusion imaging were successfully performed, and a total of 32 datasets were obtained. One CT dataset was excluded because of poor image quality. In one pig (4 datapoints), measurements of FFR could not be obtained due to a clot in the coronary artery catheter. Due to probe malfunction (lack of contact between probe and vessel), 11 measurements of CBF could not be obtained. Consequently, a total of 21 CBF measurements, 28 FFR measurements, and 31 CT datasets obtained in 7 swine were analyzed (Table 1).

Table 1. Number of datasets included in the analysis.

PIGS\DATASETS	CT	FFR	CBF
CT	7p\31ds	28ds	20ds
FFR	6p	6p\28ds	17ds
CBF	5p	4p	5p\21ds

Legend:
p: number of pigs
ds: number of datasets

At maximal vasodilation, a homogeneous increase in MBF was observed throughout the entire myocardium (Figure 3). At each level of CBF reduction the ischemic region in the LAD territory was clearly visible as defect in the color MBF maps in all 7 animals. Moreover, a progressive increase of the size of the ischemic territory was observed in each animal with increasing the severity of CBF reduction.

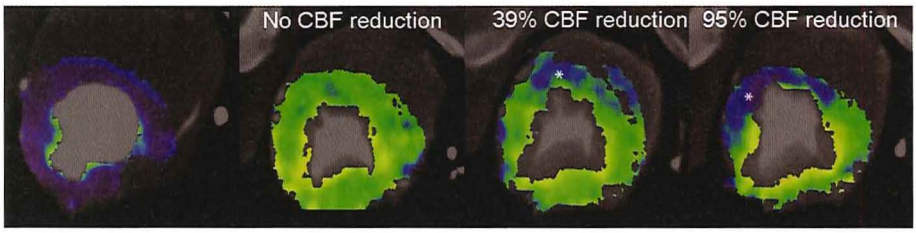

Figure 3: Response of CT-derived myocardial blood flow (CT-MBF) to different levels of coronary blood flow (CBF) reduction. Example of CT-MBF color maps of the myocardium during maximal vasodilation, intermediate CBF reduction and severe CBF reduction. The ischemic area (*) is well visible in the color-map. A progressive decrease of CT-MBF occurs with increasing severity of CBF reduction.

HEMODYNAMIC PARAMETERS

Despite the infusion of phenylephrine, blood pressure decreased from 95±3 mmHg at baseline to 85±3 mmHg during infusion of adenosine, while heart rate increased from 96±15 to 136±19 beats per minute. Animals showed a slight hemodynamic deterioration with increasing severity of coronary flow reduction as shown by the progressive decrease of aortic pressure (Table 2).

Table 2. Hemodynamic parameters and CBF, FFR, and CT-MBF of ischemic and remote myocardium during different levels of coronary blood flow CBF at the time of CT acquisition. Data are presented as median and interquartile range.

CBF REDUCTION [RANGE%]	NO [0%]	INTERMEDIATE [15-39%]	SEVERE [40-95%]	P-VALUE*
HR (bpm)	136 [117-154]	129 [118-147]	128 [116-143]	0.788
AoP (mmHg)	88 [78-99]	89 [86-94]	82 [74-91]	0.269
DISTAL CAP (MMHG)	80 [65-91]	73 [66-80]	44 [37-62] ‡	0.002
DISTAL CBF (ML/MIN)	148 [135-170]	116 [113-125] †	61 [30-83] ‡	<0.001
FFR	0.90 [0.84-1.00]	0.76 [0.65-0.91]	0.60 [0.51-0.69] ‡	<0.001
CT-MBF- ISCHEMIC (ML/G/MIN)	2.68 [2.31-2.81]	1.96 [1.83-2.33] †	1.55 [1.14-2.06] ò	<0.001
CT-MBF-REMOTE (ML/G/MIN)	2.76 [2.47-3.65]	2.51 [2.03-3.05]	3.02 [2.79-3.68]	0.162

HR: heart rate; AoP: aortic pressure; CAP: coronary artery pressure; CBF: coronary artery blood flow; FFR: fractional flow reserve; CT-MBF: CT-derived myocardial blood flow.

* p-value between CBF reduction groups (Kruskal-Wallis test)

† p-value<0.05 vs no CBF reduction (Mann-Whitney test)

‡ p-value<0.05 severe vs intermediate CBF reduction (Mann-Whitney test)

ò p-value<0.05 between CT-MBF of the LAD ischemic territory and CT-MBF of the remote myocardium (Wilcoxon Signed-Rank test)

CT-MBF OF ISCHEMIC AND REMOTE MYOCARDIUM

During normal coronary arterial inflow, maximal vasodilation with adenosine resulted in a 2.8 fold increase of CT-MBF from 0.99 [0.95-1.30] ml/g/min to 2.76 [2.47-3.65] ml/g/min (p=0.001) and a 3.7 fold increase of CBF, from 40 [25-83] ml/min to 149 [135-170] ml/min (p=0.006).

In all swine, CT-MBF of the ischemic territory decreased progressively with increasing severity of stenosis (p<0.001; Table 2). A typical response of CT-MBF to progressive flow

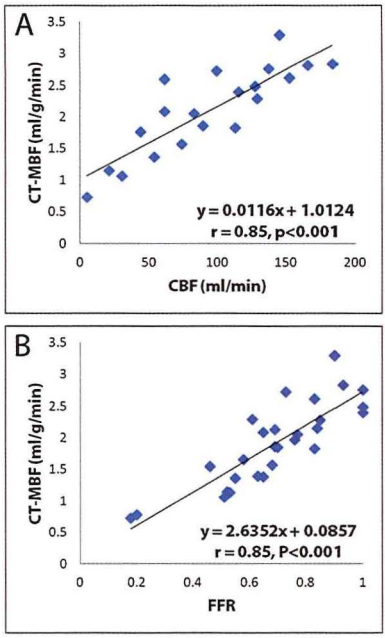

Figure 4: CT-derived myocardial blood flow (CT-MBF) versus coronary blood flow (CBF) and fractional flow reserve (FFR). Correlation between CT-MBF and (A) CBF measured by the flow probe and (B) FFR.

reductions is presented in Figure 3. CT-MBF of ischemic myocardial territories was markedly lower than CT-MBF of the remote myocardium ($p<0.001$) at severe CBF reduction.

CT-MBF correlated strongly with absolute flow measurement represented by CBF during no and various levels of CBF reduction ($r= 0.85$, $p<0.001$ Figure 4A). CT-MBF showed a similarly strong correlation with FFR ($r=0.85$, $p<0.001$) (Figure 4B).

INTRA- AND INTER-OBSERVER AGREEMENT

The mean difference of CT-MBF was 0.07 ml/g/min with a standard deviation of 0.18 ml/g/min for intra-observer measurements ($r = 0.96$; $p<0.001$). Mean difference (±standard deviation) for inter-observer measurements was 0.10 (± 0.40) ml/g/min ($r = 0.764$; $p=0.006$).

DISCUSSION

The present study assessed the diagnostic accuracy of stress dynamic DSCT quantification of MBF in ischemic and remote myocardium in a large animal model with controlled reduction in CBF under maximal vasodilation (from normal to moderate to severe CBF reduction) compared to the experimental reference standard of reference, CBF, and the clinical reference standard, FFR measurements. The major finding was that adenosine stress dynamic DSCT perfusion imaging provided regional quantification of MBF of ischemic and remote myocardium under experimental conditions which correlated very well with CBF and FFR.

CT QUANTIFICATION OF MBF

Static myocardial perfusion imaging during adenosine stress has been recently investigated in humans and showed a diagnostic accuracy comparable to SPECT to detect significant coronary stenoses [19, 20]. However, static perfusion imaging provides only qualitative information of the myocardial perfusion by comparing the attenuation of the ischemic area to the attenuation of the remote myocardium. Quantification of myocardial perfusion is possible using dynamic CT scanning and it was already investigated by electron beam CT (EBCT) in the late 1980's. EBCT was a remarkable technical development with an excellent temporal resolution allowing dynamic perfusion imaging but was limited by a rather small coverage and thick slices. Nevertheless, studies in animal models[21] and healthy humans[22] reported good correlations between EBCT -derived MBF versus microspheres[21] and versus indicator dilution methods,[22] respectively. EBCT technology has been replaced by multidetector CT technology and, due to improved temporal resolution and coverage, the latest generation scanners now allow quantitative myocardial perfusion imaging [23].Thus, George et al proved the ability of CT to quantify MBF in an experimental model using 64-multidetector CT.[15] Mahnken et al[14] and Bamberg et al [24] showed the feasibility of a novel ECG-triggered dynamic shuttle-mode scan with data being acquired at two alternating table positions in the quantification of MBF in animal and human studies, respectively. The use of two alternating table positions increased the scan coverage and the presence of two x-rays tubes provided a better temporal resolution as compared to 64-multidetector CT. The main criticism of studies so far has been that CT-MBF underestimates MBF. We observed a higher CT-MBF in the ischemic as well as in the remote myocardium than Mahnken et al,[14] and Bamberg et al.[24] which can be explained by the higher dose of adenosine in our study (500 μg/kg/min) as compared to Mahnken et al.[14] (240 μg/kg/min) and to Bamberg et al.[24] (140 μg/kg/min). In conjunction the use of phenylephrine resulted in a relatively well-maintained aortic blood pressure during adenosine infusion. Additionally, the 6 second contrast bolus was injected directly into the pulmonary artery in our study instead of a 10 seconds bolus into a peripheral ear vein. This yielded a much better defined arterial input function with better tissue discrimination and more accurate modeling. The values of MBF may differ in humans because a peripheral venous access is commonly used for contrast injection.

COMPARISON OF CT-MBF WITH CBF AND FFR

In our study we found an excellent correlation between CT-MBF and the experimental reference standard, CBF, over a wide range of blood flows. In our experimental set-up CBF provided a direct measurement of the blood flow distal to a coronary stenosis caused but direct measurements of CBF are not available in the clinical environment, although coronary blood velocity can be measured using a flow wire. Clinically, FFR was therefore introduced as indirect parameter of myocardial perfusion. FFR has been well-established as an accurate, yet invasive, parameter to assess the functionality of a coronary stenosis independent from

heart rate, blood pressure and left ventricular function. In the present study we found a good correlation between CT-MBF and FFR over a wide range of coronary flow reductions, suggesting that absolute MBF measurements with CT can provide clinically relevant information about stenosis severity. Indeed, Bamberg et al. [24] recently showed the feasibility of dynamic CT perfusion imaging for the detection of hemodynamically significant coronary artery stenoses, as defined with FFR, in a human study. These authors found a cut-off point of 75 mL/100mL/min to provide the highest discriminatory power between hemodynamically significant and non-significant coronary artery lesions. This cut-off value needs further validation in different patient populations after a standardized CT protocol developed.

LIMITATIONS

Our study has some limitations that are either related to our animal model or are more general limitations of CT technology

Animal model: First, our study was designed as a feasibility study using a relatively small number of animals. Yet, the use of multiple measurements per animal and the well-defined experimental conditions make the results reliable and reproducible as further evidenced by high correlation coefficients between CT-MBF, CBF and FFR . Second, we did not use microspheres as experimental gold standard for in vivo measurement of myocardial blood flow. Bamberg et. al provided good correlation between CT-MBF and microsphere-derived myocardial flow in pig model of LAD obstruction using the same CT technology [25]. Third, our experimental setup was designed as a single vessel LAD obstruction, therefore our results cannot be extrapolated to multi-vessel coronary artery disease. Nevertheless, we expect that this CT technology will give good results also in the situation of three vessel disease because it provides absolute quantification of regional myocardial blood flows rather than relative flows as obtained in SPECT imaging. Fourth, the pigs (mean weight±standard deviation: 34.2±3.6kg) were relatively small compared to adult humans, which may imply the need to use higher kV and mAs settings during the CT acquisition in humans. However, in a recent study performed in patients Bamberg et al [24] used successfully 100 kV and 300 mAs as we used in pigs.

CT-technology: There are several technical aspects that need further considerations. 1) An important technical limitation is the volume coverage. 64-slice CT scanners used to be limited to a single detector up to 40 mm that was not sufficient to cover the whole heart. Nowadays two alternatives are available: first, a CT system with 320 rows that can cover the whole heart in one gantry rotation[26-28], the second alternative is the shuttle mode acquisition used in our study. Although the acquisition coverage of the shuttle mode technique of 73 mm was sufficient for encompassing the entire heart of the pigs, this coverage may be not sufficient in humans, even when triggering in the systolic phase, due to the larger size of the human heart. Indeed Bamberg et al. found that one third of the scans provided incomplete coverage

of the myocardium[24]. Thus, further improvements in CT technology should aim in increasing the coverage along the z-axis. 2) We used central venous access for contrast injection , which provided a tighter input function and likely resulted in higher values of myocardial blood flow. These values may not be reproducible in patients because a peripheral venous access is commonly used in the clinical routine. 3) The addition of dynamic perfusion CT imaging to the conventional clinical cardiac CTA protocol will increase the total amount of radiation dose. Optimization of radiation dose reduction protocols should be developed with preservation of image quality. 4) Finally iodinated contrast medium in the left ventricular cavity can negatively affect the assessment of myocardial perfusion. However, this may be circumvented by using beam-hardening artifact correction algorithms to increase the accuracy of CT perfusion imaging in the quantification of myocardial blood flow [29].

CLINICAL IMPLICATIONS AND CHALLENGES

Our study shows that CT myocardial perfusion imaging can quantitatively measure MBF in experimental animals, and thereby can be used to assess stenosis severity. This observation is supported by a few small sized studies showing that CT myocardial perfusion imaging is also feasible in patients.[24, 26, 30-32]Thus, the addition of CT myocardial perfusion imaging to the standard coronary CTA provides complementary anatomical and functional information in a single, non-invasive examination which may improve patient management. Future improvements in CT technology, aimed at increasing the coverage and reducing the radiation exposure, would facilitate implementation of this non-invasive imaging technique in clinical practice.

CONCLUSIONS

The present study demonstrates that dynamic dual source CT can identify regional reductions of MBF, during pharmacological coronary vasodilation, over a wide range of flow-limiting coronary artery obstruction severities with a good correlation with coronary artery blood flow and fractional flow reserve.

ACKNOWLEDGEMENTS

We would like to dedicate this manuscript to Prof. Wim van der Giessen who sadly passed away in June 2011.

FUNDING

This research was partially financed by, and Volume Perfusion CT software was provided by, Siemens Nederland, Healthcare Sector, under a Cooperation Agreement

REFERENCES

1. Fox K, Garcia MA, Ardissino D, Buszman P, Camici PG, Crea F, Daly C, De Backer G, Hjemdahl P, Lopez-Sendon J, Marco J, Morais J, Pepper J, Sechtem U, Simoons M, Thygesen K, Priori SG, Blanc JJ, Budaj A, Camm J, Dean V, Deckers J, Dickstein K, Lekakis J, McGregor K, Metra M, Osterspey A, Tamargo J, Zamorano JL. Guidelines on the management of stable angina pectoris: Executive summary: The task force on the management of stable angina pectoris of the european society of cardiology. *Eur Heart J*. 2006;27:1341-1381
2. Shaw LJ, Berman DS, Maron DJ, Mancini GB, Hayes SW, Hartigan PM, Weintraub WS, O'Rourke RA, Dada M, Spertus JA, Chaitman BR, Friedman J, Slomka P, Heller GV, Germano G, Gosselin G, Berger P, Kostuk WJ, Schwartz RG, Knudtson M, Veledar E, Bates ER, McCallister B, Teo KK, Boden WE, Investigators C. Optimal medical therapy with or without percutaneous coronary intervention to reduce ischemic burden: Results from the clinical outcomes utilizing revascularization and aggressive drug evaluation (courage) trial nuclear substudy. *Circulation*. 2008;117:1283-1291
3. Hachamovitch R, Hayes SW, Friedman JD, Cohen I, Berman DS. Comparison of the short-term survival benefit associated with revascularization compared with medical therapy in patients with no prior coronary artery disease undergoing stress myocardial perfusion single photon emission computed tomography. *Circulation*. 2003;107:2900-2907
4. Boden WE, O'Rourke RA, Teo KK, Hartigan PM, Maron DJ, Kostuk WJ, Knudtson M, Dada M, Casperson P, Harris CL, Chaitman BR, Shaw L, Gosselin G, Nawaz S, Title LM, Gau G, Blaustein AS, Booth DC, Bates ER, Spertus JA, Berman DS, Mancini GB, Weintraub WS. Optimal medical therapy with or without pci for stable coronary disease. *N Engl J Med*. 2007;356:1503-1516
5. Legalery P, Schiele F, Seronde MF, Meneveau N, Wei H, Didier K, Blonde MC, Caulfield F, Bassand JP. One-year outcome of patients submitted to routine fractional flow reserve assessment to determine the need for angioplasty. *Eur Heart J*. 2005;26:2623-2629
6. Pijls NH, van Schaardenburgh P, Manoharan G, Boersma E, Bech JW, van't Veer M, Bar F, Hoorntje J, Koolen J, Wijns W, de Bruyne B. Percutaneous coronary intervention of functionally nonsignificant stenosis: 5-year follow-up of the defer study. *J Am Coll Cardiol*. 2007;49:2105-2111
7. Tonino PA, De Bruyne B, Pijls NH, Siebert U, Ikeno F, van' t Veer M, Klauss V, Manoharan G, Engstrom T, Oldroyd KG, Ver Lee PN, MacCarthy PA, Fearon WF, Investigators FS. Fractional flow reserve versus angiography for guiding percutaneous coronary intervention. *N Engl J Med*. 2009;360:213-224
8. Pijls NH, Fearon WF, Tonino PA, Siebert U, Ikeno F, Bornschein B, van't Veer M, Klauss V, Manoharan G, Engstrom T, Oldroyd KG, Ver Lee PN, MacCarthy PA, De Bruyne B. Fractional flow reserve versus angiography for guiding percutaneous coronary intervention in patients with multivessel coronary artery disease: 2-year follow-up of the fame (fractional flow reserve versus angiography for multivessel evaluation) study. *J Am Coll Cardiol*. 2010;56:177-184

9. Budoff MJ, Dowe D, Jollis JG, Gitter M, Sutherland J, Halamert E, Scherer M, Bellinger R, Martin A, Benton R, Delago A, Min JK. Diagnostic performance of 64-multidetector row coronary computed tomographic angiography for evaluation of coronary artery stenosis in individuals without known coronary artery disease: Results from the prospective multicenter accuracy (assessment by coronary computed tomographic angiography of individuals undergoing invasive coronary angiography) trial. *J Am Coll Cardiol*. 2008;52:1724-1732

10. Meijboom WB, Meijs MF, Schuijf JD, Cramer MJ, Mollet NR, van Mieghem CA, Nieman K, van Werkhoven JM, Pundziute G, Weustink AC, de Vos AM, Pugliese F, Rensing B, Jukema JW, Bax JJ, Prokop M, Doevendans PA, Hunink MG, Krestin GP, de Feyter PJ. Diagnostic accuracy of 64-slice computed tomography coronary angiography: A prospective, multicenter, multivendor study. *J Am Coll Cardiol*. 2008;52:2135-2144

11. Miller JM, Rochitte CE, Dewey M, Arbab-Zadeh A, Niinuma H, Gottlieb I, Paul N, Clouse ME, Shapiro EP, Hoe J, Lardo AC, Bush DE, de Roos A, Cox C, Brinker J, Lima JA. Diagnostic performance of coronary angiography by 64-row ct. *N Engl J Med*. 2008;359:2324-2336

12. Meijboom WB, Van Mieghem CA, van Pelt N, Weustink A, Pugliese F, Mollet NR, Boersma E, Regar E, van Geuns RJ, de Jaegere PJ, Serruys PW, Krestin GP, de Feyter PJ. Comprehensive assessment of coronary artery stenoses: Computed tomography coronary angiography versus conventional coronary angiography and correlation with fractional flow reserve in patients with stable angina. *J Am Coll Cardiol*. 2008;52:636-643

13. Sarno G, Decraemer I, Vanhoenacker PK, De Bruyne B, Hamilos M, Cuisset T, Wyffels E, Bartunek J, Heyndrickx GR, Wijns W. On the inappropriateness of noninvasive multidetector computed tomography coronary angiography to trigger coronary revascularization: A comparison with invasive angiography. *JACC Cardiovasc Interv*. 2009;2:550-557

14. Mahnken AH, Klotz E, Pietsch H, Schmidt B, Allmendinger T, Haberland U, Kalender WA, Flohr T. Quantitative whole heart stress perfusion ct imaging as noninvasive assessment of hemodynamics in coronary artery stenosis: Preliminary animal experience. *Invest Radiol*. 2010;45:298-305

15. George RT, Jerosch-Herold M, Silva C, Kitagawa K, Bluemke DA, Lima JA, Lardo AC. Quantification of myocardial perfusion using dynamic 64-detector computed tomography. *Invest Radiol*. 2007;42:815-822

16. Sorop O, Merkus D, de Beer VJ, Houweling B, Pistea A, McFalls EO, Boomsma F, van Beusekom HM, van der Giessen WJ, VanBavel E, Duncker DJ. Functional and structural adaptations of coronary microvessels distal to a chronic coronary artery stenosis. *Circ Res*. 2008;102:795-803

17. Duncker DJ, Stubenitsky R, Verdouw PD. Autonomic control of vasomotion in the porcine coronary circulation during treadmill exercise: Evidence for feed-forward beta-adrenergic control. *Circ Res*. 1998;82:1312-1322

18. Bamberg F, Klotz E, Flohr T, Becker A, Becker CR, Schmidt B, Wintersperger BJ, Reiser MF, Nikolaou K. Dynamic myocardial stress perfusion imaging using fast dual-source ct with alternating table positions: Initial experience. *Eur Radiol*. 2010;20:1168-1173

19. Blankstein R, Shturman LD, Rogers IS, Rocha-Filho JA, Okada DR, Sarwar A, Soni AV, Bezerra H, Ghoshhajra BB, Petranovic M, Loureiro R, Feuchtner G, Gewirtz H, Hoffmann U, Mamuya WS, Brady TJ, Cury RC. Adenosine-induced stress myocardial perfusion imaging using dual-source cardiac computed tomography. *J Am Coll Cardiol*. 2009;54:1072-1084

20. Cury RC, Magalhaes TA, Borges AC, Shiozaki AA, Lemos PA, Junior JS, Meneghetti JC, Rochitte CE. Dipyridamole stress and rest myocardial perfusion by 64-detector row computed tomography in patients with suspected coronary artery disease. *Am J Cardiol*. 2010;106:310-315

21. Rumberger JA, Feiring AJ, Lipton MJ, Higgins CB, Ell SR, Marcus ML. Use of ultrafast computed tomography to quantitate regional myocardial perfusion: A preliminary report. *J Am Coll Cardiol*. 1987;9:59-69

22. Bell MR, Lerman LO, Rumberger JA. Validation of minimally invasive measurement of myocardial perfusion using electron beam computed tomography and application in human volunteers. *Heart*. 1999;81:628-635

23. Flohr TG, Klotz E, Allmendinger T, Raupach R, Bruder H, Schmidt B. Pushing the envelope: New computed tomography techniques for cardiothoracic imaging. *J Thorac Imaging*. 2010;25:100-111

24. Bamberg F, Becker A, Schwarz F, Marcus RP, Greif M, von Ziegler F, Blankstein R, Hoffmann U, Sommer WH, Hoffmann VS, Johnson TR, Becker HC, Wintersperger BJ, Reiser MF, Nikolaou K. Detection of hemodynamically significant coronary artery stenosis: Incremental diagnostic value of dynamic ct-based myocardial perfusion imaging. *Radiology*. 2011;260:689-698

25. Bamberg F, Hinkel R, Schwarz F, Sandner TA, Baloch E, Marcus R, Becker A, Kupatt C, Wintersperger BJ, Johnson TR, Theisen D, Klotz E, Reiser MF, Nikolaou K. Accuracy of dynamic computed tomography adenosine stress myocardial perfusion imaging in estimating myocardial blood flow at various degrees of coronary artery stenosis using a porcine animal model. *Invest Radiol*. 2012;47:71-77

26. Ko BS, Cameron JD, Meredith IT, Leung M, Antonis PR, Nasis A, Crossett M, Hope SA, Lehman SJ, Troupis J, Defrance T, Seneviratne SK. Computed tomography stress myocardial perfusion imaging in patients considered for revascularization: A comparison with fractional flow reserve. *Eur Heart J*. 2011

27. George RT, Arbab-Zadeh A, Cerci RJ, Vavere AL, Kitagawa K, Dewey M, Rochitte CE, Arai AE, Paul N, Rybicki FJ, Lardo AC, Clouse ME, Lima JA. Diagnostic performance of combined noninvasive coronary angiography and myocardial perfusion imaging using 320-mdct: The ct angiography and perfusion methods of the core320 multicenter multinational diagnostic study. *AJR Am J Roentgenol*. 2011;197:829-837

28. George RT, Arbab-Zadeh A, Miller JM, Vavere AL, Bengel FM, Lardo AC, Lima JA. Computed tomography myocardial perfusion imaging with 320-row detector computed tomography accurately detects myocardial ischemia in patients with obstructive coronary artery disease. *Circ Cardiovasc Imaging*. 2012;5:333-340

29. Kitagawa K, George RT, Arbab-Zadeh A, Lima JA, Lardo AC. Characterization and correction of beam-hardening artifacts during dynamic volume ct assessment of myocardial perfusion. *Radiology*. 2010;256:111-118

30. Bastarrika G, Ramos-Duran L, Rosenblum MA, Kang DK, Rowe GW, Schoepf UJ. Adenosine-stress dynamic myocardial ct perfusion imaging: Initial clinical experience. *Invest Radiol*. 2010;45:306-313

31. Ho KT, Chua KC, Klotz E, Panknin C. Stress and rest dynamic myocardial perfusion imaging by evaluation of complete time-attenuation curves with dual-source ct. *JACC Cardiovasc Imaging*. 2010;3:811-820

32. George RT, Arbab-Zadeh A, Miller JM, Kitagawa K, Chang HJ, Bluemke DA, Becker L, Yousuf O, Texter J, Lardo AC, Lima JA. Adenosine stress 64- and 256-row detector computed tomography angiography and perfusion imaging: A pilot study evaluating the transmural extent of perfusion abnormalities to predict atherosclerosis causing myocardial ischemia. *Circ Cardiovasc Imaging*. 2009;2:174-182

CHAPTER 7

DIAGNOSTIC PERFORMANCE OF HYPERAEMIC MYOCARDIAL BLOOD FLOW OBTAINED BY DYNAMIC COMPUTED TOMOGRAPHY – DOES IT PREDICT FUNCTIONAL SIGNIFICANCE IN INTERMEDIATE CORONARY LESIONS?

2013 Submitted for publication

A Rossi
A Dharampal
A Wragg
LC Davies
RJ van Geuns
E Klotz
P Kitslaar
A Broersen
A Mathur
K Nieman
MG Hunink
PJ de Feyter
SE Petersen
F Pugliese

ABSTRACT

Objective: To evaluate the performance of quantitative hyperaemic myocardial blood flow (MBF) derived from adenosine dynamic computed tomography perfusion (CTP) imaging in the detection of functionally significant coronary lesions in patients with stable chest pain.

Background: The severity of coronary artery narrowing is a poor predictor of functional significance, in particular in intermediate lesions (30% to 70% diameter narrowing).

Methods: Computed tomography coronary angiography (CTCA) and CTP were performed in 80 patients (210 analyzable coronary vessels) referred to invasive coronary angiography (ICA). MBF (ml/100ml/min) was computed using a model-based parametric deconvolution method. The diagnostic performance of MBF in detecting functionally significant coronary lesions was compared to visual CTCA and semi-automatic quantitative computed tomography (QCT). Coronary lesions with invasive fractional flow reserve (FFR) ≤ 0.75 were defined as functionally significant.

Results: The optimal cut-off value of MBF to detect functionally significant coronary lesions was 78 ml/100ml/min. On a vessel-territory level, MBF had a larger area under the curve (0.95; 95% CI: 0.92-0.98) compared to visual CTCA (0.85; 95% CI, 0.79-0.91) and QCT (0.89; 95% CI, 0.84-0.93) (both p-values <0.001). In the analysis restricted to intermediate lesions, the specificity of visual CTCA (69%) and QCT (77%) could be improved by the subsequent use of MBF (89%).

Conclusions: MBF performed better than visual CTCA and QCT in the identification of functionally significant coronary lesions. MBF had additional value beyond CT anatomy in intermediate coronary lesions. This may have a potential to support patient management.

INTRODUCTION

Computed tomography coronary angiography (CTCA) is an established non-invasive imaging modality for the diagnosis of coronary artery disease. Similar to invasive coronary angiography (ICA), CTCA evaluates the anatomical severity of coronary lesions. Anatomical CTCA findings are poor predictors of functionally significant coronary lesions, in particular in lesions of intermediate severity (30-70% diameter reduction). Additional functional testing is often required to guide patient management. Fractional flow reserve (FFR) is commonly used during ICA for the identification of functionally significant coronary lesions to guide angioplasty [1]. Dynamic computed tomography (CT) stress perfusion imaging is a newly introduced non-invasive technique that allows the absolute quantification of myocardial blood flow (MBF). Combined with CTCA, MBF may allow a more comprehensive non-invasive evaluation of patients with suspected coronary artery disease. To date, only few animal studies [2-6] and small single-centre patient series [7-10] have shown the feasibility of this method. The purpose of this prospective study was to evaluate the diagnostic performance of MBF obtained by dynamic CT perfusion imaging during hyperaemic stress for the identification of functionally significant coronary lesions in patients with stable angina. We hypothesized that MBF would have better diagnostic performance than anatomical CTCA, in particular in lesions of intermediate severity.

METHODS

STUDY POPULATION

From March 2011 to September 2012, 157 patients with stable chest pain scheduled for invasive coronary angiography (ICA) at two large institutions were screened for inclusion into this prospective study (Figure 1). Patients underwent a computed tomography (CT) study consisting of CT coronary angiography (CTCA) and adenosine stress dynamic CT perfusion (CTP) one day to two weeks before ICA. Exclusion criteria were acute coronary syndrome, severely impaired left ventricular ejection fraction (≤35%), estimated glomerular filtration rate <60ml/min, documented or suspected allergy to iodinated contrast and contraindications to adenosine infusion such as history of severe asthma or obstructive lung disease, second or third degree atrioventricular block and a systolic blood pressure <90mmHg. The study protocol received approval by the Research Ethics Committee/Institutional Review Board at each institution and all patients gave written informed consent.

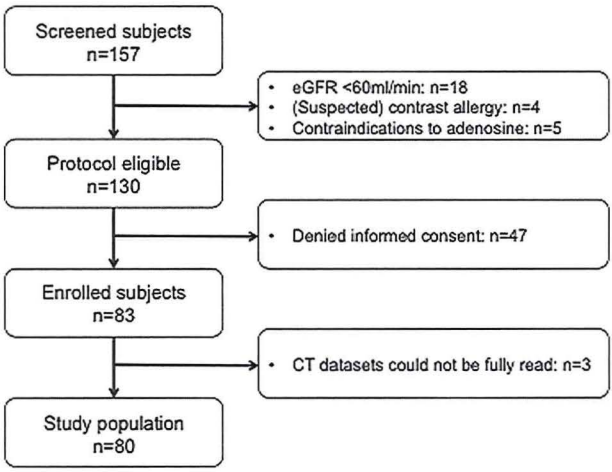

Figure 1. Inclusion procedure.

COMPUTED TOMOGRAPHY (CT) PROTOCOL

PATIENT PREPARATION

Patients abstained from caffeine (coffee, tea, chocolate, energy drinks etc.) for 18 hours and from methylxanthine-containing products, theophylline, oral dipyridamole, beta-blockers and nitrates for 24 hours before the scan. The preparation procedure is detailed in Table 1.

CT CORONARY ANGIOGRAPHY (CTCA)

A second-generation dual-source CT scanner (Somatom Definition Flash, Siemens Healthcare, Forchheim, Germany) was used at both institutions. First, all patients underwent a non-enhanced scan for calcium scoring with the Agatston method. This was followed by prospectively ECG-triggered CTCA (Adaptive Sequential, Siemens Healthcare) (Table 1). A

Table 1. Patient preparation and scan parameters.

PATIENT PREPARATION PROCEDURES AND SCAN PARAMETERS
PATIENT PREPARATION
• 18-gauge cannula in right antecubital vein for contrast injection; 20-gauge cannula in left antecubital vein for adenosine infusion;
• 30-sec breath hold practiced; if unable to hold the breath for longer than 20 s, patients were asked to exhale gently over 10 s.
NON-ENHANCED CORONARY CALCIUM SCORING
• Collimation 2 x 32 x 1.2 mm;
• Gantry rotation time 285 ms;
• Voltage 120 kV;
• Tube current-time product 75 mAs;
• Slice thickness 3 mm, reconstruction increment 1.5 mm;
• Image acquisition triggered 250 ms after the R wave.
CTCA
• Collimation 2 x 64 x 0.6 mm with z-flying focal spot (2 x 128 sections);
• Gantry rotation time 285 ms;
• Voltage/tube current-time product 100 kV/370 mAs if BMI <30; 120 kV/320 mAs if BMI >30;
• Image acquisition triggered at 60-75% of R-R interval in heart rates <65 beats/min; 35-75% of R-R interval in heart rates between 65 and 80 beats/min; 35-50% of R-R interval in heart rates >80 beats/min.
CT PERFUSION
• Collimation 2 x 32 x 1.2 mm;
• Gantry rotation time 285 ms;
• Voltage 100 kV;
• Tube current-time product 300 mAs;
• Image acquisition triggered 250 ms after the R wave.

test bolus scan was obtained with 6s delay at the level of the ascending aorta after injection of 15ml of contrast (Omnipaque 300, GE Healthcare or Ultravist 370, Schering, Berlin) followed by 40ml of saline. The main bolus consisted of 50 or 60ml of contrast (depending on the type used). The injection rates were adjusted to achieve an iodine delivery rate of 2.2 g of iodine/s (gI/s). CTCA images were reconstructed with 0.75mm slice thickness and 0.4mm increment using a medium-smooth convolution kernel (B26f).

Stress CT Perfusion (CTP)

The delay between CTCA and CTP acquisition was 10 to 15 minutes. Adenosine was infused intravenously at a dose of 140μg/kg/min. Stress CTP acquisition began 3 minutes after the start of the adenosine infusion. Stress CTP images were acquired over 30s using an ECG-triggered axial shuttle mode. The scanner alternates rapidly between 2 table positions and acquires prospectively ECG-triggered axial images in these 2 positions (Table 1). A volume of 50 or 60ml of contrast was injected with an iodine delivery rate of 2.2gI/s followed by 40ml of saline. The scan delay was calculated from the test bolus time-attenuation curve and commenced 6s before arrival of contrast in aorta. Stress CTP images were reconstructed with 3mm slice thickness and 2mm increment using a smooth-medium kernel that includes correction for iodine beam hardening (B23). The median (IQR) dose length product (DLP) associated with CTCA was 302 (215-402) Gy*cm; the median (IQR) DLP for CTP was 674 (621-748) Gy*cm.

CTCA AND CTP ANALYSIS

A flow chart of CT image analysis is given in Figure 2. Anonymized CTCA data were analyzed blindly in a core-lab based at Erasmus MC, Rotterdam. An off-line workstation with a commercially available platform (syngo 3D, MMW, Siemens Medical Solution, Erlangen, Germany) was used. If more than one lesion was present within the same vessel, the most severe lesion was selected and used in the analysis. Lesion severity was assessed visually, and then quantified using semi-automatic software (QAngioCT Research Edition v1.3.61, Medis medical imaging systems, Leiden, the Netherlands). For the latter, percentage diameter narrowing was calculated from detected lumen contours at the minimal lumen area and corresponding reference diameter values obtained from an automatic trend analysis of the vessel area [11]. The percent diameter narrowing assessed visually and measured by quantitative CT (QCT) was dichotomized us-

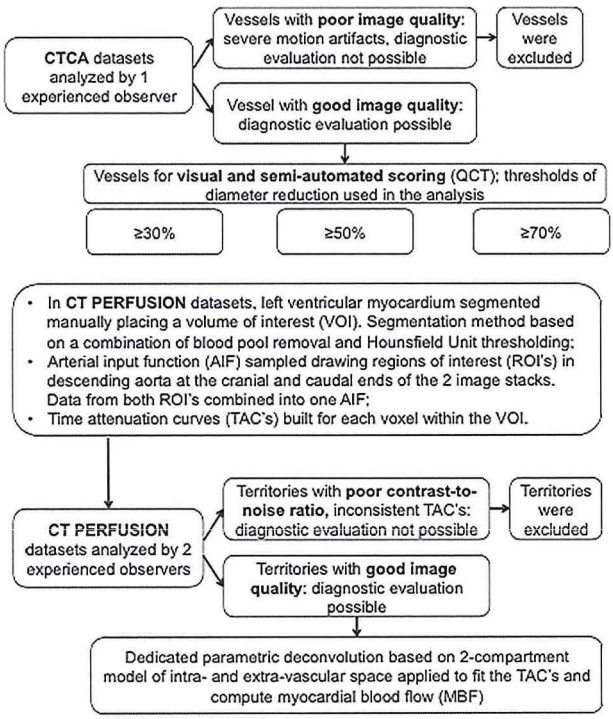

Figure 2. Flow chart of CT image analysis.

ing three thresholds, a) ≥30% vs. <30%, b) ≥50% vs. <50% and c) ≥70% vs. <70% diameter narrowing.

Anonymized stress CTP images were analyzed blindly at a core-lab based at the Centre for Advanced Cardiovascular Imaging, London. Commercial software (Volume Perfusion CT Body, Siemens) [4] was used (Figure 2). Myocardial blood flow (MBF) in each voxel was calculated as maximum slope of the fit curve/maximum arterial input function (AIF), and quantitative three-dimensional color maps representing MBF distribution in the myocardium were created. Three 10mm-thick standard short axis views of the left ventricle at basal, mid-cavity and apical levels were generated. MBF was obtained from volumes of interest (VOI's) defined by one observer (blinded to the CTCA findings) following a standard 16-segment model [12]. Individual myocardial segments supplied by the same coronary vessel based on a three vessel-territory model (LAD, LCx, and RCA) were considered as parts of the same territory. Within each territory, the myocardial segment with the lowest MBF value was selected and used in the analysis. To ensure accurate matching of coronary vessels and associated myocardial territories, coronary dominance (right, left or balanced) was used to decide which vessel (RCA, LCA or both) supplied the inferior and infero-septal segments of the myocardium.

INVASIVE CORONARY ANGIOGRAPHY (ICA) AND FRACTIONAL FLOW RESERVE (FFR)

All patients underwent ICA. During the procedure two experienced interventional cardiologists visually identified coronary lesions associated with diameter narrowing between 30% and 90%. Fractional flow reserve (FFR) was measured using a sensor-tipped 0.014-inch guidewire (Pressure Wire, Radi Medical Systems, Uppsala, Sweden). The pressure sensor was positioned just distal to the lesion and maximal myocardial hyperemia was induced by a continuous intravenous infusion of adenosine in a femoral vein (140μg/kg/minute for a minimum of 2min). FFR was calculated as the ratio of mean distal pressure measured by the pressure wire divided by the mean proximal pressure measured by the guiding catheter. ICA images were analyzed blindly on multiple projections by a single experienced observer unaware of the CT results. The most severely diseased segment in each coronary vessel was identified to derive percentage diameter narrowing using validated quantitative coronary angiography (QCA) software (QAngio® XA, 7.2, Medis, Leiden, the Netherlands).

STANDARD OF REFERENCE

If FFR was ≤0.75 lesions were classified as functionally significant; if FFR was >0.75 lesions were classified as non-significant. Critical lesions (≥90% diameter narrowing) were classified as significant while mild lesions (<30% diameter narrowing) were classified as non-significant [13].

The methods used for the adjudication of functionally significant coronary lesions (standard of reference) are detailed in Table 3.

STATISTICAL ANALYSIS

Statistical analysis was performed using commercial software (IBM SPSS Statistic, version 20; Somers, NY). Results were reported in accordance with the STARD criteria [14]. Continuous variables were presented as means ± standard deviations (SD) or medians with interquartile ranges (IQR). Categorical variables were presented as frequencies and percentages. Receiver operating characteristics (ROC) curves were built for MBF, CTCA and QCT. The optimal cut-off value of MBF was identified as the value that allowed the optimization of specificity provided that sensitivity was at least 85%. Myocardial territories with an MBF higher than the cut-off value were defined as remote myocardium. MBF in territories with functionally significant lesions were compared to remote myocardium using the Wilcoxon signed-rank test. Sensitivity analyses used the specified cut-off value of MBF. At the patient level, sensitivity and specificity were calculated as proportions with 95% confidence intervals. The vessels with the most severe findings were selected to represent the patient (lowest FFR, lowest MBF). At the vessel-territory level we adjusted for the clustered nature of the data using logistic generalized estimating equations (GEE's) [15]. Secondly, we performed a pre-specified sub-analysis in vessels directly interrogated with FFR. Thirdly, we estimated the diagnostic performance in intermediate coronary lesions defined as diameter narrowing between 30% and 70% on CTCA. The DeLong test was used to compare the areas under the curve (AUC's) of MBF to those of visual CTCA and QCT. The McNemar test was used to compare sensitivity and specificity. Intra- and inter-observer variability of MBF were assessed in 75 randomly selected myocardial territories and presented as mean difference with SD and the corresponding correlation coefficient (r). Statistical significance for all analyses was defined as $p<0.05$.

RESULTS

BASELINE CHARACTERISTICS AND ICA FINDINGS

The study population consisted of 80 patients (Figure 1). Stents were present in 13 vessels and these were excluded from analysis. Further 3 vessels were excluded due to suboptimal ICA views. One vessel could not be engaged on ICA due to an anomalous origin. Further 11 vessels and 2 myocardial territories were excluded due poor image quality on CTCA and CTP, respectively. Thus data from 210 coronary vessels and 210 corresponding myocardial territories were available for comparison and were included in the analysis.

Table 2. Baseline characteristics and main ICA findings (n=80).

CHARACTERISTICS	TOTAL (N=80)
Men/women	63/17 (79%/21%)
Age (yrs)	60 ± 10
Body mass index (kg/m2)	27 ± 4
Risk factors	
Diabetes mellitus§	16 (20%)
Hypertension†	48 (60%)
Dyslipidemia‡	53 (66%)
Current smoker	26 (33%)
History of coronary artery disease∫	35 (44%)
Agatston calcium score: median (IQR)	198 (26-618)
Right dominant coronary system	72 (90%)
Heart rate (beats/min)	
Baseline	66 ± 11
During hyperaemia	87 ± 14
Systolic blood pressure (mmHg)	
Baseline	135 ± 23
During hyperaemia	128 ± 21
Diastolic blood pressure (mmHg)	
Baseline	76 ± 11
During hyperaemia	70 ± 13
Patients with functionally significant coronary lesion*	40/80 (50%)
One-vessel disease	27/80 (34%)
Two-vessel disease	10/80 (12%)
Three-vessel disease	3/80 (4%)
Vessels with functionally significant coronary lesion*	56/210 (25%)
Right coronary artery	14/56 (23%)
Left main/left anterior descending coronary artery**	28/56 (55%)
Left circumflex artery	14/56 (23%)

Values are means, frequencies and percentages, unless otherwise specified.

§ Treatment with oral anti-diabetic medication or insulin; † Blood pressure ≥ 140/90 mmHg or treatment for hypertension; ‡ Total cholesterol > 180 mg/dl or treatment for hypercholesterolemia; ∫ Family history of coronary artery disease having first- or second- degree relatives with premature coronary artery disease (age<55 years).

* Functionally significant coronary lesion defined as FFR ≤ 0.75 or quantitative coronary angiography diameter narrowing ≥90%.

** Only one patient had significant left main disease associated with significant disease of the left anterior descending and left circumflex arteries.

Functionally significant coronary lesions were found in 56/210 (27%) vessels in 40/80 (50%) patients. There were 3/80 patients with 3-vessel disease, 10/80 patients with 2-vessel disease and 27/80 patients with 1-vessel disease. Baseline characteristics of the population are given in Table 2. FFR was measured in 68 vessels and ranged between 0.24 and 1.00 (median 0.79; IQR: 0.71-0.87). An FFR ≤0.75 was found in 25/68 (37%) vessels. The detailed breakdown of the coronary lesions encountered is given in Table 3.

Table 3. The adjudication of coronary lesions (total vessels = 210) as functionally significant (standard of reference) was based on FFR≤0.75 or ≥90% diameter narrowing on QCA. MBF tracked the expected changes according to FFR and QCA.

QCA	FFR	ADJUDICATED AS FUNCTIONALLY SIGNIFICANT	NO. LESIONS	MEDIAN MBF (IQR) [ML/100ML/MIN]
<30%	Not measured	No	111	115 (94-138)
<30%	>0.75	No	13	103 (85-139)
<30%	≤0.75	(Yes)	0	-
30%≤ICA<90%	>0.75	No	30	98 (82-115)
30%≤ICA<90%	≤0.75	Yes	24	70 (62-75)
≥90%	>0.75	(No)	0	-
≥90%	≤0.75	Yes	1	78
≥90%	Not measured	Yes	31	57 (50-65)
TOTAL VESSELS			210	

QCA = quantitative coronary angiography; FFR = fractional flow reserve; MBF = myocardial blood flow; IQR = interquartile range.

CTP AND MYOCARDIAL BLOOD FLOW (MBF)

CTP was performed 7 ± 5 days before ICA (range 1-14 days). No severe adverse reactions to adenosine or contrast were observed. The median (IQR) myocardial blood flow (MBF) in the whole sample was 97 (74-127) ml/100ml/min. Median MBF was 62 (51-74) ml/100ml/min in myocardial territories supplied by vessels with functionally significant coronary lesions and 109 (92-136) ml/100ml/min in the remote myocardium ($p<0.001$). MBF in vessels interrogated with FFR is shown in Figure 3.

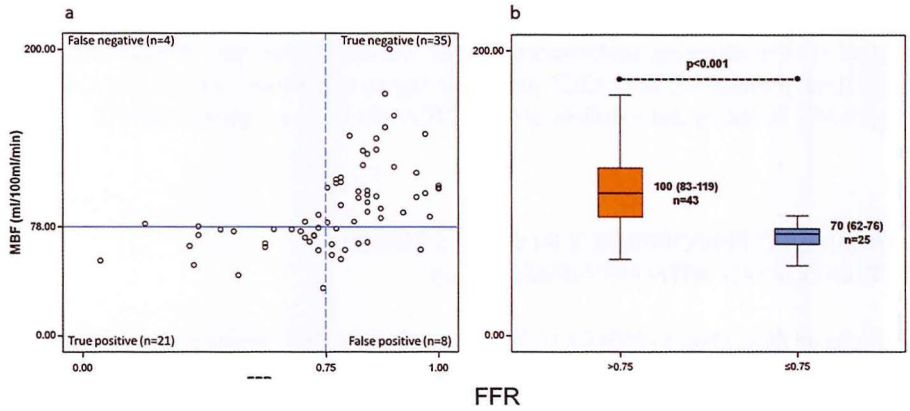

Figure 3. Hyperaemic myocardial blood flow (MBF) in vessels interrogated with FFR (n=68).
(a) Scatter plot shows MBF in a given myocardial territory and FFR in the corresponding vessel. (b) Hyperaemic MBF was lower in vessels with FFR ≤0.75 compared to FFR>0.75 *(MBF values are medians and interquartile ranges)*.

DIAGNOSTIC PERFORMANCE IN THE WHOLE SAMPLE (TOTAL VESSELS = 210)

On a vessel-territory level, MBF had an AUC of 0.95 (95% CI, 0.92-0.98, p<0.001). The MBF value that allowed the identification of all territories supplied by functionally significant lesions was 51ml/100ml/min, while the MBF value that allowed the identification of all remote myocardial territories was 103ml/100ml/min. An MBF cut-off value of 78ml/100ml/min yielded 88% sensitivity and 90% specificity (Figure 4A). Visual CTCA had an AUC of

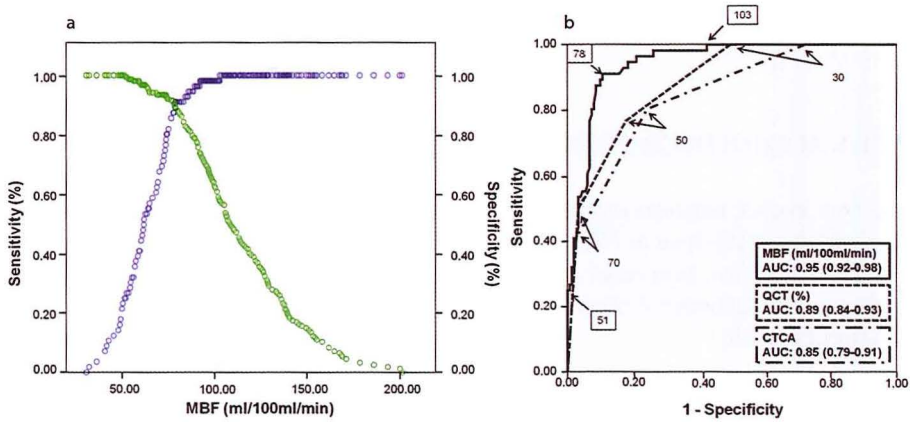

Figure 4. Diagnosis of functionally significant coronary lesion (vessel-territory level).
(a) A cut-off value for MBF of 78ml/100ml/min yielded 88% sensitivity and 90% specificity. (b) Receiver operating characteristics curves showed a better performance for MBF compared to visual CTCA and QCT (p<0.001 and p=0.0145, respectively). QCT performed better than visual CTCA (p=0.019).

0.85 (95% CI, 0.79-0.91, p<0.001) and QCT had an AUC of 0.89 (95% CI, 0.84-0.93, p<0.001). The diagnostic performance of MBF was better than that of visual CTCA and QCT (both p-values <0.001). QCT performed slightly better than visual CTCA (p=0.019) (Figure 4B). Sensitivity and specificity of MBF, CTCA and QCT are given in Table 4.

DIAGNOSTIC PERFORMANCE IN VESSELS DIRECTLY INTERROGATED WITH FFR (VESSELS = 68)

MBF had an AUC of 0.85 (95% CI, 0.76-0.94, p<0.001), 84% sensitivity and 81% specificity. Visual CTCA had an AUC of 0.69 (95% CI, 0.56-0.83, p<0.001) and QCT had an AUC of 0.78 (95% CI, 0.66-0.89, p<0.001). The diagnostic performance of MBF was better than visual CTCA and QCT (both p-values <0.001). QCT performed slightly better than visual CTCA (p<0.001) (Table 4).

DIAGNOSTIC PERFORMANCE IN INTERMEDIATE CORONARY LESIONS ON CTCA (30-70% DIAMETER REDUCTION)

In the analysis restricted to coronary lesions scored between 30% and 70% diameter reduction on CTCA, on a vessel-territory level, MBF had an AUC of 0.87 (95% CI, 0.79-0.95, p<0.001), 85% sensitivity and 89% specificity. Visual CTCA had an AUC of 0.68 (95% CI, 0.57-0.79, p=0.002) and QCT had an AUC of 0.69 (95% CI, 0.58-0.80, p=0.001). The diagnostic performance of MBF was better than visual CTCA (p=0.003) and QCT (p=0.002) due to a significantly lower false positive ratio (better specificity) (Table 5).

INTRA- AND INTER-OBSERVER AGREEMENT

The time interval between repeat readings by the same observer was >3 months. The mean absolute difference in MBF±SD between two readings by the same observer was 7±17ml/100ml/min. Intra-observer correlation was strong (r=0.9). The mean absolute difference in MBF between 2 observers was 7±18ml/100ml/min. Inter-observer correlation was strong (r=0.8).

Table 4. Diagnostic performance of visual CTCA, QCT and MBF.

	TP	TN	FP	FN	SENSITIVITY, % (95% CI)	SPECIFICITY, % (95% CI)	PPV, % (95% CI)	NPV, % (95% CI)
VESSEL-TERRITORY LEVEL								
FUNCTIONALLY SIGNIFICANT CORONARY LESION AS STANDARD OF REFERENCE (N=210)								
VISUAL CTCA-30%	56	43	111	0	100 (94-100)	28 (21-36) §	34 (27-41)	100 (92-100)
VISUAL CTCA-50%	45	117	37	11	80 (67-89)	76 (67-83) §	55 (43-66)	91 (85-95)
VISUAL CTCA-70%	24	150	4	32	43 (31-55) ∫	97 (93-99)	86 (67-95)	82 (76-87)
QCT-30%	56	76	74	0	100 (94-100)	51 (41-60) §	42 (34-51)	100 (95-100)
QCT-50%	43	127	27	13	77 (63-87)	83 (75-88)	61 (49-72)	91 (85-5)
QCT-70%	28	149	5	28	50 (37-63) ∫	97 (91-99)	85 (66-94)	84 (78-89)
MBF	49	139	15	7	88 (74-95) **	90 (82-95) **	77 (61-87) **	95 (90-98) **
SUB-ANALYSIS INCLUDING VESSELS DIRECTLY INTERROGATED WITH FFR (N=68)								
VISUAL CTCA-30%	25	3	40	0	100 (87-100)	7 (2-19) §	39 (28-51)	100 (44-100)
VISUAL CTCA-50%	18	24	19	7	72 (50-87)	56 (38-72) §	49 (32-65)	77 (58-90)
VISUAL CTCA-70%	9	40	3	16	36 (18-59) ∫	93 (81-98)	75 (43-92)	71 (58-82)
QCT-30%	25	11	32	0	100 (87-100)	26 (13-45) §	44 (31-58)	100 (74-100)
QCT 50%	16	32	11	9	64 (42-81)	74 (59-86)	59 (40-76)	78 (62-88)
QCT-70%	9	42	1	16	36 (20-57) ∫	98 (85-100)	90 (53-99)	72 (59-83)
MBF	21	35	8	4	84 (64-94) **	81 (64-92) **	72 (53-86) **	90 (77-96) **

PATIENT LEVEL								
FUNCTIONALLY SIGNIFICANT CORONARY LESION AS STANDARD OF REFERENCE (N=80)								
VISUAL CTCA-30%	40	7	33	0	100 (91-100)	18 (9-32) §	55 (43-66)	100 (65-100)
VISUAL CTCA-50%	33	25	15	7	83 (69-91)	63 (47-76) §	69 (55-80)	78 (61-89)
VISUAL CTCA-70%	21	37	3	19	53 (38-67) ∫	93 (87-97)	88 (69-96)	66 (3-77)
QCT-30%	40	16	24	0	100 (91-100)	40 (26-55)	63 (50-73)	100 (81-100)
QCT-50%	31	29	11	9	78 (63-88)	73 (57-84) §	74 (59-85)	76 (61-87)
QCT-70%	24	37	3	16	60 (45-74) ∫	93 (80-97)	89 (72-96)	70 (57-81)
MBF	36	35	5	4	90 (77-96) **	88 (74-94) **	88 (75-95) **	90 (76-96) **
SUB-ANALYSIS INCLUDING VESSELS DIRECTLY INTERROGATED WITH FFR (N=36)								
VISUAL CTCA-30%	20	0	16	0	100 (84-100)	0 (0-19)	56 (40-71)	NA
VISUAL CTCA-50%	15	4	12	5	75 (53-89)	25 (10-50) §	56 (37-72)	44 (19-73)
VISUAL CTCA-70%	10	13	3	10	50 (30-70) ∫	81 (57-93)	77(50-92)	56 (37-74)
QCT-30%	20	1	15	0	100 (84-100)	6 (1-28) §	57 (41-72)	100 (21-100)
QCT-50%	14	7	9	6	70 (48-86)	44 (23-67)	61 (41-78)	54 (29-77)
QCT-70%	10	12	4	10	50 (30-70) ∫	75 (51-90)	71 (45-88)	55 (35-73)
MBF	18	12	4	2	90 (70-97) **	75 (51-90) **	82 (62-93) **	86 (60-96) **

CTCA-30% = visual analysis with ≥30% diameter narrowing to define positive cases; CTCA-50% = visual analysis with ≥50% diameter narrowing to define positive cases; CTCA-70%= visual analysis with ≥70% diameter narrowing to define positive cases; QCT-30% = semi-automatic quantitative CTCA analysis with ≥30% diameter narrowing to define positive cases; QCT-50% = semi-automatic quantitative CTCA analysis with ≥50% diameter narrowing to define positive cases; QCT-70% = semi-automatic quantitative CTCA analysis with ≥70% diameter narrowing to define positive cases; CI = confidence interval; TP = true positive; TN = true negative; FP = false positive; FN = false negative; PPV = positive predictive value; NPV = negative predictive value.

∫ $p < 0.05$; sensitivity significantly lower than MBF's sensitivity using the McNemar test.

§ $p < 0.05$; specificity significantly lower than MBF's specificity using the McNemar test.

** MBF cut-off value: 78 ml/100ml/min.

Table 5. Diagnostic performance of visual CTCA, QCT and MBF (vessel-territory level) for lesions of intermediate severity (30-70% diameter narrowing on visual CTCA).

	TP	TN	FP	FN	SENSITIVITY, % (95% CI)	SPECIFICITY, % (95% CI)	PPV, % (95% CI)	NPV, % (95% CI)
FUNCTIONALLY SIGNIFICANT CORONARY LESION AS STANDARD OF REFERENCE (N=140)								
VISUAL CTCA-50%	22	74	33	11	67 (47-82)	69 (58-78) ∫	40 (27-57)	87 (78-93)
QCT-50%	20	82	25	13	61 (42-77)	77 (67-84) ∫	44 (31-59)	86 (78-92)
MBF	28	95	12	5	85 (69-94)	89 (78-95)	70 (50-85)	95 (89-98)
SUB-ANALYSIS INCLUDING VESSELS DIRECTLY INTERROGATED WITH FFR (N=54)								
VISUAL CTCA-50%	10	21	16	7	59 (33-81)	57 (38-74) ∫	39 (21-60)	75 (54-87)
QCT-50%	8	27	10	9	47 (24-72)	73 (56-85)	44 (22-69)	75 (58-87)
MBF	13	31	6	4	77 (53-91)	84 (64-94)	68 (40-88)	89 (75-95)

CTCA-50% = visual analysis with ≥50% diameter narrowing to define positive cases; QCT-50% = semi-automatic quantitative CTCA analysis with ≥50% diameter narrowing to define positive cases.
MBF cut-off value: 78 ml/100ml/min.
∫p <0.05; specificity significantly lower than MBF's specificity using the McNemar test.
All other abbreviations as in Table 4.

DISCUSSION

SUMMARY OF MAIN FINDINGS

In this study we evaluated the diagnostic performance of hyperaemic MBF derived from dynamic CT perfusion imaging to identify functionally significant coronary lesions. To avoid referral bias, all patients underwent ICA with FFR independently of the CT results. We used stringent positivity criteria based on FFR and ICA to define functionally significant lesions as the study endpoint. Myocardial territories supplied by functionally significant lesions could be differentiated reliably from the remote myocardium. The performance of MBF (AUC: 0.95) was better than that of CTCA and QCT (AUC's: 0.85 and 0.89, respectively). These findings were consistent on a vessel-territory level as well as on a patient-level. In the sub-analysis restricted to lesions scored as intermediate on CTCA (30% to 70% diameter narrowing), the performance of MBF (AUC: 0.87) remained better than CTCA or QCT (AUC's: 0.68 and 0.69, respectively).

MYOCARDIAL BLOOD FLOW (MBF)

Our study used a dynamic CTP technique that is fundamentally different from static techniques. Unlike static perfusion, where a single set of images is acquired at a single time point within the early arterial phase and the relative distribution of contrast during this phase is used as a surrogate marker of blood flow [16-21], dynamic CTP imaging involves repeated imaging over time to capture the inflow and washout of contrast in the myocardial tissue and vascular compartment to construct time-attenuation curves (TAC's) from which quantitative MBF can be computed [4]. In contrast to static CTP, quantitative MBF does not rely on the assumption that the best-enhanced territory is normal and can be used as reference. MBF provides independent information about each myocardial territory. Quantification of images in general results in more precise and reproducible findings. Quantitative MBF might be particularly useful in cases where relative assessment of lesions' functional significance is difficult such as patients with balanced multi-vessel disease [22, 23]. In our study, the absolute value of MBF to discriminate functionally significant lesions from non-flow limiting lesions was 78ml/100ml/min. This is in keeping with the value of 75ml/100ml/min found by Bamberg et al. [7]. Using this cut-off we could identify all functionally significant lesions in patients with three-vessel disease (Figure 5). It is noteworthy that we could not distinguish whether a hyperaemia-

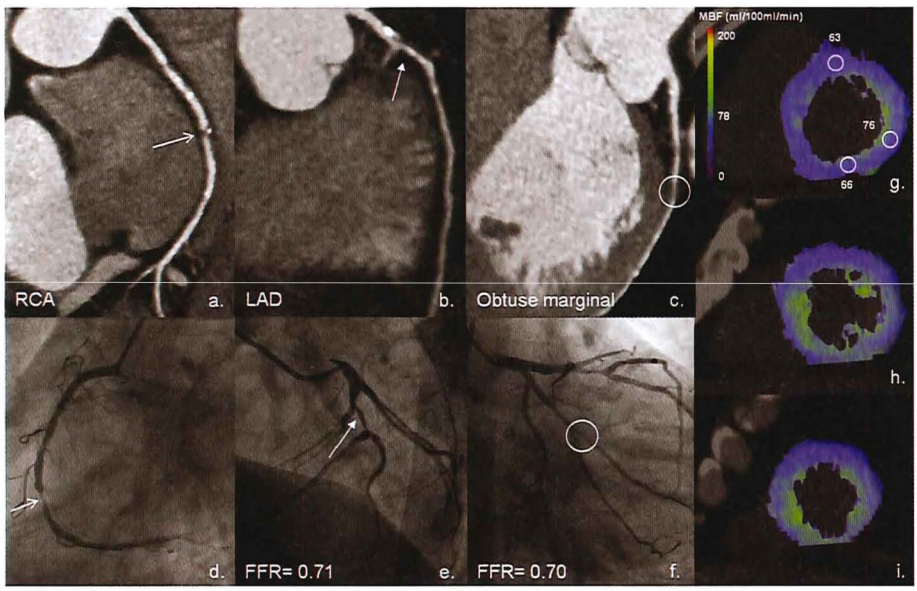

Figure 5. Dynamic CT perfusion imaging in a patient with 3-vessel disease.

64-year-old man with stable chest pain, hypertension and family history of coronary artery disease. (a-c) CTCA showed severe coronary lesion (>70% narrowing) in the mid RCA (arrow; a) and moderate lesions (50-69% narrowing) in the mid LAD (arrow; b) and in the obtuse marginal branch (circle; c). ICA confirmed the critical lesion in the mid RCA (d). Both the LAD and obtuse marginal lesions were functionally significant at FFR (e and f). Color-coded dynamic CT perfusion maps in basal (g), mid (h) and apical (i) short-axis views demonstrated reduced MBF (<78 ml/100ml/min) in the whole myocardium.

induced CTP abnormality was reversible or irreversible (myocardial scar) since this would have required further CTP scan at rest. However, FFR was our reference standard and a decrease in FFR in a lesion supplying an area of myocardial scar cannot be expected [24]. Thus in this proof-of-principle study we decided to restrict the associated radiation exposure and volume of contrast agent. The values of MBF in normal myocardium of healthy subjects during hyperaemia are in the range 200 to 500 ml/100g/min [25]. MBF values found in this study were lower. MBF measured by different imaging modalities (positron emission tomography, magnetic resonance imaging, single photon emission tomography and CT) may differ due to different uptake kinetics of the tracers or contrast agents used, different acquisition protocols and post-processing methods [10, 23, 26]. In our analysis we did not average MBF but selected the lowest MBF measurement in each vascular territory. Difficulty in temporal sampling of the hyperaemic intra-capillary first pass of contrast, which is characterized by fast flow, may be a further explanation for this difference in MBF values.

DIAGNOSTIC PERFORMANCE

Anatomical diameter narrowing is a poor indicator of flow-limiting lesion even by ICA and mismatch between anatomy and function is not unusual [13]. In this study, MBF performed well in the identification of functionally significant lesions compared to FFR, showing that non-invasive imaging has potential value to provide functional information combined with anatomy as guidance to revascularization procedures [1]. MBF had better discriminatory power than visual CTCA and QCT to identify and exclude flow-limiting lesions both on a patient-level and on a vessel-territory level. The performance of a semi-automatic quantitative method (QCT) to measure coronary artery narrowing was better than that of visual CTCA but inferior to MBF. MBF had 90% sensitivity and 88% specificity in the identification of patients with functionally significant lesions, which compared favorably to other imaging modalities such as single photon emission tomography (80% sensitivity, 76% specificity) [27], positron emission tomography (82% sensitivity, 87% specificity) and magnetic resonance imaging (82% sensitivity, 81% specificity) [26].

INTERMEDIATE CORONARY LESIONS

No lesions with <30% coronary diameter narrowing on CTCA were functionally significant and nearly all lesions with ≥70% coronary diameter narrowing were functionally significant, suggesting that in the presence of ≥70% coronary diameter narrowing on CTCA additional testing is unlikely to be helpful and patients may be referred directly to ICA to determine suitability for revascularization [28, 29]. By contrast, intermediate coronary lesions (30-70% diameter narrowing) represent a challenge as the severity of coronary artery narrowing on CTCA is a poor predictor of functional significance. Anatomical CTCA yielded both false posi-

tive and false negative findings in these lesions, in keeping with previous reports [30, 31]. Since revascularization of a coronary lesion is only justified if the lesion is functionally significant [32], we sought to evaluate whether there was an additional value of MBF over visual CTCA or QCT in intermediate coronary lesions. We followed an approach consisting of anatomical testing first (CTCA) to identify intermediate coronary lesions followed by functional testing (MBF) (Table 5). Such an approach is different from that followed by Bamberg et al. [7] where only lesions with ≥50% diameter narrowing on CTCA were reclassified based on MBF to identify functional significance. By identification of intermediate coronary lesions first, as it can be obtained from modern CTCA with low radiation exposure to the patient, CT perfusion imaging can be avoided in patients who have <30% lesions, or at least one ≥70% lesion. With this approach we observed a significant gain in discriminatory power of MBF compared to CTCA and QCT with a significant reduction of false positive findings. In this context, the possibility of non-invasive FFR measurement, albeit still computationally difficult, has been reported with promising results [33] and may further enhance the clinical value of CT in patients with coronary artery disease.

LIMITATIONS

Our study was performed in selected stable patients referred to ICA who consented to participate in this study. Vessels and myocardial territories with poor CT image quality were excluded, as were patients with acute coronary syndromes. This study should be considered a proof-of-principle study and it remains to be demonstrated whether a similar high diagnostic performance of MBF can be achieved in less selected populations. Invasive FFR, considered a reliable standard of reference, reflects the functional consequence of narrowing in epicardial coronary vessels, whereas myocardial blood flow (MBF) depends on epicardial coronary disease as well as myocardial microvascular dysfunction. However, in our study the presence of significant microvascular dysfunction was largely avoided by exclusion of patients with severely impaired left ventricular ejection fraction. Not all vessels were interrogated with FFR. FFR was not performed in angiographically normal vessels, in vessels with <30% diameter narrowing or with ≥90% diameter narrowing, which is in agreement with generally accepted clinical standards. Combining CTCA with CT perfusion imaging will increase patient radiation exposure. Technical developments such as more sophisticated detector arrays and iterative reconstruction algorithms may decrease radiation exposure in the near future. In addition, the combined approach requires a double dose of contrast agent, which necessitates careful selection of patients without impaired renal function.

CONCLUSIONS

The CT evaluation of coronary artery anatomy and hyperaemic MBF performs well as an integrated diagnostic tool to detect functionally significant lesions in patients with stable angina, in particular in patients with intermediate coronary lesions. Future comparative effectiveness studies are warranted to assess the performance of such combined anatomic-physiologic approach in a single non-invasive imaging test in less selected patient populations.

ACKNOWLEDGEMENTS

This work forms part of the research areas contributing to the translational research portfolio of the Cardiovascular Biomedical Research Unit at Barts which is supported and funded by the National Institute for Health Research (NIHR). This study was partly supported by a grant from the FP7-CP-FP 2007 project (grant agreement 222915, EVINCI).

REFERENCES

1. De Bruyne B, Pijls NH, Kalesan B, Barbato E, Tonino PA, Piroth Z, Jagic N, Mobius-Winckler S, Rioufol G, Witt N, Kala P, MacCarthy P, Engstrom T, Oldroyd KG, Mavromatis K, Manoharan G, Verlee P, Frobert O, Curzen N, Johnson JB, Juni P, Fearon WF. Fractional flow reserve-guided pci versus medical therapy in stable coronary disease. *N Engl J Med*. 2012;367:991-1001
2. Bamberg F, Hinkel R, Schwarz F, Sandner TA, Baloch E, Marcus R, Becker A, Kupatt C, Wintersperger BJ, Johnson TR, Theisen D, Klotz E, Reiser MF, Nikolaou K. Accuracy of dynamic computed tomography adenosine stress myocardial perfusion imaging in estimating myocardial blood flow at various degrees of coronary artery stenosis using a porcine animal model. *Invest Radiol*. 2012;47:71-77
3. George RT, Jerosch-Herold M, Silva C, Kitagawa K, Bluemke DA, Lima JA, Lardo AC. Quantification of myocardial perfusion using dynamic 64-detector computed tomography. *Invest Radiol*. 2007;42:815-822
4. Mahnken AH, Klotz E, Pietsch H, Schmidt B, Allmendinger T, Haberland U, Kalender WA, Flohr T. Quantitative whole heart stress perfusion ct imaging as noninvasive assessment of hemodynamics in coronary artery stenosis: Preliminary animal experience. *Investigative radiology*. 2010;45:298-305
5. Rossi A, Uitterdijk A, Dijkshoorn M, Klotz E, Dharampal A, van Straten M, van der Giessen WJ, Mollet N, van Geuns RJ, Krestin GP, Duncker DJ, de Feyter PJ, Merkus D. Quantification of myocardial blood flow by adenosine-stress ct perfusion imaging in pigs during various degrees of stenosis correlates well with coronary artery blood flow and fractional flow reserve. *Eur Heart J Cardiovasc Imaging*. 2012
6. So A, Hsieh J, Li JY, Hadway J, Kong HF, Lee TY. Quantitative myocardial perfusion measurement using ct perfusion: A validation study in a porcine model of reperfused acute myocardial infarction. *The international journal of cardiovascular imaging*. 2012;28:1237-1248
7. Bamberg F, Becker A, Schwarz F, Marcus RP, Greif M, von Ziegler F, Blankstein R, Hoffmann U, Sommer WH, Hoffmann VS, Johnson TR, Becker HC, Wintersperger BJ, Reiser MF, Nikolaou K. Detection of hemodynamically significant coronary artery stenosis: Incremental diagnostic value of dynamic ct-based myocardial perfusion imaging. *Radiology*. 2011;260:689-698
8. Ho KT, Chua KC, Klotz E, Panknin C. Stress and rest dynamic myocardial perfusion imaging by evaluation of complete time-attenuation curves with dual-source ct. *JACC Cardiovasc Imaging*. 2010;3:811-820
9. Wang Y, Qin L, Shi X, Zeng Y, Jing H, Schoepf UJ, Jin Z. Adenosine-stress dynamic myocardial perfusion imaging with second-generation dual-source ct: Comparison with conventional catheter coronary angiography and spect nuclear myocardial perfusion imaging. *AJR Am J Roentgenol*. 2012;198:521-529
10. So A, Wisenberg G, Islam A, Amann J, Romano W, Brown J, Humen D, Jablonsky G, Li JY, Hsieh J, Lee TY. Non-invasive assessment of functionally relevant coronary artery stenoses with quantitative ct perfusion: Preliminary clinical experiences. *Eur Radiol*. 2012;22:39-50
11. Boogers MJ, Schuijf JD, Kitslaar PH, van Werkhoven JM, de Graaf FR, Boersma E, van Velzen JE, Dijkstra J, Adame IM, Kroft LJ, de Roos A, Schreur JH, Heijenbrok MW, Jukema JW, Reiber JH, Bax JJ. Automated quantification of stenosis severity on 64-slice ct: A comparison with quantitative coronary angiography. *JACC Cardiovasc Imaging*. 2010;3:699-709

12. Cerqueira MD, Weissman NJ, Dilsizian V, Jacobs AK, Kaul S, Laskey WK, Pennell DJ, Rumberger JA, Ryan T, Verani MS. Standardized myocardial segmentation and nomenclature for tomographic imaging of the heart: A statement for healthcare professionals from the cardiac imaging committee of the council on clinical cardiology of the american heart association. *Circulation*. 2002;105:539-542
13. Tonino PA, Fearon WF, De Bruyne B, Oldroyd KG, Leesar MA, Ver Lee PN, Maccarthy PA, Van't Veer M, Pijls NH. Angiographic versus functional severity of coronary artery stenoses in the fame study fractional flow reserve versus angiography in multivessel evaluation. *J Am Coll Cardiol*. 2010;55:2816-2821
14. Bossuyt PM, Reitsma JB, Bruns DE, Gatsonis CA, Glasziou PP, Irwig LM, Lijmer JG, Moher D, Rennie D, de Vet HC. Towards complete and accurate reporting of studies of diagnostic accuracy: The stard initiative. *Bmj*. 2003;326:41-44
15. Genders TS, Spronk S, Stijnen T, Steyerberg EW, Lesaffre E, Hunink MG. Methods for calculating sensitivity and specificity of clustered data: A tutorial. *Radiology*. 2012;265:910-916
16. Blankstein R, Shturman LD, Rogers IS, Rocha-Filho JA, Okada DR, Sarwar A, Soni AV, Bezerra H, Ghoshhajra BB, Petranovic M, Loureiro R, Feuchtner G, Gewirtz H, Hoffmann U, Mamuya WS, Brady TJ, Cury RC. Adenosine-induced stress myocardial perfusion imaging using dual-source cardiac computed tomography. *J Am Coll Cardiol*. 2009;54:1072-1084
17. Feuchtner G, Goetti R, Plass A, Wieser M, Scheffel H, Wyss C, Stolzmann P, Donati O, Schnabl J, Falk V, Alkadhi H, Leschka S, Cury RC. Adenosine stress high-pitch 128-slice dual-source myocardial computed tomography perfusion for imaging of reversible myocardial ischemia: Comparison with magnetic resonance imaging. *Circ Cardiovasc Imaging*. 2011;4:540-549
18. George RT, Arbab-Zadeh A, Miller JM, Vavere AL, Bengel FM, Lardo AC, Lima JA. Computed tomography myocardial perfusion imaging with 320-row detector computed tomography accurately detects myocardial ischemia in patients with obstructive coronary artery disease. *Circ Cardiovasc Imaging*. 2012;5:333-340
19. Ko BS, Cameron JD, Meredith IT, Leung M, Antonis PR, Nasis A, Crossett M, Hope SA, Lehman SJ, Troupis J, DeFrance T, Seneviratne SK. Computed tomography stress myocardial perfusion imaging in patients considered for revascularization: A comparison with fractional flow reserve. *Eur Heart J*. 2012;33:67-77
20. Rocha-Filho JA, Blankstein R, Shturman LD, Bezerra HG, Okada DR, Rogers IS, Ghoshhajra B, Hoffmann U, Feuchtner G, Mamuya WS, Brady TJ, Cury RC. Incremental value of adenosine-induced stress myocardial perfusion imaging with dual-source ct at cardiac ct angiography. *Radiology*. 2010;254:410-419
21. Techasith T, Cury RC. Stress myocardial ct perfusion: An update and future perspective. *JACC Cardiovasc Imaging*. 2011;4:905-916
22. Hajjiri MM, Leavitt MB, Zheng H, Spooner AE, Fischman AJ, Gewirtz H. Comparison of positron emission tomography measurement of adenosine-stimulated absolute myocardial blood flow versus relative myocardial tracer content for physiological assessment of coronary artery stenosis severity and location. *JACC Cardiovasc Imaging*. 2009;2:751-758

23. Kajander SA, Joutsiniemi E, Saraste M, Pietila M, Ukkonen H, Saraste A, Sipila HT, Teras M, Maki M, Airaksinen J, Hartiala J, Knuuti J. Clinical value of absolute quantification of myocardial perfusion with (15) o-water in coronary artery disease. *Circ Cardiovasc Imaging.* 2011;4:678-684
24. Pijls NH, Sels JW. Functional measurement of coronary stenosis. *J Am Coll Cardiol.* 2012;59:1045-1057
25. Chareonthaitawee P, Kaufmann PA, Rimoldi O, Camici PG. Heterogeneity of resting and hyperemic myocardial blood flow in healthy humans. *Cardiovascular research.* 2001;50:151-161
26. Morton G, Chiribiri A, Ishida M, Hussain ST, Schuster A, Indermuehle A, Perera D, Knuuti J, Baker S, Hedstrom E, Schleyer P, O'Doherty M, Barrington S, Nagel E. Quantification of absolute myocardial perfusion in patients with coronary artery disease: Comparison between cardiovascular magnetic resonance and positron emission tomography. *J Am Coll Cardiol.* 2012;60:1546-1555
27. Hacker M, Rieber J, Schmid R, Lafougere C, Tausig A, Theisen K, Klaus V, Tiling R. Comparison of tc-99m sestamibi spect with fractional flow reserve in patients with intermediate coronary artery stenoses. *J Nucl Cardiol.* 2005;12:645-654
28. Gaemperli O, Schepis T, Valenta I, Koepfli P, Husmann L, Scheffel H, Leschka S, Eberli FR, Luscher TF, Alkadhi H, Kaufmann PA. Functionally relevant coronary artery disease: Comparison of 64-section ct angiography with myocardial perfusion spect. *Radiology.* 2008;248:414-423
29. Nicol ED, Stirrup J, Reyes E, Roughton M, Padley SP, Rubens MB, Underwood SR. Sixty-four-slice computed tomography coronary angiography compared with myocardial perfusion scintigraphy for the diagnosis of functionally significant coronary stenoses in patients with a low to intermediate likelihood of coronary artery disease. *J Nucl Cardiol.* 2008;15:311-318
30. Meijboom WB, Van Mieghem CA, van Pelt N, Weustink A, Pugliese F, Mollet NR, Boersma E, Regar E, van Geuns RJ, de Jaegere PJ, Serruys PW, Krestin GP, de Feyter PJ. Comprehensive assessment of coronary artery stenoses: Computed tomography coronary angiography versus conventional coronary angiography and correlation with fractional flow reserve in patients with stable angina. *J Am Coll Cardiol.* 2008;52:636-643
31. Sarno G, Decraemer I, Vanhoenacker PK, De Bruyne B, Hamilos M, Cuisset T, Wyffels E, Bartunek J, Heyndrickx GR, Wijns W. On the inappropriateness of noninvasive multidetector computed tomography coronary angiography to trigger coronary revascularization: A comparison with invasive angiography. *JACC. Cardiovascular interventions.* 2009;2:550-557
32. Wijns W, Kolh P, Danchin N, Di Mario C, Falk V, Folliguet T, Garg S, Huber K, James S, Knuuti J, Lopez-Sendon J, Marco J, Menicanti L, Ostojic M, Piepoli MF, Pirlet C, Pomar JL, Reifart N, Ribichini FL, Schalij MJ, Sergeant P, Serruys PW, Silber S, Sousa Uva M, Taggart D. Guidelines on myocardial revascularization. *Eur Heart J.* 2010;31:2501-2555
33. Min JK, Leipsic J, Pencina MJ, Berman DS, Koo BK, van Mieghem C, Erglis A, Lin FY, Dunning AM, Apruzzese P, Budoff MJ, Cole JH, Jaffer FA, Leon MB, Malpeso J, Mancini GB, Park SJ, Schwartz RS, Shaw LJ, Mauri L. Diagnostic accuracy of fractional flow reserve from anatomic ct angiography. *Jama.* 2012;308:1237-1245

CHAPTER 8

PATIENT WITH MICROVASCULAR OBSTRUCTION AND MYOCARDIAL BRIDGING: MULTIMODALITY APPROACH WITH DYNAMIC CT PERFUSION IMAGING, INVASIVE CORONARY ANGIOGRAPHY, INDEX OF MICROVASCULAR RESISTANCE AND FRACTIONAL FLOW RESERVE

2013 (submitted for publication)

A Rossi
A Dharampal
PJ de Feyter
C Schultz

A male aged 53y with hypercholesterolaemia presented with exertional dyspnoea. Exercise ECG was negative for ischaemia. Coronary calcium score was high (618 Agatston units). CT-angiography indicated intermediate lesions in the right, RCA, (A) the left anterior descending, LAD, (B) and the left circumflex, LCx, (C) coronary arteries (arrows). Adenosine CT-perfusion showed reduced myocardial blood flow (MBF) in the left ventricle antero-septal and inferior walls, but not in the lateral wall, respectively 78, 65 and 100 ml/100ml/min (D). Invasive coronary angiography demonstrated intermediate lesions in the RCA (E), LAD (F) and LCx (H) and myocardial bridging in the mid LAD (F: diastolic phase; G: systolic phase). Fractional flow reserve was reduced in the LAD (0.85 proximal to bridging, 0.76 distal to bridging) but not in the RCA (0.84) or LCx (0.87). The index of microvascular resistance (IMR) was substantially elevated in the RCA (IMR=35, normal: <20).

Adenosine CT-perfusion provides new possibilities for investigating cardiac microvascular disease non-invasively by combining epicardial coronary anatomy and MBF.

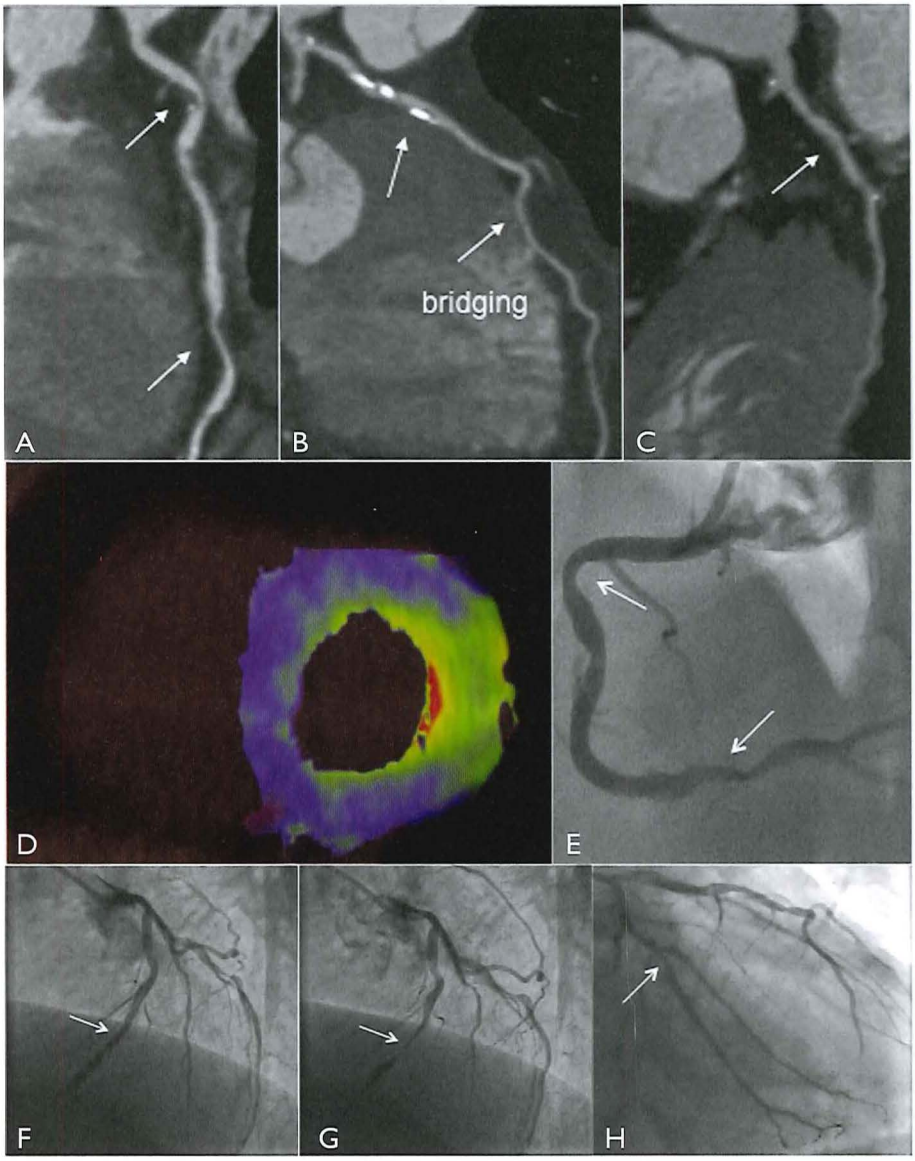
A
B
bridging
C
D
E
F
G
H

PART 2: AORTIC VALVE STENOSIS

CHAPTER 9

ASCENDING AORTA DILATATION IN PATIENTS WITH BICUSPID AORTIC VALVE: PROSPECTIVE CMR STUDY.

European Radiology, 2012; 23(3): 642-649

A Rossi
D van der Linde
SC Yap
S Kirschbaum
T Lapinskas
T Springeling
M Witsenburg
J Cuypers
A Moelker
GP Krestin
A van Dijk
M Johnson
RJ van Geuns
JW Roos-Hesselink.

ABSTRACT

Background: The aim of this study was to evaluate the natural progression of aortic dilatation and its association with aortic valve stenosis (AoS) in patients with bicuspid aortic valve (BAV).

Methods: Prospective study of aorta dilatation in patients with BAV and AoS using cardiac magnetic resonance (CMR). Aortic root, ascending aorta, aortic peak velocity, left ventricular systolic and diastolic function and mass were assessed at baseline and at 3-years follow-up.

Results: Of the 33 enrolled patients, 5 needed surgery, while 28 patients (17 male; mean age: 31 ±8 years) completed the study. Aortic diameters significantly increased at aortic annulus, sinus of Valsalva and tubular ascending aorta levels ($P<0.05$). The number of patients with dilated tubular ascending aorta increased from 32% to 43%. No significant increase in sino-tubular-junction diameter was observed. Aortic peak velocity, ejection fraction and myocardial mass significantly increased while the early/late filling ratio significantly decreased at follow-up ($P<0.05$). The progression rate of the ascending aorta diameter correlated weakly with the aortic peak velocity at baseline ($R^2=0.16$, $P=0.04$).

Conclusion: BAV patients with AoS showed a progressive increase of aortic diameters with maximal expression at the level of the ascending aorta. The progression of aortic dilatation correlated weakly with the severity of AoS.

INTRODUCTION

Bicuspid aortic valve (BAV) is the most common congenital heart defect with an estimated prevalence of 0.5% - 2% [1]. Patients with BAV show an increased risk of developing aortic valve dysfunction and dilatation of the thoracic aorta [2, 3]. There is still controversy whether the pathogenesis of the dilatation of the ascending aorta in BAV patients is caused by a genetic predisposition or that the aortic valvular stenosis causes post-stenotic dilatation due to blood flow turbulences (haemodynamic theory). In addition, despite the high prevalence of BAV disease in the general population, longitudinal data investigating the natural history of the disease process is scarce.

Therefore the aims of this study were to prospectively evaluate the natural progression of ascending aorta dilatation in asymptomatic BAV patients with aortic stenosis (AoS) and its association with the haemodynamic progression of valvular stenosis using cardiovascular magnetic resonance (CMR) as reference standard.

METHODS

STUDY DESIGN AND POPULATION

This prospective study included asymptomatic patients with BAV and AoS. Consecutive patients visiting the out-patient clinic of our hospital were invited to participate. Inclusion criteria were age between 18 and 50 years, a bicuspid aortic valve and a peak flow velocity over the valve above 2.5 m/s based on echocardiographic measurements. Exclusion criteria were sub-valvular or supra-valvular aortic stenosis, severe aortic regurgitation, symptoms, previous aortic valve replacement or a concomitant significant mitral valve lesion. Patients underwent CMR at baseline and after 3-years of follow-up. Patients who did not complete the follow-up were excluded from further analysis. The study protocol was approved by the institutional review board of our university hospital. All patients gave written informed consent.

CARDIAC MAGNETIC RESONANCE

CMR imaging was performed at 1.5T (Signa CV/I, GE Medical Systems at baseline upgraded to Signa Discovery 450, GE Healthcare, Milwaukee, Wisconsin at follow-up). Patients were placed in supine position and entered feet first into the magnet. A dedicated cardiac coil (4 channels coil at baseline and 8 channels coil at follow-up) was placed on the thorax of each patient and used for the acquisition of the images. All the studies were analysed on a remote workstation. CAAS- MRV (version 3.1; Pie Medical Imaging, Maastricht, The Netherlands) was used for the left ventricular (LV) function evaluation. Quantitative flow measurements

were performed using CINE software (version 3.4, GE Medical System, Milwaukee, Wisconsin, USA).

LV FUNCTION

Cine MR images were obtained using a breath-holding ECG triggered balanced steady state free precession (SSFP) pulse sequence. Imaging parameters included the following: FOV 36-40 x 28-32 cm; matrix 224 x 196; TR: 3.4 milliseconds; TE: 1.5 ms; flip angle 45 degrees; 12 views per segment. Slice thickness was 8 mm with a gap of 2 mm. These parameters resulted in a temporal resolution per image of 41 ms with a heart rate of 60 bpm. First, three rapid surveys were obtained for the determination of the cardiac position and orientation; 2- and 4-chamber cine MR images were then obtained. The series of short axis images were obtained from the reference images provided by the 2- and 4- chamber end-diastolic images at the end of expiration. Approximately 10 to 12 slices were acquired to cover the entire length of the heart. For all patients LV function was analysed using both a combination of the short axis view and the long axis views [4]. Endocardial and epicardial contours were automatically detected by dedicated software and manually corrected on each cardiac phase [4,5]. The papillary muscles were considered as being part of the blood pool. End-diastolic volume (EDV), end-systolic volume (ESV), ejection fraction (EF), stroke volume (SV) and cardiac output (CO) were calculated for each patient at both baseline and follow-up times and presented either as absolute numbers or indexed to body surface area (BSA).

Time-volumes curves of the left ventricle were plotted as volume versus time during the diastolic phase for the determination of LV diastolic function. The volumetric filling curves were also transformed to the first derivative to obtain early and late profile [6]. Peak early filling rate (PEFR), time to PEFR, peak late filling rate (PLFR) and early/late ratio were calculated. Heart rate (HR) was recorded during CMR acquisition.

AORTIC DIAMETERS

Cine SSFP images for the measurements of the aortic diameters were acquired in the oblique and double oblique sagittal plane of the left ventricular outflow tract (LVOT). The diameter of the ascending aorta was measured at four different levels: aortic annulus, defined as the hinge points of the atrio-ventricular valve (level 1), sinus of Valsava, defined as the mid point of the aortic sinus of Valsalva (level 2), sino-tubular junction (level 3) and tubular portion of the ascending aorta, at the level of the pulmonary trunk (level 4) (Figure 1). At each level the external diameter was measured perpendicular to the axis of blood flow during peak systole [7]. Aortic measurements were presented either as absolute numbers or indexed to BSA.

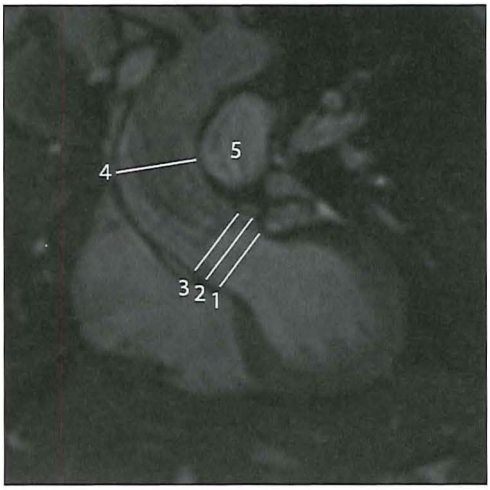

Figure 1. Measurements of the aortic diameters. The oblique sagittal SPSS view of the aorta shows the measurements of the aortic root: at the level of the aortic annulus (1), the sinus of Valsalva (2), the sinotubular junction (3) and the tubular portion of ascending aorta (4) at the level of the pulmonary trunk (5).

Images were assessed by two independent observers (AR and TL). One observer who was blinded to the previous results measured the datasets twice, at least 12 weeks after the first measurement.

AORTIC VALVE FUNCTION

A retrospective gated velocity-encoded sequence during expiratory breath-holds was used (FOV: 36-40 x 16-20 cm; TR: 6.5ms; TE: 3.1ms; flip angle: 30°; matrix: 256x128). The 3-chamber view was used to plan three velocity-mapping planes parallel to aortic valve as described previously [8]. Regions of interest (ROI) were drawn on each of the 30 frames of the velocity-encoded sequence to include the aortic valve and the aorta depending on slice position. Peak velocities were extracted for the greatest velocity recorded in any pixel within the ROI. Aortic valve area (AVA) was calculated using the continuity equation as previously described [8].

STATISTICAL ANALYSIS

Statistical analysis was performed using SPSS software (version 17.0, SPSS Inc., Chicago, Illinois, USA). Continuous variables were tested for normality using the Kolmogorov-Smirnov test. Continuous data are expressed as mean ± standard deviation (SD) and qualitative variables as count and percentage. Differences of baseline characteristics between the group of patients who completed the study and the group of patients who interrupted the study were tested using the Mann-Whitney U test. Continuous variables between the two different timepoints were compared by the paired samples t-test if the data were normally distributed, or the Wilcoxon signed ranks test for non-normal data. Annual rates of progression of aortic diameters were calculated and expressed as means±SD. Linear regression models were performed between the progression rate of ascending aorta diameter and aortic peak velocity at baseline and diameter of ascending aorta at baseline. Intra- and inter-observer variability

Table 1. Baseline characteristics of the overall BAV population and grouped according to the completion of the study

POPULATION VARIABLE	TOTAL POPULATION (N=33)	POPULATION WITH BASELINE AND FOLLOW-UP CMR (N=28)	POPULATION WHO UNDERWENT AORTIC SURGERY (N=5)	P-VALUE
Age (years)	32±8	32±8	38±9	0.108
Men	22 (67%)	17 (61%)	5 (100%)	0.068
Systolic blood pressure (mmHg)	132±15	132±15	130±17	0.706
Diastolic blood pressure (mmHg)	76±10	75±9	83±10	0.138
EF (%)	56±8	57±7	54±12	0.209
SV (ml)	115±36	112±38	131±17	0.098
CO (L/min)	7.7±2.4	7.5±2.6	8.6±1.6	0.192
Mass (g)	133±42	124±38	184±27	0.009
Aortic annulus (mm)	27±6	26±7	30±3	0.119
Sinus of Valsalva (mm)	33±5	33±6	34±4	0.615
Sino-tubular junction (mm)	29±5	28±5	31±5	0.340
Tubular ascending aorta (mm)	38±7	37±6	44±5	0.022
Aortic peak velocity (cm/sec)	335±80	319±74	423±53	0.009

Data are reported as mean±SD or n (%).
SV = stroke volume; EF= ejection fraction; CO= cardiac output

of each aortic diameter were assessed in 25 randomly selected patients and presented as mean difference (measure of precision) with SD (measure of accuracy) and the corresponding correlation coefficient (r).
A *P*-value <0.050 was considered significant.

RESULTS

DEMOGRAPHIC CHARACTERISTICS

Thirty-three asymptomatic patients were enrolled in the study and underwent baseline CMR. During follow-up five patients needed surgical correction of their aortic stenosis. Two of them underwent a Bentall procedure and three a isolated aortic valve replacement. The mean time±SD between study inclusion and aortic valve replacement was 21±11 months. These 5 patients were excluded from further analysis.

Table 2. Comparison of LV haemodynamic parameters and mass at baseline and follow-up (n=28).

	BASELINE	FOLLOW-UP	P-VALUE
EDV			
Absolute (ml)	197±65	198±61	0.929
Indexed (ml/m²)	103±31	103±29	0.716
ESV			
Absolute (ml)	86±32	81±32	0.010
Indexed (ml/m²)	45±17	43±16	0.009
EF (%)	57±7	59±7	<0.001
SV			
Absolute (ml)	112±38	116±35	0.104
Indexed (ml/m²)	59±17	61±17	0.078
CO (L/min)	7.5±2.6	7.9±2.1	0.246
Mass			
Absolute (g)	124±38	128±39	0.006
Indexed (g/m²)	65±18	67±18	0.011
Heart rate (bpm)	68±10	69±10	0.649
PEFR (ml/s)	509±187	571±148	0.601
PLFR (ml/s)	281±210	362±164	0.067
TPEFR (s)	140±39	153±33	0.226
Early/late ratio	2.4±1.1	1.8±0.7	0.032

Data are reported as mean±SD.
EDV = end-diastolic volume; ESV = end-systolic volume; EF = ejection fraction; SV = stroke volume; CO = cardiac output; PEFR = peak early filling rate; PLFR = peak late filling rate; TPEFR = time to peak filling rate.

Twenty-eight patients completed the study and underwent follow-up CMR. Mean follow-up was 34±6 months. Seventeen patients (61%) were male. The age ranged from 21 to 49 years (31±8 years). Mean BSA was 1.9±0.2. Twenty-three/28 (82%) patients showed no or mild aortic regurgitation at echocardiography while 5/28 (18%) showed moderate aortic regurgitation. Baseline characteristics of all patients are reported in Table 1. Myocardial mass, diameter of tubular ascending aorta and aortic peak velocity were significantly higher in the group of patients who underwent surgery.

LV PARAMETERS AND MASS

Changes in LV haemodynamic parameters and mass are described in Table 2. Ejection fraction and LV mass significantly increased from baseline to follow-up ($P<0.001$ and $P=0.006$, respectively). End- systolic volume significantly decreased ($p=0.01$). No significant changes over time were observed for EDV, SV and CO. The early/late ratio was significantly lower at follow-up compared to baseline ($P=0.032$).

AORTIC DIAMETERS AND VALVULAR STENOSIS

The largest diameter was found at the level of the tubular ascending aorta. Of the 28 patients, 9 (32%) showed dilatation of the tubular portion of the ascending aorta (> 4 cm) at baseline. The number of patients with dilated aorta increased to 12/28 at follow up (43%). Absolute aortic diameters significantly increased during follow-up at the levels of aortic annulus, sinus of Valsava and tubular portion of ascending aorta. No significant changes were observed at the level of sino-tubular junction (Table 3, Figure 2). Aortic diameters at all levels were significantly larger in the subgroup of patients with moderate aortic regurgitation compared with the group of patients with no or mild aortic regurgitation ($P<0.05$).

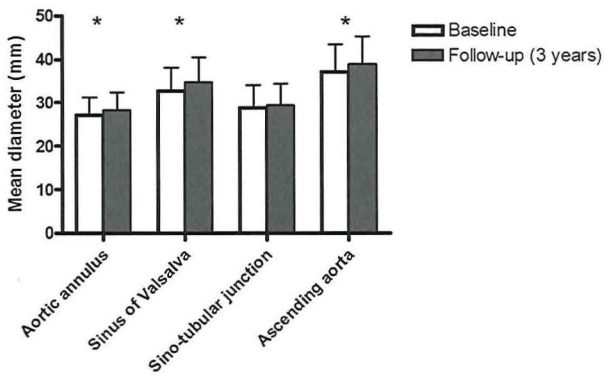

Figure 2. Comparison of aortic diameters and valvular stenosis at baseline and follow-up.
* P-value<0.05

Table 3. Comparison of aortic diameters and valvular stenosis at baseline and follow-up (n=28).

	BASELINE	FOLLOW-UP	P-VALUE	PROGRESSION RATES
Aortic Annulus				
Absolute (mm)	26±7	28±4	0.011	0.6±1.1 mm/year
Indexed (mm/m²)	14±2	15±2	0.010	
Sinus of Valsalva				
Absolute (mm)	33±6	35±6	0.001	0.8±1.1 mm/year
Indexed (mm/m²)	17±3	18±3	<0.001	
Sino-tubular junction				
Absolute (mm)	28±5	29±5	0.168	0.2±1.2 mm/year
Indexed (mm/m²)	15±3	16±3	0.229	
Tubular ascending aorta				
Absolute (mm)	37±6	39±6	<0.001	0.7±0.6 mm/year
Indexed (mm/m2)	20±3	21±4	<0.001	
Aortic peak velocity (cm/s)	319±74	348±94	0.010	11±21 cm/s/year

Data are reported as mean±SD

The mean progression rate of the tubular portion of the ascending aorta diameter was 0.7±0.6 mm/year (Table 3). In the overall population, the mean aortic peak velocity increased significantly at follow up (P=0.010) with a mean increase of 11±21 cm/s/year (Table 3). Aortic valve area significantly decreased from 1.4 cm^2 at baseline to 1.2 cm^2 at follow-up (P=0.004).

The patients were classified in three different groups based on the mean progression rate of the tubular portion of ascending aorta diameter. Fourteen patients (50%) showed a progression rate between 0 and 0.5 mm/year ("slow progression group", mean progression rate: 0.2±0.2 mm/year), 8 patients (28.6%) had a progression rate between 0.5 and 1.0 mm/year ("moderate progression group", mean progression rate: 0.7±0.1 mm/year), while 6 patients (21.4%) had a progression rate>1.0 mm/year ("fast progression group", mean progression rate: 1.7±0.4 mm/year). Baseline characteristics and aortic diameters did not differ

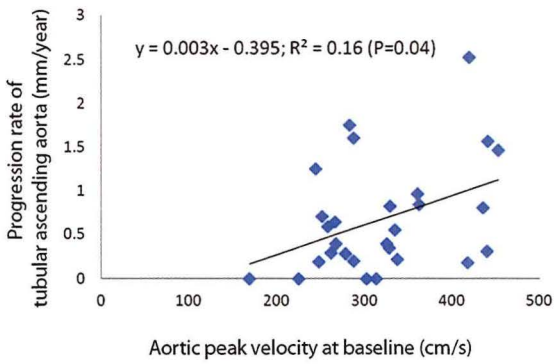

Figure 3. Regression line between the progression rate of tubular ascending aorta diameter and aortic peak velocity at baseline.

Table 4. Intra- and inter-observer variability of aortic diameters by CMR

	INTRA-OBSERVER VARIABILITY		INTER-OBSERVER VARIABILITY	
Variable	Absolute mean difference	r	Absolute mean difference	r
Aortic annulus (mm)	0.8±5.5	0.6	0.1±6.1	0.5
Sinus of Valsalva (mm)	0.4±4.2	0.7	1.4±3.1	0.8
Sino-tubular junction (mm)	1.0±2.9	0.8	0.3±3.1	0.8
Tubular ascending aorta (mm)	0.2±0.8	0.9	0.2±2.2	0.9

Data are reported as mean±SD.

within the different subgroups (P>0.05). The peak velocity over the aortic valve at baseline was 300±71 cm/s in the "slow progression group", 325±63 cm/s in the "moderate progression group" and 354±93 cm/s in the "fast progression group"; P=0.443.

The progression rate of the tubular portion of the ascending aorta diameter calculated in the overall population correlated weakly with the aortic peak velocity at baseline: R^2=0.16, P=0.04, Figure 3. No significant correlation was found between the progression rate of the tubular portion of the ascending aorta diameter and the diameter of the tubular portion of the ascending aorta at baseline: R^2=0.01; P=0.631.

The results of inter-observer and intra-observer variability of aortic diameters are reported in Table 4.

DISCUSSION

To our knowledge the present study is the first investigating the natural progression of aortic dimensions and aortic valve function in adult BAV patients with AoS using a prospective design and CMR as reference standard. This study showed that patients with BAV experienced a progressive increase in thoracic aortic dilatation and severity of aortic stenosis over time and that the rate of aortic dilatation was weekly correlated with the aortic peak velocity at baseline.

NATURAL HISTORY OF BAV PATIENTS

The natural history of patients with BAV and AoS differs from that of patients with stenotic tricuspid aortic valve in two aspects. Firstly, BAV patients show an earlier onset of significant aortic valve stenosis and regurgitation, already during the third or fourth decade of life. In

our study population the annual change of aortic jet velocity was 11 cm/s/year, which is in concordance with previous echocardiographic studies [9-11]. We found a concomitant increase in LV mass. As previously shown, hypertrophy is an initial adaptive response to pressure overload, which may lead to adverse consequences in the long run [12]. In our population, we observed a reduced ESV over time with a consequent increased ejection fraction. This has not been described before. An early decrease in diastolic function was also observed. This may be related to the stiffer ventricle due to the significant increase in LV mass. As shown in previous clinical studies LV diastolic dysfunction may precede LV systolic dysfunction [13]. In the 5 patients who underwent surgery during the study the mean ejection fraction at baseline was slightly lower. The exact point at which to intervene in asymptomatic patients with severe AoS is still disputed, but perhaps more detailed longitudinal studies will reveal that the development of LV diastolic and systolic dysfunction in association with LV mass thickness can be used as indicators of the need for intervention.

The second difference is the dilatation of the ascending aorta which is a common finding in BAV patients [14]. Indeed, up to 50% of BAV patients with normally functioning aortic valve show aortic dilatation [15, 16]. The prevalence of aortic dilatation in our cohort, as composed by BAV patients with aortic stenosis, was 32% at baseline and increased to 43% at follow-up. Only a few echocardiographic studies have estimated the rate of progression of aortic dilatation over time [17-19]. Similarly to the findings of Ferencik and Pape [18], we observed a significant progressive increase of aortic dimensions at all levels with the exception of the sino-tubular junction where the mean diameter remained unchanged over time. A possible explanation may be a different expression at this level of matrix protein and tissue inhibitor of metalloproteinases compared with the other sites of the aortic root and the tubular portion of the ascending aorta [20]. In agreement with previous echocardiographic studies, in our study the largest diameter was measured at the level of the tubular portion of the ascending aorta. It has been reported previously that dilatation at this level occurs more rapidly than in other segments [21]. In our study, the mean progression rate was 0.7 mm per year, which is slightly slower than the progression rate of 0.9 mm per year reported by Ferencik and Pape [18]. The younger age of our patients may explain the slower progression rate of aortic dilatation observed in our study.

ASSOCIATION BETWEEN AoS AND AORTIC DILATATION

Currently, there are two theories explaining the aortopathy observed in BAV patients [22]. The first theory suggests that the association of aortic dilatation with BAV may be secondary to an intrinsic aortic wall pathology, resulting in weakness of the aortic wall and consequent dilatation. Indeed, marked degenerative changes of the aortic wall, including cystic medial necrosis [23] and loss of elastic elements [24], have been described in the aorta of BAV patients. The second theory suggests that there may also be some haemodynamic factors that contribute to the aortic dilatation, although dilatation has been described in the absence of AoS

and regurgitation. The haemodynamic theory is based on the idea that the orientation and the morphology of a BAV cause turbulent blood flow in the ascending aorta and an increase in aortic wall shear stress. Hope et al [25, 26] demonstrated recently an abnormal systolic helical flow in BAV patients which was not found in any of the healthy volunteers or patients with a tricuspid aortic valve. We found a significant correlation, although weak, between aortic peak velocity at baseline and progression of aortic dilatation. The high aortic peak velocity with concomitant turbulence in the aortic root and in the tubular portion of the ascending aorta may be one of the mechanisms in the development of aortic dilatation[27]. Although we expect indeed this to be a cause effect relation, we cannot exclude a genetic origin based on these findings, as both severity of aortic stenosis and aortic dilatation may be just an effect of time. Our study is the first to identify a relationship between the severity of the aortic stenosis and the rate of progression of the dilatation of the tubular portion of the thoracic aorta. This is still not overwhelming evidence and more studies on long-term outcome in native BAV patients and patients after isolated aortic valve replacement are needed to understand better the underlying mechanism of aortic dilatation. This is clinically relevant, as it will influence the surgical techniques employed and the frequency of aortic screening [28, 29].

DIAGNOSTIC MANAGEMENT OF BAV PATIENTS

In BAV patients diameters of aortic root and ascending aorta should be monitored periodically due to the increase risk of developing concurrent tubular ascending aortic aneurysm that may require surgical repair [30]. Transthoracic echocardiography (TTE) is a widely used, non-invasive imaging investigation but the mid ascending aorta can be difficult to examine with ultrasound. In recent guidelines of the European Society of Cardiology the use of CMR is suggested as the first line investigation for the assessment of aortic diameters as a guide for the therapy of the patient [31]. It has been proven that measurements of the diameters of the entire thoracic aorta can be performed accurately with SSFP technique and with high contrast between vessels and surrounding tissues with good intra- and inter-observer variability [32]. In addition CMR can provide other information such as reliable judgment of systolic and diastolic LV function, valve assessment, aortic distensibility and pulse wave velocity.

LIMITATIONS

This study has some limitations that are either related to our study design or are more general limitations of MR technology.

STUDY DESIGN

Firstly, the number of patients enrolled in the study was small and three-year follow-up was relatively short. Secondly, we decided to include only BAV patients with AoS, so our findings

cannot be translated to BAV patients without stenosis. In addition, the exclusion of patients who underwent surgery may have led to an underestimation of the incidence and rate of progression of aortic dilatation. Finally, we did not look at the different BAV morphologies or at the specific dilatation pattern, which may play a role in the haemodynamic theory of BAV-aortopathy [33, 34].

MR TECHNOLOGY

Although several validation studies have shown that anterograde velocity as measured by CMR correlates well with TTE, CMR has a trend to underestimate the aortic peak velocity and the mean pressure gradient [35, 36], Moreover, differently from cardiac CT, CMR does not provide information of valvular and aortic calcifications [33].

CONCLUSIONS

Our study demonstrates that in adult asymptomatic patients with BAV and AoS there is a progressive increase of aortic diameters over time, which is maximal at the level of the tubular portion of the ascending aorta. The weak correlation between the progression of aortic dilatation and AoS severity partially supports the hemodynamic theory of causation of the aortopathy associated with BAV.

REFERENCES

1. Ward C. Clinical significance of the bicuspid aortic valve. *Heart*. 2000;83:81-85
2. Roberts WC, Ko JM. Frequency by decades of unicuspid, bicuspid, and tricuspid aortic valves in adults having isolated aortic valve replacement for aortic stenosis, with or without associated aortic regurgitation. *Circulation*. 2005;111:920-925
3. Roberts WC, Morrow AG, McIntosh CL, Jones M, Epstein SE. Congenitally bicuspid aortic valve causing severe, pure aortic regurgitation without superimposed infective endocarditis. Analysis of 13 patients requiring aortic valve replacement. *Am J Cardiol*. 1981;47:206-209
4. Kirschbaum SW, Baks T, Gronenschild EH, Aben JP, Weustink AC, Wielopolski PA, Krestin GP, de Feyter PJ, van Geuns RJ. Addition of the long-axis information to short-axis contours reduces interstudy variability of left-ventricular analysis in cardiac magnetic resonance studies. *Invest Radiol*. 2008;43:1-6
5. van Geuns RJ, Baks T, Gronenschild EH, Aben JP, Wielopolski PA, Cademartiri F, de Feyter PJ. Automatic quantitative left ventricular analysis of cine mr images by using three-dimensional information for contour detection. *Radiology*. 2006;240:215-221
6. Kudelka AM, Turner DA, Liebson PR, Macioch JE, Wang JZ, Barron JT. Comparison of cine magnetic resonance imaging and doppler echocardiography for evaluation of left ventricular diastolic function. *Am J Cardiol*. 1997;80:384-386
7. Hiratzka LF, Bakris GL, Beckman JA, Bersin RM, Carr VF, Casey DE, Jr., Eagle KA, Hermann LK, Isselbacher EM, Kazerooni EA, Kouchoukos NT, Lytle BW, Milewicz DM, Reich DL, Sen S, Shinn JA, Svensson LG, Williams DM. 2010 accf/aha/aats/acr/asa/sca/scai/sir/sts/svm guidelines for the diagnosis and management of patients with thoracic aortic disease. A report of the american college of cardiology foundation/american heart association task force on practice guidelines, american association for thoracic surgery, american college of radiology,american stroke association, society of cardiovascular anesthesiologists, society for cardiovascular angiography and interventions, society of interventional radiology, society of thoracic surgeons,and society for vascular medicine. *J Am Coll Cardiol*. 2010;55:e27-e129
8. Yap SC, van Geuns RJ, Meijboom FJ, Kirschbaum SW, McGhie JS, Simoons ML, Kilner PJ, Roos-Hesselink JW. A simplified continuity equation approach to the quantification of stenotic bicuspid aortic valves using velocity-encoded cardiovascular magnetic resonance. *J Cardiovasc Magn Reson*. 2007;9:899-906
9. Michelena HI, Desjardins VA, Avierinos JF, Russo A, Nkomo VT, Sundt TM, Pellikka PA, Tajik AJ, Enriquez-Sarano M. Natural history of asymptomatic patients with normally functioning or minimally dysfunctional bicuspid aortic valve in the community. *Circulation*. 2008;117:2776-2784
10. Yap SC, Kouwenhoven GC, Takkenberg JJ, Galema TW, Meijboom FJ, van Domburg R, Simoons ML, Roos-Hesselink JW. Congenital aortic stenosis in adults: Rate of progression and predictors of clinical outcome. *Int J Cardiol*. 2007;122:224-231
11. van der Linde D, Yap SC, van Dijk AP, Budts W, Pieper PG, van der Burgh PH, Mulder BJ, Witsenburg M, Cuypers JA, Lindemans J, Takkenberg JJ, Roos-Hesselink JW. Effects of rosuvastatin on progression of stenosis in adult patients with congenital aortic stenosis (procas trial). *Am J Cardiol*. 2011;108:265-271

12. Kupari M, Turto H, Lommi J. Left ventricular hypertrophy in aortic valve stenosis: Preventive or promotive of systolic dysfunction and heart failure? *Eur Heart J*. 2005;26:1790-1796
13. Mandinov L, Eberli FR, Seiler C, Hess OM. Diastolic heart failure. *Cardiovasc Res*. 2000;45:813-825
14. Beroukhim RS, Kruzick TL, Taylor AL, Gao D, Yetman AT. Progression of aortic dilation in children with a functionally normal bicuspid aortic valve. *Am J Cardiol*. 2006;98:828-830
15. Nistri S, Sorbo MD, Marin M, Palisi M, Scognamiglio R, Thiene G. Aortic root dilatation in young men with normally functioning bicuspid aortic valves. *Heart*. 1999;82:19-22
16. Hahn RT, Roman MJ, Mogtader AH, Devereux RB. Association of aortic dilation with regurgitant, stenotic and functionally normal bicuspid aortic valves. *J Am Coll Cardiol*. 1992;19:283-288
17. La Canna G, Ficarra E, Tsagalau E, Nardi M, Morandini A, Chieffo A, Maisano F, Alfieri O. Progression rate of ascending aortic dilation in patients with normally functioning bicuspid and tricuspid aortic valves. *Am J Cardiol*. 2006;98:249-253
18. Ferencik M, Pape LA. Changes in size of ascending aorta and aortic valve function with time in patients with congenitally bicuspid aortic valves. *Am J Cardiol*. 2003;92:43-46
19. Novaro GM, Griffin BP. Congenital bicuspid aortic valve and rate of ascending aortic dilatation. *Am J Cardiol*. 2004;93:525-526
20. Mohamed SA, Noack F, Schoellermann K, Karluss A, Radtke A, Schult-Badusche D, Radke PW, Wenzel BE, Sievers HH. Elevation of matrix metalloproteinases in different areas of ascending aortic aneurysms in patients with bicuspid and tricuspid aortic valves. *ScientificWorldJournal*. 2012;2012:806261
21. Thanassoulis G, Yip JW, Filion K, Jamorski M, Webb G, Siu SC, Therrien J. Retrospective study to identify predictors of the presence and rapid progression of aortic dilatation in patients with bicuspid aortic valves. *Nat Clin Pract Cardiovasc Med*. 2008;5:821-828
22. Girdauskas E, Borger MA, Secknus MA, Girdauskas G, Kuntze T. Is aortopathy in bicuspid aortic valve disease a congenital defect or a result of abnormal hemodynamics? A critical reappraisal of a one-sided argument. *Eur J Cardiothorac Surg*. 2011;39:809-814
23. McKusick VA. Association of congenital bicuspid aortic valve and erdheim's cystic medial necrosis. *Lancet*. 1972;1:1026-1027
24. Roberts CS, Roberts WC. Dissection of the aorta associated with congenital malformation of the aortic valve. *J Am Coll Cardiol*. 1991;17:712-716
25. Hope MD, Hope TA, Meadows AK, Ordovas KG, Urbania TH, Alley MT, Higgins CB. Bicuspid aortic valve: Four-dimensional mr evaluation of ascending aortic systolic flow patterns. *Radiology*. 2010;255:53-61
26. Hope MD, Meadows AK, Hope TA, Ordovas KG, Reddy GP, Alley MT, Higgins CB. Images in cardiovascular medicine. Evaluation of bicuspid aortic valve and aortic coarctation with 4d flow magnetic resonance imaging. *Circulation*. 2008;117:2818-2819
27. Robicsek F, Thubrikar MJ, Cook JW, Fowler B. The congenitally bicuspid aortic valve: How does it function? Why does it fail? *Ann Thorac Surg*. 2004;77:177-185

28. Doss M, Risteski P, Sirat S, Bakhtiary F, Martens S, Moritz A. Aortic root stability in bicuspid aortic valve disease: Patch augmentation plus reduction aortoplasty versus modified david type repair. *Eur J Cardiothorac Surg*. 2010;38:523-527

29. Badiu CC, Eichinger W, Bleiziffer S, Hermes G, Hettich I, Krane M, Bauernschmitt R, Lange R. Should root replacement with aortic valve-sparing be offered to patients with bicuspid valves or severe aortic regurgitation? *Eur J Cardiothorac Surg*. 2010;38:515-522

30. Svensson LG, Blackstone EH, Cosgrove DM, 3rd. Surgical options in young adults with aortic valve disease. *Curr Probl Cardiol*. 2003;28:417-480

31. Baumgartner H, Bonhoeffer P, De Groot NM, de Haan F, Deanfield JE, Galie N, Gatzoulis MA, Gohlke-Baerwolf C, Kaemmerer H, Kilner P, Meijboom F, Mulder BJ, Oechslin E, Oliver JM, Serraf A, Szatmari A, Thaulow E, Vouhe PR, Walma E, Vahanian A, Auricchio A, Bax J, Ceconi C, Dean V, Filippatos G, Funck-Brentano C, Hobbs R, Kearney P, McDonagh T, Popescu BA, Reiner Z, Sechtem U, Sirnes PA, Tendera M, Vardas P, Widimsky P, Swan L, Andreotti F, Beghetti M, Borggrefe M, Bozio A, Brecker S, Budts W, Hess J, Hirsch R, Jondeau G, Kokkonen J, Kozelj M, Kucukoglu S, Laan M, Lionis C, Metreveli I, Moons P, Pieper PG, Pilossoff V, Popelova J, Price S, Roos-Hesselink J, Uva MS, Tornos P, Trindade PT, Ukkonen H, Walker H, Webb GD, Westby J, Task Force on the Management of Grown-up Congenital Heart Disease of the European Society of C. Esc guidelines for the management of grown-up congenital heart disease (new version 2010). *Eur Heart J*. 2010;31:2915-2957

32. Groth M, Henes FO, Mullerleile K, Bannas P, Adam G, Regier M. Accuracy of thoracic aortic measurements assessed by contrast enhanced and unenhanced magnetic resonance imaging. *Eur J Radiol*. 2011

33. Wuest W, Anders K, Schuhbaeck A, May MS, Gauss S, Marwan M, Arnold M, Ensminger S, Muschiol G, Daniel WG, Uder M, Achenbach S. Dual source multidetector ct-angiography before transcatheter aortic valve implantation (tavi) using a high-pitch spiral acquisition mode. *Eur Radiol*. 2012;22:51-58

34. Ferda J, Linhartova K, Kreuzberg B. Comparison of the aortic valve calcium content in the bicuspid and tricuspid stenotic aortic valve using non-enhanced 64-detector-row-computed tomography with prospective ecg-triggering. *European journal of radiology*. 2008;68:471-475

35. John AS, Dill T, Brandt RR, Rau M, Ricken W, Bachmann G, Hamm CW. Magnetic resonance to assess the aortic valve area in aortic stenosis: How does it compare to current diagnostic standards? *J Am Coll Cardiol*. 2003;42:519-526

36. Caruthers SD, Lin SJ, Brown P, Watkins MP, Williams TA, Lehr KA, Wickline SA. Practical value of cardiac magnetic resonance imaging for clinical quantification of aortic valve stenosis: Comparison with echocardiography. *Circulation*. 2003;108:2236-2243

CHAPTER 10

ASCENDING AORTIC DIAMETERS IN CONGENITAL AORTIC STENOSIS: CARDIAC MAGNETIC RESONANCE VERSUS TRANSTHORACIC ECHOCARDIOGRAPHY

Echocardiography 2013. Epub ahead of print.

D van der Linde
A Rossi
SC Yap
JS McGhie
A E van den Bosch
SWM Kirschbaum
B Russo
APJ van Dijk
A Moelker
GP Krestin
R-JM van Geuns
JW Roos-Hesselink

ABSTRACT

Objectives/background: Congenital aortic stenosis (AS) is the most common obstructive left heart lesion in the young adult population and often complicated by aortic dilatation. Our objective was to evaluate accuracy of aortic imaging with transthoracic echocardiography (TTE) compared to cardiac magnetic resonance (CMR).

Methods: Aortic diameters were measured at 4 levels by CMR and TTE. Agreement and concordance were assessed by Pearson's correlation and Bland-Altman analysis.

Results: Fifty-nine patients (age 33±8 years; 66% male) with congenital AS and a bicuspid aortic valve (BAV) were included. Aortic diameters were generally smaller with TTE than with CMR. The best correlation was found at the level of the sinotubular junction ($R^2 = 0.78$) with a bias of 1.46 mm (limits of agreement: -5.47 to +8.39 mm). In patients with an aortic aneurysm >40 mm (n=29) the correlation and agreement between TTE and CMR were found to be less good when compared to patients with normal aortic diameters, especially at the level of the proximal ascending aorta. The correlation and agreement between both imaging modalities was better in patients with type 1 BAV compared to type 2 BAV. Intra- and interobserver variability was smaller with CMR (1.8-5.9%) compared to TTE (6.9-15.0%).

Conclusions: CMR was found to be superior to TTE for imaging of the aorta in patients with congenital AS, especially at the level of the proximal ascending aorta when an aortic aneurysm is present. Therefore, ideally CMR should be performed at least once to ensure an ascending aortic aneurysm is not missed.

BACKGROUND

Congenital valvular aortic stenosis (AS) is responsible for approximately 4% of all congenital heart defects [1]. The underlying cause for congenital AS is usually a bicuspid aortic valve (BAV), which is strongly associated with aortic dilatation [2,3]. Since both the valve and the aorta can be affected, active surveillance of both structures is indicated. Stringent follow-up is necessary to determine the optimal timing of surgical replacement of the aortic valve and/or ascending aorta [4]. Two-dimensional transthoracic echocardiography (TTE) has become the clinical standard for evaluation of AS severity [5]. Recent ESC guidelines consider cardiac magnetic resonance (CMR) superior to TTE for imaging of the ascending aorta [6]. However, no study has ever focused on agreement between both imaging techniques at the various aortic levels in this patient group.

The purpose of the present study was to evaluate correlation and agreement between CMR and TTE measurements of aortic diameters in young adult patients with congenital AS.

METHODS

We prospectively included asymptomatic adult patients with congenital valvular AS who visited the outpatient clinic for Adult Congenital Heart Disease of the Erasmus Medical Center Rotterdam and Radboud University Nijmegen Medical Center. Inclusion criteria were: age 18-50 years, BAV and peak aortic velocity >2.5 m/s based on echocardiographic measurements. Patients with general contraindications for CMR (pacemaker, metallic implants or claustrophobia), previous aortic valve replacement, or concomitant severe mitral or aortic regurgitation were excluded. Patients underwent TTE and CMR on the same day. The study protocol was approved by the Medical Ethics Committee, and all patients gave written informed consent.

CARDIAC MAGNETIC RESONANCE

CMR imaging was performed using a 1.5T scanner (Signa Discovery 450, GE Healthcare, Milwaukee, Wisconsin). The patient was placed in supine position and a dedicated cardiac coil was placed on the thorax of the patient. CMR image acquisitions and analyses were performed by an experienced investigator blinded to TTE results.

Cine magnetic resonance long axis 3-chamber view images were obtained using a breath-holding electrocardiogram triggered balanced steady state free precession (SSFP) pulse sequence for a standard ventricular function examination. The parameters of the SSFP sequence were: field of view 360-400 x 280-320 mm^2; matrix 224 x 196; repetition time: 3.4

ms; echo time: 1.5 ms; flip angle: 45 degrees; 12 views per segment; slice thickness 8 mm; gap of 2 mm; temporal resolution 41 ms. CAAS-MRV (version 3.1; Pie Medical Imaging, Maastricht, The Netherlands) was used for the left ventricular function evaluation.

End-diastolic tubular ascending aortic diameters were measured in the oblique sagittal view (Figure 1A). End-diastolic internal aortic diameters were measured at three levels in the 3-chamber view images: aortic annulus, sinus of Valsalva and sinotubular junction (Figure 1B). At each level the measurement was taken perpendicular to the long axis of the aorta.

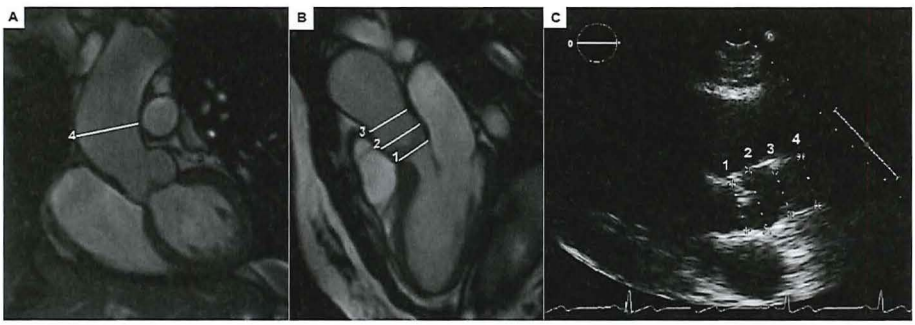

Figure 1. Aortic measurements.
Multimodality imaging of the aorta showing measurements of the aortic diameters at the level of the aortic annulus (1), sinus of Valsalva (2), sinotubular junction (3) and ascending aorta (4) by (A, B) cardiac magnetic resonance (the oblique sagittal and 3-chamber view) and (C) two-dimensional transthoracic echocardiography (parasternal long-axis view).

TRANSTHORACIC ECHOCARDIOGRAPHY

TTE examinations were performed and analyzed by experienced sonographers (blinded to CMR data) using commercially ultrasound systems (Sonos 7500, iE33 and iE33 xMATRIX X5-1, Philips Medical Systems, Best, The Netherlands). According to EAE/ASE guidelines, AS severity was evaluated by peak aortic velocity, mean transaortic gradient and continuity equation aortic valve area [5]. The end-diastolic diameter of the aortic valve annulus, sinus of Valsalva, sinotubular junction and proximal ascending aorta were measured from leading edge to leading edge in the parasternal long-axis view (Figure 1C). An aortic aneurysm was defined as a diameter of >40 mm in one or more aortic diameter measurements. BAV morphology was determined in the parasternal short-axis view according to the orientation of the commissures [7,8]. Type 1 BAV is a fusion of the right and left coronary cusps. In type 2 BAV the non-coronary and right coronary cusps are fused. Type 3 BAV involves a fusion of the non-coronary and left coronary cusps.

STATISTICAL ANALYSIS

Statistical analyses were performed using Statistical Package for Social Sciences, version 19.0 (SPSS, Chicago, Illinois) and GraphPad, version 5.0 (GraphPad Software, Inc, La Jolla, California). Significance was defined as $p<0.05$. Continuous data are expressed as mean ± standard deviation (SD). Categorical variables are summarized by the use of frequency and percentage. The normality of the data was verified with a Shapiro-Wilk test and histograms. Correlations between CMR and TTE measurements were assessed by linear regression analysis and Pearson's correlations. Bland-Altman analysis was used to determine bias (mean of the difference) with 95% limits of agreement (± 1.96 SD) [9]. To compare aortic diameters measured with both imaging modalities, a paired Student's t-test was performed. The reproducibility of the TTE and CMR measurements was evaluated in 25 randomly selected patients. We expressed the intra-observer and inter-observer variability by the coefficient of

Table 1. Patient characteristics

	PATIENTS (N=59)
Age (years)	33 ± 8
Male gender, n(%)	39 (66)
Systolic blood pressure (mmHg)	132 ± 15
Diastolic blood pressure (mmHg)	76 ± 9
Body surface area (m2)	1.94 ± 0.25
Peak aortic valve velocity (m/s)	3.6 ± 0.8
Ejection fraction (%) *	58 ± 7
Left ventricular mass (g) *	133 ± 40
Aortic aneurysm (>40 mm), n (%)	29 (49.2)
Bicuspid aortic valve morphology, n (%) †	
Type 1 (fusion right and left coronary cusp)	28 (47.5)
Type 2 (fusion non-coronary and right coronary cusp)	26 (44.1)
Aortic valve calcification, n(%) ‡	20 (34)
Aortic regurgitation, n(%) ‡	
None	38 (64)
Mild	11 (19)
Moderate	10 (17)
Severe	0 (0)

Data are presented as mean ± SD, or as n(%) when frequencies.

* Derived from cardiac magnetic resonance measurements.

† In 5 patients the bicuspid aortic valve morphology could not be determined.

‡ Derived from transthoracic echocardiography measurements.

variation (CV), which is defined as the SD of the difference between the two readings (or readers) divided by their mean value, times 100.

RESULTS

Fifty-nine patients with congenital AS were included in this study and completed the imaging protocols without difficulty. All patients were in sinus rhythm and New York Heart Association Class I. Patient characteristics are reported in Table 1.

Figure 2 shows correlation and agreement for aortic diameter measurements by TTE and CMR. Aortic diameters measured by TTE were generally smaller than aortic diameters measured by CMR (Table 2). The best agreement was found at the aortic annulus level (bias 0.23 mm, limits of agreement: -6.47 to +6.94 mm; correlation R^2 = 0.63; Figure 2A,E). The best correlation was found at the level of the sinotubular junction (R^2 = 0.78) with a bias of 1.46 mm (limits of agreement: -5.47 to +8.39 mm) (Figure 2C,G). At the level of

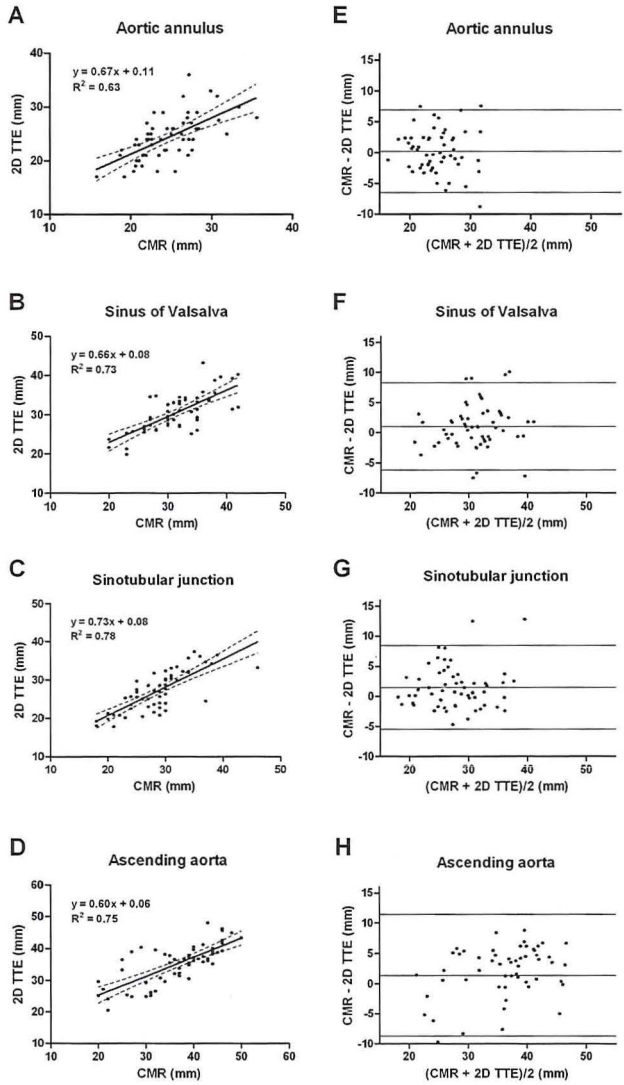

Figure 2. Aortic diameters: comparison between CMR and TTE

Comparison between cardiac magnetic resonance and two-dimensional transthoracic echocardiography measurements of aortic diameters at the level of the (A, E) aortic annulus, (B, F) sinus of Valsalva, (C, G) sinotubular junction and (D, H) ascending aorta, as shown by regression lines (left) and Bland-Altman plots (right).

Table 2. Aortic diameters.

	TTE	CMR	P-VALUE
Aortic annulus (mm)	24.3 ± 4.1	24.5 ± 3.9	0.606
Sinus of Valsalva (mm)	30.6 ± 4.7	31.6 ± 5.2	0.041
Sinotubular junction (mm)	27.1 ± 5.2	28.5 ± 5.5	0.003
Ascending aorta (mm)	35.2 ± 6.2	36.6 ± 7.8	0.048

Data are presented as mean ± SD.
CMR = cardiac magnetic resonance; TTE = transthoracic echocardiography.

the sinus of Valsalva, the correlation and agreement were good (R^2 = 0.73; bias 1.02 mm, limits of agreement: -6.22 to +8.25 mm; Figure 2B,F). The agreement was least at the level of the proximal ascending aorta (R^2 = 0.75; bias 1.36 mm, limits of agreement: -8.70 to +11.42 mm; Figure 2D,H).

Table 3. Correlation and agreement in patients with and without an aortic aneurysm.

	NO ANEURYSM N=30	ANEURYSM (>40 MM) N=29
Annulus		
Diameter TTE versus CMR (mm)	22.7 ± 3.5 vs. 22.8 ± 2.7	25.9 ± 4.1 vs. 26.3 ± 4.1
P-value Diameter TTE versus CMR	p = 0.854	p = 0.619
Correlation	R2 = 0.58	R2 = 0.55
Bias (95% limits of agreement)	0.10 (-5.59 to 5.79)	0.37 (-7.31 to 8.04)
Sinus of Valsalva		
Diameter TTE versus CMR (mm)	28.7 ± 4.2 vs. 28.8 ± 4.5	32.5 ± 4.6 vs. 34.5 ± 4.3
P-value Diameter TTE versus CMR	p = 0.920	p = 0.008
Correlation	R2 = 0.68	R2 = 0.65
Bias (95% limits of agreement)	0.07 (-6.73 to 6.86)	1.97 (-5.34 to 9.27)
Sinotubular junction		
Diameter TTE versus CMR (mm)	24.4 ± 4.4 vs. 26.0 ± 4.2	29.8 ± 4.4 vs. 31.0 ± 5.5
P-value Diameter TTE versus CMR	p = 0.006	p= 0.110
Correlation	R2 = 0.75	R2 = 0.69
Bias (95% limits of agreement)	1.69 (-4.24 to 7.61)	1.23 (-6.67 to 9.13)
Ascending aorta		
Diameter TTE versus CMR (mm)	31.0 ± 5.5 vs. 31.2 ± 6.4	39.5 ± 3.5 vs. 42.0 ± 4.8
P-value Diameter TTE versus CMR	p = 0.808	p = 0.009
Correlation	R2 = 0.59	R2 = 0.40
Bias (95% limits of agreement)	0.24 (-10.27 to 10.76)	2.48 (-6.77 to 11.73)

Reported data are expressed as mean ± SD.
CMR = cardiac magnetic resonance, TTE= transthoracic echocardiography.

PATIENTS WITH AND WITHOUT AORTIC ANEURYSM

Twenty-nine patients (49%) were found to have an aortic aneurysm (>40 mm in at least 1 of the measurement levels). Table 3 shows the results of the correlation and agreement between CMR and TTE in patients with and without an aortic aneurysm. Especially at the level of the proximal ascending aorta the correlation between both imaging techniques was lower in patients with an aortic aneurysms compared to patients with normal aortic diameters (respectively R^2=0.40 versus R^2=0.59;Table 3). Bland-Altman analysis shows that the bias and limits of agreement were also worse in patients with an aortic aneurysm as compared to patients without an aortic aneurysm (Table 3, Figure 3).

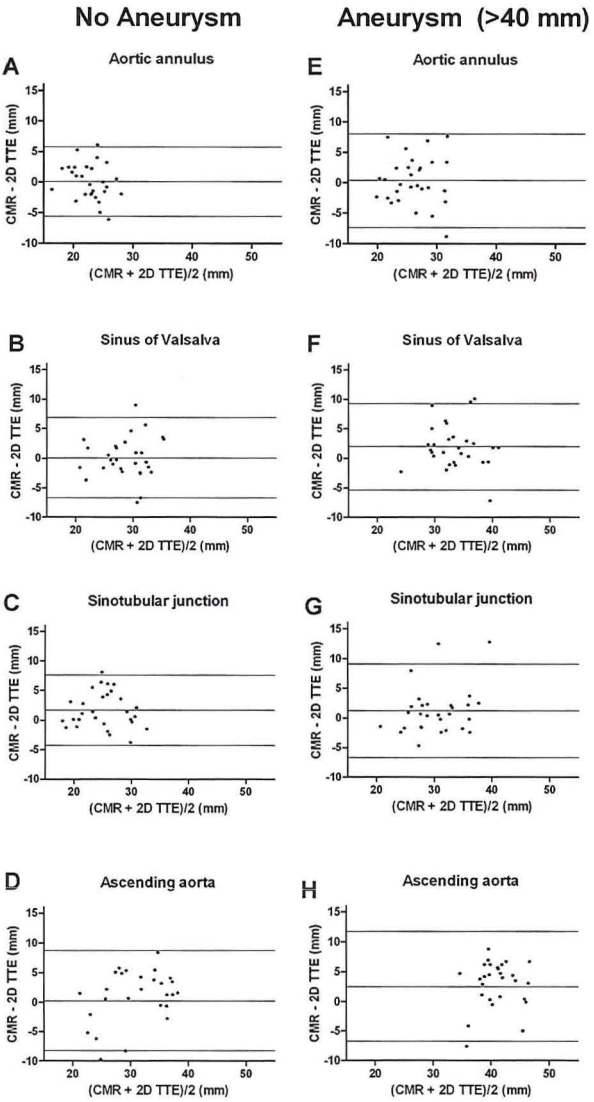

Figure 3. Agreement between CMR and TTE in patients with normal aortic diameters and aneurysms.

Bland-Altman plots demonstrating the comparison between cardiac magnetic resonance and two-dimensional transthoracic echocardiography measurements of aortic diameters at the level of the (A, E) aortic annulus, (B, F) sinus of Valsalva, (C, G) sinotubular junction and (D, H) ascending aorta, in patients with (right) and without (left) an aortic aneurysm.

BICUSPID AORTIC VALVE MORPHOLOGY

Twenty-eight patients were found to have a fusion of the right and left coronary cusp (Type 1 BAV) and 26 patients were found have a

fusion of the non-coronary and right coronary cusp (Type 2 BAV). No patients exhibited a type 3 BAV. In 5 patients the BAV morphology could not be determined with certainty. In six patients with a type 2 BAV the aortic root showed marked asymmetry on the TTE short-axis view.

Table 4 and Figure 4 show the results of the correlation and agreement analyses between CMR and TTE comparing patients with type 1 and 2 BAV. The correlation and agreement between both imaging techniques was better in patients with type 1 BAV at all aortic levels.

Table 4. Correlation and agreement according to bicuspid aortic valve morphology.

	TYPE 1 BAV (FUSION RIGHT AND LEFT CORONARY CUSP) N=28	TYPE 2 BAV (FUSION NON-CORONARY AND RIGHT CORONARY CUSP) N=26
Annulus		
Diameter TTE versus CMR (mm)	22.4 ± 3.4 vs. 22.7 ± 3.1	26.2 ± 3.9 vs. 26.5 ± 3.7
P-value Diameter TTE versus CMR	p = 0.606	p = 0.718
Correlation	R2 = 0.57	R2 = 0.44
Bias (95% limits of agreement)	0.30 (-5.63 to 6.23)	0.28 (-7.61 to 8.19)
Sinus of Valsalva		
Diameter TTE versus CMR (mm)	29.6 ± 5.0 vs. 29.1 ± 4.3	33.5 ± 4.7 vs. 32.3 ± 4.8
P-value Diameter TTE versus CMR	p = 0.348	p = 0.169
Correlation	R2 = 0.81	R2 = 0.58
Bias (95% limits of agreement)	-0.54 (-6.26 to 5.18)	-1.20 (-9.68 to 7.28)
Sinotubular junction		
Diameter TTE versus CMR (mm)	26.5 ± 4.9 vs. 25.7 ± 5.1	30.7 ± 5.4 vs. 28.8 ± 4.6
P-value Diameter TTE versus CMR	p = 0.108	p= 0.034
Correlation	R2 = 0.87	R2 = 0.67
Bias (95% limits of agreement)	-0.82 (-5.86 to 4.21)	-1.82 (-9.94 to 6.30)
Ascending aorta		
Diameter TTE versus CMR (mm)	34.0 ± 8.7 vs. 32.8 ± 7.4	37.9 ± 6.1 vs. 36.8 ± 3.6
P-value Diameter TTE versus CMR	p = 0.181	p = 0.363
Correlation	R2 = 0.85	R2 = 0.33
Bias (95% limits of agreement)	-1.22 (-10.25 to 7.81)	-1.08 (-12.79 to 10.62)

Reported data are expressed as mean ± SD.
BAV = bicuspid aortic valve, CMR = cardiac magnetic resonance, TTE= transthoracic echocardiography.

INTRA- AND INTEROBSERVER VARIABILITY

The intra- and interobserver variability data are displayed in Table 5. Intra-observer variability was between 2.4 and 11.2%. Interobserver agreement demonstrated more variation and

was between 1.8 and 15.0%. The highest variation was found at the level of the annulus (5.4-15%) and the smallest variation at the level of the proximal ascending aorta (1.8-8.2%). Variability was generally smaller with CMR (1.8-5.9%) compared to TTE (6.9-15.0%).

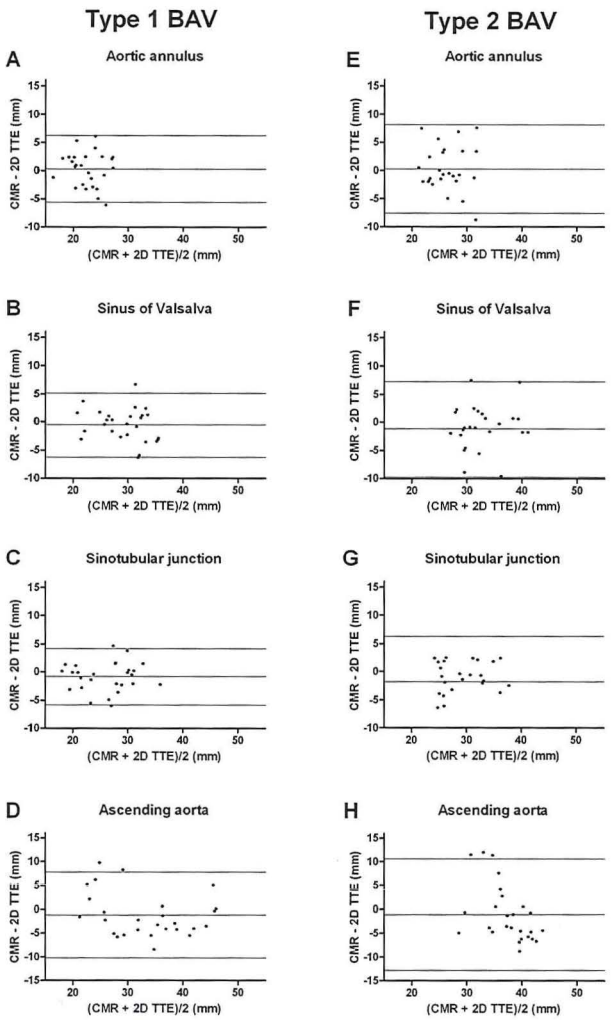

Figure 4. Agreement between CMR and TTE according to bicuspid aortic valve morphology.

Bland-Altman plots demonstrating the comparison between cardiac magnetic resonance and two-dimensional transthoracic echocardiography measurements of aortic diameters at the level of the (A, E) aortic annulus, (B, F) sinus of Valsalva, (C, G) sinotubular junction and (D, H) ascending aorta, in patients with type 1 (left) and type 2 (right) bicuspid aortic valve morphology.

DISCUSSION

The present study systematically investigated correlation and concordance of aortic diameters at different levels using CMR and TTE as imaging modalities in patients with congenital AS due to BAV disease. The results demonstrated that although there seems to be good concordance between both imaging modalities, aortic diameter measurements are slightly smaller (approximately 1 mm) with TTE compared to CMR. In general, the agreement between both imaging techniques was quite good, but least at the level of the proximal ascending aorta, especially in patients with an aortic aneurysm. Measurement reproducibility was better with CMR than with TTE.

Table 5. Intra- and interobserver variability.

	INTRA-OBSERVER VARIABILITY			INTER-OBSERVER VARIABILITY		
	Mean difference ± SD	Mean value ± SD	CV	Mean difference ± SD	Mean value ± SD	CV
TTE						
Annulus	0.5 ± 2.4	24.5 ± 3.8	10.0%	1.6 ± 3.8	25.0 ± 4.1	15.0%
Sinus of Valsalva	0.1 ± 2.2	31.9 ± 5.4	6.9%	0.8 ± 2.8	32.3 ± 5.2	8.7%
Sinotubular junction	1.5 ± 3.2	28.2 ± 4.8	11.2%	1.7 ± 3.9	28.2 ± 5.1	13.8%
Ascending aorta	1.1 ± 3.0	37.2 ± 6.3	7.9%	0.1 ± 3.0	36.6 ± 6.6	8.2%
CMR						
Annulus	0.3 ± 1.4	24.2 ± 2.8	5.9%	0.1 ± 1.3	23.9 ± 3.1	5.4%
Sinus of Valsalva	0.1 ± 0.8	30.1 ± 4.0	2.7%	0.1 ± 1.4	26.5 ± 4.8	5.3%
Sinotubular junction	0.2 ± 0.7	26.8 ± 4.8	2.6%	0.4 ± 1.0	29.9 ± 4.3	3.5%
Ascending aorta	0.1 ± 0.9	36.8 ± 5.2	2.4%	0.1 ± 0.7	36.9 ± 5.3	1.8%

Reported data are expressed as mean ± SD. Coefficient of variability (CV): expressed as a percentage of the SD of the difference divided by the mean of the two measurements. Aortic diameters are measured in mm.

CMR = cardiac magnetic resonance; CV = coefficient of variability; SD = standard deviation; TTE = transthoracic echocardiography.

AORTIC DIAMETER ASSESSMENT IN BAV: WHICH METHOD TO USE?

Aortic dilatation in BAV disease is especially present at the level of the ascending aorta [10-13]. Therefore, it is of uttermost importance to correctly visualize and measure this part of the aorta. This study clearly showed that the correlation and agreement between CMR and TTE were quite good in patients with normal aortic diameters. Intra- and inter observer variability were better with CMR. These findings confirm several studies in other patient populations [14-19]. However, in patients with an aortic aneurysm >40 mm, the correlation and agreement between both imaging modalities were worse, especially at the level of the proximal ascending aorta. This phenomenon might be explained by the fact that in patients with an ascending aortic aneurysm, TTE acoustic windows might be suboptimal and transection planes incorrect.

In addition, BAV morphology seemed to influence the accuracy of aortic diameters. The correlation and agreement between CMR and TTE were better at all levels in patients with a type 1 BAV as compared to patients with a type 2 BAV. An explanation for this finding might be that the aortic diameters tended to be larger in patients with type 2 BAV as compared to type 1 BAV. Furthermore, we hypothesize that the difference in accuracy according to BAV morphology could be due to the fact that 6 patients in the type 2 BAV group exhibited marked aortic root asymmetry, while none of the patients with a type 1 BAV exhibited marked aortic root asymmetry. The noncircular geometry could be a problem for the aortic measurements in the parasternal long-axis view, because 2D TTE cannot guarantee crossing in the center or prevent oblique transections. Unfortunately our group of 6 patients with aortic root asymmetry was too small to accurately test our hypothesis or draw firm conclusions. Further studies focusing on comparing CMR and TTE in patients with and without aortic root asymmetry are warranted.

STUDY LIMITATIONS

The limited sample size is an evident limitation of this study. Furthermore, we did not assess a true gold standard for aortic measurement, which is considered to be direct perioperative measurement. Acoustic shadowing artifact created by aortic valve calcification was not controlled for and could have limited the accuracy and available acoustic windows of TTE. Furthermore, we have to acknowledge that the proximal ascending aorta was measured in the left-right dimension by CMR and in the anterior-posterior dimension by TTE. Since the ascending aorta is typically symmetric, this probably did not affect our results to a large extent. Finally, the results of this study specifically address adult patients with congenital AS and BAV disease, and may not be generalizable to degenerative, calcific AS.

CLINICAL RECOMMENDATIONS

Correct imaging of the aorta is crucial in clinical decision making process regarding surgical interventions in BAV and associated aortic aneurysms [4]. Elective aortic surgery is advised when the aortic diameter reaches 50 mm to avoid acute dissection or rupture [4]. Our study confirms recent ESC guidelines for grown-up congenital heart disease stating that CMR is mainly required to assess aortic dilatation when occurring distal to the sinotubular junction [6]. Thus, when available, CMR should be used at least once in all BAV patients to exclude presence of an ascending aortic aneurysm and might also be the preferred method for follow-up when an aortic aneurysm is suspected and/or confirmed.

For this young asymptomatic patient population computed tomography or transesophageal echocardiography are generally not considered first choice because of the disadvantage of respectively radiation exposure and invasiveness, but there might be a role for three-dimensional TTE [20, 21].

Because of certain disadvantages of CMR (contraindicated use in patients with claustrophobia and metallic implants, prolonged duration of imaging acquisition, higher costs and often limited availability), echocardiography is often the most pragmatic choice in routine clinical practice. When availability of CMR is limited, we advise to perform both TTE and CMR at baseline and assess agreement between both techniques in respect to aortic diameter measurements at all 4 levels in the individual patient. When both imaging techniques agree well and aortic diameter is <40 mm, TTE can be used for regular follow-up. In case of good agreement and an aortic diameter >40 mm, we suggest to repeat CMR at least every 4 years. In case TTE and CMR show poor agreement in that individual patient (>5 mm difference), TTE cannot be used as a reliable tool to assess aortic diameter. In these patients, CMR should be the preferred method for follow-up of aortic diameters; once every 3 to 4 years when aortic diameter is <40 mm, every 1 to 2 years when aortic diameter is >40 mm, and even more frequently when the diameter approaches 50 mm.

CONCLUSIONS

In patients with congenital AS, aortic diameter measurements are slightly smaller with TTE compared to CMR and the reproducibility of CMR is better. Agreement between both imaging modalities is good in patients with normal aortic diameters, however poor in patients with an aortic aneurysm. In addition, the agreement between CMR and TTE seems to be lower in patients with a type 2 BAV morphology.

Since BAV associated aortic dilatation mainly occurs at the ascending aortic level, CMR should be performed at least once to ensure that an aortic aneurysm at this level is not missed and might be the preferred method for aortic aneurysm follow-up.

REFERENCES

1. van der Linde D, Konings EE, Slager MA, et al: Birth prevalence of congenital heart disease worldwide: a systematic review and meta-analysis. J Am Coll Cardiol 2011;58:2241-2247.
2. Siu SC, Silversides CK. Bicuspid aortic valve disease: J Am Coll Cardiol 2010;55:2789-2800.
3. Yap SC, Takkenberg JJ, Witsenburg M, Meijboom FJ, Roos-Hesselink JW: Aortic stenosis at young adult age. Expert Rev Cardiovasc Ther 2005;3:1087-1098.
4. Hiratzka LF, Bakris GL, Beckman JA, et al: 2010 ACCF/AHA/AATS/ACR/ASA/SCA/SCAI/SIR/STS/SVM guidelines for the diagnosis and management of patients with Thoracic Aortic Disease: a report of the American College of Cardiology Foundation/American Heart Association Task Force on Practice Guidelines, American Association for Thoracic Surgery, American College of Radiology, American Stroke Association, Society of Cardiovascular Anesthesiologists, Society for Cardiovascular Angiography and Interventions, Society of Interventional Radiology, Society of Thoracic Surgeons, and Society for Vascular Medicine. J Am Coll Cardiol 2010;55:e27-e129.
5. Baumgartner H, Hung J, Bermejo J, et al: Echocardiographic assessment of valve stenosis: EAE/ASE recommendations for clinical practice. Eur J Echocardiogr 2009;10:1-25.
6. Kilner PJ, Geva T, Kaemmerer H, Trindade PT, Schwitter J, Webb GD: Recommendations for cardiovascular magnetic resonance in adults with congenital heart disease from the respective working groups of the European Society of Cardiology. Eur Heart J 2010;31:794-805.
7. Schaefer BM, Lewin MB, Stout KK, et al: The bicuspid aortic valve: an integrated phenotypic classification of leaflet morphology and aortic root shape. Heart 2008;94:1634-8.
8. Jassal DS, Bhagirath KM, Tam JW, et al: Association of Bicuspid aortic valve morphology and aortic root dimensions: a substudy of the aortic stenosis progression observation measuring effects of rosuvastatin (ASTRONOMER) study. Echocardiography 2010;27:174-9.
9. Bland JM, Altman DG: Statistical methods for assessing agreement between two methods of clinical measurement. Lancet 1986;1:307-310.
10. Hahn RT, Roman MJ, Mogtader AH, Devereux RB: Association of aortic dilation with regurgitant, stenotic and functionally normal bicuspid aortic valves. J Am Coll Cardiol 1992;19:283–288.
11. Novaro GM, Griffin BP: Congenital bicuspid aortic valve and rate of ascending aortic dilatation. Am J Cardiol 2004;93:525–526.
12. Della Corte A, Bancone C, Quarto C, et al: Predictors of ascending aortic dilatation with bicuspid aortic valve: a wide spectrum of disease expression. Eur J Cardiothorac Surg 2007;31:397-405.
13. Van der Linde D, Yap SC, Van Dijk AP, et al: Effects of Rosuvastatin on Progression of Stenosis in Adult Patients With Congenital Aortic Stenosis (PROCAS trial). Am J Cardiol 2011;108:265-271.
14. Paelinck BP, Van Herck PL, Rodrigus I, et al: Comparison of magnetic resonance imaging of aortic valve stenosis and aortic root to multimodality imaging for selection of transcatheter aortic valve implantation candidates. Am J Cardiol. 2011;108:92-98.

15. Joziasse IC, Vink A, Cramer MJ, et al: Bicuspid stenotic aortic valves: clinical characteristics and morphological assessment using MRI and echocardiography. Neth Heart J. 2011;19:119-125.
16. von Knobelsdorff-Brenkenhoff F, Rudolph A, Wassmuth R, Abdel-Aty H, Schulz-Menger J: Aortic dilatation in patients with prosthetic aortic valve: comparison of MRI and echocardiography. J Heart Valve Dis 2010;19:349-356.
17. Smíd M, Ferda J, Baxa J, et al: Aortic annulus and ascending aorta: comparison of preoperative and perioperative measurement in patients with aortic stenosis. Eur J Radiol 2010;74:152-155.
18. Jabbour A, Ismail TF, Moat N, et al: Multimodality imaging in transcatheter aortic valve implantation and post-procedural aortic regurgitation: comparison among cardiovascular magnetic resonance, cardiac computed tomography, and echocardiography. J Am Coll Cardiol. 2011;58:2165-2173.
19. Lanzarini L, Larizza D, Prete G, et al: Aortic dimensions in Turner's syndrome: two-dimensional echocardiography versus magnetic resonance imaging. J Cardiovasc Med (Hagerstown). 2007;8:428-437.
20. Joshi D, Bicer EI, Donmez C, et al. Incremental value of live/real time three-dimensional transesophageal echocardiography over the two-dimensional technique in the assessment of aortic aneurysm and dissection. Echocardiography 2012;29:620-30.
21. Tsang JF, Lytwyn M, Farag A, et al: Multimodality imaging of aortic dimensions: comparison of transthoracic echocardiography with multidetector row computed tomography. Echocardiography 2012;29:735-41.

CHAPTER 11

AORTIC ANNULUS AND LEAFLET CALCIFICATION FROM CONTRAST MSCT PREDICT THE NEED FOR BALOON POST-DILATATION AFTER TAVI WITH MEDTRONIC COREVALVE PROSTHESIS

Eurointervention, 2011; 7(5): 564-572

C Schultz
A Rossi
N van Mieghem
R van der Boon
S-L Papadopoulou
R van Domburg
A Moelker
N Mollet
GP Krestin
RJ van Geuns
K Nieman
PJ de Feyter
PW Serruys
P de Jaegere

ABSTRACT

Aims: We compared the measurement of aortic leaflet calcification on contrast and non-contrast MSCT and investigated predictors of balloon post-dilatation after TAVI.

Methods and Results: In 110 patients, who had TAVI with a Medtronic Corevalve prosthesis (MCS) for symptomatic aortic stenosis, calcification of the aortic root was measured on non-contrast MSCT (conventionally) and on contrast MSCT (signal attenuation>450 Houndsfield units). Calcium volume was underestimated on contrast- vs. non-contrast MSCT: median [IQ-range] = 759 [466-1295] vs. 2016 [1376-3262]. The difference between the two methods increased with higher calcium volumes. Calcium mass was only slightly underestimated on contrast vs non-contrast MSCT: median [IQ-range] = 441 [268-809] vs. 555 [341-950] and there was no association between the differences and increasing calcium mass. Balloon post-dilatation was performed after TAVI in 11 patients. Balloon post-dilatation was associated with higher aortic leaflet calcium ($p<0.01$), aortic annulus diameters ($p<0.01$) and lower annulus to prosthesis area ($p=0.01$). The ability to discriminate the need for balloon post-dilatation was excellent for aortic leaflet calcium (area under ROC curve>0.80), moderate for aortic annulus dimensions (area under ROC=0.69) and poor for prosthesis to annulus ratio (area under ROC=0.36).

Conclusions: Dense aortic leaflet calcification measured on contrast MSCT discerned well the need for balloon post-dilatation after TAVI. Non-contrast MSCT may no longer be needed to quantify aortic root calcium before TAVI.

INTRODUCTION

Transcutaneous aortic valve implantation (TAVI) improves prognosis of patients with severe aortic stenosis who are deemed at too high a risk for surgical valve replacement (SAVR)[1]. Heavy calcification of the aortic root is an almost universal finding in patients with severe symptomatic aortic stenosis [2]. The gold standard for the measurement of calcification is standardized non-contrast MSCT, yet the precise anatomical distribution of calcification can be better appreciated on contrast MSCT, which usually shows dense calcification of the aortic leaflets. Balloon valvuloplasty is essential to crack open the calcified valve before it can be crossed with the TAVI prosthesis [3,4]. The calcified aortic leaflets are then pushed aside and trapped by the prosthesis during implantation. Apposition of a sealing skirt to the disrupted aortic leaflets and or to the surrounding tissues within a few millimeters below them is necessary to prevent paravalvular aortic regurgitation (PAR) for both types of commercially available TAVI prostheses. It is likely that the calcified leaflets also play an important role in preventing device embolisation after deployment. Yet,dense calcification may contribute to deformation of the deployed frame of the prosthesis, which may result in malapposition and paraprosthetic aortic valve regurgitation.

Another factor which may cause PAR after TAVI is undersizing, where the prosthesis is small relative the native annulus [5]. Prosthesis size selection is based on the measurement of the aortic annulus [6,7]. Yet, during SAVR the aortic annulus is partially decalcified before sizing proceeds under direct vision, whereas during TAVI sizing relies on non-invasive imaging without prior decalcification.

When significant PAR is encountered after deployment of the prosthesis balloon post-dilatation of the frame (BAVF) may reduce the amount of regurgitation, but carries the risks of potential damage to the new valve leaflets as well as of vascular sequelae that may result from the additional instrumentation [8-11]. Yet if it were possible to identify *a priori* which patients would be at risk of requiring BAVF, it may be possible to modify the procedure so as to obviate the need for it, for example by selecting a larger pre-dilatation balloon or larger size prosthesis. This study investigates first the measurement of aortic valve calcification on contrast vs non-contrast MSCT and second the clinical and anatomical determinants of BAVF after TAVI.

METHODS

POPULATION

The study population consisted of 110 patients who received TAVI and who had a MSCT for pre-procedure planning. No patients were specifically excluded, but MSCT was not performed on patients with an estimated glomerular filtration rate below 20ml/min.

MSCT WITHOUT CONTRAST ENHANCEMENT

A scan without contrast enhancement was available in 98 of 110 patients because it was initially not performed in patients with previous CABG or coronary stents. The non-contrast MSCT acquisition was performed in a prospectively ECG-triggered, sequential (step and shoot) mode with a reference tube current of 80 mAs, a tube voltage of 120kV and slice thickness of 3mm in the early or mid diastolic heart phase depending on the heart rate. For analysis on a dedicated cardiovascular CT workstation (MMWP,Siemens AG, Forchheim, Germany) the aortic root was defined as the stretching from the caudal aspect of the aortic annulus to the origin of the left main stem as seen on axial images [12]. The threshold for the detection of calcium was set at 130HU. Agatston score, calcium volume and mass were measured[13-17]. In cases where aortic root calcification was confluent with calcium in adjacent structures (mitral annulus, ascending aorta, coronary arteries) only the stack of images that contained the aortic root were selected.

CONTRAST ENHANCED MSCT

The MSCT acquisition method using 64-slice dual-source CT has been described before[18]. In brief, the acquisition was performed using the spiral scan mode, a variable table speed (depending on the heart rate), no ECG-triggered tube output modulation, and ECG-gated image reconstruction. Further acquisition parameters: detector collimation 2 x 32 x 0.6 mm with rapid alternation of focal spot position in the Z-axis (Z-sharp®), roentgen tube rotation time 330 ms, tube voltage 120 kV. The scan ranged from the top of the aortic arch to the diaphragm. The volume of iodinated contrast material was adapted to the expected scan time. A 50-60 ml bolus of iodixanol (Visipaque® 320 mg I/ml, GE Health Care, Eindhoven, The Netherlands) was injected in an antecubital vein at a flow rate of 4.5 ml/s followed by a second contrast bolus of 30-40 at 3.0 ml/s. Bolus tracking was used to trigger the start of the scan with the arrival of contrast in aortic root. Reconstructions were made in end systole using a single-segmental reconstruction algorithm with slice thickness 1.5 mm; increment 0.4 mm; medium-to-smooth convolution kernel (B26f) resulting in a spatial resolution of 0.6-0.7 mm in-plane and 0.4-0.5 mm through-plane and a temporal resolution of 83ms. The radiation doses ranged from 8 to 20 mSv depending on body habitus and table speed.

The aortic annulus was defined as a virtual ring with 3 anchor points at the bases of the 3 aortic leaflets[19]. This definition was visually reproduced by setting up a viewing plane axial to the aortic root as described before [20]. The minimum and maximum diameters and area of the annulus were measured. Propriety software was developed to allow measurement of aortic leaflet calcification on a contrast MSCT (3mensio Medical Imaging, Bilthoven, the Netherlands). On images axial to the aortic annulus a region of interest was defined from the aortic annulus to the most cranial aspect of the aortic leaflets. The threshold for detecting calcification in the region of interest was set at 450 Houndsfield units (HU) which was

approximately 150 HU above contrast density of the blood pool when sampled just above the aortic leaflets in the majority of patients. This was found to be the lowest level at which contrast was not detected as calcium. Non-detection of contrast was visually verified. If necessary the region of interest was then edited to ensure that calcification detection was limited to the three aortic leaflets (Figure 1). Calcium volume and mass was measured. The density of calcium can be determined from the amount of signal attenuation [16,17]. Due to the high signal attenuation threshold selected for the detection of calcium it was anticipated that only dense calcium would be measured on contrast MSCT.

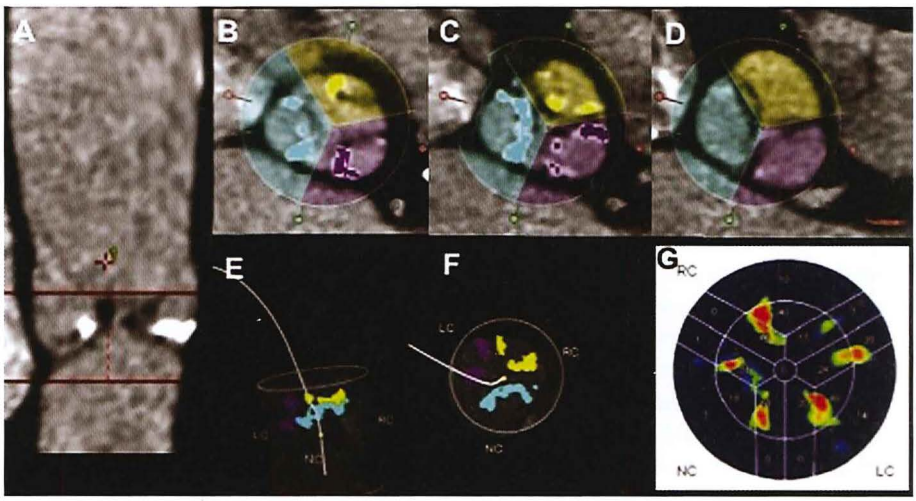

Figure 1: Calcium quantification on aortic leaflets on contrast MSCT.
On two longitudinal views the region of interest was defined from the base of the 3 aortic leaflets to just above the aortic leaflets (Panel A). The threshold for detecting calcification was set at 450 Houndsfield units (HU) which was approximately 150 Houndsfield units (HU) above contrast density of the blood pool when sampled just above the aortic leaflets in the majority of patients. This was found to be the lowest level at which contrast was not detected as calcium. Non-detection of contrast was visually verified at different levels and if necessary the region of interest was then edited (Panels B-D) to ensure that calcification detection was limited to and measured individually for the three aortic leaflets. The correct segmented calcium was also verified on 3D views (Panels E, F). Panel G shows a collapsed (2D) calcium density plot after segmentation.

RELEVANT ASPECTS OF THE TAVI PROCEDURE

The patient selection and TAVI implantation procedure has been described before [21]. As is the case in the majority of TAVI procedures performed worldwide a cine-aortogram was performed after device deployment to assess device position and to detect and grade aortic regurgitation [11]. A 6 french pigtail catheter was placed in the outflow part of the frame just above the commissures of the prosthesis leaflets. 20ml of radiographic contrast was injected with a power injector at a rate of 20ml/s. Aortic regurgitation (AR) was graded by the operator during the implantation procedure according to the method of Sellers: grade 0= no

AR, grade 1=trace, grade 2= mild, grade 3= moderate, grade 4=severe [22]. In the event of aortic regurgitation grade 3 or 4 one of 2 approaches were taken. BAVF was performed if the operators judged that the AR may be reduced by improved apposition of the sealing skirt to the tissues surrounding the inflow of the prosthesis. Alternatively, if a too deep position of the prosthesis inflow below the annulus was judged to be the cause of AR then a second valve was implanted (valve in valve)[23].

COMPARISON OF CALCIUM MEASUREMENT ON CONTRAST AND NON-CONTRAST MSCT

Given the much higher threshold for the detection of calcification (on average 450HU vs 130HU) we anticipated that calcium score would be underestimated on the contrast MSCT relative to the conventional non-contrast method. In order to compare the measurement of aortic leaflet calcification by the two methods (contrast- compared to non-contrast MSCT) 47 patients were selected with calcification largely limited to the aortic leaflets and with no or limited calcification in the adjacent structures so as to ensure that the regions of interest corresponded as closely as possible. This was necessary because 1) aortic leaflet calcification may have an effect on the need for BAVF whereas additional aortic root calcification in the wall of the aorta, mitral valve or coronary ostia would not, 2) the region of interest on the non-contrast images is defined on images axial to the patient and fine anatomical detail cannot be readily appreciated whereas on the contrast MSCT the region of interest is defined on images axial to the aortic annulus and calcification of individual leaflets can be measured.

STATISTICAL ANALYSIS

Correlation coefficients and Bland- Altman plots were used for the comparison of measurement of aortic leaflet calcification on contrast and non-contrast MSCT. Calcification score data were not normally distributed and are given as median [interquartile range]. Normally distributed data are given as mean (SD). For comparison between groups Student's t-test or the Mann-Whitney U-test were used. The odds ratio and 95% confidence interval was used to investigate the association between the exposure variables (calcium volume, mass) and outcome (BAVF). To determine which variable best discriminated the need for BAVF receiver operator characteristic (ROC) curves were plotted (sensitivity vs 1-specificity) and the areas under the curve were calculated. Statistical significance was defined as $p<0.05$. SPSS 15.0 was used.

RESULTS

DEMOGRAPHICS

Clinical and anatomical details of the study population are given in Table 1. The calcium burden of the aortic root and leaflets was high in all patients, Table 1. The degree of calcification was highest for the non-coronary leaflet (calcium mass median [IQR] = 187 [121-

Table 1: Clinical and anatomical characteristics of the patients who did and did not have balloon post-dilatation of the frame (BAVF) during TAVI.

N[%]; MEAN (SD); MEDIAN [IQ-RANGE]	ALL N=110	NO BAVF N=99	BAVF N=11	P-VALUE
Age (y)	80 (7)	81 (7)	79 (8)	
Female:male	62:48	57:42	5:6	
Height (cm)	167 (9)	167 (9)	168 (11)	
Weight (kg)	73 (14)	72 (14)	75 (13)	
BMI (kg/m^2)	26 (4)	26 (4)	27 (4)	
Serum creatinine (µmol/l)	91 [71-117]	87 [70-117]	103 [91-144]	0.06
LV function				
- normal	66 (60)	59 (60)	7 (64)	
- mild to moderate	34 (31)	31 (31)	3 (27)	
- poor	10 (9)	9 (9)	1 (9)	
Echo annulus	23 (2)	23 (2)	23 (2)	
Euroscore	15 (9)	15 (9)	12 (9)	
MSCT annulus diameter				
- Minimum	21.7 (2.6)	21.5 (2.5)	23.0 (3.1)	0.03
- Maximum	26.9 (2.6)	26.6 (2.4)	28.8 (3.4)	0.01
- Mean	24.1 (2.3)	23.9 (2.2)	25.9 (3.1)	<0.01
Aortic root calcium				
- Agatston	2904 [2008-4484]	2841 [1909 to 4239]	4729 [4010 to 7871]	<0.01
- Volume	2333 [1577-3695]	2231 [1506 to 3595]	3710 [3277 to 6156]	<0.01
- Mass	647 [402-1138]	606 [380 to 1014]	1166 [872 to 1925]	<0.01
Total aortic leaflet calcium				
- Volume	783 [531-1421]	759 [502 to 1278]	1545 [1295 to 2186]	<0.01
- Mass	442 [295-911]	420 [290 to 802]	1003[809 to 1395]	<0.01
Depth of implantation				
- Non-coronary sinus	8.2 (3.5)	8.1 (3.5)	8.9 (3.6)	NS
- Left coronary sinus	8.9 (3.6)	8.7 (3.6)	10.0 (3.8)	NS
Prosthesis size implanted 26:29	35:75	33:66	2:9	
Prosthesis inflow to annulus area	1.38 (0.21)	1.40 (0.20)	1.25 (0.24)	0.02
Prosthesis inflow to annulus diameter	1.17 (0.09)	1.18 (0.09)	1.11 (0.11)	0.01

360]), followed by the right (calcium mass= 138 [67-249]) and left coronary leaflets (calcium mass= 129 [62-217).

AR grade 3-4 was seen immediately after device implantation in 15 of 110 patients. In 4 of these 15 patients a second MCS was immediately implanted (valve in valve), which resulted in AR grade 1-2 in all 4 patients. In 11 of these 15 patients BAVF was performed, which resulted in AR grade ≤2 in 8 of 11 patients. One further patient received a second prosthesis (valve in valve) that improved the AR grading to trivial. The grade of AR spontaneously reduced to grade 2 in the first week after TAVI in another patient. One other patient with persistent AR grade 3 despite BAVF died 12 days after the procedure. With the exception of this patient there were no patients with PAR grade >2 on echocardiography 1 week after TAVI. BAVF was associated with the development of a VSD in one patient who had an unusually long ventricular membranous septum[24].

COMPARISON OF CALCIUM VOLUME AND MASS ON CONTRAST AND NON-CONTRAST MSCT

In the 47 patients with calcification limited to aortic leaflets the measurements of both calcium volume and mass where lower on contrast- when compared to non-contrast MSCT: calcium volume median [IQ-range] = 759 [466 to 1295] vs. 2016 [1376 to 3262]; calcium mass = 441 [268 to 809] vs. 555 [341 to 950]. There was a high degree of correlation between the contrast and non-contrast MSCT measurement of both calcium volume and mass (respectively r=0.93 and r=0.95), Figure 2. The Bland- Altman plot showed that there was a negative bias for the measurement of calcium volume on contrast scans and the difference between the two methods increased as calcium volume increased (correlation coefficient r=0.90), Figure 2. In contrast the calcium mass was also underestimated on contrast MSCT but there was no association between the difference between the two methods and increasing calcium values (correlation coefficient r=0.17), Figure 3.

CHARACTERISTICS OF PATIENTS WHO REQUIRED BAVF

There were no differences in the clinical characteristics of patients who did and did not have BAVF (Table 1). On pre-procedural MSCT the patients who required PABV had a larger annulus dimensions (minimum, maximum, mean diameters), a higher degree of aortic root calcification on non-contrast MSCT and higher levels of aortic leaflet calcification on contrast MSCT, Table 1. The ratio of nominal prosthesis inflow to annulus dimensions was lower in patients who received BAVF when compared to those who did not, Table 1. There was no difference depth of implantation between the two groups.

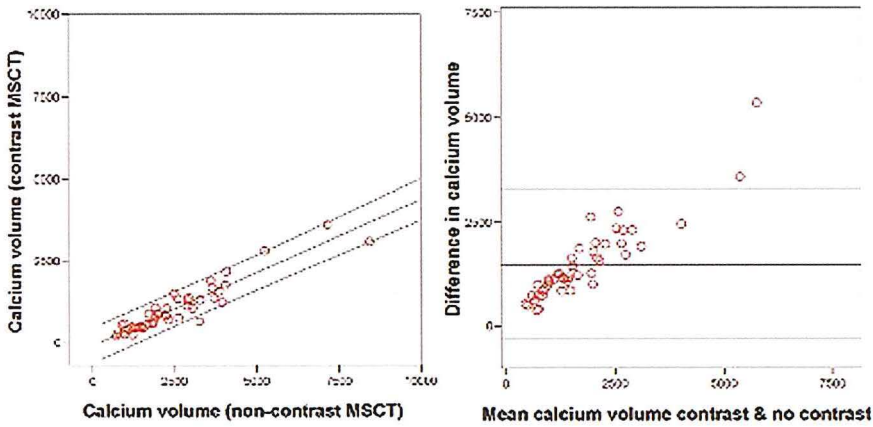

Figure 2: Scatter plot (left panel) and Bland-Altman plot (right panel) of calcium volume measured on contrast and non-contrast MSCT.

The linear regression lines with 95% confidence intervals are shown for scatterplot (left panel: intercept -99, slope 0.45, R-squared =0.86). Reference lines represent the mean difference±2SD for the Bland-Altman plot (right panel).

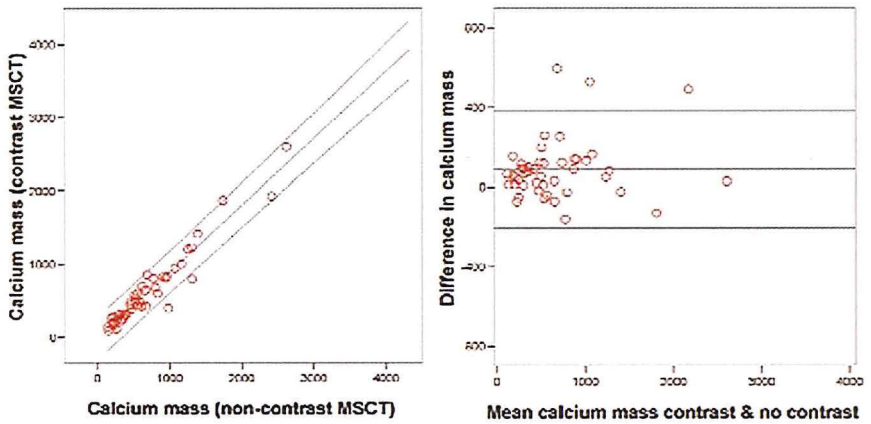

Figure 3: Scatterplot (left panel) and Bland-Altman plot (right panel) of calcium mass measured on contrast and non-contrast MSCT.

The linear regression lines with 95% confidence intervals are shown for the scatterplot (left panel: intercept -26, slope 0.91, R-squared =0.93). Reference lines represent the mean difference±2SD for the Bland-Altman plot (right panel).

The implanted prosthesis was correctly or over-sized based on the sagittal annulus measurement from echocardiography in all patients who subsequently required BAVF. Yet if sizing was based on the maximum annulus diameter obtained from MSCT, which is not accurately measured on 2D echocardiography, the selected prosthesis would have been undersized in

8 of 11 patients who required BAVF. If the sizing was based on the mean annulus diameter obtained from MSCT the selected prosthesis would have been undersized in 5 of 11 patients who required BAVF and oversized in one patient. Undersizing, defined as a mean annulus diameter ≥23.5 for a size 26 and ≥27.5 for a size 29 MCS implant, was associated with BAVF: odds ratio (95% CI) = 11.0 (2.7-45).

An aortic leaflet dense calcium mass ≥800 (contrast MSCT) was more frequent in cases who had BAVF than those who did not (91% vs 25%) and was significantly associated with BAVF: odds ratio (95% CI) = 29.6 (3.6 to 242.9). 29% of patients with an aortic leaflet dense calcium mass ≥800 required BAVF compared to 1% of those with a dense calcium mass <800. Similar data were seen for an aortic leaflet dense calcium volume ≥1200 (contrast MSCT), which was seen respectively in 91% and 26% of patients who did and did not have BAVF. On non-contrast MSCT an Agaston score ≥3000 was seen in all patients who had BAVF and in 43% of those who did not. When evaluated by ROC curve all measures of aortic root or aortic leaflet calcium showed excellent discrimination for the requirement of BAVF (all >0.80, Table 2), whereas the discriminatory value of aortic annulus dimensions was moderate (0.68) and that of prosthesis to annulus ratio was poor (0.39), Table 2.

Table 2: Receiver operating characteristic (ROC) curves plotted as sensitivity vs. 1 minus specificity and areas under the curves were calculated to determine which variable was best able to discriminate the need for BAVF.

TEST VARIABLE	AREA UNDER THE ROC CURVE
Aortic Root Calcium (non-contrast MSCT)	
Volume	0.82*
Mass	0.80*
Agatston	0.83*
Aortic Leaflet Calcium (contrast MSCT)	
Volume	0.81
Mass	0.81
Annulus diameter	
Mean	0.68
Minimum	0.68
Maximum	0.69
Prosthesis to annulus area	0.36
Prosthesis to annulus diameter	0.36

* As determined in the subset of 98 patients with a non-contrast MSCT of which 9 underwent BAVF

DISCUSSION

This study shows firstly that quantification of mass and volume of dense calcium of the aortic leaflets on contrast MSCT is feasible and secondly that it allows the detection of dense calcifications that increase the risk of needing post-dilatation after TAVI. Dense calcium was a predictor of BAVF in the present study and others [25]. Less dense calcification is unlikely to affect procedural outcome. This concept is supported by the observation in the present study that calcifications measured on both contrast- and non-contrast MSCT discriminated the need for BAVF equally, despite the fact that spots of calcium with mild to moderate density (<450HU) are not detectable on contrast MSCT.

Although semi-quantitative estimation of calcification burden on the aortic leaflets on echocardiography has been described [2] the measurement of calcium non-contrast MSCT (Agatston score, volume, mass) has to be considered the gold standard [26, 27]. We report that calcium volume is underestimated on contrast- when compared to non-contrast MSCT and the degree of underestimation increases with increasing levels of root Ca volume. In contrast the mass measurement did not show a similar increasing bias. This may be explained by the fact that less dense calcium that will not be detected on contrast scans (<450HU) may have a substantial volume but relatively little mass. These data indicate measurement of calcium on contrast MSCT may lead to significant misclassification when small amounts of calcification have prognostic implications for example in the coronary arteries[13]. Yet only dense aortic leaflet calcification (Agatston score >3000 on non-contrast MSCT, mass ≥800, volume ≥1200 on contrast MSCT) was a risk marker for BAVF during TAVI in this and another study[25]. The ability to easily measure dense aortic root calcification contrast MSCT may eliminate the need for an additional non-contrast MSCT before TAVI. This would reduce the radiation dose of a pre-TAVI MSCT scan by approximately 1-2mSv on average, depending on the scanning protocol used.

PAR is common post TAVI but is mostly mild whereas haemodynamically significant AR (grade 3 to 4) is reported in approximately 1 to 5% of patients[8,25]. This is in part because haemodynamically significant PAR is not well tolerated in elderly patients with stiff ventricles. Consequently it is almost always ameliorated by additional measures during the implantation procedure, even when it does not lead to acute haemodynamic compromise. Treatment options include BAVF in order to improve apposition of the sealing skirt at the inflow of the frame to surrounding tissues, or, if a too deep implantation is the principle cause a second prosthesis may be deployed (valve in valve). We observed haemodynamically significant AR (grade ≥3) in 14 patients (15%) after TAVI of which 10% was first treated with BAVF and 4% were treated with implantation of a second valve. Another study of similar size reported PAR grade ≥3 in 9% of patients of which 3% were treated with implantation of a second valve after BAVF failed to improve the AR[25]. In that study BAVF was performed in a larger proportion i.e. 34% of patients because the threshold was lower i.e. patients with PAR grade 2 also underwent BAVF. In our study PAR grade ≥3 was seen in only 1 patient on follow up echocardiography 1 week after TAVI. It is thought that the nitinol frame of the MCS continues

to expansion of within 48 hours after device release. Consequently PAR may be expected to reduce further within this period without BAVF. The additional instrumentation during BAVF may carry an incremental risk of complications, although the risk is small and clearly considerably lower than for BAV of the native valve. A case report suggested that caution may be warranted when post-dilatation is performed in patients with a ventricular membranous septum that extends a relatively long way below the aortic annulus [24]. However, as there is currently no technique to eliminate the calcium during TAVI and the current frame technology does not fully accommodate the surrounding anatomy, additional BAVF is integral part of TAVI, fortunately at low risk. In patients who receive a surgical aortic valve prosthesis aortic calcification is a marker of adverse procedural outcome. There is currently no evidence that this calcification predicts an adverse outcome after TAVI, although the case series have been relatively small.

We report that aortic annulus dimensions and the ratio of nominal prosthesis to annulus size were higher in patients who required BAVF when compared to those who did not. Two studies of respectively 74 and 53 patients reported similar findings based on 2D echocardiographic measurements[5,29]. In the present study there was substantial overlap between the two groups. However, annulus dimensions discriminated less well the need for BAVF than did quantification of calcifications. These data suggest that relative undersizing, if not too extreme, may exacerbate the effects of dense calcification rather than being the primary cause of haemodynamically significant AR requiring BAVF. Furthermore the availability of larger prosthesis sizes in combination with sizing based on mean annulus dimensions from a 3D imaging modality such as MSCT, 3DTEE or CMRI may reduce the need for BAVF, although this would require further study.

LIMITATIONS

This is a relatively small study and should be viewed as hypothesis generating. Since the analysis method for the quantification of calcium on the contrast and non-contrast scans are different and non-contrast scans do not allow appreciation of fine anatomical detail it is not possible to exactly match the regions of interest on the two types of scan. Other factors that may affect the detection of calcium between contrast and non-contrast scans include differences in scanner type, body habitus, the radiation dose, slice thickness, reconstruction increment in addition to the presence or absence of contrast [17,30-33]. Despite that these differences can not be adjusted for the ability to discriminate the need for BAVF was similar for calcium measured on both contrast and non-contrast MSCT .

CONCLUSIONS

Dense aortic leaflet calcification can be quantified sufficiently on contrast MSCT to allow prediction of haemodynamically significant PAR during TAVI requiring BAVF after device release. On contrast MSCT an aortic leaflet calcium mass >800, a calcium volume > 1200, larger annulus dimensions and nominal prosthesis inflow to annulus ratio were associated with BAVF during TAVI. Aortic root or aortic leaflet calcium on respectively non-contrast and contrast MSCT showed excellent discrimination for the requirement of BAVF, whereas the discriminatory value of aortic annulus dimensions was moderate.

REFERENCES

1. Leon MB, Smith CR, Mack M, Miller DC, Moses JW, Svensson LG, Tuzcu EM, Webb JG, Fontana GP, Makkar RR, Brown DL, Block PC, Guyton RA, Pichard AD, Bavaria JE, Herrmann HC, Douglas PS, Petersen JL, Akin JJ, Anderson WN, Wang D, Pocock S; PARTNER Trial Investigators. Transcatheter aortic-valve implantation for aortic stenosis in patients who cannot undergo surgery. *N Engl J Med.* 2010; 21; 363: 1597-607.
2. Rosenhek R, Binder T, Porenta G, Lang I, Christ G, Schemper M, Maurer G, Baumgartner H.Predictors of outcome in severe, asymptomatic aortic stenosis. *N Engl J Med.* 2000; 31: 611-7.
3. Grube E, Laborde JC, Gerckens U, Felderhoff T, Sauren B, Buellesfeld L, Mueller R, Menichelli M, Schmidt T, Zickmann B, Iversen S, Stone GW.Percutaneous implantation of the CoreValve self-expanding valve prosthesis in high-risk patients with aortic valve disease: the Siegburg first-in-man study. *Circulation.* 2006; 114:1616-24.
4. Cribier A, Eltchaninoff H, Tron C, Bauer F, Agatiello C, Sebagh L, Bash A, Nusimovici D, Litzler PY, Bessou JP, Leon MB.Early experience with percutaneous transcatheter implantation of heart valve prosthesis for the treatment of end-stage inoperable patients with calcific aortic stenosis.*J Am Coll Cardiol.* 2004; 43:698-703.
5. Détaint D, Lepage L, Himbert D, Brochet E, Messika-Zeitoun D, Iung B, Vahanian A. Determinants of significant paravalvular regurgitation after transcatheter aortic valve: implantation impact of device and annulus discongruence. *JACC Cardiovasc Interv.* 2009; 2: 821-7.
6. Schultz CJ, Moelker A, Piazza N, Tzikas A, Otten A, Nuis RJ, Neefjes LA, van Geuns RJ, de Feyter P, Krestin G, Serruys PW, de Jaegere PP. Three dimensional evaluation of the aortic annulus using multislice computer tomography: are manufacturer's guidelines for sizing for percutaneous aortic valve replacement helpful? *Eur Heart J.* 2010; 31: 849-56.
7. Messika-Zeitoun D, Serfaty JM, Brochet E, Ducrocq G, Lepage L, Detaint D, Hyafil F, Himbert D, Pasi N, Laissy JP, Iung B, Vahanian. A.Multimodal assessment of the aortic annulus diameter: implications for transcatheter aortic valve implantation. *J Am Coll Cardiol.* 2010; 55: 186-94.
8. Koos R, Mahnken AH, Dohmen G, Brehmer K, Günther RW, Autschbach R, Marx N, Hoffmann R. Association of aortic valve calcification severity with the degree of aortic regurgitation after transcatheter aortic valve implantation. *Int J Cardiol.* 2010 Epub ahead of print.
9. Himbert D, Descoutures F, Al-Attar N, Iung B, Ducrocq G, Détaint D, Brochet E, Messika-Zeitoun D, Francis F, Ibrahim H, Nataf P, Vahanian A. Results of transfemoral or transapical aortic valve implantation following a uniform assessment in high-risk patients with aortic stenosis. *J Am Coll Cardiol.* 2009; 54: 303-11.
10. Rodés-Cabau J, Dumont E, Doyle D. "Valve-in-valve" for the treatment of paravalvular leaks following transcatheter aortic valve implantation. *Catheter Cardiovasc Interv.* 2009; 74: 1116-9.
11. Zahn R, Gerckens U, Grube E, Linke A, Sievert H, Eggebrecht H, Hambrecht R, Sack S, Hauptmann KE, Richardt G, Figulla HR, Senges J; on behalf of the German Transcatheter Aortic Valve Interventions—Registry Investigators. Transcatheter aortic valve implantation: first results from a multi-centre real-world registry. *Eur Heart J.* 2011; 32: 198-204.

12. Messika-Zeitoun D, Aubry MC, Detaint D, Bielak LF, Peyser PA, Sheedy PF, Turner ST, Breen JF, Scott C, Tajik AJ, Enriquez-Sarano M. Evaluation and clinical implications of aortic valve calcification measured by electron-beam computed tomography. *Circulation.* 2004; 110: 356-62.
13. van der Bijl N, Joemai RM, Geleijns J, Bax JJ, Schuijf JD, de Roos A, Kroft LJ. Assessment of Agatston coronary artery calcium score using contrast-enhanced CT coronary angiography. *AJR Am J Roentgenol.* 2010; 195: 1299-305.
14. Agatston AS, Janowitz WR, Hildner FJ, Zusmer NR, Viamonte M Jr, Detrano R. Quantification of coronary artery calcium using ultrafast computed tomography. *J Am Coll Cardiol.* 1990; 15: 827-32.
15. Callister TQ, Cooil B, Raya SP, Lippolis NJ, Russo DJ, Raggi P. Coronary artery disease: improved reproducibility of calcium scoring with an electron-beam CT volumetric method. *Radiology.* 1998; 208: 807-14
16. Hong C, Becker CR, Schoepf UJ, Ohnesorge B, Bruening R, Reiser MF. Coronary artery calcium: absolute quantification in nonenhanced and contrast-enhanced multi-detector row CT studies. *Radiology.* 2002; 223: 474-80.
17. Ohnesorge B, Flohr T, Fischbach R, Kopp AF, Knez A, Schröder S, Schöpf UJ, Crispin A, Klotz E, Reiser MF, Becker CR. Reproducibility of coronary calcium quantification in repeat examinations with retrospectively ECG-gated multisection spiral CT. *Eur Radiol.* 2002; 12: 1532-40.
18. Schultz CJ, Weustink A, Piazza N, Otten A, Mollet N, Krestin G, van Geuns RJ, de Feyter P, Serruys PW, de Jaegere P. Geometry and degree of apposition of the CoreValve ReValving system with multislice computed tomography after implantation in patients with aortic stenosis. *J Am Coll Cardiol.* 2009; 54: 911-8.
19. Piazza N, de Jaegere P, Schultz C, Becker AE, Serruys PW, Anderson RH. Anatomy of the aortic valvar complex and its implications for transcatheter implantation of the aortic valve. *Circ Cardiovasc Interv.* 2008; 1: 74-81.
20. Schultz C, Moelker A, Tzikas A, Piazza N, de Feyter P, van Geuns RJ, Serruys PW, Krestin GP, de Jaegere P. The use of MSCT for the evaluation of the aortic root before transcutaneous aortic valve implantation: the Rotterdam approach. *EuroIntervention.* 2010; 6: 505-11.
21. de Jaegere P, Kappetein AP, Knook M, Ilmer B, van der Woerd D, Deryck Y, de Ronde M, Boks R, Sianos G, Ligthart J, Laborde JC, Bogers A, Serruys PW. Percutaneous aortic valve replacement in a patient who could not undergo surgical treatment. A case report with the CoreValve aortic valve prosthesis. *EuroIntervention.* 2006; 1: 475-9.
22. Sellers RD, Levy MJ, Amplatz K, Lillehei CW. Left retrograde cardioangography in acquired cardiac disease: Technic indications and interpretations in 700 cases. *Am J Cardiol.* 1964; 14: 437-47.
23. Piazza N, Schultz C, de Jaegere PP, Serruys PW. Implantation of two self-expanding aortic bioprosthetic valves during the same procedure-Insights into valve-in-valve implantation ("Russian doll concept"). *Catheter Cardiovasc Interv.* 2009; 73: 530-9.
24. Tzikas A, Schultz C, Piazza N, van Geuns RJ, Serruys PW, de Jaegere PP. Perforation of the membranous interventricular septum after transcatheter aortic valve implantation. *Circ Cardiovasc Interv.* 2009; 2: 582-3.

25. John D, Buellesfeld L, Yuecel S, Mueller R, Latsios G, Beucher H, Gerckens U, Grube E. Correlation of Device landing zone calcification and acute procedural success in patients undergoing transcatheter aortic valve implantations with the self-expanding CoreValve prosthesis. *JACC Cardiovasc Interv.* 2010; 3: 233-43.
26. McCollough CH, Ulzheimer S, Halliburton SS, Shanneik K, White RD, Kalender WA. Coronary artery calcium: a multi-institutional, multimanufacturer international standard for quantification at cardiac CT. *Radiology.* 2007; 243: 527-38.
27. Koos R, Mahnken AH, Kühl HP, Mühlenbruch G, Mevissen V, Stork L, Dronskowski R, Langebartels G, Autschbach R, Ortlepp JR. Quantification of aortic valve calcification using multislice spiral computed tomography: comparison with atomic absorption spectroscopy. *Invest Radiol.* 2006; 41: 485-9.
28. Ben-Dor I, Pichard AD, Satler LF, Goldstein SA, Syed AI, Gaglia MA Jr, Weissman G, Maluenda G, Gonzalez MA, Wakabayashi K, Collins SD, Torguson R, Okubagzi P, Xue Z, Kent KM, Lindsay J, Waksman R. Complications and outcome of balloon aortic valvuloplasty in high-risk or inoperable patients. *JACC Cardiovasc Interv.* 2010; 3: 1150-6.
29. Delgado V, Ng AC, van de Veire NR, van der Kley F, Schuijf JD, Tops LF, de Weger A, Tavilla G, de Roos A, Kroft LJ, Schalij MJ, Bax JJ. Transcatheter aortic valve implantation: role of multi-detector row computed tomography to evaluate prosthesis positioning and deployment in relation to valve function. *Eur Heart J.* 2010; 31: 1114-23.
30. Horiguchi J, Matsuura N, Yamamoto H, Hirai N, Kiguchi M, Fujioka C, Kitagawa T, Kohno N, Ito K. Variability of repeated coronary artery calcium measurements by 1.25-mm- and 2.5-mm-thickness images on prospective electrocardiograph-triggered 64-slice CT. *Eur Radiol.* 2008; 18: 209-16.
31. Schlosser T, Hunold P, Schmermund A, Kühl H, Waltering KU, Debatin JF, Barkhausen J. Coronary artery calcium score: influence of reconstruction interval at 16-detector row CT with retrospective electrocardiographic gating. *Radiology.* 2004; 233: 586-9.
32. Arnold BA, Budoff MJ, Child J, Xiang P, Mao SS. Coronary calcium test phantom containing true CaHA microspheres for evaluation of advanced CT calcium scoring methods. *J Cardiovasc Comput Tomogr.* 2010; 4: 322-9.

PART 3: PREGNANCY AND HEART DISEASE

CHAPTER 12

QUANTITATIVE CARDIOVASCULAR MAGNETIC RESONANCE IN PREGNANT WOMEN: CROSS-SECTIONAL ANALYSIS OF PHYSIOLOGICAL PARAMETERS THROUGHOUT PREGNANCY AND THE IMPACT OF THE SUPINE POSITION.

Journal of Cardiovascular Magnetic Resonance, 2011; 13 (1): 31-37

A Rossi
J Cornette
MR Johnson
Y Karamermer
T Springeling
P Opic
A Moelker
GP Krestin
E Steegers
J Roos-Hesselink
R-JM van Geuns

ABSTRACT

Background: There are physiological reasons for the effects of positioning on hemodynamic variables and cardiac dimensions related to altered intra-abdominal and intra-thoracic pressures. This problem is especially evident in pregnant women due to the additional aorto-caval compression by the enlarged uterus. The purpose of this study was to investigate the effect of postural changes on cardiac dimensions and function during mid and late pregnancy using cardiovascular magnetic resonance (CMR).

Methods: Healthy non-pregnant women, pregnant women at 20th week of gestation and at 32nd week of gestation without history of cardiac disease were recruited to the study and underwent CMR in supine and left lateral positions. Cardiac hemodynamic parameters and dimensions were measured and compared between both positions.

Results: Five non-pregnant women, 6 healthy pregnant women at mid pregnancy and 8 healthy pregnant women at late pregnancy were enrolled in the study. In the group of non-pregnant women left ventricular (LV) cardiac output (CO) significantly decreased by 9% ($p=0.043$) and right ventricular (RV) end-diastolic volume (EDV) significantly increased by 5% ($p=0.043$) from the supine to the left lateral position. During mid pregnancy LV ejection fraction (EF), stroke volume (SV), left atrium lateral diameter and left atrial supero-inferior diameter increased significantly from the supine position to the left lateral position: 8%, 27%, 5% and 11%, respectively ($p<0.05$). RV EDV, SV and right atrium supero-inferior diameter significantly increased from the supine to the left lateral position: 25%, 31% and 13% ($p<0.05$), respectively. During late pregnancy a significant increment of LV EF, EDV, SV and CO was observed in the left lateral position: 11%, 21%, 35% and 24% ($p<0.05$), respectively. Left atrial diameters were significantly larger in the left lateral position compared to the supine position ($p<0.05$). RV CO was significantly increased in the left lateral position compared to the supine position ($p<0.05$).

Conclusions: During pregnancy positional changes affect significantly cardiac hemodynamic parameters and dimensions. Pregnant women who need serial studies by CMR should be imaged in a consistent position. From as early as 20 weeks the left lateral position should be preferred on the supine position because it positively affects venous return, SV and CO.

BACKGROUND

Increasing numbers of women with pre-existing heart disease are reaching childbearing age and are deciding to become pregnant [1]. Pregnancy induces marked physiological changes in cardiac parameters, with a 30-50% increase in cardiac output, through an increase both in stroke volume and heart rate [2]. While usually well tolerated in healthy pregnant women, these changes can induce adverse effect in women with pre-existing heart disease on both right and left-sided lesions [3, 4]. Therefore, heart function should be closely monitored during pregnancy in these patients. Echocardiography has been used for many years but cardiovascular magnetic resonance (CMR) is more reliable in the context of congenital heart disease [5]. To date, most data have been derived using echocardiography with the patients in lateral position [6], while CMR is usually performed in supine position. As aortocaval compression is important in advanced pregnancy [7, 8] data of both techniques can not be compared. Many women with complex cardiac conditions will require CMR during pregnancy, however there is relatively little data regarding both the use of CMR during pregnancy and of the impact of supine and lateral positions on cardiac parameters. The purpose of this study was to investigate the impact of maternal position on cardiac parameters derived from CMR during 2nd and 3rd trimesters of pregnancy in normal women.

METHODS

PATIENT SELECTION

Healthy non-pregnant women, pregnant women at 20th week of gestation and at 32nd week of gestation with no history of cardiac disease were recruited to the study between June 2009 and January 2010. Study participants underwent CMR in supine and left lateral positions. Exclusion criteria were the common contraindications for CMR studies (pacemaker, cochlea implants and claustrophobia). The study was approved by the institutional review board and each subject gave informed consent.

CMR PROTOCOL

CMR was performed using a 1.5T scanner (Signa CV/I, GE Medical System, Milwaukee, WI). Firstly the patient was placed in the supine position and entered feet first into the magnet. A dedicated cardiac 8 channels coil was placed on the thorax of the subject and used for the acquisition of the images. CMR cines were obtained using a breath-holding ECG triggered balanced steady state free precession sequence. Imaging parameters were as follows: FOV 36-40 x 28-32 cm; matrix 224 x 196; TR: 3.4 milliseconds; TE: 1.5 milliseconds; flip angle 45 degrees; 12 views per segment. Slice thickness was 8 mm with a gap of 2 mm. These

parameters resulted in a temporal resolution per image of 41 milliseconds. At first, three rapid surveys were obtained for the determination of the cardiac position and orientation; two- and four-chamber cine MR images were then obtained. The series of short axis (SA) images were obtained from the reference images provided by the two- and four- chamber end-diastolic images at the end of expiration. Approximately 10 to 12 slices were acquired to cover the entire length of the heart. Directly after the first CMR study, the subject was repositioned on the left lateral side position for the second examination. The acquisition of images was performed by the same operator.

IMAGE ANALYSIS

All the studies were analysed on a remote workstation using the CAAS-MRV (version 3.2; Pie Medical Imaging, Maastricht, The Netherlands).

Left end-diastolic volume (EDV) and end-systolic volume (ESV) were calculated using a combination of classic SA and long-axis images. The long-axis view was used to limit the extend of volumes at the base and at the apex of the heart. The Simpson rule was used to calculate volumes based on the SA images where the first basal and the last apical were only partially included relating to the area outlined on two- and four- chamber images. More details about this approach have been previously reported [9]. The papillary muscles were considered as being part of the blood pool shortening the analysis time without compromising the accuracy of LV volumes compared to standard short-axis technique [10]. Ejection fraction (EF) was calculated as (EDV – ESV)/EDV. Cardiac output (CO) was calculated from stroke volume (SV) and heart rate (HR). Left atrium volume (LAvol) was measured using a combination of the two- and four chamber views in the diastolic phase of the atria. Lateral (LAlat) and supero-inferior (LAsi) left atrial diameters were measured on a four-chamber view during

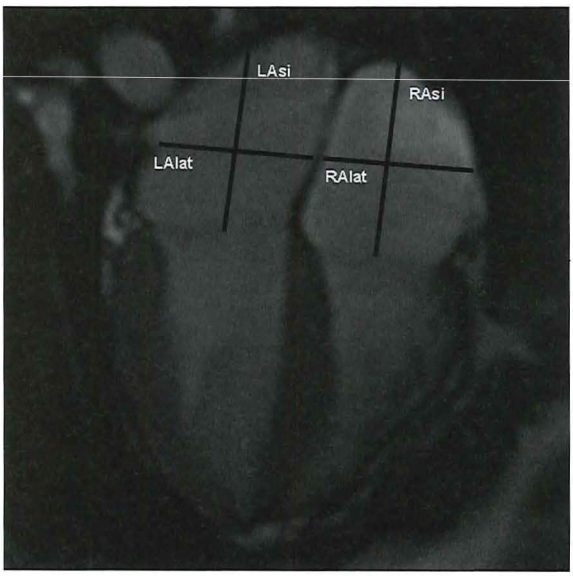

Figure 1. Cardiac dimensions: four-chamber end-systolic view.
LAlat: left atrium lateral diameter; LAsi: left atrium supero-inferior diameter; RAlat: right atrium lateral diameter: RAsi: right atrium supero-inferior diameter.

the phase of cardiac cycle with the largest left atrium (Figure 1). The lateral diameter was taken from the perpendicular constructed from the midpoint of the LAsi diameter extending to the atrial borders. The LAsi dimension corresponds to a line bisecting the left atrium and extending from the midpoint of the mitral annulus to the midpoint of the superior left atrium.

Right EF, EDV, ESV, SV and CO were calculated using cine images acquired in SA view, parallel to the tricuspid valve annulus and applying the same methods of the left ventricular hemodynamic measurements without long-axis corrections. In addition, lateral (RAlat) and supero-inferior (RAsi) right atrium diameters were taken during the phase of the cardiac cycle with the largest right atrium, on a four-chamber view (Figure 1). The RAlat diameter corresponds to the line extending from the atrial borders and perpendicular to the RAsi diameter. The RAsi diameter is the line from the midpoint of the tricuspid valve to the midpoint of the superior right atrium.

Due to the low inter-observer variability reported in a previous study [11] image analysis was performed by one operator with 3 years-experience in CMR. The operator was blinded to the same patient at the other position. CMR analyses were performed in a random order at different days.

ANALYSIS BY GESTATIONAL WEEK

The patients were categorized into 3 groups according to gestational age. The first group consists of non-pregnant controls, the second group of women in the 20th gestational week and the third group of women in the 32nd gestational week.

STATISTICAL ANALYSIS

All analyses were done using SPSS 15 (SPSS Inc.) software. Parametric data were reported as mean ± standard deviation. For each gestational group mean values of HR, EDV, ESV, EF, SV, CO, left and right atrium diameters of supine and left lateral positions were tested for significance, using Wilcoxon's two sample test. A p-value <0.05 was considered significant. The percentage of change in the measure of left ventricle (LV) and right ventricle (RV) parameters (X) and left atrium (LA) and right atrium (RA) parameters (X) between supine and left lateral position was calculated using the following formula:

$$\text{percentage change in } X = [(X_{lateral} - X_{supine})/X_{supine}] \times 100.$$

RESULTS

A total of 14 healthy women with singleton pregnancies (30.3±5.2 years) were included in the study. Five non-pregnant women (29.4±5.7 years) were recruited as controls. The time interval between the examinations in supine and left lateral position ranged between 8 and 12 minutes. Table 1 gives the data regarding hemodynamic parameters and cardiac dimensions as related to gestational week and maternal posture. Percentage differences of cardiac volumes between supine and left lateral position are graphically reported in Figure 2 and 3 and will be reported in more detail below.

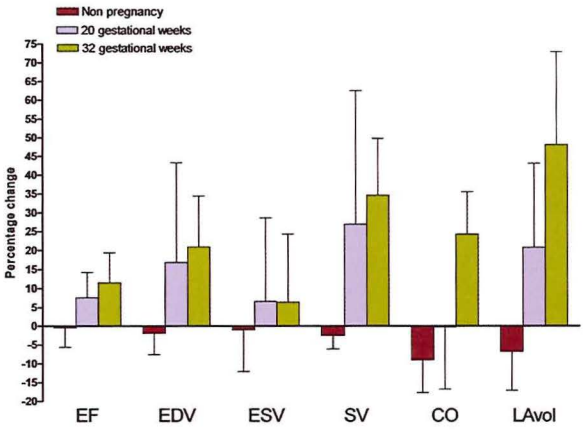

Figure 2. Percentage differences of hemodynamic parameters of left side of the heart.

EF (ejection fraction: %), EDV (end-diastolic volume: ml), ESV (end-systolic volume: ml), SV (stroke volume: ml), CO (cardiac output: L/min), LAvol (left atrium volume: ml)

Percentage difference from supine to left lateral position is calculated with the following formula:

$X(\%) = [(X_{lateral} - X_{supine})/(X_{supine})]$ x100 where X is a cardiac parameter.

Figure 3. Percentage differences of hemodynamic parameters of right side of the heart.

EF (ejection fraction: %), EDV (end-diastolic volume: ml), ESV (end-systolic volume: ml), SV (stroke volume: ml), CO (cardiac output: L/min), LAvol (left atrium volume: ml)

Percentage difference from supine to left lateral position is calculated with the following formula:

$X(\%) = [(X_{lateral} - X_{supine})/(X_{supine})]$ x100 where X is a cardiac parameter.

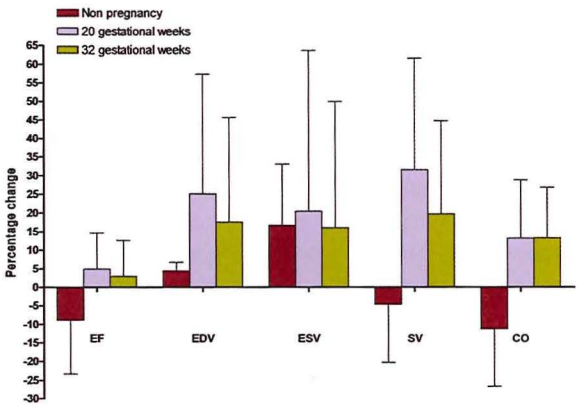

Table 1. Influence of position related to gestational weeks.

	PRE PREGNANCY (N=5)			T20 (N=6)			T32 (N=8)		
	Supine position Mean (SD)	Left lateral position Mean (SD)	p-value╬	Supine position Mean (SD)	Left lateral position Mean (SD)	p-value╬	Supine position Mean (SD)	Left lateral position Mean (SD)	p-value╬
LEFT ATRIUM AND LEFT VENTRICLE									
HR	78.2 (12.7)	73.0 (12.1)	0.180	80.5 (11.3)	72.3 (5.3)	0.104	80.8 (15.7)	75.2 (10.6)	0.237
EF (%)	56.2 (3.5)	55.9 (4.3)	0.686	53.8 (4.4)	57.8 (4.6)	0.046	51.8 (7.2)	57.7 (8.0)	0.012
EDV (ml)	156.5 (23.3)	153.5 (24.7)	0.686	140.8 (37.1)	157.4 (20.7)	0.115	138.4 (22.1)	166.1 (25.6)	0.012
ESV (ml)	68.6 (12.7)	67.8 (14.1)	0.893	64.6 (17.9)	66.5 (11.8)	0.917	67.1 (16.4)	71.4 (22.3)	0.484
SV (ml)	87.8 (12.9)	85.7 (13.4)	0.223	76.0 (21.1)	90.9 (13.4)	0.028	71.2 (12.2)	94.8 (13.1)	0.012
CO (L/min)	6.8 (0.8)	6.2 (1.2)	0.043	6.5 (1.1)	6.5 (1.6)	0.917	5.6 (0.7)	6.9 (0.9)	0.012
LA vol (ml)	65.5 (13.3)	57.1 (15.8)	0.068	51.8 (12.7)	60.8 (10.3)	0.028	49.0 (20.9)	68.6 (15.7)	0.012
LA lat (mm)	39.7 (2.8)	37.8 (3.3)	0.080	35.0 (3.9)	36.7 (3.7)	0.028	35.4 (2.4)	40.7 (3.7)	0.012
LA si (mm)	45.1 (6.7)	43.7 (3.4)	0.500	40.3 (3.9)	44.9 (3.2)	0.027	39.7 (6.3)	44.7 (8.2)	0.025
RIGHT ATRIUM AND RIGHT VENTRICLE									
EF (%)	51.5 (5.5)	46.4 (4.0)	0.225	50.5 (3.4)	52.9 (4.7)	0.249	53.2 (6.8)	54.6 (6.6)	0.575
EDV (ml)	161.0 (24.8)	168.6 (29.2)	0.043	132.0 (34.6)	156.1 (22.3)	0.028	138.8 (37.3)	155.9 (22.6)	0.161
ESV (ml)	78.7 (18.8)	90.5 (17.6)	0.080	65.1 (16.5)	73.1 (8.9)	0.463	65.7 (22.6)	71.8 (18.7)	0.484
SV (ml)	82.3 (10.7)	78.1 (14.1)	0.345	66.9 (19.3)	84.1 (16.9)	0.028	73.1 (17.2)	84.1 (7.9)	0.050
CO (L/min)	6.4 (1.0)	5.6 (1.1)	0.138	5.3 (1.5)	5.9 (1.8)	0.075	5.6 (0.6)	6.3 (0.7)	0.025
RA lat (mm)	34.4 (5.0)	33.5 (5.2)	0.345	32.4 (4.0)	33.2 (5.2)	0.500	33.9 (6.2)	36.2 (7.1)	0.484
RA si (mm)	47.5 (2.8)	45.9 (4.4)	0.345	40.4 (4.4)	45.1 (5.6)	0.042	44.5 (6.0)	45.2 (7.8)	0.889

T20: 20th gestational week; T32: 32nd gestational week.

EF (ejection fraction), EDV (end-diastolic volume), ESV (end-systolic volume), SV (stroke volume), CO (cardiac output), LAvol (left atrium volume), LAlat (left atrium lateral diameter), LAsi (left atrium supero-inferior diameter), RAlat (right atrium lateral diameter), RAsi (right atrium supero-inferior diameter).

PRE PREGNANCY

HR did show a slight although not significantly decrease between supine and left lateral position: 78±12 versus 73±12. Left CO significantly decreased by 9% ($p=0.043$) and right EDV significantly increased by 5% ($p=0.043$). There were no other significant changes of hemodynamic parameters and cardiac dimensions between the two recumbent positions.

20 GESTATIONAL WEEKS

Six pregnant women were in the 20th gestational week. HR was 80±11 bpm in the supine position and 72±5 in the left lateral position ($p=0.15$). A significant increment of EF and SV of the left ventricle was observed between the supine and the left lateral position: 8% ($p=0.046$) and 27% ($p=0.028$), respectively. Left atrial dimensions increased significantly between the supine and the left lateral position by 5% for LAlat ($p=0.028$) and by 11% for LAsi ($p=0.027$). Regarding the right side of the heart, EDV increased by 25% (0.028) and SV increased by 31% (0.028) between the supine and the left lateral position. RAsi significantly increased by 13% ($p=0.042$) between the supine and the left lateral position.

32 GESTATIONAL WEEKS

Eight pregnant women were in the 32nd gestational week. HR did not significantly change between the supine and the left lateral position: 81±16 versus 75±8 bpm ($p=0.237$). A significant increment of EF, EDV, SV and CO was observed between the supine and the left lateral position: 11% ($p=0.012$), 21% ($p=0.012$), 35% ($p=0.012$) and 24% ($p=0.012$), respectively. Left atrial dimensions increased significantly between the supine and the left lateral position by 15% for LAlat ($p=0.012$) and by 13% for LAsi ($p=0.025$). No significant changes of right hemodynamic parameters and dimensions were observed between the two recumbent positions with the only exception of CO ($p=0.025$).

IMPACT OF GESTATIONAL AGE

A progressive increase of percentage changes of hemodynamic parameters and cardiac dimensions of the left side of the heart was found throughout gestation. The only exception was the percentage change of ESV which substantially did not change between 20 and 32 weeks of gestation. During late pregnancy left ventricle CO significantly increased between supine and left lateral position; the percentage of increment at 32 weeks was 24%. This was associated to an increase of 21% of left ventricle EDV. A significant increase in LA dimensions

was also found. The difference between the two recumbent positions was less clear at 20th gestational week with an increase of left ventricle EDV and LA dimensions but with no clear impact on CO. For the right side of the heart we observed a similar trend of increment of ventricular and atrial dimensions at 20 weeks but no further increase during late pregnancy.

DISCUSSION

This study investigated how the supine and the left lateral positions during CMR affects heart rate, cardiac volumes and dimensions at different gestational ages. To our knowledge this is the first study investigating the effect of two recumbent positions on cardiovascular hemodynamic measurements and changes in cardiac dimensions during pregnancy using CMR. The data show a clear difference between the two positions, which become more marked as pregnancy advances but are significant from as early as 20 weeks. There were minimal changes in the non-pregnant subjects. The existing data from non-pregnant humans with regards to the effect of different positions on hemodynamic parameters are limited and sometimes conflicting. Some report that cardiac output is higher in the supine position compared to the right or left lateral position [12, 13], while others have shown that cardiac output is higher in the left lateral position than in the supine position [14] and still others that there is no difference in either position [15, 16]. In our series, we found that there was no significant effect on hemodynamic parameters and cardiac dimensions of moving from the supine to the left lateral position in non-pregnant women. However, we did observe a non significant decline in both heart rate and stroke volume leading to a borderline significant reduction in cardiac output.

Pregnancy itself is a circulatory burden with a significant impact on the cardiovascular system. Cardiac output increases 30-50% above pre-pregnancy levels. In addition, when a pregnant woman lies flat on her back, the gravid uterus partially compresses the inferior vena cava with the consequent reduction of venous filling load and cardiac output [2, 17]. From our data it appears that the increase of left atrial volume accounts for the majority in increase in stroke volume. As such it seems that the relief of caval obstruction (preload) is far more important that the relief of aortic compression (afterload) for the increase in cardiac output. In our series the significant increase in LA dimensions and the trend to increase EDV in the left lateral position suggest an increased venous return in this position which is already present at 20 gestational weeks. The effect of the gravid uterus compressing the abdominal vessels might be enforced by the increase in plasma volume even as early as 20 weeks of pregnancy [2]. An increase of right atrial pressure [18] and left and right ventricular peak systolic and end-diastolic pressures [19] in the left lateral position can also help to explain the increased venous return. It is of interest to observe that the heart rate was higher in the supine position compensating for the fall in stroke volume in this position [16] in an attempt to recover cardiac output. This could be partly explained by the fact that during mid-late pregnancy the suppression of cardiac vagal activity and the enhancement of cardiac sympathetic activity are greater in the supine position [20] than in the lateral position. In this series left ventricle EDV, EF, CO and SV increase significantly

from the supine to left lateral position. These findings are easily explained: the change from the supine to the lateral position relieves the compression on the vena cava from the gravid uterus. The increasing venous return leads to an increased SV and so CO. Ueland et al [16] demonstrated that a change in position from the supine to the left lateral side produced a rise in CO by 8% at 20 to 24 weeks gestation, 13.6% at 28 to 32 weeks gestation and 28.5% at term in a group of eleven healthy pregnant women. We observed that the SV increased by approximately 27% at 20 weeks gestation. At 32 weeks gestation SV increased significantly by 35%. In our series turning to the left lateral position we observed an increment of the SV of the right ventricle which is more evident in the mid than in the late pregnancy. More studies are needed to better explain the consistency of this finding.

Some concerns may develop regarding the use of CMR in pregnant patients. Most studies evaluating MR safety during pregnancy do not show ill effects on the fetus [21-23]. It is anyway good practice to avoid MR studies during the first trimester of pregnancy although it can be used if clinical indicated. All our patients were studied during the second or third trimester of pregnancy.

Several limitations of this study should be highlighted. First, our results should be tested in a larger sample of women including women with cardiac disease. Indeed the normal physiological respond to pregnancy could be different in patients with congenital or acquired cardiovascular diseases. In addition, the small sample size may justify the large standard deviation in our series. Second, because the interval between each MR acquisition was between 8 and 12 minutes it is possible that cardiac parameters had not returned to baseline. Additional studies using more time points and also investigating the reverse change from lateral to supine could clarify this interesting subject. Third, this study is a cross-sectional study. The effects of the position on cardiac hemodynamic should preferably be studied in a prospective-longitudinal study investigating the same population at different gestational times.

CONCLUSION

In the non-pregnant state, turning from supine to left lateral position have minimal effect on cardiac parameters. During pregnancy, from as early as 20 weeks, turning to the left lateral position has positive effects on cardiac hemodynamics inducing a significant increase of venous return, SV and CO. Pregnant women requiring CMR should be studied in a consistent position for serial studies and the left lateral position is preferred from early pregnancy onwards, also to limit uteroplacental hypoperfusion.

REFERENCES

1. Drenthen W, Pieper PG, Roos-Hesselink JW, van Lottum WA, Voors AA, Mulder BJ, van Dijk AP, Vliegen HW, Yap SC, Moons P, Ebels T, van Veldhuisen DJ, Investigators Z. Outcome of pregnancy in women with congenital heart disease: A literature review. *J Am Coll Cardiol*. 2007;49:2303-2311
2. Karamermer Y, Roos-Hesselink JW. Pregnancy and adult congenital heart disease. *Expert Rev Cardiovasc Ther*. 2007;5:859-869
3. Uebing A, Arvanitis P, Li W, Diller GP, Babu-Narayan SV, Okonko D, Koltsida E, Papadopoulos M, Johnson MR, Lupton MG, Yentis SM, Steer PJ, Gatzoulis MA. Effect of pregnancy on clinical status and ventricular function in women with heart disease. *Int J Cardiol*. 2010;139:50-59
4. Tzemos N, Silversides CK, Colman JM, Therrien J, Webb GD, Mason J, Cocoara E, Sermer M, Siu SC. Late cardiac outcomes after pregnancy in women with congenital aortic stenosis. *Am Heart J*. 2009;157:474-480
5. Kilner PJ, Geva T, Kaemmerer H, Trindade PT, Schwitter J, Webb GD. Recommendations for cardiovascular magnetic resonance in adults with congenital heart disease from the respective working groups of the european society of cardiology. *Eur Heart J*. 2010;31:794-805
6. Del Bene R, Barletta G, Mello G, Lazzeri C, Mecacci F, Parretti E, Martini E, Vecchiarino S, Franchi F, La Villa G. Cardiovascular function in pregnancy: Effects of posture. *BJOG*. 2001;108:344-352
7. Flo K, Wilsgaard T, Vartun A, Acharya G. A longitudinal study of the relationship between maternal cardiac output measured by impedance cardiography and uterine artery blood flow in the second half of pregnancy. *BJOG*. 2010;117:837-844
8. Pump B, Talleruphuus U, Christensen NJ, Warberg J, Norsk P. Effects of supine, prone, and lateral positions on cardiovascular and renal variables in humans. *Am J Physiol Regul Integr Comp Physiol*. 2002;283:R174-180
9. Kirschbaum SW, Baks T, Gronenschild EH, Aben JP, Weustink AC, Wielopolski PA, Krestin GP, de Feyter PJ, van Geuns RJ. Addition of the long-axis information to short-axis contours reduces interstudy variability of left-ventricular analysis in cardiac magnetic resonance studies. *Invest Radiol*. 2008;43:1-6
10. Sievers B, Kirchberg S, Bakan A, Franken U, Trappe HJ. Impact of papillary muscles in ventricular volume and ejection fraction assessment by cardiovascular magnetic resonance. *J Cardiovasc Magn Reson*. 2004;6:9-16
11. van Geuns RJ, Baks T, Gronenschild EH, Aben JP, Wielopolski PA, Cademartiri F, de Feyter PJ. Automatic quantitative left ventricular analysis of cine mr images by using three-dimensional information for contour detection. *Radiology*. 2006;240:215-221
12. Newman B, Derrington C, Dore C. Cardiac output and the recumbent position in late pregnancy. *Anaesthesia*. 1983;38:332-335
13. Atkins AJ, Watt JM, Milan P, Davies P, Crawford JS. The influence of posture upon cardiovascular dynamics throughout pregnancy. *Eur J Obstet Gynecol Reprod Biol*. 1981;12:357-372
14. Doering L, Dracup K. Comparisons of cardiac output in supine and lateral positions. *Nurs Res*. 1988;37:114-118

15. Lange RA, Katz J, McBride W, Moore DM, Jr., Hillis LD. Effects of supine and lateral positions on cardiac output and intracardiac pressures. *Am J Cardiol*. 1988;62:330-333

16. Ueland K, Novy MJ, Peterson EN, Metcalfe J. Maternal cardiovascular dynamics. Iv. The influence of gestational age on the maternal cardiovascular response to posture and exercise. *Am J Obstet Gynecol*. 1969;104:856-864

17. Robson SC, Hunter S, Boys RJ, Dunlop W. Serial study of factors influencing changes in cardiac output during human pregnancy. *Am J Physiol*. 1989;256:H1060-1065

18. Lees MM, Scott DB, Kerr MG, Taylor SH. The circulatory effects of recumbent postural change in late pregnancy. *Clin Sci*. 1967;32:453-465

19. Nakao S, Come PC, Miller MJ, Momomura S, Sahagian P, Ransil BJ, Grossman W. Effects of supine and lateral positions on cardiac output and intracardiac pressures: An experimental study. *Circulation*. 1986;73:579-585

20. Kuo CD, Chen GY, Yang MJ, Tsai YS. The effect of position on autonomic nervous activity in late pregnancy. *Anaesthesia*. 1997;52:1161-1165

21. Clements H, Stephenson T, Gabriel V, Harrison T, Millar M, Smyth A, Tong W, Linton CJ. Rationalised prescribing for community acquired pneumonia: A closed loop audit. *Arch Dis Child*. 2000;83:320-324

22. Kok RD, de Vries MM, Heerschap A, van den Berg PP. Absence of harmful effects of magnetic resonance exposure at 1.5 t in utero during the third trimester of pregnancy: A follow-up study. *Magn Reson Imaging*. 2004;22:851-854

23. Kanal E, Barkovich AJ, Bell C, Borgstede JP, Bradley WG, Jr., Froelich JW, Gilk T, Gimbel JR, Gosbee J, Kuhni-Kaminski E, Lester JW, Jr., Nyenhuis J, Parag Y, Schaefer DJ, Sebek-Scoumis EA, Weinreb J, Zaremba LA, Wilcox P, Lucey L, Sass N, Safety ACRBRPoM. Acr guidance document for safe mr practices: 2007. AJR Am J Roentgenol. 2007;188:1447-1474

CHAPTER 13

HEMODYNAMIC ADAPTATION TO PREGNANCY IN PATIENTS WITH STRUCTURAL HEART DISEASE: A PROSPECTIVE MRI STUDY

Submitted for publication

A Rossi
J Cornette
TP Ruys
D Rizopoulos
Y Karamermer
E Steegers
M Ouhlous
GP Krestin
R-J van Geuns
JW Roos-Hesselink

ABSTRACT

Purpose: During pregnancy the cardiovascular system of healthy women is capable to accommodate the increased hemodynamic demands. This adaptation process may be compromised in women with heart disease. The aim of this pilot study was to use cardiac magnetic resonance (CMR) to study the effects of pregnancy on cardiac hemodynamic parameters in women with structural heart disease.

Material and methods: Women with structural heart disease (acquired or congenital) were included in our study if they came for preconception counseling or when they presented at the outpatient clinic before 20 weeks gestation and agreed to participate. CMR acquisitions were performed at four time points: before pregnancy if possible, at 20 weeks and 32 weeks of gestation and six months postpartum. Left (L) and right (R) end-diastolic volume (EDV), end-systolic volume (ESV), and ejection fraction (EF) were calculated.

Results: Before pregnancy 17 women with heart disease agreed to participate in the study and underwent baseline MRI. Of these patients 6 did not become pregnant and were excluded from further analysis. In the first trimester another 13 patients were enrolled so the final study population consisted of 24 women. Heart rate significantly increased during pregnancy ($p<0.001$). After an initial rise LV ejection fraction progressively decreased from 20 to 32 weeks: $61\% \pm 2\%$ and $58\% \pm 2\%$, respectively ($p=0.01$). Both right EDV and ESV significantly decreased in the third trimester of pregnancy compared to the second trimester ($p<0.05$). The RV EF did not change. When comparing the measurements before and after pregnancy no significant changes were observed in any of the hemodynamic parameters ($p>0.05$).

Conclusions: In this prospective CMR study of women with pre-existing structural heart disease, ejection fraction showed a decrease between 20 and 32 weeks. Pregnancy did not have a negative impact on right and left ventricular function.

INTRODUCTION

During pregnancy the cardiovascular system of healthy women is capable to accommodate the increased hemodynamic demands. This adaptation process may be compromised in women with heart disease [1,2].

Nowadays, the number of women with heart disease who decide to become pregnant is increasing. Despite the advances in medical and surgical care of patients with heart disease, which have led to improved survival and outcome, cardiac disease remains the most common cause of mortality during pregnancy [3]. Patients with known cardiac disease should be evaluated before pregnancy and informed about the risks of pregnancy [2]. Only scarce longitudinal data are available on the cardiac adaptation to pregnancy in women with heart disease. Possible irreversible effects on maternal cardiac function have been described in some specific patient groups, but robust data are lacking. This information is essential for adequate counseling.

Cardiac magnetic resonance (CMR) has become the reference standard in the assessment of cardiac hemodynamic parameters and ventricular function and it can safely be performed after the first gestational trimester [4]. Until now, the few existing studies have all been performed with echocardiography [5]. The accuracy of various echocardiographic methods to reflect systolic function, especially in subjects with structural heart disease, can be questioned.

The aim of this pilot study was to use CMR to evaluate the effects of pregnancy on cardiac hemodynamic parameters in women with structural heart disease.

MATERIALS AND METHODS

STUDY POPULATION

This prospective observational study was conducted between 2007 and 2010 in a joint collaboration between the departments of Cardiology, Radiology and Obstetrics at Erasmus MC. During this period women with structural heart disease (acquired or congenital) were invited to participate. They were included if they came for preconception counseling or when they presented at the outpatient clinic before 20 weeks gestation and agreed to participate. CMR acquisitions were performed at four time points: before pregnancy if possible, at 20 weeks and 32 weeks of gestation and six months postpartum.

The study was approved by the Medical Ethical Committee and all women gave written informed consent. The population presented in this study is a part of a larger population previously described [6].

CMR PROTOCOL AND IMAGE ANALYSIS

CMR imaging was performed using a 1.5T scanner (Signa CV/I, GE Medical System, Milwaukee, WI). The woman was placed in the supine position and entered head first into the magnet. A dedicated cardiac 8 channels coil was placed on the thorax of the subject and used for the acquisition of the images. Cine CMR images were obtained using a breath-holding ECG triggered balanced steady state free precession. Imaging parameters were as follows: FOV 36-40 x 28-32 cm; matrix 224 x 196; TR: 3.4 milliseconds; TE: 1.5 milliseconds; flip angle 45 degrees; 12 views per segment. Slice thickness was 8 mm with a gap of 2 mm. These parameters resulted in a temporal resolution per image of 41 milliseconds. At first, three rapid surveys were obtained for the determination of the cardiac position and orientation; two- and four-chamber cine CMR images were then obtained. The series of short axis (SA) images were obtained from the reference images provided by the two- and four- chamber end-diastolic images at the end of expiration. Approximately 10 to 12 slices were acquired to cover the entire length of the heart.

All studies were analysed on a remote workstation using the CAAS- MRV (version 3.3; Pie Medical Imaging, Maastricht, The Netherlands).

Left end-diastolic volume (EDV) and end-systolic volume (ESV) were calculated using a combination of classic SA and long-axis images. The long-axis view was used to limit the extend of volumes at the base and at the apex of the heart. The Simpson rule was used to calculate volumes based on the SA images where the first basal and the last apical were only partially included relating to the area outlined on two- and four- chamber images. More details about this approach have been previously reported [7]. The papillary muscles were considered as being part of the blood pool shortening the analysis time without compromising the accuracy of LV volumes compared to standard short-axis technique. Ejection fraction (EF) was calculated as (EDV – ESV)/EDV.

In patients with transposition of great arteries the systemic right ventricle, defined as the ventricle supporting the systemic circulation, was used for the calculation of LV parameters. In addition right EF, EDV, and ESV, were calculated using cine images acquired in short axis view, parallel to the tricuspid valve annulus and applying the same methods of the left ventricular hemodynamic measurements without long-axis corrections.

STATISTICAL ANALYSIS

Continuous variables are presented as mean and standard deviation (SD); categorical data were presented as frequencies and percentages. To account for the correlation in the measurements taken from the same patient we performed a repeated measurements analysis for each parameter using linear mixed effects models [8]. Time was treated as a factor variable with

four levels, namely *pre-pregnancy, trimester 1, trimester 2, and post-pregnancy*. The models' assumptions were validated using residuals plots. This type of analysis was chosen over ANOVA for repeated measurements to account for missing data in the datasets. Statistical analysis was performed in R version 2.15.0 (2012-03-30) using package nlme (version 3.1-103) and IBM SPSS Statistic (version 20). The significance level was set to 0.05. No multiple testing corrections have been applied, and therefore the following results should be used as indicative results and not to form strong conclusions.

RESULTS

STUDY POPULATION

Before pregnancy 17 women with heart disease agreed to participate in the study and underwent baseline MRI. Of these patients 6 did not become pregnant and were excluded from further analysis. In the first trimester another 13 patients were enrolled so the final study population consisted of 24 women. Baseline characteristics are described in Table 1. The mean age at the moment of delivery was 31 ±5 years. All women were in New York Heart Association (NYHA) functional class I before pregnancy.

Table 1. Baseline characteristics.

PATIENT	AGE*	G/P	DIAGNOSIS	SURGERY
1	25	2/0	Tetralogy of Fallot.	+
2	33	1/0	Marfan Syndrome.	no
3	30	2/0	Tetralogy of Fallot with pulmonary artery atresia.	+
4	23	2/0	Multiple VSD. Mitral valve defect.	+
5	37	1/0	Aortic stenosis	+
6	25	1/0	Small VSD; ASD type 2.	no
7	36	3/1	Mitral valve stenosis.	+
8	30	2/1	Tetralogy of Fallot. Pulmonary valve stenosis.	+
9	34	2/1	Cardiomyopathy adriamicyn induced .	no
10	30	1/0	Aortic coartation; patent ductus arteriosus; VSD; supra-valve pulmonary stenosis.	+
11	31	1/0	BAV. Aortic coartation.	+
12	41	3/2	Mitral valve defect.	no

13	39	7/3	Aortic coartation.	+
14	31	2/1	Aortic coartation.	+
15	26	1/0	Transposition of the great arteries (Mustard).	+
16	32	3/2	Aortic coartation. BAV. Dilated ascending aorta.	+
17	30	2/0	Tetralogy of Fallot.	+
18	27	2/1	Stenotic pulmonary valve.	+
19	33	2/1	Aortic arch hypoplasia. Patent ductus arteriosus	+
20	27	1/0	VSD. Tricuspid valve regurgitation.	no
21	37	2/0	ASD type 2.	+
22	28	2/1	Ebstein's anomaly.	+
23	27	1/0	Aortic coartation.	+
24	30	1/0	BAV.	+

* Maternal Age P = Parity
ASD = atrial septal defect; VSD = ventricular septal defect; BAV = bicuspid aortic valve.

CLINICAL OUTCOMES

Pregnancy duration was a mean of 40±2 weeks. All pregnancies were singletons. There were 20/24 (83%) vaginal deliveries and 4/24 (17%) deliveries by cesarean section. Of the 20 vaginal deliveries, 3 (15%) were complicated by postpartum hemorrhage and none in the cesarean section group. There were no intrauterine or neonatal deaths. The mean birth weight was 3300±559 grams.

EVOLUTION OF CARDIAC HEMODYNAMIC PARAMETERS DURING PREGNANCY

Evolution of hemodynamic parameters of the study population before, during and after pregnancy are reported in Table 2 and Figure 1. Systolic and diastolic blood pressures showed a trend, although not statistically significant, to decrease in the second trimester followed by a slight increase in the third trimester. Heart rate significantly increased during pregnancy. After an initial rise LV ejection fraction progressively decreased from 20 to 32 weeks. When comparing the measurements before and after pregnancy no significant changes were observed in any of the hemodynamic parameters ($p>0.05$) (Table

Table 2. Hemodynamic data.

VARIABLE	PRE-PREGNANCY	TRIMESTER 2	TRIMESTER 3	POST-PREGNANCY	P-VALUE*	P-VALUE* (TRIMESTER 2 VS TRIMESTER 3)	P-VALUE* (PRE- VS POST-PREGNANCY)
No. participants	11	24	24	17			
SBP, mmHg	120	118	118	119	0.6323	NA	NA
DBD, mmHg	73	68	70	70	0.5118	NA	NA
Heart rate, bpm	69	79	84	72	<0.001	0.160	0.979
LEFT VENTRICLE							
EF (%)	55 (2)	61 (2)	58 (2)	56 (2)	<0.001	0.011	0.862
EDV (ml)	160 (8)	187 (7)	182 (7)	162 (7)	<0.001	0.725	0.995
ESV (ml)	72 (5)	74 (4)	78 (4)	72 (5)	0.150	NA	NA
Mass (g)	75 (3)	77 (2)	80 (2)	75 (2)	0.067	NA	NA
RIGHT VENTRICLE							
EF (%)	51 (3)	55 (2)	55 (2)	52 (2)	0.261	NA	NA
EDV (ml)	160 (9)	197 (8)	168 (8)	159 (9)	<0.001	<0.001	0.999
ESV (ml)	79 (7)	92 (6)	80 (6)	77 (7)	0.001	0.019	0.995

* P-values from linear-mixed-effects model.Data are presented as mean±SD. SBD indicates systolic blood pressure; DBP diastolic blood pressure; EF ejection fraction; EDV end diastolic volume; ESV end systolic volume; SV stroke volume; CO cardiac output; NA non-assessable.

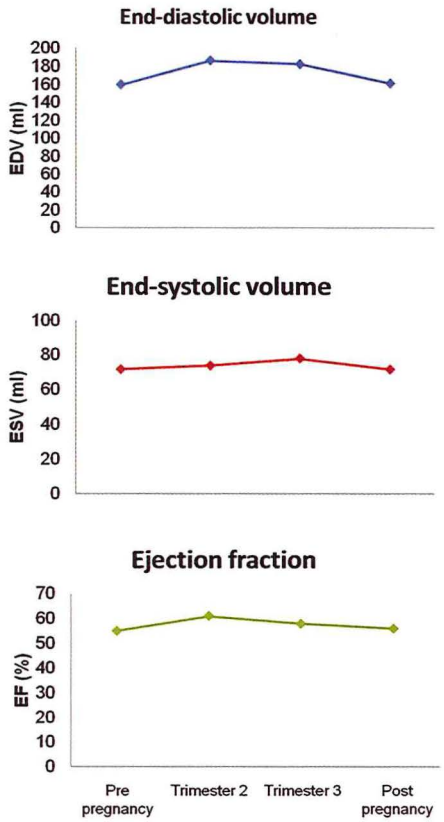

Figure 1. Left ventricular end-diastolic volume (EDV), end-systolic volume (ESV) and ejection fraction (EF) evolution during pregnancy.

2). Outcomes of the right ventricle are reported in Table 2. Both right EDV and ESV significantly decreased in the third trimester of pregnancy compared to the second trimester. The RV EF did not change. In the Mustard patient with a systemic right ventricle no differences were found between pre- and post-pregnancy.

DISCUSSION

In this prospective pilot-study we investigated the hemodynamic adaptation to pregnancy in women with structural heart disease. CMR was performed before pregnancy, at 20 and 32 gestational weeks and 6 months postpartum. After an initial rise LV ejection fraction progressively decreased from 20 to 32 weeks. Our data suggest that pregnancy in women with pre-existing structural heart disease is not associated with an irreversible impairment of ventricular systolic function.

EVOLUTION OF CARDIAC HEMODYNAMIC PARAMETERS

In the past echocardiography was used to assess changes in cardiac hemodynamics in healthy pregnant women. These studies showed that pregnancy induces marked physiological changes in cardiac parameters, with a 30-50% increase in cardiac output, through an increase both in stroke volume and heart rate. This is caused by a decrease in total vascular resistance, mainly due to peripheral arterial vasodilatation, mediated by progesterone and vasodilators such as nitric oxide in combination with low-resistance flow in the uteroplacental bed. In normal pregnancy heart rate and cardiac output gradually increase in the first two trimesters of pregnancy. In the third trimester heart rate further increases, while cardiac output only slightly increases towards the end of pregnancy. In addition, ventricular volumes and ventricular wall thickness increase during normal pregnancy. Cardiovascular hemodynamic state returns back to the pre-pregnancy state within 6 months postpartum [9 10].

In women with heart disease hemodynamic changes in pregnancy can exceed the compensatory possibilities of their compromised circulation and induce adverse maternal and fetal outcomes. In our study LV ejection fraction increased in the second trimester but decreased from 20 to 32 weeks of pregnancy. This is an unexpected finding and it may be caused by limited adaptation of the ventricular function in patients with structural heart disease. Negative consequences of the fall in LV ejection fraction and consequently increased heart rate might be a negative effect on uteroplacental perfusion which might became inadequate. Abnormal uteroplacental perfusion is shown to be associated with offspring outcome and may be influence by cardiovascular status. Babies from mothers with heart disease typically have a lower birth weight and are more often born prematurely [11].

EFFECTS OF PREGNANCY IN PATIENTS WITH HEART DISEASE

Similarly to a previous echocardiography study [12], in our population ejection fraction and cardiac dimensions of the left and right ventricle showed no changes 6 months after pregnancy compared with pre-pregnancy values. These findings suggest that pregnancy did not have an irreversible effect on ventricular dimensions or function in women with structural heart disease. Our data are in contrast with previous echocardiography reports [6, 13, 14]. Cornette et al. [6] demonstrated a permanent reduction in LV systolic function. In that study the ejection fraction was measured using the Teicholz method. That is not the optimal method and probably CMR provides more reliable data. However, larger numbers are clearly warranted to answer the question if pregnancy causes an irreversible impact on the heart. Guèdes et al [13] reported an irreversible negative effect on systemic ventricular function in 3 of 28 pregnancies amongst 16 women (with a previous atrial switch procedure for transposition of the great arteries). In this study the follow-up time was longer after pregnancy compared to our folow-up; therefore it might have been a coincidental finding and part of the natural history of the disease. Kamiya et al. [14] demonstrated that left ventricular size and function did not change due to pregnancy in 25 women with repaired tetrology of Fallot, but the right ventricular dimensions remained increased at 6 months after delivery. The use of different imaging modalities may explain some of the differences that we found in our population. In our study CMR is the reference standard for assessing left ventricular dimensions and function; in addition, CMR allows a more reliable and precise estimation of right ventricular function in patients with congenital heart disease [2].

Finally, in our population LV mass showed a trend, although not statistically significant, to increase during pregnancy. LV mass values were in the normal range but substantially lower if compared with the values presented in the echocardiographic study by Cornette et al. [6]. Possible explanations are that echocardiography is less accurate and reproducible than CMR for LV mass calculation and it is affected by the LV geometry [15].

LIMITATIONS

Our study was designed as a pilot study and therefore the number of patients is limited. The distribution of structural heart disease is quite heterogeneous in our population and the limited number of patients did not allow for pathology specific pattern analysis. A matched control group for direct comparison is missing as we have chosen not to perform CMR in healthy pregnant women. However, this would have been very interesting and might be considered in the future.

CONCLUSIONS

In this prospective CMR study of women with pre-existing structural heart disease, ejection fraction showed a decrease between 20 and 32 weeks. Pregnancy did not have a negative impact on right and left ventricular function. Larger prospective multicenter studies are warranted to further investigate the impact of pregnancy on cardiac function in specific patient groups.

REFERENCES

1. Robson SC, Hunter S, Boys RJ, Dunlop W. Serial study of factors influencing changes in cardiac output during human pregnancy. Am J Physiol. 1989;256:H1060-1065
2. Baumgartner H, Bonhoeffer P, De Groot NM, de Haan F, Deanfield JE, Galie N, Gatzoulis MA, Gohlke-Baerwolf C, Kaemmerer H, Kilner P, Meijboom F, Mulder BJ, Oechslin E, Oliver JM, Serraf A, Szatmari A, Thaulow E, Vouhe PR, Walma E. Esc guidelines for the management of grown-up congenital heart disease (new version 2010). Eur Heart J. 2010;31:2915-2957
3. Saving mothers' lives: Reviewing maternal deaths to make motherhood safer: 2006–2008. BJOG: An International Journal of Obstetrics & Gynaecology. 2011;118:1-203
4. Chen MM, Coakley FV, Kaimal A, Laros RK, Jr. Guidelines for computed tomography and magnetic resonance imaging use during pregnancy and lactation. Obstet Gynecol. 2008;112:333-340
5. Lesniak-Sobelga A, Tracz W, KostKiewicz M, Podolec P, Pasowicz M. Clinical and echocardiographic assessment of pregnant women with valvular heart diseases--maternal and fetal outcome. Int J Cardiol. 2004;94:15-23
6. Cornette J, Ruys TP, Rossi A, Rizopoulos D, Takkenberg JJ, Karamermer Y, Opic P, Van den Bosch AE, Geleijnse ML, Duvekot JJ, Steegers EA, Roos-Hesselink JW. Hemodynamic adaptation to pregnancy in women with structural heart disease. Int J Cardiol. 2012
7. Kirschbaum SW, Baks T, Gronenschild EH, Aben JP, Weustink AC, Wielopolski PA, Krestin GP, de Feyter PJ, van Geuns RJ. Addition of the long-axis information to short-axis contours reduces interstudy variability of left-ventricular analysis in cardiac magnetic resonance studies. Invest Radiol. 2008;43:1-6
8. G. Verbeke GM. Linear mixed models for longitudinal data. Springer, New York; 2000.
9. Duvekot JJ, Peeters LL. Maternal cardiovascular hemodynamic adaptation to pregnancy. Obstet Gynecol Surv. 1994;49:S1-14
10. van Oppen AC, Stigter RH, Bruinse HW. Cardiac output in normal pregnancy: A critical review. Obstet Gynecol. 1996;87:310-318
11. Roos-Hesselink JW, Ruys TP, Stein JI, Thilen U, Webb GD, Niwa K, Kaemmerer H, Baumgartner H, Budts W, Maggioni AP, Tavazzi L, Taha N, Johnson MR, Hall R. Outcome of pregnancy in patients with structural or ischaemic heart disease: Results of a registry of the european society of cardiology. Eur Heart J. 2012
12. Uebing A, Arvanitis P, Li W, Diller GP, Babu-Narayan SV, Okonko D, Koltsida E, Papadopoulos M, Johnson MR, Lupton MG, Yentis SM, Steer PJ, Gatzoulis MA. Effect of pregnancy on clinical status and ventricular function in women with heart disease. Int J Cardiol. 2010;139:50-59
13. Guedes A, Mercier LA, Leduc L, Berube L, Marcotte F, Dore A. Impact of pregnancy on the systemic right ventricle after a mustard operation for transposition of the great arteries. J Am Coll Cardiol. 2004;44:433-437
14. Kamiya CA, Iwamiya T, Neki R, Katsuragi S, Kawasaki K, Miyoshi T, Sasaki Y, Osato K, Murohara T, Ikeda T. Outcome of pregnancy and effects on the right heart in women with repaired tetralogy of fallot. Circ J. 2012;76:957-963

15. Perdrix L, Mansencal N, Cocheteux B, Chatellier G, Bissery A, Diebold B, Mousseaux E, Abergel E. How to calculate left ventricular mass in routine practice? An echocardiographic versus cardiac magnetic resonance study. Arch Cardiovasc Dis. 2011;104:343-351

SUMMARY AND CONCLUSIONS

CHAPTER 14

SUMMARY

ISCHEMIC HEART DISEASE

CHAPTER 2

CT coronary angiography (CTCA) has matured in recent years, as a robust non-invasive imaging technique. The high negative predictive value of CTCA effectively identifies patients without significant coronary artery disease (CAD). This supports the alternative use of CTCA as an effective gatekeeper for invasive coronary angiography (ICA) to functional tests. The high sensitivity indicates that CTCA enables to detect the majority of patients with significant CAD, but at the cost of a high false positive rate due to overestimation of the severity of stenoses. CTCA is an anatomic imaging modality that cannot reliably predict functionally significant coronary stenoses. Current guidelines indicate that revascularization should only be applied to coronary stenoses that are functionally significant. Further non-invasive functional testing is recommended in CT- anatomic non-high risk patients, which in case of ischemia may be referred for revascularization. CT- anatomic high-risk patients may be directly referred to ICA with fractional flow reserve (FFR) to guide functional lesion revascularization. Preliminary studies have shown that the combination of CT-anatomy and CT-function in one examination is feasible but future comparative effectiveness studies are warranted to assess the clinical value of such combined anatomic-physiologic approach.

CHAPTER 3

CTCA has been challenged during past years because of (unacceptable) high increased lifetime attributable risk estimates of developing cancer associated with high radiation exposure. Dual Source CT (DSCT) systems provide two different low dose CTCA protocols: a prospective high-pitch spiral protocol which allows CT data acquisition of the entire heart within 1 heart beat and a prospective sequential protocol for patients with low and high heart rates. We have evaluated these new methods in 459 symptomatic patients referred for CTCA. ICA was the reference standard of the study. Patients with a heart rate below 65 bpm (Group A) were randomized between high-pitch spiral versus narrow-window sequential CTCA protocols while patients with a heart rate above 65 bpm (Group B) were randomized between wide-window sequential versus retrospective spiral protocols.

In Group A high-pitch spiral CTCA yielded a lower per segment sensitivity compared to sequential CTCA. Specificity, PPV and NPV were comparable but radiation dose was lower. In group B diagnostic performance of the two protocols was comparable. Radiation dose of sequential CTCA was lower compared to retrospective CTCA. Our results suggest that a sequential CTCA protocols should be the first choice in patients undergoing CTCA, combining high diagnostic performance with few non-assessable segments and relatively low radiation exposure.

CHAPTER 4

Coronary lesions with a diameter narrowing ≥ 50% on visual CTCA are generally considered for referral to ICA. However, visual CTCA is often inaccurate in detecting functionally significant coronary lesions. We compared the diagnostic performance of quantitative CTCA in terms of minimal lumen area (MLA), percentage area stenosis (AS), and plaque burden, with visual CTCA for the detection of functionally significant coronary lesions based on FFR in ninety-nine patients with stable chest pain. Specificity of visual CTCA was lower than that of MLA, %AS and plaque burden: 42%, 68%, 76% and 63% respectively. Our results suggest that quantitative CTCA improves the prediction of functionally significant coronary lesions compared to visual CTCA but it remains insufficient. Functional assessment is still needed, especially in coronary lesions of moderate stenosis, to guide patient management.

CHAPTER 5

The safety and feasibility of stress myocardial CT perfusion imaging has been recently demonstrated. The addition of myocardial CT perfusion imaging to the standard anatomical CTCA examinations provides complementary functional information in a single examination which may be helpful to improve patient management and outcome. An overview of (1) the physiology of coronary circulation and myocardial perfusion, (2) the technical pre-requisites, challenges, and mathematical modeling related to CT perfusion imaging, (3) the recent advances in CT scanners and CT perfusion protocols, (4) the interpretation of CT perfusion images, (5) the current literature, and (6) future directions for research are discussed.

CHAPTER 6

We quantified regional CT-derived myocardial blood flow (MBF) by dynamic stress CT perfusion imaging at different degrees of coronary flow reduction in a well-established large animal model. Coronary artery blood flow (CBF) and FFR were the experimental reference standard and the clinical reference standard, respectively. The major finding of the study was that dynamic stress CT perfusion imaging provided regional quantification of MBF of ischemic and remote myocardium, which correlated very well with CBF and FFR. Our animal study suggests that adenosine stress CT perfusion imaging may provide useful information for patient management.

CHAPTER 7

We evaluated the performance of quantitative hyperemic MBF derived from dynamic stress CT perfusion imaging to detect of functionally significant coronary lesions in eighty patients with stable chest pain. The optimal cut-off value of MBF to detect functionally significant coronary lesions was 78 ml/100ml/min. On a vessel-territory level, MBF had a significantly (p-values <0.001) higher overall diagnostic performance (area under curve: 0.95) compared to visual CTCA (area under curve: 0.85) and quantitative CT (QCT) (area under curve: 0.89). In the analysis restricted to intermediate lesions (30-70% lumen narrowing on visual CTCA), the specificity of visual CTCA (69%) and QCT (77%) was improved by the subsequent use of MBF (89%). In conclusion, the CT evaluation of coronary artery anatomy and hyperemic MBF performs well as an integrated diagnostic tool to detect functionally significant lesions in patients with stable angina, in particular in patients with intermediate coronary lesions.

CHAPTER 8

Dynamic stress CT perfusion imaging provides new possibilities for non-invasively investigating cardiac microvascular disease by combining epicardial coronary anatomy and MBF.

AORTIC VALVE STENOSIS

CHAPTER 9

There is still controversy concerning whether the pathogenesis of the dilatation of ascending aorta in BAV patients is caused by a genetic predisposition or by the aortic valve stenosis causing a post-stenotic dilatation due to blood flow turbulence. In our prospective study we evaluated the natural progression of aortic dilatation in twenty-eight asymptomatic patients with BAV and aortic valve stenosis. Aortic root, tubular ascending aorta, aortic peak velocity, left ventricular systolic and diastolic function and mass were quantified by cardiac magnetic resonance (CMR) at baseline and at three-years follow-up. This study showed that there was a progressive increase of aortic diameters over time, which is maximal at the level of the tubular portion of the ascending aorta. A week but significant correlation was found between the progression of aortic dilatation and the severity of aortic valve stenosis partially supporting the haemodynamic theory for the etiology of aortopathy associated with BAV.

CHAPTER 10

The underlying cause for congenital aortic stenosis is usually a bicuspid aortic valve (BAV), which is strongly associated with aortic dilatation. In BAV patients diameters of the aortic root and tubular ascending aorta should be monitored periodically because of the increased risk of developing concurrent ascending aortic aneurysms that may require surgical repair. Elective aortic surgery is advised when the aortic diameter reaches 50 mm to avoid acute dissection or rupture. Our study confirms recent ESC guidelines stating that CMR is manly required to assess aortic dilatation when it occurs distal to the sino-tubular junction. We measured aortic diameters at four levels by CMR and transthoracic echocardiography (TTE) in fifty-nine patients with congenital aortic stenosis and a BAV. We found a good agreement between both imaging modalities but TTE slightly underestimated aortic diameters. In patients with aortic aneurysm >40 mm the agreement between CMR and TTE was lower than in patients with normal aortic diameters, especially at the level of the tubular ascending aorta. Intra- and inter-observer variability was smaller with CMR. As BAV-associated aortic dilatation occurs mainly at the level of the ascending aorta, our results suggest that CMR should be performed at least once to ensure that an aortic aneurysm at this level is not missed. CMR might be the preferred method for aortic aneurysm follow-up.

CHAPTER 11

Heavy calcification of the aortic root may result in malposition and paraprosthetic aortic valve regurgitation (PAR) in patients with severe aortic stenosis undergoing transcatheter aortic valve implantation (TAVI). This often results in the need for balloon post-dilatation (PDP) after TAVI, which carries the risks of potential damage to the new valve leaflets and of vascular sequelae due to the additional instrumentation. Our results suggest that the quantification of mass and volume of dense calcium of the aortic leaflets on contrast cardiac CT is feasible. On contrast cardiac CT, an aortic leaflet calcium mass >800, a calcium volume >1200, larger annulus dimensions and nominal prosthesis inflow to annulus ratio were associated with PDP during TAVI. Aortic root or aortic leaflet calcium on respectively non-contrast and contrast-enhanced cardiac CT showed excellent discrimination for the requirement of PDP, whereas the discriminatory value of aortic annulus dimensions was moderate. Non-contrast cardiac CT may no longer be needed to quantify aortic root calcium before TAVI.

PREGNANCY AND HEART DISEASE

CHAPTER 12

There are physiological reasons for the effect of positioning for MR examinations during pregnancy on hemodynamic variables and cardiac dimensions. These are related to altered intra-abdominal and intra-thoracic pressures. Cardiac hemodynamic parameters and dimensions were assessed using CMR in 5 healthy non-pregnant women, 6 pregnant women at 20th week of gestation and 8 women at 32nd week of gestation without history of cardiac disease in both supine and left lateral decubitus. In the non-pregnant state, turning from supine to left lateral decubitus position has minimal effect on cardiac parameters. During pregnancy, from as early as 20 weeks, turning to the left lateral decubitus has positive effects on cardiac hemodynamics inducing a significant increase of venous return, stroke volume and cardiac output. These results suggest that pregnant women requiring CMR should be studied in a consistent position for serial studies and the left lateral decubitus position should be preferred from early pregnancy onwards.

CHAPTER 13

During pregnancy the cardiovascular system of healthy women is capable to accommodate the increased hemodynamic demands. This adaptation process may be compromised in women with heart disease. In our longitudinal, prospective study we investigated the hemodynamic adaptation to pregnancy in twenty-four women with structural heart disease. CMR was performed before pregnancy, at 20 and 32 gestational weeks and 6 months postpartum. After an initial rise the left ventricular ejection fraction progressively decreased from 20 to 32 weeks. Ejection fraction of the left and right ventricle showed no changes 6 months after pregnancy compared to pre-pregnancy levels. Our study suggests that pregnancy in women with pre-existing structural heart disease is not associated with an irreversible impairment of ventricular systolic function.

SAMENVATTING

ISCHEMISCHE HARTZIEKTE

HOOFDSTUK 2

In recente jaren is CT coronaire angiografie (CTCA) uitgerijpt tot een robuste niet-invasieve beeldvormingstechniek. Patiënten zonder significante vernauwingen in de kransslagaderen (*coronary artery disease*; CAD) worden goed identificeert door de hoge negatief voorspellende waarde van CT. Hiermee wordt het gebruik van CT als effectief alternatief voor invasieve coronaire angiografie (ICA) ondersteunt. De hoge sensitiviteit geeft aan dat de meeste patiënten met significante afwijkingen in de kranslagaderen door CTCA worden opgespoord, echter er zijn veel vals positieve bevindingen waarbij de ernst van de vernauwing wordt overgeschat met deze methode. CTCA is een anatomische beeldvormende modaliteit en het kan niet betrouwbar bepalen of een vernauwing leidt tot een significante functionele invloed. De huidige richtlijnen geven aan dat alleen de significante coronaire vernauwingen die leiden tot zuurstoftekort, moeten worden behandeld met revascularisatie. In patiënten waarbij de bevindingen met anatomische CT niet als hoog-risico wordt aangemerkt, wordt het aangeraden om verder non-invasieve functionele onderzoeken te verrichten, waarbij een verwijzing voor revascularisatie in het geval van ischemie een mogelijkheid is. Patiënten die vanwege de anatomische CT wel als hoog-risico wordt aangemerkt kunnen direct gestuurd worden voor ICA met meting van de bloedstroom (*fractional flow reserve*; FFR), Hiermee kan de indicatie voor revascularisatie beter worden gesteld. De eerste resultaten tonen aan dat het haalbaar lijkt om zowel de anatomisch als de functionele CT in een onderzoek te doen, toch is het zinnig om eerst de klinische waarde van zo'n gecombineerde anatomisch-fysiologisch aanpak te bestuderen met vergelijkingsstudies naar effectiviteit.

HOOFDSTUK 3

Doordat hoge-dosis straling, over het hele leven gezien, een (onacceptabel) verhoogde kans geeft op het ontwikkelen van een tumor, is CTCA de laatste jaren onder vuur komen te staan. Duaal-bron CT (*dual source CT*; DSCT) systemen hebben twee verschillende CTCA protocollen met lage-dosis straling: een prospectief hoge-pitch spiraal protocol geeft CT dataverzameling van het hele hart binnen 1 hartslag en een prospectiefvolgend protocol kan gebruikt worden met zowel lage als hoge hartslag. Wij hebben deze nieuwe protocollen getoetst in 459 symptomatische patiënten diet voor CTCA waren verwezen. ICA werd als controle gebruikt. Patiënten met een hartslag onder 65 slagen per minuut (Groep A) waren random verdeeld tussen een hoge-pitch spiraal protocol en een nauw-venster opeenvolgend protocol, en patiënten met een hartslag boven 65 slagen per minuut (Groep B) waren random verdeeld tussen een breed-venster opeenvolgend protocol en een retrospectief spiraal protocol.

In Groep A, hoge-pitch spiraal, CTCA was minder gevoelig per segment dan opeenvolgend CTCA. Specificiteit, positief voorspellende waarde en negatief voorspellende waarde waren vergelijkbaar, maar de hoeveelheid straling was lager. In Groep B, deden de beide protocollen het even goed wat betreft diagnostische uitkomst. Opeenvolgend CTCA gaf minder straling dan retrospectieve CTCA. Onze resultaten geven aan dat opeenvolgende protocollen als eerste keus moeten dienen bij CTCA, omdat deze protocollen een goede diagnostische werking combineren met weinig segmenten die niet beoordeeld kunnen worden en een relatief lage stralen belasting.

HOOFDSTUK 4

Als vernauwingen van de kransslagaderen op CTCA met het oog geschat worden meer dan 50% te zijn, wordt de patient meestal doorverwezen voor ICA. Toch zijn visuele schattingen op CTCA vaak niet accuraat als het gaat om de detectie van significante laesies. In 99 patiënten met stabiele pijn op de borst hebben we de diagnostische werking van kwantitatief CTCA met visuele CTCA vergeleken wat betreft het detecteren van significante vernauwingen in de kransslagaderen, zoals aangegeven met FFR. Hiervoor werd de minimale lumen doorsnede (*minimal lumen area*, MLA), als percentage doorsnee vernauwing (*area stenosis*, AS), en plaque belasting gemeten. Gevoeligheid van visueel CTCA was lager dan gevoeligheid van MLA, %AS, en plaque belasting: respectievelijk 42%, 68%, 76% en 63%. Uit ons resultaten mag men concluderen dat kwantitatief CTCA beter is dan visueel CTCA in het voorspellen van laesies van functioneel belang, maar toch is kwantitatief CTCA onvoldoende. Functionele toetsen zijn nog steeds nodig voor het bepalen van de optimale behandeling, vooral in laesies met een matige vernauwing.

HOOFDSTUK 5

Recent is de veiligheid en bruikbaarheid van myocardiale CT perfusie beeldvorming gedemonstreerd. Het toevoegen van myocardiale CT perfusie protocollen aan de standaard anatomische CTCA onderzoeken geeft complementaire functionele informatie in een enkel onderzoek, die van mogelijk toegevoegde waarde kan zijn bij het management van de behandeling. In dit hoofdstuk wordt een overzicht van en discussie over (1) de fysiologie van coronaire bloedstroming en myocardiale perfusie, (2) technische voorwaarden, uitdagingen, en mathematische modellen gerelateerd aan CT perfusie beeldvorming, (3) de recente vooruitgang in CT scanners en in CT perfusie protocollen, (4) de interpretatie van CT perfusie beelden, (5) de huidige literatuur, en (6) toekomstige onderzoeksrichtingen gegeven.

HOOFDSTUK 6

In een bekend model voor grote dieren hebben we dynamisch stress CT perfusie beeldvorming gebruikt om regionale CT-afgeleide myocardiale bloeddoorstroming (*myocardial blood flow*, MBF) te meten bij verschillende graden van coronaire stroombeperking. De bloedstroom door de kransslagaderen (*coronary artery blood flow*, CBF) was de controle binnen dit onderzoek en FFR was de klinische standaard. De hoofdbevinding was dat dynamisch stress CT perfusie beeldvorming regionale kwantificatie geeft van MBF in zowel ischemisch alsook remote myocardium, welk ook goed correleert met CBF en FFR. Deze dierstudie geeft aanleiding te denken dat adenosine stress CT perfusie beeldvorming bruikbare informatie voor de patiëntenzorg kan geven.

HOOFDSTUK 7

In 80 patiënten met stabiele pijn op de borst hebben we geëvalueerd hoe goed kwantitatieve hyperemische MBF gemeten op dynamische stress CT perfusie beelden kransslagader laesies van functioneel belang kan vaststellen. De optimale MBF-grenswaarde voor de detectie van laesies van functioneel belang was 78 ml/ 100 ml/ min. Op het niveau van het vaatgebied, had MBF (AUC: 0.95) een significant beter diagnostische werking dan visueel CTCA (AUC: 0.85) en kwantitatief CTCA (AUC: 0.89) ($p<0.001$). In een analyse van middelgrote laesies (30-70% lumenvernauwing op visueel CTCA) kon de specificiteit van visueel CTCA (69%) en kwantitatief CTCA (77%) met behulp van daarop volgende MBF (89%) verbeterd worden. Concluderend, doen CT evaluatie van kransslagader anatomie en hyperemie het goed als geïntegreerd diagnostisch gereedschap voor de opsporing van laesies van functioneel belang in patiënten met stabiele angina, vooral in patiënten met middelgrote laesies.

HOOFDSTUK 8

Dynamisch stress CT perfusie beeldvorming geeft nieuwe mogelijkheden voor het niet-invasief onderzoeken van cardiale microvaatziekte door de combinatie van epicardiale coronaire anatomie en MBF.

VERNAUWING VAN DE AORTAKLEP

HOOFDSTUK 9

Of de pathogenese van dilatatie van de aorta in patienten met een tweeslippige aortaklep (bicuspide aortaklep, BAV) wordt veroorzaakt door een genetische aanleg of door turbulentie in de bloedstroom direct na een aortaklepvernauwing, is een punt waarover de meningen verschillen. We hebben het natuurlijk verloop van aortadilatatie gevolgd in een prospectieve studie onder 28 asymptomatische BAV patiënten met stenose van de klep. Cardiale Magnetisch Resonantie (CMR) vond plaats bij de start van de studie en 3 jaar later, waarbij de afmetingen van de aortawortel en eerste deel van de aorta, maar ook de aorta pieksnelheid, systolische en diastolische afmetingen van de linkerkamer, en de linker kamer massa werden gemeten. Deze studie laat zien dat de aorta dilatatie gestaag toeneemt over tijd, en de dilatatie is het meest uitgesproken op het niveau van de zogenaamde sinus van valsalva en verderop in de aorta ascendens. Een zwakke doch significante correlatie tussen het verloop van de aortadilatatie en de graad van vernauwing van de aortaklep werd gevonden, wat deels de hemodynamische theorie over BAV aortopathie etiologie ondersteunt.

HOOFDSTUK 10

De onderliggende oorzaak van aangeboren aortavernauwing is bijna altijd een BAV, wat ook een sterke correlatie met aortadilatatie heeft. Het is belangrijk om de breedte van de aortawortel en aorta ascendens in BAV patiënten regelmatig te controleren. Dit vanwege het verhoogde risico op een scheur in de aorta (dissectie) dat deze patiënten lopen. Electieve chirurgie bij een aortadilatatie van meer dan 55 mm wordt aangeraden om een acute dissectie of ruptuur te voorkomen. Ons studie bevestigt de recente ESC richtlijn waarin CMR wordt geadviseerd om aortadilatatie ook meer distaal in de aorta ascendens te beoordelen. In 59 patiënten met een aangeboren aortaklepvernauwing en BAV hebben we de aortadiameter op 4 verschillende niveaus gemeten. Dit met behulp van CMR en transthoracale echocardiografie (TTE). De modaliteiten waren in overeenstemming met elkaar, maar TTE onderschat de aortadimensie licht. De overeenstemming tussen CMR en TTE was minder in patiënten met een aortaverwijding >40 mm dan in patiënten met normale aortadimensies. Intra-en inter-observer variatie was minder met CMR. Gezien de BAV-geassocieerde aortadilatatie vooral plaatsvindt op het niveau van de stijgende aorta, geven onze resultaten aan dat CMR ten minste één keer gedaan moet worden om te zorgen dat een verwijding op dit niveau wordt niet overgeslagen. CMR lijkt de voorkeursmethode voor het volgen van aortaverwijding.

HOOFDSTUK 11

In patiënten met een ernstig vernauwde aortaklep die een aortaklep geimplanteerd krijgen via de lies (*transcatheter aortic valve implantation*, TAVI) , kan zware verkalking van de aortastam voorkomen wat impact heeft op de ligging en kan leiden tot lekkage langs de nieuwe klep (paravalvulaire aorta regurgitatie: PAR). Vaak betekent dit dat ballon post-dilatatie (PDP) na TAVI nodig is, wat een risico met zich meebrengt van schade aan de nieuwe klep of van vasculaire gevolgen van de additionele instrumenten. Ons resultaten geven aan dat het mogelijk is de massa en inhoud van hard kalk in de aorta klepbladente kwantificeren op cardiale CT. PDP tijdens TAVI was geassocieerd met aortaklepalkmassa >800, kalkinhoud >1200, grotere annulus afmetingen, op contrast cardiale CT. Met het meten van kalk in de aortastam of aorta klepop respectievelijk niet-contrast en contrast cardiale CT konden we erg goed bepalen of PDP nodig was, terwijl aorta annulus afmetingen minder goed aangaf of PDP nodig was. Mogelijk is non-contrast cardiale CT niet meer nodig om de kalk in de aortastam voorafgaande aan TAVI te bepalen.

ZWANGERSCHAP EN HARTZIEKTE

HOOFDSTUK 12

Er zijn fysiologische redenen waarom hemodynamische parameters en cardiale afmetingen varieren afhankelijk van de positie van de proefpersoon bij MRI tijdens de zwangerschap. Deze zijn gerelateerd aan veranderde intra-abdominale en intra-thoracale drukken. Cardiale hemodynamische parameters en afmetingen werden bepaald met CMR in vrouwen zonder bekende hartziekte: 5 gezonde, niet-zwangere vrouwen, 6 vrouwen in de 20e week van de zwangerschap, en 8 vrouwen in de 32e week van de zwangerschap. Metingen werden verricht zowel als de vrouw op de rug lag alsook als ze op de linkerzij lag. Bij de niet-zwangere vrouwen was er weinig effect van ligging op cardiale parameters. Tijdens de zwangerschap, zelfs al bij 20 weken, had de linkerzijligging een gunstige effect op de cardiale hemodynamische parameters, waaronder een significante toename in veneuze retour, slagvolume en hartminuutvolume. Deze resultaten geven aan dat zwangere vrouwen die een CMR nodig hebben tijdens de zwangerschap consistent in linker zijligging gescand dienen te worden

HOOFDSTUK 13

Het cardiovasculaire systeem van gezonde vrouwen kan de toegenomen hemodynamische eisen van een zwangerschap goed aan. In vrouwen met een hartziekte kan de adaptatie aan de zwangerschap beperkt zijn. Wij hebben de hemodynamische adaptatie aan zwangerschap bestudeerd in een longitudinale, prospectieve studie van 24 vrouwen met een structurele

hartziekte. Proefpersonen ondergingen CMR voor de zwangerschap, bij 20 en 32 weken zwangerschap en 6 maanden na de bevalling. Na initieel omhoog te gaan, werd de linkerkamer ejectie fractie lager tussen de 20 en 32 weken. De ejectie fractie van zowel de rechter- als linkerkamer was hetzelfde 6 maanden na de bevalling als voor de zwangerschap. Ons studie geeft aan dat zwangerschap in vrouwen met een bekende structurele hartziekte geen onherstelbaar effect heeft op het hart.

GENERAL DISCUSSION AND CONCLUSIONS

This thesis investigated novel applications and limitations of cardiac CT and cardiac MR based on a quantitative approach. In this general discussion we will address the outcomes of our studies against the background of the published literature.

ISCHEMIC HEART DISEASE

HOW TO REDUCE RADIATION DOSE IN CARDIAC IMAGING.

The recent years showed an overall increase in the use of cardiac and CT coronary imaging. The radiation dose of earlier CT scanners was worrisome with an effective radiation dose ranging from 4 mSv to 30 mSv [1]. Einstein et al. [2] demonstrated that radiation exposure from 64-slice CT coronary angiography (CTCA) is associated with a relatively wide variation in lifetime attributable risk of cancer in relation to patient age and sex.

The strenght of CTCA is its high negative predictive value. Preliminary data suggest that CTCA may be used as first line diagnostic test in patients with low-to-intermediate pretest probability of having coronary artery disease (CAD) [3]. As first line test, CTCA should be as safe and as minimally invasive as possible because the majority of patients do not have obstructive CAD. In an effort to minimize radiation dose from CTCA several methods for dose reduction have been developed.

Dual source, second generation (128-slice) CT (DSCT) systems provide two low dose scan protocols: a high-pitch spiral protocol, which allows CT data acquisition of the entire heart within 1 heart beat with a radiation dose below 1 mSv, and a prospective sequential protocol for patients with low and high heart rates. The effect on radiation dose and on diagnostic performance of these two low dose protocols in patients with various heart rates is currently debated [4-6]. The major finding of our prospective randomized study (*Chapter 3*) is that sequential CTCA outperforms high pitch-spiral CTCA on a per segment level in patients with a heart rate below 65 beats per minute (bpm). We demostrated that a negative high-pitch spiral CTCA does not reliably exclude the presence of an obstructive stenosis due to the higher rate of non-assessable segments mainly caused by motion artefacts. The use of β-blockers is highly suggested to reduce the heart rate below 65 bpm which allows to select a low dose scan protocol. Alternatively, when the heart rate is above 65 bpm despite the administration of β-blockers, a wide-window sequential CTCA protocol can be used as it provides a comparable diagnostic performance than retrospective CTCA but at significant lower radiation dose. There are some limitations of our study. First, we included exclusively patients with stable heart rates and therefore our results do not apply to patients with arrhythmia. Second, the cut-off value of 65 bpm was extrapolated from data acquired with retrospective CTCA protocols; it is debatable if the same cut-off value is suitable also for sequential CTCA protocols.

Iterative reconstruction has been introduced most recently in cardiac CT, and preliminary data suggest that these sophisticated reconstruction algorithms may allow a further reduction in radiation dose of approximately 40% [7-9]. Future studies are mandatory to determine the correct settings for sequential acquisition protocols.

INTEGRATED ANATOMIC-PHYSIOLOGICAL INFORMATION OF CAD SEVERITY BY CARDIAC CT: THE "HOLY GRAIL"?

Results from large prospective, observational registries and multicenter randomized controlled trials support a symptom benefit and potential risk reduction of revascularization of patients with moderate to severe ischaemia [10-12]. There has been considerable discussion regarding the ability of CTCA to identify functionally significant coronary stenoses. Various studies have demonstrated a mismatch of angiographic stenosis severity measures for the detection of ischaemia compared to myocardial perfusion scintigraphy (MPS) [13] or fractional flow reserve (FFR) [14, 15].

This mismatch between anatomy and function in cardiac imaging has initiated intense research to assess the feasibility of new, non-invasive diagnostic techniques. In a substudy of the FAME trial Tonino et al. [16] showed a high rate of non-functionally significant lesions in the range of an angiographic severity of 50% to 70% diameter stenosis. In our study (*Chapter 4*) we investigated whether the analysis of quantitative CTCA parameters could improve the prediction of functionally significant lesions compared to visual CTCA without further irradiation, contrast, or drug administration. Similarly to Tonino et al., in our study 54% of the coronary stenoses with an angiographic severity between 50% and 70% based on visual assessment were not functionally significant. The use of quantitative CTCA decreased the number of misclassified lesions by half, mainly by reducing the number of lesions incorrectly classified as functionally significant. However, quantitative CTCA improved specificity but at the loss of sensitivity. Our results suggest that quantitative CTCA improves the prediction of flow-limiting lesions compared to visual assessment but remains insufficient for routine clinical practice. Functional assessment is still needed for lesions of moderate severity to guide patient management.

The modest association between anatomic measurements and functional assessment was already demonstrated by Gould et al. [17] who found that stenosis severity as low as 40% can cause ischemia. This may be explained by the complexity of factors leading to myocardial ischemia. As proposed by Marzilli et al. [18] obstructive epicardial coronary stenosis is only one of the contributors to myocardial ischemia and inflammation, endothelial dysfunction, microvascular dysfunction, platelet dysfunction, thrombosis and vasomotor dysfunction should be also considered.

Similar results emerged from pooled analysis examining the association between myocardial perfusion scans (MPS) and CTCA findings [19]. Coronary stenoses judged as <50% at the per-patient level generally revealed a normal MPS, explaining the high negative predictive value of CTCA. Conversely, only half of the coronary stenoses graded as >50% at CTCA was associated with abnormal MPS. These findings demonstrated that anatomic measures of stenosis severity and functional measures of myocardial perfusion provide potentially complementary information regarding CAD.

Recently, numerous single centre studies have demonstrated the feasibility of stress CT perfusion imaging [20-23]. The goal of these studies was to add incremental value to the assessment of coronary stenosis severity with CTCA for the detection of functionally significant coronary stenoses, by providing integrated anatomic-physiological information of CAD severity. Static myocardial perfusion imaging by CT during adenosine stress has been recently investigated in humans and showed a diagnostic accuracy comparable to MPS to detect significant coronary stenoses [20, 21]. However, static perfusion imaging provides only qualitative information of the myocardial perfusion by comparing the attenuation of the ischemic area to the attenuation of the remote myocardium. Quantification of myocardial perfusion is possible using dynamic CT scanning and it was already investigated by electron beam CT (EBCT) in the late 1980's [24, 25]. EBCT technology has been replaced by multidetector CT technology and, due to improved temporal resolution and coverage, the latest generation CT scanners now allow quantitative myocardial perfusion imaging. The first exciting study about dynamic CT perfusion imaging was performed by George et al. who proved the ability of CT to quantify myocardial blood flow (MBF) in an experimental, canine model using 64-multidetector CT [26].

Recently a novel dynamic shuttle mode technique using DSCT has been introduced [27]. In *Chapter 6* we determine whether adenosine stress dynamic CT perfusion imaging by DSCT enables non-invasive quantification of regional MBF in an animal model with various degrees of coronary flow reduction. We found an excellent correlation between MBF and the experimental reference standard, coronary blood flow (CBF), over a wide range of flow values. CBF provides a direct measure of the blood flow distal to a coronary stenosis but direct assessment of CBF is not available in the clinical environment, although coronary blood velocity can be measured using a flow wire. FFR was therefore introduced as indirect parameter of myocardial perfusion. We found a good correlation between MBF and FFR over a wide range of coronary flow reductions.

Microspheres are usually used as experimental gold standard for in vivo measurement of myocardial blood flow. We did not use them in our experiment. However, Bamberg et al. [28] provided good correlation between MBF and microsphere-derived myocardial flow in a pig model of LAD obstruction using the same CT technology. Our experimental setup was designed as a single vessel LAD obstruction. Nevertheless, we expect that this CT technology will give good results also in the situation of multi-vessel disease because it provides absolute quantification of regional MBF rather than relative flows as obtained in MPS. These animal

findings suggest that absolute MBF measurements with CT are feasible and may provide clinically relevant information about the functional impact of coronary stenoses.

We then evaluated the diagnostic performance of MBF obtained by dynamic CT perfusion imaging using DSCT during hyperemic stress for the identification of functionally significant coronary lesions based on FFR in patients with stable angina referred to invasive coronary angiography (ICA) (*Chapter 7*). Our hypothesis was that MBF would have a better diagnostic performance than visual and quantitative CTCA, in particular in intermediate coronary stenoses (30%-70% lumen narrowing).

In our study, the absolute value of MBF to discriminate functionally significant stenoses from non-flow limiting lesions was 78 ml/100ml/min. This is in agreement with the value of 75 ml/100ml/min found by Bamberg et al. [22]. The main criticism has been that MBF assessed by CT is lower compared to positron emission tomography (PET) values, the clinical reference standard for in vivo quantification of MBF [29]. We think that MBF measured by different imaging modalities (positron emission tomography, magnetic resonance imaging, single photon emission tomography and CT) may differ due to different uptake kinetics of the used tracers or contrast agents, different acquisition protocols, and different post-processing methods [30-32].

We found that MBF had better discriminatory power than visual CTCA and quantitative CTCA to identify or exclude flow-limiting lesions both on a patient-level and on a vessel-territory level. The performance of quantitative CTCA to measure coronary artery narrowing was better than that of visual CTCA but inferior than MBF. Lesions with <30% lumen narrowing on CTCA were not functionally significant and nearly all coronary stenoses >70% lumen narrowing on CTCA were functionally significant. By contrast, intermediate grade coronary stenoses represent the most challenging situation: indeed anatomical CTCA measurements yelded both false positive and false negative findings in such lesions. We advise that in the presence of >70% coronary diameter narrowing on CTCA patients may be referred directly to ICA to determine suitability for revascularization. Patients with coronary stenoses <30% lumen narrowing should be treated with optimal medical therapy and modification of risk factors. CT perfusion imaging should be reserved only when intermediate coronary stenoses are identified first on CTCA.

There are several technical aspects related to dynamic CT perfusion imaging that need further considerations. An important technical limitation is the limited volume coverage. The acquisition coverage of the shuttle mode technique is 73 mm which is not always sufficient to encompass the entire heart even when triggering in the systolic phase. Further improvements in CT technology should aim to increase the coverage along the z-axis. The addition of dynamic perfusion CT imaging to the conventional clinical CTCA protocol will increase the total amount of radiation dose. Optimization of radiation dose reduction protocols should be developed with preservation of image quality.

The introduction of CT perfusion imaging will be a boost to further the clinical use of CTCA.

"Now the work begins. Steps need to be taken, questions need to be answered and additional layers need to be avoided" [35]. Future comparative effectiveness studies are warranted to assess the performance of such combined anatomic-physiologic approach in a single non-invasive imaging test in general patient populations.

Recently, the possibility of a non-invasive FFR computation [33] and the measure of transluminal contrast attenuation gradients as a surrogate measure of coronary blood flow [34] have been investigated with promising results. Conversely to stress CT perfusion imaging, both methods do not need the administration of adenosine, additional contrast material and additional radiation dose. Further research should be focused on comparing the diagnostic performance of these two novel techniques with stress CT perfusion imaging.

AORTIC VALVE STENOSIS

AORTIC DILATATION IN PATIENTS WITH BICUSPID AORTIC VALVE: GENETICS OR HEMODYNAMICS?

Aortopathy in bicuspid aortic valve (BAV) is a challenging clinical issue. Patients with bicuspid aortic valve (BAV) are at significantly higher risk for aortic dissection and have larger aortic dimensions than patients with a normal trileaflet aortic valve [36, 37]. So far the pathogenesis of aortic dilatation in BAV patients has been related to a genetic disorder resulting in weakness of the aortic wall and consequent dilatation. Marked degenerative changes of the aortic wall, including cystic medial necrosis [38] and loss of elastic elements [37], have been described in the aorta of BAV patients. This hypothesis was strongly supported by an association between a novel mutation in the NOTCH1 gene and the development of BAV [39]. Moreover, aortic dilatation in BAV was reported to be disproportional to coexisting valvular lesions or to be present in patients without significant valve dysfunction [40, 41] or after successful aortic valve replacement (AVR) [42]. By contrast, the haemodynamic theory is based on the idea that the orientation and the morphology of a BAV may cause turbulent blood flow in the ascending aorta and an increase in aortic wall shear stress. Hope et al. [43, 44] demonstrated recently an abnormal systolic helical flow in BAV patients which was not found in any of the healthy volunteers or patients with a tricuspid aortic valve. We found a significant correlation, although weak, between aortic peak velocity at baseline and progression of aortic dilatation (*Chapter 9*). The high aortic peak velocity with concomitant turbulence in the aortic root and in the tubular portion of the ascending aorta may be one of the mechanisms in the development of aortic dilatation. Although we expect this to be indeed a cause effect relation, we cannot exclude a genetic origin based on these findings, as both severity of aortic stenosis and aortic dilatation may be just an effect of time. Our results are also supported by a recent study by Kim et al. [45] who found a significant correlation between the severity of aortic stenosis and the diameter at the level of the tubular ascending aorta. Nevertheless, this is still not overwhelming evidence and more studies on long-term outcome in native BAV patients and patients

after isolated AVR are needed to better understand the underlying mechanism of aortic dilatation. This is clinically relevant, as it might influence the pharmacological therapy, the surgical techniques employed, and the frequency of aortic screening.

DIAGNOSTIC WORK-UP OF PATIENTS WITH BICUSPID AORTIC VALVE: TRANSTHORACIC ECHOCARDIOGRAPHY OR CARDIAC MAGNETIC RESONANCE?

In patients with BAV the optimal timing of surgical repair for aortic dilatation is determined by the natural course of the disease, by the risk of surgery, and by the post-surgical outcome. Elective aortic surgery is advised when the aortic diameter reaches 55 mm to avoid acute dissection or rupture. Therefore in BAV patients serial imaging of the aorta is mandatory to estimate optimal timing of surgery [46]. For this young population there is the need for a non-invasive imaging modality, which allows accurate and reproducible measurements of the aortic root and tubular ascending aorta. So far, transthoracic echocardiography (TTE) has been widely used as non-invasive imaging modality for BAV patients follow-up, but the mid ascending aorta can be difficult to examine with ultrasound [47]. Cardiac magnetic resonance (CMR) can provide accurate measurements of the diameters of the entire thoracic aorta with high contrast between vessels and surrounding tissues and with good intra- and inter-observer agreement [48]. The results of our study (*Chapter 10*) confirm recent ESC guidelines stating that CMR is manly required to assess aortic dilatation when it occurs distal to the sino-tubular junction [49]. We advise to perform both TTE and CMR at baseline and assess agreement between both techniques when availability of CMR is limited. When both imaging techniques agree well and aortic diameter is <40 mm, TTE can be used for regular follow-up. In case of good agreement and an aortic diameter >40 mm, we suggest to repeat CMR at least every 4 years. In case TTE and CMR show poor agreement in a certain individual patient (>5 mm difference), TTE cannot be used as a reliable tool to assess aortic diameter. In such patients, CMR should be the preferred method for follow-up of aortic diameters; once every 3 to 4 years when the aortic diameter is <40 mm, every 1 to 2 years when the aortic diameter is >40 mm, and even more frequently when the diameter approaches 55 mm.

TRANSCATHETER AORTIC VALVE IMPLANTATION: A POSSIBLE ALTERNATIVE TO SURGERY FOR BICUSPID AORTIC VALVE PATIENTS?

Transcatheter aortic valve implantation (TAVI) has emerged as an attractive alternative to surgery in patients with symptomatic aortic stenosis and contraindications to surgery or in selected patients at high risk for surgery. So far, because of its specific anatomic characteristics, BAV is still considered a contraindication to TAVI, and there have been only a few reported cases of TAVI in patients with BAVs [50-53]. Although the prevalence of BAV decreases in the elderly, a

recent study reported a 22% prevalence in excised stenotic aortic valves in octogenarians [54, 55]. The exact prevalence of BAV remained unclear, because it may have been underestimated due to the difficulty of diagnosis using echocardiography in these severely calcified valves.

Several reasons precluded the use of TAVI in patients with BAV: (1) the high frequency of aortic annular diameters that are too large, not suitable for currently available transcatheter valves; (2) the asymmetric distribution of calcification may preclude the full expansion of the prosthesis and increase the risk for paravalvular aortic regurgitation; and (3) associated lesions of the ascending aorta may also have curbed the use of TAVI.

So far, multimodality imaging has been proved to have a crucial role for an accurate preoperative assessment of the anatomy before TAVI in patients with tricuspid aortic valve and aortic stenosis (*Chapter 11*). Future studies are warranted to investigate such an integrative approach in BAV patients as possible candidates for TAVI.

PREGNANCY AND HEART DISEASE

DOES PREGNANCY INDUCE IRREVERSIBLE EFFECTS IN PATIENTS WITH STRUCTURAL HEART DISEASE?

Most research on haemdynamic adaptation to pregnancy, both in healthy pregnants as in pathologic conditions is performed with TTE. The advantage of TTE is that it is non-invasive, readily available, and commonly used in clinical practice. Also, it offers information on various aspects of systolic and diastolic cardiac function. Most ultrasound volume estimations and mass calculations are dependant on geometric assumption which are not always met during pregnancy and in subjects with structural heart defects. This may result in an inaccurate estimation of haemodynamic cardiac parameters. CMR is more reliable in the assessment of left and right ventricular function. Because aortocaval compression is important in advanced pregnancy we advise that pregnant women requiring CMR should be studied in a consistent position for serial studies and the left lateral position should be preferred from early pregnancy onwards (*Chapter 12*).

Possible irreversible effects on maternal cardiac function induced by pregnancy have been described in some specific patient groups [56-58]. In contrast to previous ultrasound findings by Cornette et al. [56], our CMR data (*Chapter 13*) suggest that pregnancy in women with pre-existing structural heart disease is not associated with an irreversible impairment of left ventricular systolic function. The absence of difference before and after pregnancy is in accordance with Uebings et al. [59] who could not observe a detrimental effect of pregnancy on postpartum ventricular function, except in women with tetralogy of Fallot (TOF). Similarly, Kamiya et al. [57] demonstrated that left ventricular size and function did not change due to pregnancy in women with repaired TOF, but the right ventricular dimensions remained in-

creased at 6 months after delivery. Another interesting finding of our study is that we did not find the reversible eccentric hypertrophy described in healthy pregnant women with an increase in myocardial mass up to 50%. This is considered as a compensatory mechanism to overcome increased preload and afterload that accompany the progressing gestation. Left venricular mass values were in the normal range but substantially lower if compared with the values presented in the echocardiographic study by Cornette et al [56]. Possible explanations are that echocardiography is less accurate and reproducible than CMR for LV mass calculation and it is affected by the LV geometry [60].

Larger patient numbers are clearly warranted to answer the question if pregnancy causes an irreversible impact on the heart. A matched control group for direct comparison was missed in our study as we chose not to perform CMR in healthy pregnant women. However, this would have been very interesting and might be considered in the future.

CONCLUSIONS

The accurate and reproducible quantification of morphological and functional cardiac parameters is crucial for the determination of appropriate therapeutic procedures, monitoring disease progression and response, timing of surgery and prognostic stratification in patients with congenital and acquired cardiac disease.

PhD PORTFOLIO

Name PhD student:	Alexia Rossi
Erasmus MC Department:	Radiology/ Cardiology
Research School:	Cardiovascular research School (COEUR), Erasmus MC
PhD period:	January 2009 – December 2012
Promotors:	Prof. Dr JW Roos-Hesselink Prof. Dr GP Krestin

EDUCATION AND TRAINING

1994-1998	Scientific High School Degree (Scientific High School "E. Torricelli")
1998-2004	Laurea in Medicina e Chirurgia (University of Trieste)
2004	Professional licensure to practice
2004-2008	Specialty Training in Diagnostic Imaging, subspecialty training: Cardiovascular (University of Trieste)
2007-2008	Research fellowship in cardiac MR at the Departments of Cardiology and Radiology - Erasmus MC, Rotterdam, The Netherlands.

PhD TRAINING (42.6 ECTS)

IN-DEPTH COURSES (14.8 ECTS)

2009	Congenital heart disease COEUR course
2009	Biostatistic for Clinicians Netherlands Institute for Health Science (NIHES)

2009 Diagnostic Research
Netherlands Institute for Health Science (NIHES)

2009 Classical Methods for Data Analysis
Netherlands Institute for Health Science (NIHES)

2010 English Biomedical Writing and Communication
Erasmus MC

2009-2011 5 COEUR seminaries

ORAL PRESENTATIONS AT INTERNATIONAL MEETINGS (14.2 ECTS)

2008 43° Congresso Nazionale SIRM (5 days)
Visibilità del lume intrastent nei vasi intracoronarici con angiografia TC a doppia sorgente. Influenza di indice di massa corporea, frequenza cardiaca e diametro dello stent.

2008 European Society of Cardiovascular Radiology (3 days)
Assessment of left ventricle time-dependent parameters: semi-automated versus manual contour tracing in cardiac magnetic imaging.

2008 Radiological Society of North America (5 days)
A simplified continuity equation approach to the quantification of stenotic highly calcified aortic valves using velocity encoded CMR: comparison with conventional invasive cardiac catheterization.

2010 Cardiac problems in pregnancy (3 days)
Quantitative cardiac magnetic resonance: supine or left lateral position?

2010 44° Congresso Nazionale SIRM (5 days)
Accuratezza diagnostica dell' ECG da sforzo e della scintigrafia miocardica nella diagnostica della malattia coronarica: confronto head to head con l'angiografia coronarica con tomografia computerizzata.

Acquisizione high pitch spiral versus acquisizione step and shoot in angiografia coronarica con TC a doppia sorgente di seconda generazione: qualita' dell'immagine e dose. Risultati preliminary.

2010 Radiological Society of North America (6 days)
Quantitative Cardiac Magnetic Resonance in Pregnant Women: Supine or Left Lateral Position?

2011 European Congress of Radiology (5 days)
Quantification of regional myocardial perfusion at different levels of stenosis in a large animal model using dynamic perfusion CT

Temporal resolution in dual source CT: comparison between standard single energy scans and dual nergy scans with a dedicated, mixed reconstruction technique.

2011 Radiological Society of North America (6 days)
Diagnostic Performance of 128-slice Dual Source CT Coronary Angiography Using Three Different Scan Protocols: A Randomized Study.

Myocardial Stress Perfusion Imaging Using Dual Source CT: Quantification of Myocardial Blood Flow at Different Levels of Coronary Flow Reduction in A Large Animal Model.

2012 European Congress of Radiology (5 days)
A randomised study to test the diagnostic performance of 128-slice dual source CT coronary angiography in patients with various heart rates using 3 low-dose scan protocols.

Iterative reconstruction (IR) improves image quality and diagnostic confidence of CT delayed enhancement imaging for the detection of myocardial infarction: preliminary results.

INVITED LECTURES AT INTERNATIONAL MEETINGS (1.8 ECTS)

2008 Somatom World Summit (3 days)
CT coronary stent imaging.

2010 Siemens CT userdag (1 day)
Cardiac CT in ischemic heart disease: beyond CT coronary angiography.

2010 Avanzamenti tecnici e applicazioni cliniche dell'imaging cardiovascolare: luci ed ombre (1 day)
TAC delle coronarie e triple rule-out.

POSTER PRESENTATION AT INTERNATIONAL MEETINGS (7.8 ECTS)

2008 Society of Cardiovascular Magnetic Resonance
The reduction in number of short axis series for MR left ventricular analysis using a combined long-axis and short axis analysis strategy

2008 European Society of Cardiovascular Radiology (3 days)
A simplified continuity equation approach to the quantification of stenotic highly calcified aortic valves using velocity-encoded CMR: comparison with conventional invasive cardiac catheterization.

The number of short axis series for MRI left ventricular analysis can be reduced when a combined long-axis and short-axis analysis strategy is used.

2009 European Congress of Radiology (5 days)
Role of CT angiography and cardiovascular magnetic resonance in the selection of patients suitable for Percutaneous Aortic Valve Replacement.

2009 Radiological Society of North America (6 days)
Myocardial perfusion imaging using Dual Source Computed Tomography

Cardiac perfusion and delayed enhancement imaging using dual energy computed tomography.

2010 Society of Cardiovascular Magnetic Resonance
Cardiac magnetic resonance in pregnant women: supine or left lateral position?

2010 European Congress of Radiology (5 days)
Cardiac perfusion and delayed enhancement using DSCT.

2010 Radiological Society of North America (6 days)
Diagnostic clinical applications of dual source CT.

2011 Society of Cardiovascular Magnetic Resonance
Changes in ascending aorta dimensions, aortic valve function and sistolic ventricular function over time in patients with congenital aortic stenosis.

2011 American college of Cardiology (4 days)
Quantification of myocardial perfusion defects in a large animal model using dynamic dual source computed tomography.

2011 ICNC10 (2 days)
Quantification of myocardial perfusion defects in a large animal model using dynamic dual source CT.

TEACHING (4.0 ECTS)

2009 Supervising several research fellows from foreign countries in training for cardiovascular imaging

LIST OF PUBLICATIONS

PUBLICATIONS IN PEER-REVIEWED INTERNATIONAL JOURNALS

1) Shahzad R, van Walsum T, Schaap M, ***Rossi A***, Klein S, Weustink AC, de Feyter PJ, van Vliet LJ, Niessen WJ.
Vessel specific coronary artery calcium scoring: an automatic system (2013).
Academic Radiology 20 (1): 1-9

2) Dharampal AS, Papadopoulou SL, ***Rossi A***, Weustink AC, Mollet NR, Meijboom WB, Neefjes LA, Nieman K, Boersma E, de Feijter PJ, Krestin GP.
Computed tomography coronary angiography accuracy in women and men at low to intermediate risk of coronary artery disease (2012).
European Radiology 22 (11): 2415-23

3) Papadopoulou SL, Brugaletta S, Garcia-Garcia HM, ***Rossi A***, Girasis C, Dharampal AS, Neefjes LA, Ligthart J, Nieman K, Krestin GP, Serruys PW, de Feyter PJ.
Assessment of atherosclerotic plaques at coronary bifurcations with multidetector computed tomography angiography and intravascular ultrasound-virtual histology (2012).
European Heart Journal Cardiovascular Imaging 13 (8): 635-42.

4) Papadopoulou SL, Neefjes LA, Garcia-Garcia HM, Flu WJ, ***Rossi A***, Dharampal AS, Kitslaar PH, Mollet NR, Veldhof S, Nieman K, Stone GW, Serruys PW, Krestin GP, de Feyter PJ.
Natural history of coronary atherosclerosis by multislice computed tomography (2012).
JACC Cardiovasc Imaging 5 (3 Suppl): S28-37.

5) Maffei E, Messalli G, Martini C, Nieman K, Catalano O, ***Rossi A***, Seitun S, Guarricci AL, Tedeschi C, Mollet NR, Cademartiri F.
Left and right ventricle assessment with cardiac CT: validation study vs Cardiac MR (2012).
European Radiology 22(5): 1041-1049

6) Maffei E, Nieman K, Martini C, Catalano O, Seitun S, Arcadi T, Malago' R, ***Rossi A***, Clemente A, Mollet NR, Cademartiri F.
Classification of noncalcified coronary atherosclerotic plaque components on CT coronary angiography: impact of vascular attenuation and density thresholds (2012).
Radiologia Medica 117(2): 230-241

7) Neefjes LA, Ten Kate GJ, ***Rossi A***, Nieman K, Galema-Boers AJ, Langendonk JG, Weustink AC, Mollet NR, Sijbrands EJ, Krestin GP, de Feyter PJ. *Accelerated subclinical coronary atherosclerosis in patients with familial hypercholesterolemia (2011).*
Atherosclerosis 219(2):721-727

8) Gruszczynska K, Kirschbaum S, Baks T, Moelker A, Duncker DJ, ***Rossi A***, Baron J, de Feyter PJ, Krestin GP, van Geuns RJ.
Different algorithms for quantitative analysis of myocardial infarction with DE MRI: comparison with autopsy specimen measurements (2011).
Academic Radiology 18(12):1529-1536

9) Neefjes LA, Dharampal AS, ***Rossi A***, Nieman K, Weustink AC, Dijkshoorn ML, Ten Kate GJ, Dedic A, Papadopoulou SL, van Straten M, Cademartiri F, Krestin GP, de Feyter PJ, Mollet NR.
Image quality and radiation exposure using different low-dose scan protocols in dual-source CT coronary angiography: randomized study (2011).
Radiology 261(3):779-786

10) Schultz C, ***Rossi A***, van Mieghem N, van der Boon R, Papadopoulou SL, van Domburg R, Moelker A, Mollet N, Krestin G, van Geuns RJ, Nieman K, de Feyter P, Serruys PW, de Jaegere P.
Aortic annulus dimensions and leaflet calcification from contrast MSCT predict the need for balloon post-dilatation after TAVI with the Medtronic CoreValve prosthesis (2011).
Eurointervention 7(5):564-572

11) Maffei E, Messalli G, Martini C, ***Rossi A***, van Pelt N, van Geuns RJ, Weustink AC, Mollet NR, Nieman K, Aldrovani A, Imbriaco M, Bogaert J, Cademartiri F. *Magnetic resonance assessment of left ventricular volumes and mass using a single-breath-hold 3D k-t BLAST cine b-SSFP in comparison with multiple-breath-hold 2D cine b-SSFP (2011).*
Insights Imaging 2: 39-45

12) ***Rossi A***, Cornette J, Johnson MR, Karamermer Y, Springeling T, Opic P, Moelker A, Krestin GP, Steegers E, Roos-Hesselink J, van Geuns RJ. *Quantitative cardiovascular magnetic resonance in pregnant women: cross-sectional analysis of physiological parameters throughout pregnancy and the impact of the supine position (2011).*
Journal of Cardiovascular Magnetic Resonance 13 (1): 31-37

13) Dharampal AS, ***Rossi A***, de Feyter PJ.
Computed tomography-coronary angiography in the detection of coronary artery disease (2011).
Journal of Cardiovascular Medicine 12 (8): 554-561

14) Kirschbaum SW, Nieman K, Springeling T, Weustink AC, Ramcharitar S, Mieghem C, ***Rossi A***, Duckers E, Serruys PW, Boersma E, de Feyter PJ, van Geuns RJ.
Non-invasive diagnostic workup of patients with suspected stable angina by combined computed tomography coronary angiography and magnetic resonance perfusion imaging (2011).
Circulation Journal: Official Journal of the Japanese Circulation Society 75 (7): 1678-1684

15) Neefjes LA, Ten Kate GJ, ***Rossi A***, Galema-Boers AJ, Langendonk JG, Weustink AC, Moelker A, Nieman K, Mollet NR, Krestin GP, Sijbrands EJ, de Feyter PJ.
CT coronary plaque burden in asymptomatic patients with familial hypercholesterolaemia (2011).
Heart 97 (14): 1151-1157

16) Kirschbaum SW, Springeling T, ***Rossi A***, Duckers E, Gutiérrez-Chico JL, Regar E, de Feyter PJ, van Geuns RJ.
Comparison of adenosine magnetic resonance perfusion imaging with invasive coronary flow reserve and fractional flow reserve in patients with suspected coronary artery disease (2011).
International Journal of Cardiology 147 (1): 184-186

17) Maffei E, Martini C, De Crescenzo S, Arcadi T, Clemente A, Capuano E, ***Rossi A***, Malagò R, Mollet N, Weustink A, Tedeschi C, La Grutta L, Seitun S, Igoren Guaricci A, Cademartiri F.
Low dose CT of the heart: a quantum leap into a new era of cardiovascular imaging (2010).
Radiologia Medica 115 (8): 1179-1207

18) Kirschbaum SW, ***Rossi A***, van Domburg RT, Gruszczynska K, Krestin GP, Serruys PW, Duncker DJ, de Feyter PJ, van Geuns RJ.
Contractile reserve in segments with nontransmural infarction in chronic dysfunctional myocardium using low-dose dobutamine CMR (2010).
JACC Cardiovascular Imaging 3 (6): 614-622

19) Schultz CJ, Moelker AD, Tzikas A, ***Rossi A***, van Geuns RJ, de Feyter PJ, Serruys PW
Cardiac CT: necessary for precise sizigi for transcatheter aortic implantation (2010).
Eurointervention 6 Supplemento: G: G6-G13

20) Martini C, Palumbo A, Maffei E, ***Rossi A***, Rengo M, Malagò R, Dijkshoorn M, Weustink A, Mollet N, Krestin G, Cademartiri F.
Dose reduction in spiral CT coronary angiography with dual source equipment. Part II. Dose surplus due to slope-up and slope-down of prospective tube current modulation in a phantom model (2010).
Radiologia Medica 115 (1): 36-50

21) Martini C, Palumbo A, Maffei E, ***Rossi A***, Rengo M, Malagò R, Dijkshoorn M, Weustink A, Mollet N, Krestin G, Cademartiri F.
Dose reduction in spiral CT coronary angiography with dual-source equipment. Part I. A phantom study applying different prospective tube current modulation algorithms (2009).
Radiologia Medica 114 (7): 1037-1052

22) Cademartiri F, Aldrovandi A, Palumbo A, Maffei E, Fusaro M, Tresoldi S, Messalli G, ***Rossi A***, Rengo M, Pugliese F, Salamousas BV, Reverberi C, Meijboom WB, Mollet NR, Ardissino D, De Feyter PJ.
Multislice computed tomography coronary angiography: clinical applications (2007).
Minerva Cardioangiologica 55(5): 647-58.

AHEAD OF PRINT

23) Weustink AC, Neefjes LA, ***Rossi A***, Meijboom WB, Nieman K, Capuano E, Boersma E, Mollet NR, Krestin GP, de Feyter PJ.
Diagnostic performance of exercise bicycle testing and single-photon emission computed tomography: comparison with 64-slice computed tomography coronary angiography.
The International Journal of Cardiovascular Imaging. Epub ahead of print: 08.01.2011.

24) Kirschbaum SW, ***Rossi A***, Boersma E, Springeling T, van de Ent M, Krestin GP, Serruys PW, Duncker DJ, de Feyter PJ, van Geuns RJ.
Combining magnetic resonance viability variables better predicts improvement of myocardial function prior to percutaneous coronary intervention.
International Journal of Cardiology. Epub ahead of print: 15.03.2011

25) Dharampal AS, ***Rossi A***, Papadopoulou SL, Weustink AC, Boersma E, Nieman K, Chen CH, Dijkshoorn M, Mollet NR, Krestin GP, de Feyter PJ.
Is there a difference in the diagnostic accuracy of computed tomography coronary angiography between women and men?
Coronary Artery Disease. Epub ahead of print: 20.05.2011.

26) Dedic A, ***Rossi A***, Ten Kate GJ, Neefjes LA, Galema TW, Moelker A, van Domburg RT, Schultz CJ, Mollet NR, de Feyter PJ, Nieman K.
First-line evaluation of coronary artery disease with coronary calcium scanning or exercise electrocardiography.
International Journal of Cardiology. Epub ahead of print: 18.06.2011

27) Schultz CJ, Tzikas A, Moelker A, ***Rossi A***, Nuis RJ, Geleijnse MM, van Mieghem N, Krestin GP, de Feyter P, Serruys PW, de Jaegere PP.
Correlates on MSCT of paravalvular aortic regurgitation after transcatheter aortic valve implantation using the medtronic corevalve prosthesis.
Catheterization and cardiovascular intervention: official journal of the Society for Cardiac Angiography and Intervention. Epub ahead of print: 25.07.2011

28) Kirişli HA, Gupta V, Kirschbaum SW, ***Rossi A***, Metz CT, Schaap M, van Geuns RJ, Mollet N, Lelieveldt BP, Reiber JH, van Walsum T, Niessen WJ. *Comprehensive visualization of multimodal cardiac imaging data for assessment of coronary artery disease: first clinical results of the SMARTVis tool.* International Journal of Computer Assisted Radiology and Surgery. Epub ahead of print: 25.09.2011

29) Dedic A, Ten Kate GJ, Neefjes LA, ***Rossi A***, Dharampal A, Rood PP, Galema TW, Schultz C, Ouhlous M, Moelker A, de Feyter PJ, Nieman K.
Coronary CT angiography outperforms calcium imaging in the triage of acute coronary syndrome.
International Journal of Cardiology. Epub ahead of print: 07.05.2012

30) ***Rossi A***, Uitterdijk A, Dijkshoorn M, Klotz E, Dharampal A, van Straten M, van der Giessen WJ, Mollet N, van Geuns RJ, Krestin GP, Duncker DJ, de Feyter PJ, Merkus D.
Quantification of myocardial blood flow by adenosine-stress CT perfusion imaging in pigs during various degrees of stenosis correlates well with coronary artery blood flow and fractional flow reserve.
European Heart Journal Cardiovascular Imaging. Epub ahead of print: 26.07.2012

31) ***Rossi A***, van der Linde D, Yap SC, Lapinskas T, Kirschbaum S, Springeling T, Witsenburg M, Cuypers J, Moelker A, Krestin GP, van Dijk A, Johnson M, van Geuns RJ, Roos-Hesselink JW.
Ascending aorta dilatation in patients with bicuspid aortic valve stenosis: a prospective CMR study.
European Radiology. Epub ahead of print: 26.09.2012

32) Neefjes LA, ***Rossi A***, Genders TS, Nieman K, Papadopoulou SL, Dharampal AS, Schultz CJ, Weustink AC, Dijkshoorn ML, Ten Kate GJ, Dedic A, van Straten M, Cademartiri F, Hunink MG, Krestin GP, de Feyter PJ, Mollet NR.
Diagnostic accuracy of 128-slice dual-source CT coronary angiography: a randomized comparison of different acquisition protocols.
European Radiology. Epub ahead of print: 07.10.2012

33) Cornette J, Ruys TP, ***Rossi A***, Rizopoulos D, Takkenberg JJ, Karamermer Y, Opić P, Van den Bosch AE, Geleijnse ML, Duvekot JJ, Steegers EA, Roos-Hesselink JW.
Hemodynamic adaptation to pregnancy in women with structural heart disease.
International Journal of Cardiololy. Epub ahead of print: 11.11.2012

34) Papadopoulou SL, Garcia-Garcia HM, ***Rossi A***, Girasis C, Dharampal AS, Kitslaar PH, Krestin GP, de Feyter PJ.
Reproducibility of computed tomography angiography data analysis using semiautomated plaque quantification software: implications for the design of longitudinal studies.
International Journal of Cardiovascular Imaging. Epub ahead of print: 07.12.2012

35) van der Linde D, ***Rossi A***, Yap SC, McGhie JS, van den Bosch AE, Kirschbaum SW, Russo B, van Dijk AP, Moelker A, Krestin GP, van Geuns RJ, Roos-Hesselink JW.
Ascending Aortic Diameters in Congenital Aortic Stenosis: Cardiac Magnetic Resonance versus Transthoracic Echocardiography.
Echocardiography. Epub ahead of print: 11.01.2013

BOOK CHAPTERS

1) Capuano E, Weustink A, ***Rossi A***, Dijkshoorn MR, Cademartiri F, Mollet NR.
Case studies: acute coronary sybdrome. CT coronary angiography.
An atlas of investigation and diagnosis. Clinical Publishing

2) Weustink A, Pugliese F, Capuano E, ***Rossi A***, Dijkshoorn MR, Mollet NR.
Case studies: secondaty prevention. CT coronary angiography.
An atlas of investigation and diagnosis. Clinical Publishing

3) Palumbo A, Maffei E, Martini C, ***Rossi A***, Dijkshoorn MR, Cademartiri F.
Case studies: triple rule-out and other findings. CT coronary angiography.
An atlas of investigation and diagnosis. Clinical Publishing

4) Capuano E, Dijkshoorn MR, ***Rossi A***, Cademartiri F, Mollet NR.
New horizons in cardiac CT technology. CT coronary angiography.
An atlas of investigation and diagnosis. Clinical Publishing

ACKNOWLEDGEMENTS

In 2007 I spent one year as a research fellow in the Radiology Department of Erasmus University Medical Center, Rotterdam. At that time I "fell in love" with research. In 2009 I started the incredible experience of this research thesis.

This book would not exist without the help and support of all my collegues, friends, and family.

TO MY PROMOTERS, CO-PROMOTER AND PHD COMMITTEE MEMBERS

Dear Professor Gabriel Krestin, thank you for making this project possible. I will always be grateful for your unconditional faith in every moment of this long and, by definition, not easy trip.

Dear Professor Jolien Roos-Hesselink, thank you for your supervision in the field of congenital heart disease as well as for your psychological support in all the critical situations I faced with.

Dear Professor Pim de Feyter, my mentor, thank you for teaching me how to think in and for scientific research. I will never forget our long stimulating discussions, your tireless help and enthusiasm in dealing with the difficulties of research. Thank you for always beliving in this book, even when I did not, and for encouraging me throughout.

Dear Francesca Pugliese, a collegue but first of all a beloved friend. I admire your strenght of mind and the love you put in everything you do. Thank you for your scientific help and support, thank you for everything that you have done for me. Ti voglio bene!

Dear Professor Maria Cova, you have been the first person who belived in me. Thanks for helping me to chose my own path in this world.

Dear Robert-Jan van Geuns, you have been a great supervisor. Thank you for your enthusiasm and motivation.

The inner committee members: Prof. dr. Roos-Hesselink, Prof. dr. GP Krestin, Prof. dr. JHC Reber, Prof. dr. MGM Hunink and Prof. dr. A Bogers; the plenary committee members, Prof. dr. M Simoons, Prof. MA Cova and dr. F Pugliese, thank you for all the efforts in reading and improving this thesis.

TO MY PARANYMPHS

Dear Anoeshka, you know already that this book is also your book. Thank you for your friendship, for the sleepless nights working together in the office, for the help in patient recruitment. We have grown up together during these four years and I hope we will always be in touch in the future.

Dear Rahil, at the beginning we were collegues, then we have became friends. Your smile and good mood, your willing to make new experiences and to try new foods have made the time in Rotterdam pleasant and funny. I know that I can count on you. Thank you for your friendship and your support.

TO MY COLLEGUES

Dear Lisan, Tirza and Elina, we shared the same office but not only. We shared the joy but also the tears related to this experience. Your support has been essential for me.

During these four years I had the privilege to work with a lot of brilliant scientists and clinicians from different methodologies and lines of research.

Thanks to Nico Mollet, Admir Dedic, Gert-Jan ten Kate, Kei, Koen Nieman, Filippo Cademartiri, Annick Weustink, Sharon Kirschbaum, Bob Meijboom, Carl Schultz, Marco Rengo, Ermanno Capuano, Mara Bonardi, Valentina Silvestri, Brunella Russo, Tomas Lapinskas, Adriaan Moelker, and Mohamed Ouhlous from the Non-Invasive Cardiac Imaging group. Dear Mo, thanks for your time, your constant support and precious advices. Dear Kei, thanks for visiting me in Italy and in Rotterdam. You are an awesome friend and I hope I will visit you in Japan in the near future.

A special thank you to the Experimental Cardiology Group: Prof. dr. Dirk Duncker, Daphne Merkus, Andre Uitterdijk, Oana Sorop, Heleen van Beusekom, Nienke van Ditzhuijzen, Mieke van de Heuvel and Prof. dr. Wim van der Giessen who sadly passed away. I have learnt a lot from you and I really appreciate all the efforts that you have put in our common projects.

I would like to thank the BIGR group and in particular Prof. Wiro Niessen, Hortense Kirişli and Rahil Shahzad. I really enjoyed discovering a bit the complex and interesting world of biomedical imaging.

Thanks to Jurgen Ligthart, Nico Bruining, Petra Opic, Titia Ruys, Denise van der Linde, Jerome Cornette, and Dimitris Rizopoulos for their cooperation in several projects.

A special mention should be made to the great team of all radiographers of Erasmus MC.

Dear Marcel, thanks so much for your precious teaching and for your time scanning CT with me during the weekends and the nights. Dear Ronald, thanks for your willingness and for your constant help. Big thanks to Marcel van Straten, for his continous patience with my endless questions. I cannot forget Gavin Huston. Dear Gavin, thanks for your advices and for your help. A special thank you is for Piotr Wielopolski.

Linda Everse, you have been a great support for me during these years. Thanks for the long chats, for the advices and for your friendship.

Big thanks to Ton Everaers. Dear Ton, you have made a great job with the cover of this book!

Big thanks to Marja Thijse, Esther Kara, Fania Jarmohamed and the staff of the Radiology secretariaat. A special mention to Mart Rentmeester. Dear Mart, thanks for your help and for solving all problems related to my computer. I would like also to thank Jolanda Meijer for her precious help during these years.

TO MY DEAREST FRIENDS AND FAMILY

I have met a lot of people from different countries during these four years in Holland, my big family in Rotterdam.

Dear Carmen, Gianluca, Antonio, thank you for your friendship and constant help.

Dear Laura, Pierluigi and Agata, thanks for your unlimited love and for always making me feel at home.

Alessandro and Gaia, I really admire your resolution and courage. Gaia, thanks for your precious advices and for your constant support.

Dear Elina, I consider you one of my best friends. I miss our brainstorming but I especially miss our coffees in the morning, our dinners after work, our chats. Thanks because you were next to me in all the difficult moments of the past years. I wish all the best to you and Chris, I love you both!

Dear Brunella, we had a really nice time together. I don't know how to thank you for your friendship.

Dear Salvatore, we had really an "excellent" time together. It was really a pity to meet you in the last months of your stay in Rotterdam. I wish you all the best for your future life.

Dear Giulia P, thanks for the fun, the unconditional support and hospitality. I hope you will visit me soon in Trieste.

Dear Giulia A, we had fun together! I wish you all the best for the future.

Dear Ermanno, thanks for all the trips around the world, for your constant help and support.

Miroslav, Oscar, Lurdes, Francesco C, Francesco A, Valerio, Valentina, Silvana, Francesca, Claudia, Alessandro, Federico, Paolo, Marialuisa, Marta, Giulia, Anna, Davide, Sara it has been a pleasure to meet all of you!

Elisa e Gigi, grazie per aver condiviso con me i momenti belli e brutti di questo lungo percorso. Vi voglio bene!

Grazie a tutta la mia famiglia in Italia. Un grazie speciale a mia zia Nadia per aver sempre creduto in me e per essermi sempre stata vicina in ogni momento della mia vita.

Mamma Eliana, papà Giuseppe, non riuscirò mai a ringraziarvi abbastanza per il sostegno che mi avete dato durante questi anni. Grazie per avermi sempre appoggiato incondizionatamente. Grazie per avermi sempre lasciato scegliere liberamente. Tutto questo non sarebbe stato possibile senza il vostro infinito amore. Vi voglio bene!

ABOUT THE AUTHOR

Alexia Rossi was born on March 16th 1979 in Pordenone, Italy. She started Medial School in 1998 at Trieste University. In 2004 she obtained her medical degree. In the same year she started her specialization in Radiology at Cattinara Hospital in Trieste, Italy. During her training, in 2007, she spent one year at the Department of Radiology of Erasmus Medical Center in Rotterdam, The Netherlands, as research fellow in cardiac MR. She finished her Radiology training in November 2008. In 2009 she moved again to Rotterdam where she started her training in cardiac CT and in cardiac MR, and also her PhD research under the supervision of Professor JW Roos-Hesselink (Department of Cardiology), of Professor PJ de Feyter (Department of Radiology and Department of Interventional Cardiology) and Professor GP Krestin (Department of Radiology). Her achievements in the role of quantification in non-invasive cardiac imaging are summarized in this PhD thesis.

At the present time (2013), Alexia works at Cattinara Hospital, Trieste, Italy, in cardiovascular CT and MR.

ABBREVATIONS

AIF:	arterial input function
AoS:	aortic stenosis
AR:	aortic regurgitation
AS:	area stenosis
AVA:	aortic valve area
BAV:	bicuspid aortic valve
CAD:	coronary artery disease
CABG:	coronary artery by-pass graft
CBF:	coronary blood flow
CCTA:	coronary CT angiography
CFR:	coronary flow reserve
CMR:	cardiac magnetic resonance
CO:	cardiac output
CT:	computed tomography
CTCA:	CT coronary angiography
CTP:	CT perfusion
CX:	circumflex
DBP:	diastolic blood pressure
DSCT:	dual source CT
EBCT:	electrom beam tomography
ECG:	electrocardiogram
EDV:	end-diastolic volume
EF:	ejection fraction
ESV:	end-systolic volume
FFR:	fractional flow reserve
FN:	false negative
FP:	false positive
HR:	heart rate
ICA:	invasive coronary angiography
IVUS:	intra-vascular ultrasound
LAD:	left anterior descending
LV:	left ventricle
LVOT:	left ventricle outflow tract
MBF:	myocardial blood flow
MI:	myocardial infarction
MLA:	minimum lumen area
MSCT:	multislice CT
MTT:	mean transit time
NPV:	negative predictive value
PAR:	paraprosthetic aortic regurgitation
PCI:	percutaneous coronary intervention
PEFR:	peak early filling rate
PLFR:	peak late filling rate

PPV:	positive predictive value
QCT:	quantitative computed tomography
RCA:	right coronary artery
ROI:	region of interest
SAVR:	surgical valve replacement
SBP:	systolic blood pressure
SSFP:	steady state free precession
SV:	stroke volume
TAC:	time attenuation curve
TAVI:	transcatheter aortic valve replacement
TN:	true negative
TP:	true positive
TTE:	transthoracic echocardiography
VOI:	volume of interest